Synaptic Transmission in the Rat Medial Superior Olivary Nucleus.

A thesis submitted for the degree of
Doctor of Philosophy
at the University of Leicester

By

Amanda Jane Smith B.Sc.
Department of Cell Physiology and Pharmacology
University of Leicester.

June 1998.

ProQuest LLC
789 East Eisenhower Parkway
P.O. Box 1346
Ann Arbor, MI 48106-1346

Synaptic Transmission in the Rat Medial Superior Olivary Nucleus.

Amanda J. Smith.

The medial superior olivary (MSO) nucleus forms part of the binaural auditory pathway in the brain stem where it is involved in sound source localisation. It detects interaural time differences (ITDs) of sounds arriving at the two ears by functioning as a coincidence detector of the bilateral excitatory inputs from spherical bushy cells of the anterior ventral cochlear nuclei (AVCN). The MSO also receives a unilateral inhibitory synaptic input from globular bushy cells of the contralateral AVCN, via the medial nucleus of the trapezoid body (MNTB). Investigations in this thesis focus on the inhibitory synaptic input.

Transverse brain stem slices were prepared from 6-13 day old Lister Hooded rats and whole cell patch clamp recordings were made from visually identified MSO neurones. Synaptic currents were evoked using a bipolar platinum stimulating electrode positioned over the ipsilateral MNTB.

The excitatory synaptic input from the contralateral AVCN was mediated by glutamate receptors. Inhibitory postsynaptic currents (IPSCs), generated by stimulation of the ipsilateral MNTB reversed around the chloride equilibrium potential and were blocked by 1μM strychnine, suggesting them to be glycine receptor mediated. The IPSCs had a mean 10-90% rise time of 0.71±0.12ms (n=9) and decayed over a double exponential time course with time constants of 8.54±0.44ms and 41.50±1.84ms (n=81) at 25°C. The decay time course of the IPSC had a Q_{10} of ~2 and was slightly voltage-dependent. The IPSCs were also modulated by 5HT, metabotropic glutamate and $GABA_B$ receptors, the latter of which, based on miniature current analysis was suggested to be via a presynaptic site.

This work confirms that there is a functional synapse between the MNTB and MSO which is mediated by the inhibitory transmitter, glycine and hence suggests that models of sound source localisation should incorporate this important observation.

Acknowledgements

I would like to thank everyone in the Department of Cell Physiology and Pharmacology for their friendly support over the last three years and thanks to the Wellcome Trust for the funding.

I would particularly like to thank my supervisor, Ian Forsythe for his guidance and continued encouragement throughout my PhD.

In addition, I would like to thank Julie Turner and Ian Brooks for all their hard work on the immunohistochemistry - I know I seemed to be asking the impossible! Thanks also to Stuart Johnson for allowing me to use his confocal images of neurones in this thesis and to David Maconochie for his perseverance with the miniatures! Thank you John Clarke, Diane Everitt, Julie Turner and Ian Brooks for all the technical support.

Special thanks must go to my lab. colleagues over the years: Ian F., Helen, Margaret, Matt, Zoltan, Ian B., Steve, Jo and Julie. You have all been an endless source of knowledge and fun throughout!

Thanks also to the many people who have shared the highs and lows with me over a pint or two! - Gareth, Chris, Matt, Julie, Gayle, Chris, Steve, Ian, Jo, Ali and many more.....

Thank you also James for your constant love and encouragement and for coping with all my stress without complaint. I wouldn't have been able to do this without you keeping me sane over the last few months!

Finally, I would like to thank my family for their never ending love and support and the many word of wisdom they have given me. Thank you for everything mam and dad, I could not have done it without you.

TABLE OF CONTENTS

LIST OF FIGURES

Chapter 1 - Introduction

1 Introduction

The medial superior olivary (MSO) nucleus in the brain stem plays an important role in mammals as part of a mechanism involved in sound source localisation. The aim of this thesis is to provide the reader with some understanding of the complexities of the synaptic projections the MSO receives. Particular emphasis will be placed on the characteristics of the glycine-mediated input the MSO receives from the ipsilateral medial nucleus of the trapezoid body (MNTB).

To examine this in detail the introduction covers a number of subject matters. It begins with a description of the anatomy and physiology of the auditory system and goes on to provide some background information of the neurotransmitter, glycine and its ligand-gated receptor-ion channel complex. The introduction finishes by providing some detail of the properties of cell membranes and the techniques used to study them.

1.1 The Auditory System

The interpretation of sound is a process which involves the transduction of sound arriving as compression waves at the ear into neural signals in the brain. This process gives information about the sound, including its loudness, frequency and location, providing a complex perception of the sound. This section begins with an overview of the anatomical arrangement of the auditory system and goes on to describe some of the history and current opinions of the way mammals localise a sound source using what is known as binaural processing. Particular emphasis will be placed on the role played by the MSO.

1.11 Auditory Anatomy

The mammalian auditory system is complex but comprises several common basic features. It firstly uses a signal transduction system in the cochlea of the ear which converts mechanical sound waves to neural signals. From here the auditory (VIIIth) nerve projects centrally to the brain stem where several nuclei and a variety of neurotransmitters are used to interpret the signal arriving from the ear. Nuclei in the brain stem are the first point in the auditory pathway which receive bilateral input from both ears, making it also the first point of binaural processing (Ramón y Cajal, 1909 (from Grothe & Sanes, 1994); Poljak, 1926; Stotler, 1953,

Warr, 1966). From the brain stem, a number of bilateral parallel pathways ascend and converge in the inferior colliculus (IC) in the midbrain. The IC then projects information to the auditory cortex via the medial geniculate nucleus (MGN) (reviewed by Helfert, Snead & Altschuler, 1991).

1.111 The Ear

The ear comprises three main structures: the outer ear which includes the pinna and tympanic membrane (or eardrum); the middle ear which contains the malleus, incus and stapes bones; and the inner ear which contains the cochlea and semicircular canals which are involved in the vestibular system.

Sound occurs as a series of pressure waves in air (or some other medium) which are detected by the movement of the tympanic membrane in the outer ear, which is exquisitely sensitive to pressure changes. The cochlea in the inner ear is where the receptor cells, or hair cells are located. Different regions of the cochlea are maximally sensitive to different frequencies of sound, creating a tonotopic organisation which is preserved throughout the auditory pathway. When a hair cell is mechanically displaced by pressure waves originating from the tympanic membrane, its membrane depolarises. The signal is then transmitted centrally via the auditory (VIIIth) nerve. There is a one-to-one ratio of synaptic connection between each hair cell and each neurone of the auditory nerve.

1.112 The Auditory Nerve

The auditory nerve comprises type I and type II spiral ganglion cells which receive afferent input from hair cells of the cochlea. Where the auditory nerve enters the cochlear nucleus (CN), each axon bifurcates such that ascending branches pass toward the anterior ventral CN (AVCN) and descending branches converge into the posterior ventral CN (PVCN) and the dorsal CN (DCN) (reviewed by Helfert, Snead & Altschuler, 1991). Tonotopy is maintained in these bifurcated nerves such that each subdivision of the CN will respond across a range of frequencies of stimulation (reviewed by Moore, 1986).

1.113 Cochlear Nucleus

Each fibre of the auditory nerve forms an obligatory synapse at the CN. The CN comprises three major sub-divisions (AVCN, PVCN & DCN), each of which contains a variety of cell types (Osen, 1969; Brawer, Morest & Kane, 1974). The main neuronal types in the CN are called bushy, stellate, octopus, multipolar, fusiform and granule cells, all of which have distinctive morphological features. The tonotopic arrangement observed in the auditory nerve is maintained in the VCN (Bourk, Mielcarz & Norris, 1981) but is more complex and less well understood in the DCN (Leake and Snyder, 1989).

The ventral part of the CN is most relevant to this study since it contains neurones which synapse both directly and indirectly onto MSO neurones. Briefly, I will describe some of the basic morphological features of the VCN (reviewed by Helfert, Snead & Altschuler, 1991; Moore, 1986). Four major cell types are found in the VCN; spherical bushy cells, globular bushy cells, octopus cells and multipolar/stellate cells.

Spherical bushy cells are located in the anterior ventral cochlear nucleus (AVCN) and show a size gradient where the largest cells are located at the anterior end and the smallest cells at the dorsal end. They receive a giant excitatory calyceal synapse called an endbulb of Held from the auditory nerve (Held, 1893; Isaacson & Walmsley, 1995a). They project ipsilaterally to the lateral superior olivary (LSO) nucleus and bilaterally to the MSO nucleus (reviewed by Cant, 1991; see section *1.114* and figure 1.1).

Globular bushy cells provide the input to the contralateral medial nucleus of the trapezoid body (MNTB) via a giant excitatory calyceal synapse (Forsythe, 1994) called the calyx of Held (Held, 1893) which in turn projects an inhibitory synapse to the LSO and MSO nuclei (see section *1.114* and figure 1.1). These cells have an oval or round soma and are 20-28μm diameter. They appear similar to the spherical bushy cells but their outlines are more irregular. They also receive a giant excitatory synaptic input from the auditory nerve (Isaacson & Walmsley, 1995a) via a calyceal synapse called the endbulb of Held (Held, 1893).

The two bushy cell types are characterised by round cells bodies and tufted dendritic arbours (Brawer, Morest & Kane, 1974). There is a tight temporal coding between auditory nerve cells and bushy cells which may be important for encoding of timing cues used in sound source localisation (Rhode, Oertel & Smith, 1983; Wu & Oertel, 1984; Pfeiffer, 1966).

Figure 1.1 **Schematic representation in the transverse plane of some synaptic connections in the auditory brain stem.**

The auditory ($VIII^{th}$) nerve projects to neurones in the cochlear nucleus (CN). Bushy cells in the anterior ventral CN (AVCN) each receive an excitatory input from the auditory nerve via a calyceal synapse called the endbulb of Held. Spherical bushy cells of the AVCN send a bilateral excitatory projection to the medial superior olivary (MSO) nucleus and a unilateral excitatory projection to the lateral superior olivary (LSO) nucleus (on the ipsilateral side; open symbols, O). Globular bushy cells send an excitatory synaptic projection to the contralateral medial nucleus of the trapezoid body (MNTB). The MNTB then projects an inhibitory synapse to the homolateral MSO and LSO (closed symbols, ●).

MSO principal neurones are bipolar and are arranged such that one primary dendrite projects laterally toward the ipsilateral AVCN and one medially toward the midline. Each primary dendrite then receives excitatory synaptic inputs from spherical bushy cells such that ipsilateral AVCN neurones synapse on the lateral dendrite, and contralateral AVCN neurones synapse on the medial dendrite (See text).

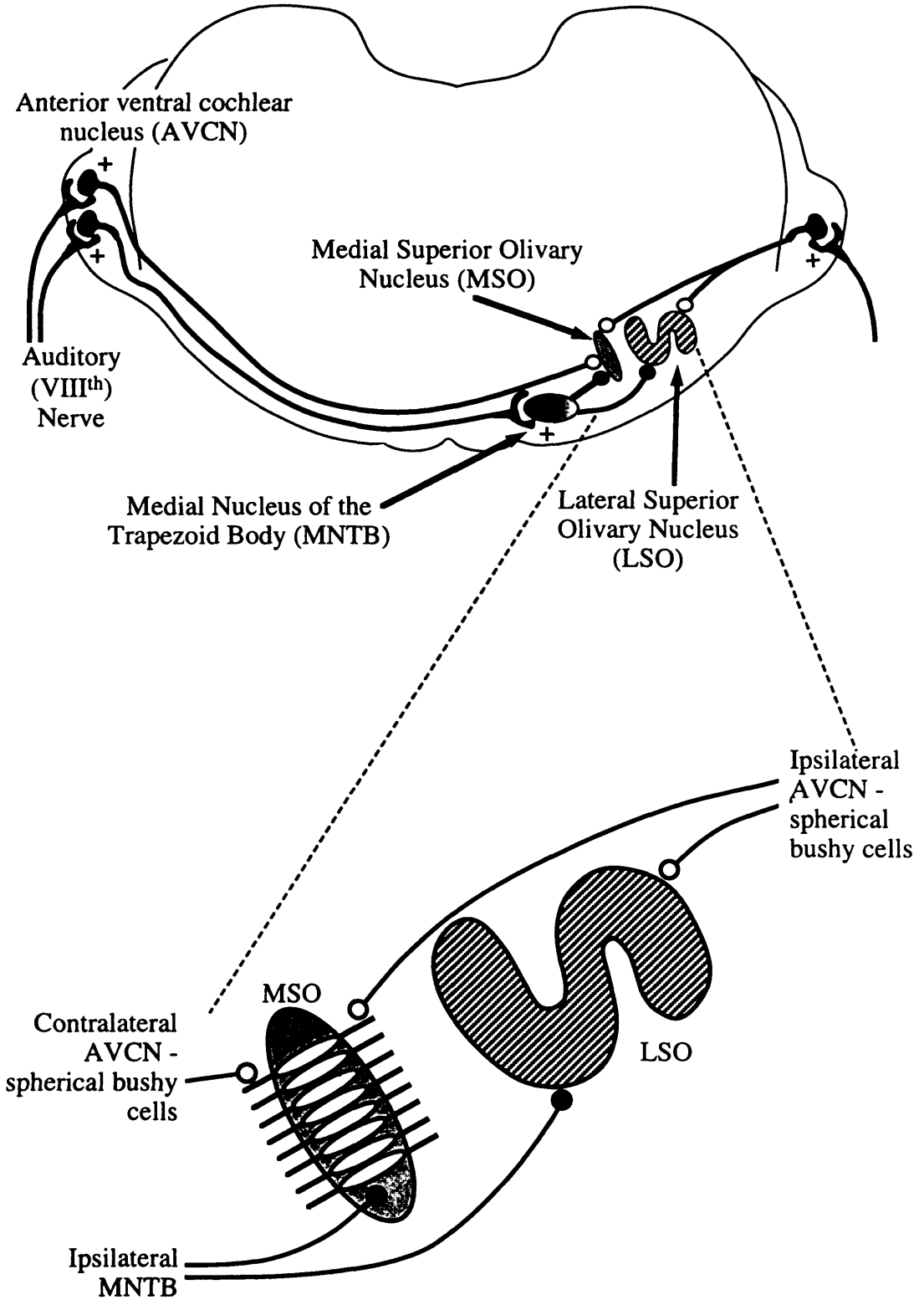
Anterior ventral cochlear nucleus (AVCN)
Medial Superior Olivary Nucleus (MSO)
Auditory (VIIIth) Nerve
Medial Nucleus of the Trapezoid Body (MNTB)
Lateral Superior Olivary Nucleus (LSO)
Ipsilateral AVCN - spherical bushy cells
MSO
LSO
Contralateral AVCN - spherical bushy cells
Ipsilateral MNTB

Octopus cells are named as such because they possess thick dendrites which arise from one side of the cell body, much like an octopus. They are located at the posterior tip of the VCN and are fairly large (~30-35μm diameter) (reviewed by Moore, 1986).

Stellate cells vary in size (from ~15-35μm diameter), have long dendrites which vary considerably in their branching patterns and are scattered throughout the VCN (Brawer, Morest & Kane, 1974). They are so named because of their 'star' shape, and they project mainly to the inferior colliculus (IC). They too receive an excitatory synaptic input from the auditory nerve (Isaacson & Walmsley, 1995a).

1.114 Superior Olivary Complex

The superior olivary complex (SOC) is a binaural processing centre in the brain stem. Figure 1.1 shows a schematic representation of some of its nuclei, particularly those relevant to this thesis. A major output of the VCN is to the SOC where spherical bushy cells project excitatory axons ipsilaterally to the lateral superior olivary (LSO) nucleus and bilaterally to the medial superior olivary (MSO) nuclei . In addition globular bushy cells project contralaterally to the medial nucleus of the trapezoid body (MNTB) from where an inhibitory synaptic projection goes to the homolateral MSO and LSO. It is these three; the MNTB, MSO and LSO which are the principal nuclei of the SOC. They are surrounded by several smaller nuclei, collectively known as the periolivary nuclei (PON).

Medial Nucleus of the Trapezoid Body (MNTB)

The MNTB is so named because of its position among trapezoid body axons. It comprises three cell types (Morest, 1968): principal, elongated and stellate/multipolar cells. The principal neurones are the most prevalent and are readily recognised by their round somas and relatively large size (~16-22μm diameter in rats) (Morest, 1968; Banks & Smith, 1992). The MNTB retains the tonotopic organisation seen earlier in the auditory pathway, with neurones positioned ventromedially responding to high frequencies, and dorsolaterally to low frequencies (Guinan, Norris & Guinan, 1972). The principal neurones receive a single secure giant glutamatergic synaptic input from globular bushy cells of the AVCN (Forsythe 1994). This synapse is a specialised calyceal synapse called the calyx of Held (Held, 1893). The principal neurones will faithfully preserve the temporal pattern of action potentials from the

AVCN (Forsythe & Barnes-Davies, 1993a; Brew & Forsythe, 1995; Wang *et al.*, 1998) which in turn preserve that from the auditory nerve. Several studies suggest that the principal neurones are glycinergic (Bledsoe *et al.*, 1990; Helfert *et al.*, 1989; Moore & Caspary, 1983; Peyret *et al.*, 1987; Wenthold *et al.*, 1987; Friauf, Hammerschmidt & Kirsch, 1997) and the MSO and LSO are known to receive a glycinergic inhibitory input from the MNTB (see below). The MNTB therefore appears to function as an inverting relay, projecting inhibitory inputs to the ipsilateral MSO and LSO (figure 1.1).

Lateral Superior Olivary Nucleus (LSO)

The LSO forms a distinctive S, U or W shape depending on the species and is therefore readily identifiable. The gaps between the folds in the structure are the major sites through which the afferent axons enter the LSO. The LSO receives a binaural input and encodes interaural intensity differences (IIDs) of sound arriving at the two ears (reviewed by Irvine, 1986; Yin & Chan, 1988) (see section *1.12* later) although there is also some evidence that LSO neurones are sensitive to interaural time differences (ITDs) (Caird & Klinke, 1983; Wu & Kelly, 1992). The cat and gerbil LSO contain at least five morphologically distinct cells types but principal neurones comprise approximately three quarters of the neuronal population. Principal neurones are multipolar with discoid dendritic organisation. They are arranged in laminar sheets perpendicular to the transverse axis of the LSO and in transverse sections the principal cell bodies appear fusiform and bipolar (Helfert & Schwartz, 1986, 1987; Scheibel & Scheibel, 1974).

As previously mentioned, the LSO receives an ipsilateral excitatory projection from the spherical bushy cells of the AVCN using glutamate as the neurotransmitter, probably via non-NMDA receptor ion channels (Stotler, 1953; Warr, 1966; Cant & Casseday, 1986; Caspary & Faingold, 1989; reviewed by Cant, 1991). However, Wu & Kelly (1994, 1995) also demonstrated an inhibitory ipsilateral input in mouse LSO. The LSO also receives an inhibitory glycine-mediated input from the globular bushy cells of the contralateral AVCN, via the MNTB as a relay (Moore & Caspary, 1983; Glendenning & Baker, 1988; Sanes, 1990; Wu & Kelly, 1992; Wenthold *et al.* 1987; Banks & Smith, 1992) (figure 1.1). Once again, the tonotopic organisation seen thus far in the auditory pathway is maintained in the LSO where isofrequency planes are oriented perpendicular to its curvatures and the dorsolateral region encodes lower frequencies of sound than the ventromedial region (Tsuchitani & Boudreau, 1966; Guinan, Norris & Guinan, 1972). However, the LSO also contains a biased

representation of the cochlear as it contains more high- than low-frequency cells (Tsuchitani & Boudreau, 1966, Guinan, Norris & Guinan, 1972). The LSO projects rostrally, bilaterally and tonotopically via the lateral lemniscus (LL) to the central nucleus of the inferior colliculus (IC), dorsal nucleus of the LL (DNLL) and less-so to the ventral nucleus of the LL (VNLL) (reviewed by Casseday & Covey, 1987). A substantial proportion of this projection is thought to be inhibitory, although some is excitatory (Oliver, Beckius & Shneiderman, 1995, Godfrey *et al.*, 1988).

Medial Superior Olivary Nucleus (MSO)

The MSO comprises a band of cells which although smaller than the LSO also receives a bilateral input and is equally important in binaural processing. It is involved in sound source localisation by encoding interaural time differences (ITDs) between sound arriving at the two ears (reviewed by Irvine, 1986; Yin & Chan, 1988; see section *1.12*). The MSO contains three major cell types (Kiss & Majorossy, 1983; Smith, 1995): principal or fusiform, multipolar and marginal cells. The principal cells were first described in 1898 by LaVilla (from Kiss & Majorossy, 1983) and are the most prominent of the MSO neuronal cell types. They are bipolar neurones and are oriented perpendicular to the axis of the nucleus in the transverse plane such that one dendrite projects medially toward the midline and one laterally toward the ipsilateral AVCN (Ramón y Cajal, 1909 (from Irvine, 1969); Stotler, 1953; Warr, 1966; see figure 1.1).

The axons of the principal neurones arise perpendicularly from the cell somas or from within ~45μm of the soma on side of the lateral primary dendrite (Stotler, 1953; Smith, 1995; Kiss & Majorossy, 1983). Most MSO neurones project to the ipsilateral central nucleus of the IC and to nuclei of the LL, especially the DNLL (reviewed by Casseday & Covey, 1987). A minor projection is also sent to the contralateral IC. An excitatory amino acid neurotransmitter is thought to be used by most MSO neurones, suggesting the major pathway from the MSO to be excitatory (Oliver, Beckius & Shneiderman, 1995; Godfrey *et al.*, 1988).

Once again, the tonotopic representation of frequencies is maintained in the MSO, where dorsally located neurones are most responsive to low frequency sounds and higher frequency sounds are detected most effectively by ventrally located neurones (Guinan, Norris & Guinan, 1972; Kuwabara & Zook, 1992).

The bipolar dendrites of MSO principal neurones receive a bilateral excitatory input from spherical bushy cells of the AVCN, with the ipsilateral input synapsing on the lateral dendrite, and the contralateral input passing through the MNTB to synapse on the medial dendrite (Cant & Casseday 1986; Warr, 1966; Clark, 1969; Lindsey, 1975; Stotler, 1953) (figure 1.1). It is this bilateral input which was originally thought to be responsible for the involvement of the MSO in sound source localisation (see section *1.12*) which would explain the relative paucity of knowledge about the inhibitory projection.

It is however now well established that MSO principal neurones also receive an inhibitory synaptic input from the ipsilateral MNTB. Some evidence supporting this are as follows. Firstly the MNTB is known to project glycinergic inhibitory inputs to the LSO (Moore & Caspary, 1983; Glendenning & Baker, 1988; Sanes, 1990; Wu & Kelly, 1992) and it was thought the same may happen to the MSO. Also, an inhibitory glycinergic synaptic projection from the lateral NTB (LNTB) to the MSO has been identified in bats and rodents (Cant & Hyson, 1992; Kuwabara & Zook, 1992; Helfert *et al.*, 1989). Kuwabara & Zook (1992), Banks & Smith (1992) and Grothe & Sanes (1993, 1994) have also provided direct evidence of a projection from the MNTB to the MSO, in bats and rodents. Electrophysiological experiments *in vivo* have also provided some indirect evidence for synaptic inhibition. For example, many MSO neurones when delivered a binaural stimulus at specific ITDs have a lower firing rate than elicited by a monaural stimulus, a phenomenon known as out-of-phase suppression (Goldberg & Brown, 1969; Langford, 1984; Yin & Chan, 1990). Interestingly, Clark (1969) conducted an ultrastructural study of the location the synaptic projections the MSO receives. He noted that the bilateral dendrites projecting from each MSO neurone, were largely surrounded by synapses containing excitatory vesicles. Inhibitory synaptic vesicles on the dendrites were restricted only to the regions at the junction of the dendrite with the cell body. Comparatively, he noted that inhibitory and excitatory vesicles were distributed in almost equal proportions on the cell body surface of the MSO. Clark (1969) identified the function of the synaptic vesicle (i.e. excitatory or inhibitory) based on their shape. This was based on work by Uchizono (1967) and Bodian (1966) who hypothesised that spherical shaped vesicles are excitatory, whilst flat vesicles are inhibitory. More recent ultrastructural studies using a similar method of identification of synapses (Brunso-Bechtold, Henkel & Linville, 1990; Oliver, Beckius & Schneiderman, 1995) have also demonstrated that the synaptic projections to LSO and MSO are segregated in a similar manner. Further support of the location of synaptic inputs to the MSO was provided by Kuwabara & Zook (1992) who

demonstrated that the axon collaterals from principal neurones of the MNTB formed small boutons on the somata of the central cell column of the MSO.

1.12 Sound Source Localisation

The localisation of a sound source in auditory space at least in part depends on a binaural auditory pathway. In 1907, Lord Rayleigh proposed the duplex theory of sound localisation. His theory incorporated two methods of sound source localisation, those of interaural intensity and phase differences which are used to localise high- and low- frequency sounds, respectively. Since this original model, it is now established that mammals, including humans do indeed primarily use these two cues of interaural time (or phase) differences (ITDs) and interaural intensity differences (IIDs) to localise low- and high frequency sounds, respectively (Masterton & Diamond, 1967; Masterton & Imig, 1984). This is consistent with the finding by Guinan, Norris & Guinan (1972) that there are considerably more neurones in the MSO with low best frequencies (BFs) than with high BFs, and more neurones in the LSO with high BFs than low BFs. They found that more than half of MSO neurones had BFs of 0-4kHz but only about a quarter of LSO neurones had BFs in this range. In addition, Smith (1995) found that all high-, medium- and low-best frequency neurones in the MSO had a converging input to the lowest frequency region of the MSO.

Two of the principal nuclei in the SOC are the LSO and MSO. These represent the first site of binaural processing (Ramón y Cajal, 1909 (from Grothe & Sanes, 1994); Poljak, 1926; Stotler, 1953; Warr, 1966) in the auditory pathway and are thought to encode IIDs and ITDs, respectively (reviewed by Irvine, 1986; Yin & Chan 1988). The LSO is therefore thought to be responsible for localisation of higher frequency sounds than the MSO.

As described above, the LSO receives a direct excitatory projection from the ipsilateral AVCN and an indirect inhibitory projection from the contralateral AVCN. The combination of these inputs permits the computation of IIDs. Comparatively, the MSO processes ITDs and acts as a coincidence detector. Traditionally, this processing was thought to occur as a result of the coincidence of the bilateral excitatory projection the MSO receives from spherical bushy cells of the AVCN, but is now thought to also involve the inhibitory input from the MNTB (see section *1.121*).

1.121 Interaural Time Differences (ITDs)

In 1948, Jeffress proposed a model of sound source localisation comprising delay lines and coincidence detectors. Figure 1.2 is a schematised representation of the Jeffress model. The delay lines in the model are created by varying axonal path lengths and the coincidence detectors are the binaural neurones (A-E, figure 1.2) that respond maximally when they receive simultaneous input from the two ears. This occurs when the interaural time difference is exactly compensated by the delay introduced by the pattern of innervation. For example, stimulation of neurone 'B' in figure 1.2 may arise from a sound arriving at the left ear fractionally before the right ear, whilst a sound arriving at exactly the same moment at each ear will stimulate neurone 'C' maximally. Since the neurones respond to interaural time differences, they act as an auditory 'place map', providing information about the location of a sound source.

Axons of the nucleus magnocellularis in the barn owl act as delay lines and neurones of the nucleus laminaris act as coincidence detectors (Sullivan & Konishi, 1986; Carr & Konishi, 1988, 1990). The nucleus laminaris and nucleus magnocellularis are the avian equivalents of the mammalian MSO and VCN, respectively. Jeffress (1948) proposed some part of the SOC to be the coincidence detector in mammals. The arrangement of principal neurones in the MSO (described in section *1.114*, also see figure 1.1) and their ability to compare timing of inputs lends them to this task with the bipolar principal neurones being the coincidence detectors and the axons projecting from the ipsilateral and contralateral VCN forming the delay lines (Crow, Rupert & Moushegian, 1978; Goldberg & Brown 1969). Only a small amount of work has been done on the MSO *in vivo* (Caird & Klinke, 1983; Yin & Chan, 1990; Goldberg & Brown, 1968, 1969; Langford, 1984) but findings from the studies were consistent with the theories of coincidence detection (reviewed by Yost & Dye, 1991). Most theories of coincidence detection stem from the Jeffress model (1948) and incorporate only excitatory synaptic projections (e.g. Colburn, Han & Culotta, 1990; Han & Colburn, 1993) despite the knowledge that the MSO and LSO each receive an inhibitory projection. However, Colburn, Han & Culotta (1990) proposed that the inhibitory projection is involved in temporal processing and functions as a modulator of the excitatory synaptic pathway. Later, a model proposed by Han & Colburn (1993) supported this hypothesis by suggesting that the inhibitory input provides relatively slow (tenths of seconds), long term adjustments to the excitatory input, a function which could be useful in tuning the cell population to particular directions,

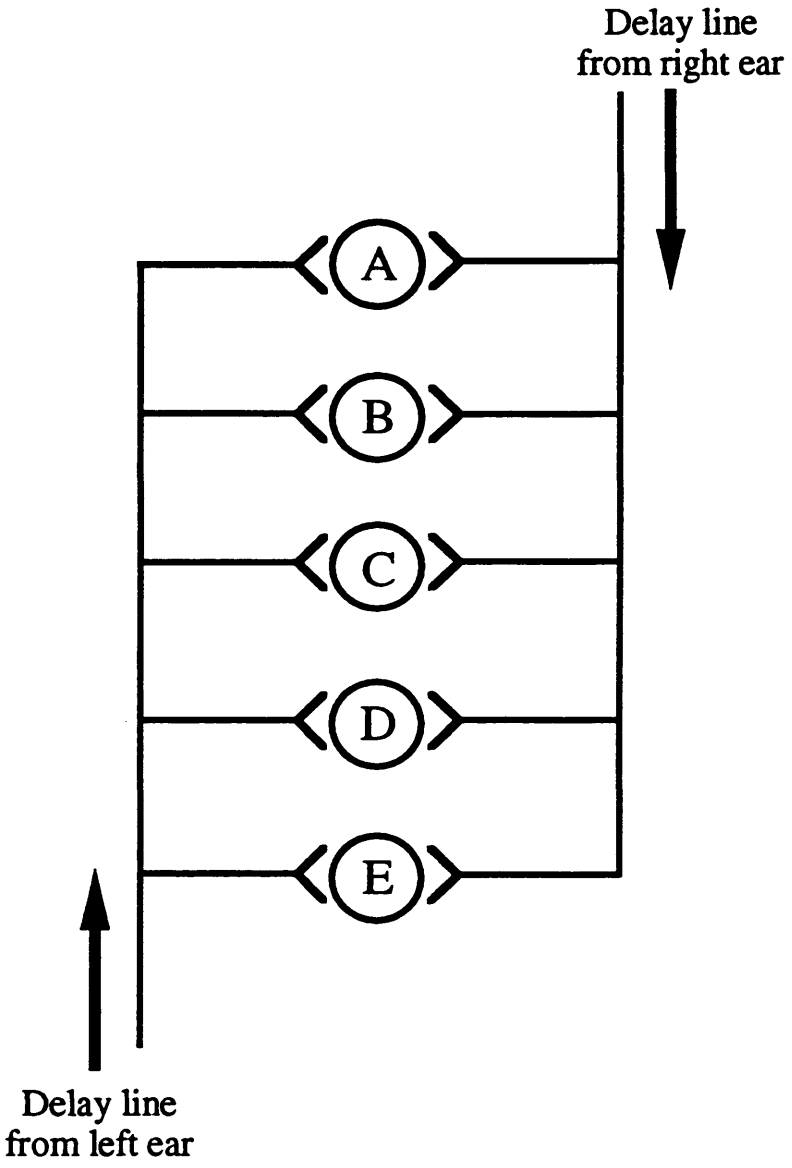

Figure 1.2 **Schematic representation of the delay line hypothesis used in sound source localisation**

The hypothesis proposed by Jeffress (1948) requires delay lines and coincidence detectors. The delay lines are created by varying axonal path lengths and the coincidence detectors are the binaural neurones (A-E).

See text for details.

Figure redrawn from Carr (1993).

frequencies or levels. Brughera *et al.* (1996) more recently attempted to incorporate inhibition into their model of the MSO and although they failed to prescribe a role to the inhibition, they suggested that it is involved in localisation of transient stimuli rather than steady state tones. Grothe & Sanes (1993, 1994) have also proposed experimentally that in addition to coincidence of excitatory synaptic transmission, synaptic inhibition is also important in the functioning of the MSO as a coincidence detector. In addition, Funabiki, Koyano & Ohmori (1998) demonstrated in the avian nucleus laminaris that an inhibitory, GABA mediated input to these neurones sharpens their coincidence detection ability.

1.2 Glycine and the Glycine Receptor

Since it is thought that synaptic transmission between the MNTB and MSO is mediated by the inhibitory neurotransmitter glycine, it is appropriate to introduce some of the history of glycine and its associated receptor.

Glycine is a simple amino acid with the following structure:

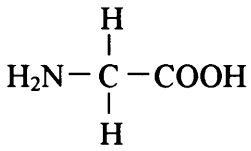

Its distribution and proposal as a neurotransmitter in the spinal cord of the cat was first described by Aprison & Werman (1965) and Graham *et al.* (1967). The establishment of it and γ-aminobutyric acid (GABA) as inhibitory neurotransmitters was reviewed by Aprison and Daly in 1978. The inhibitory actions of glycine and GABA occur by the activation of postsynaptic receptors opening an integral chloride ion channel. GABA and glycine receptor subunits combine to form a receptor-chloride ion channel complex (figure 1.3). Opening of the chloride channel results in membrane hyperpolarisation by increased membrane chloride conductance (Coombs, Eccles & Fatt, 1955).

Conventionally, GABA is thought to predominate as the inhibitory neurotransmitter in the cerebral cortex, diencephalon and cerebellum whilst glycine is important in the spinal cord and brain stem (reviewed by Aprison & Daly, 1978; Becker, 1992; Betz & Becker, 1988). Other studies however have suggested that the occurrence of glycine is more widespread throughout the CNS (Becker, Betz & Schröder, 1993) and glycine receptors are also implicated in the

Figure 1.3 **Schematic diagram showing the primary and quaternary structure of the glycine receptor.**

(A) Primary structure of the α subunit of the glycine receptor. It comprises 4 transmembrane segments (M1-M4). The N-terminal extracellular domain contains the agonist and antagonist binding site. M2 lines the chloride channel pore.

(B) Quaternary structure of the glycine receptor. It comprises 5 subunits ($\alpha_3\beta_2$) arranged as a quasisymmetrical pentamer. The M2 region of each subunit lines the channel pore, through which chloride ions flow. Gephyrin is a polypeptide located on the postsynaptic membrane and is thought to anchor the glycine receptor to the membrane.

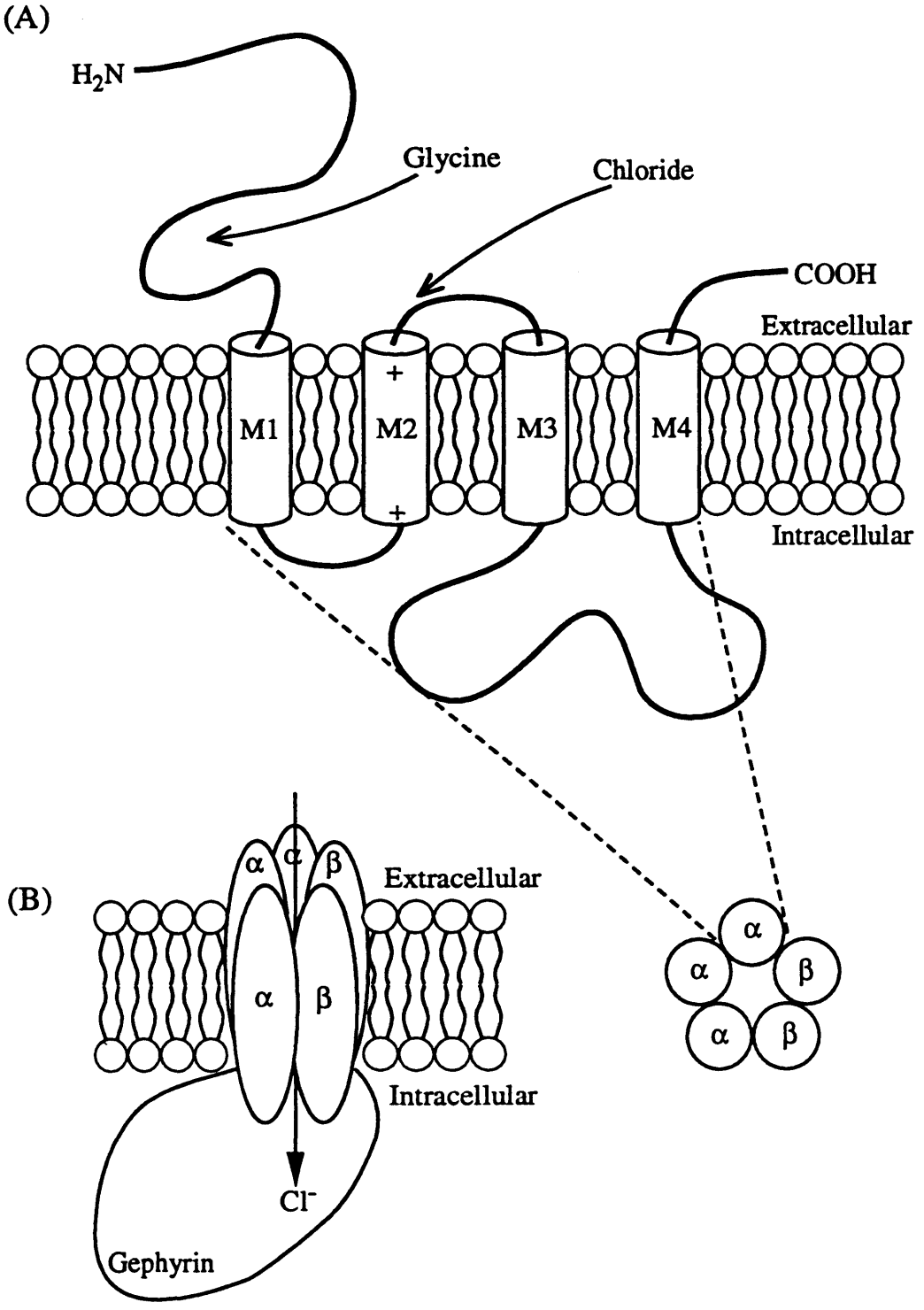
(A)
H_2N
Glycine
Chloride
COOH
Extracellular
M1
M2
M3
M4
+
+
Intracellular
α
α
β
α
β
(B)
Extracellular
α
β
Intracellular
Cl^-
Gephyrin
α
α
β
α
β

sensory, auditory and visual pathways (Becker, 1992; Zarbin, Wamsley & Kuhar, 1981). A large proportion of this study has entailed the examination of glycine mediated synaptic currents resulting from stimulation of the synaptic projection from the MNTB to the MSO. Evidence that glycine is acting as the inhibitory neurotransmitter at this synapse was described in section *1.1*.

Glycine receptors were described by Young and Snyder (1973, 1974) using antagonist binding studies. This entailed the radiolabelling of strychnine, forming [^{3}H]-strychnine. Strychnine, derived from the seeds of an Indian tree, *Strychnos nux vomica*, is a well established and potent glycine receptor antagonist (Barron & Guth, 1987; Curtis *et al.*, 1968; Curtis, Duggan & Johnston, 1971; Ryall, Piercey & Polosa, 1972; Davidoff, Aprison & Werman, 1969) although at higher concentrations it may interact with other non-glycinergic receptors (reviewed by Barron & Guth, 1987). Binding of [^{3}H]-strychnine to spinal cord membranes served as a radioligand binding assay since it competed for glycine receptor occupation. [^{3}H]-strychnine binding was antagonised by the following amino acids in this order of potency: glycine > β-alanine > taurine >> L-alanine, L-serine > proline (Young & Snyder, 1973).

1.21 Glycine Receptor Structure

1.211 Quaternary Structure

The glycine receptor was the first ligand-gated ion channel to be isolated from the mammalian nervous system (Pfeiffer, Graham & Betz, 1982). Its purification from adult mammalian spinal cord revealed the presence of three different polypeptides of molecular weights 48kDa, 58kDa and 93kDa (Pfeiffer, Graham & Betz, 1982; Graham *et al.*, 1985; Becker *et al.*, 1986). Pfeiffer, Graham & Betz (1982) estimated the total molecular mass of the glycine receptor to be 246±6.0kDa. Consistent with this Betz *et al.* (1983) proposed that the glycine receptor comprised two 48kDa subunits and one each of the 58kDa and 93kDa subunits.

Langosch, Thomas & Betz (1988) later estimated the total molecular mass of the glycine receptor to be 260kDa. They found it to comprise five subunits, forming a quasisymmetrical pentameric structure with a proposed stoichiometry of 3α (48kDa) and 2β (58kDa) subunits (figure 1.3). Bormann, Hamill & Sakmann (1987) calculated the open pore diameter based on this stoichiometry to be 0.58nm. This is very similar to that of ~0.52nm determined experimentally using patch clamp studies (Bormann, Hamill & Salmann, 1987). Patch clamp

studies have also revealed that the channel is anion selective and that in 145mM symmetrical chloride, although multiple conductance states exist, the main single channel conductance is ~45pS (Hamill, Bormann & Sakmann, 1983; Takahashi & Momiyama, 1991; Twyman & MacDonald, 1991).

1.212 Gephyrin

The proposed pentameric stoichiometry (Langosch, Thomas & Betz, 1988) did not include the copurifying 93kDa polypeptide identified by Pfeiffer, Graham & Betz (1982), Graham *et al.* (1985) and Becker *et al.*, (1986). However this could be accounted for by the finding that the 93kDa polypeptide is in fact a peripheral membrane protein (Schmitt *et al.*, 1987) which is located on the cytoplasmic face of the postsynaptic glycine receptor complex (Triller *et al.*, 1985; Altschuler *et al.*, 1986). Its localisation and ability to bind polymerised tubulin (Kirsch *et al.*, 1991) means that it is thought to anchor the glycine receptor to the postsynaptic membrane, hence the name gephyrin, from the Greek for bridge. However, there is evidence to suggest that the localisation of gephyrin is not exclusively consistent with glycine receptor localisation since the gephyrin gene is expressed in many brain areas where α subunit mRNAs are not expressed (Malosio *et al.*, 1991; Kirsch *et al.*, 1993). Gephyrin expression has also been demonstrated in the postsynaptic membrane at GABAergic synapses in the retina and spinal cord (Sassoè-Pognetto *et al.*, 1995; Todd *et al.*, 1995).

1.213 Agonist and Antagonist Binding

The α subunit of the glycine receptor is believed to be the site of agonist and antagonist binding. This was determined using antagonist binding studies where [^{3}H]-strychnine was incorporated into the 48kDa polypeptide of the glycine receptor (Graham, Pfeiffer & Betz, 1983; Pfeiffer, Graham & Betz, 1982; Graham *et al.*, 1985; Becker *et al.*, 1986). Application of either glycine or strychnine blocked this [^{3}H]-strychnine labelling, suggesting that the agonist and antagonist binding sites are both situated on the 48kDa subunit (Graham, Pfeiffer & Betz, 1983; Graham *et al.*, 1985; Becker *et al.*, 1986; Pfeiffer, Graham & Betz, 1982). However, though closely related, the agonist and antagonist binding sites are not thought to be identical since displacement by unlabelled strychnine requires a lower concentration than glycine. The IC_{50} for displacement of 2nM [^{3}H]-strychnine using unlabelled strychnine was 7.9±2.2nM and for glycine, 32.0±6.0μM (Marvizón *et al.*, 1986). Also, protein modifications

and changes in ionic conditions can prevent the displacement of [^{3}H]-strychnine by glycine, but not by unlabelled strychnine (Young & Snyder, 1974; Marvizón *et al.*, 1986).

Cloning of the α subunit has permitted more detailed analysis of the agonist and antagonist binding sites. Grenningloh *et al.* (1987) assigned the agonist binding site to the amino acid residues 190-196 and the antagonist binding site between residues 197 and 202. The existence of different isoforms of glycine receptor (see section *1.22*) with different antagonist binding properties has been the focus of a lot of work in attempting to elucidate the exact location of the agonist and antagonist binding sites. Site directed mutagenesis studies by Kuhse, Schmeiden & Betz (1990a) for example, revealed residue 167 to be important in both agonist and antagonist binding since substitution of this glutamate residue for glycine altered the pharmacology of the receptor. Site directed mutagenesis studies by Vandenberg *et al.*, (1992) and Vandenberg, Handford & Schofield (1992) have shown that two distinct subsites between positions160 and 220of the human α1 subunit are important in agonist and antagonist binding. These and other data (reviewed by Kuhse, Betz & Kirsch, 1995) have led to the postulation by Schmieden, Kuhse & Betz, (1992) of a multi-site model of ligand-binding on the glycine receptor. This model includes both low- and high-affinity agonist binding sites and the tertiary structure of each subunit incorporates these sites located in appropriate positions on the receptor.

Homo-oligomeric chloride channels can be expressed in cell lines or *Xenopus* oocytes, are gated by glycine, taurine and β-alanine and are competitively blocked by strychnine. Hill coefficients for these channels are ~2.5-4.2, suggesting that around three glycine molecules must bind to the receptor to open the channel (Schmieden *et al.*, 1989; Bormann *et al.*, 1993; Schmieden, Kuhse & Betz, (1992)).

1.214 Primary Structure

Figure 1.3 shows a simplified representation of the primary structure of the α subunit of the glycine receptor. Peptide mapping and recognition by the same monoclonal antibodies of the α and β subunits (Pfeiffer *et al.*, 1984) demonstrates high homology between these subunits, suggesting that they may be evolutionarily related. cDNA sequencing has revealed that each subunit contains four hydrophobic segments, M1-M4 which are long enough to span a lipid bilayer as an α helix (Grenningloh *et al.*, 1987, 1990). The N-terminal extracellular domain contains a pair of cysteine residues which may stabilise the structure by forming a disulphide

bridge (Grenningloh *et al.*, 1987, 1990). There is also an intracellular hydrophilic loop which separates segments M3 and M4 and the M2 hydrophobic domain is thought to line the channel pore (Grenningloh *et al.*, 1987, 1990; Betz, 1990).

1.215 Homology Between Ligand-Gated Ion Channels

There is a great deal of homology between ligand-gated ion channels, both in the amino acid sequence of the subunits and the structural organisation of those subunits. The primary structure of each subunit of the glycine receptor described above is similar to those of the nicotinic acetylcholine (nACh) receptor (Noda *et al.*, 1983; Changeux, Giraudat & Dennis, 1987) and the $GABA_A$ receptor (Schofield *et al.*, 1987; Levitan *et al.*, 1988). In addition, the quaternary structure of the glycine receptor, comprising 3α and 2β subunits (Langosch, Thomas & Betz, 1988) is very similar to that of the nACh receptor which is also arranged as a pentamer, $\alpha_2\beta\gamma\delta$ (Hucho, 1986; Changeux, Giraudat & Dennis, 1987).

The M2 hydrophobic region of each subunit of the nACh receptor has been established as the pore lining region of the ion channel (Giraudat *et al.*, 1986; Hucho, 1986; Imoto *et al.*, 1986). This region also is highly conserved between the $GABA_A$ receptor and glycine receptor subunits and contains many uncharged polar amino acid residues which are thought to form the lining for their respective ion channel pore (Betz, 1990).

The homology demonstrated between the ligand-gated ion channels means that ion channels such as the nACh receptor, the $GABA_A$ receptor and the glycine receptor constitute members of a ligand-gated ion channel superfamily with conserved primary and quaternary architecture (Unwin, 1989; Betz, 1990).

1.22 Developmental Profile of the Glycine Receptor

The developmental heterogeneity of the glycine receptor in the rodent spinal cord is now well established (Akagi & Miledi, 1988; Becker, Hoch & Betz, 1988). Our knowledge of the difference in expression can be traced back to 1884 and 1885 when Falck (from Becker, Hoch & Betz, 1988) observed that new born rats were relatively immune to strychnine. In more recent years deduction of the relative affinities of the adult and neonatal glycine receptors ($GlyR_A$ or α_1, and $GlyR_N$ or α_2, respectively) to strychnine can explain this. $GlyR_A$ binds strychnine with a high affinity (K_D=4.0nm; Becker, Hoch & Betz, 1988) and its pentameric

structure comprises $3\alpha_1$ subunits (48kDa) and 2β subunits (Langosch, Thomas & Betz, 1988). Comparatively, $GlyR_N$ has a lower affinity for strychnine (K_D=6.8nm) and its pentameric structure comprises $3\alpha_2$ subunits (49kDa) and 2β subunits (Becker, Hoch & Betz, 1988; Hoch, Betz & Becker, 1989).

The variants of the α subunit are highly homologous (Grenningloh *et al.*, 1987; Kuhse, Schmieden & Betz, 1990b; Malosio *et al.*, 1991) and have been studied using both [^{3}H]-strychnine and monoclonal antibody binding (Benavides *et al.*, 1981; Becker, Hoch & Betz, 1988; Friauf, Hammerschmidt & Kirsch, 1997).

All currently known glycine receptor α subunits are recognised by the monoclonal antibody mAb4a. The α_1 subunit of $GlyR_A$ carries an additional N-terminal epitope which is selectively recognised by the monoclonal antibody mAb2b. (Becker, Hoch & Betz, 1988, Pfeiffer *et al.*, 1984). In 1990(a), Kuhse, Schmieden & Betz found, using site directed mutagenesis that exchange of a single amino acid, residue 167 from glutamate to glycine produces a receptor with pharmacological characteristics of the neonatal glycine receptor. Friauf, Hammerschmidt & Kirsch (1997) exploited the sensitivity of α_1 glycine receptors to monoclonal antibodies in the brain stem of rats. They noted that in adults, α_1 glycine receptor subunits were distributed at most relay stations in the auditory pathway, whilst in foetal rats, no immunoreactivity was observed. They observed a gradual increase in immunoreactivity from postnatal day 0 (P0) through to about P21, in most auditory nuclei. The MSO however, displayed no immunoreactivity until around P8 but reached adult-like levels by P21.

In addition to pharmacological and immunohistochemical differences between $GlyR_A$ and $GlyR_N$, patch clamp studies have also revealed differences between these channels with respect to their single channel open times. Takahashi *et al.* (1992) recorded single channel currents from homomeric α_1 and α_2 glycine receptors expressed in *Xenopus* oocytes and compared them to those recorded from native glycine receptors in rat spinal neurones, over the developmental period embryonic day 20 (E20) to P22. They found that the single channel conductances were similar over this period but that the kinetics accelerated. Estimations of the single channel open times of α_1 homomeric channels was similarly as short as the mature glycine receptors (2.38ms and 2.01ms at P18, respectively), whilst the homomeric α_2 channels and native neonatal channels had longer open times (174ms and 39.9ms at E20, respectively). In addition, Krupp, Larmet & Feltz (1994) also noted that the decay time course of glycine mediated postsynaptic currents in sympathetic preganglionic neurones speeded up with age.

1.3 **Electrophysiology**

The major technique employed throughout this study was that of electrophysiological recording. It is an elegant technique which permits the examination of cell membrane properties such that a detailed picture of the membrane and cell structure may be established. In this project it has also been used to study in detail the synaptic inputs the MSO receives and in particular that of the inhibitory input projecting from the MNTB. This section first introduces some basic properties of cell membranes and goes on to describe some of the electrophysiological techniques used to examine these properties.

1.31 Cell Membranes

Cells are surrounded by a membrane comprising a lipid bilayer which is impermeable to the passage of ions (charged particles), sugars or amino acids. Therefore, the membrane essentially separates the inside and the outside of the cell's environment but is interspersed by integral proteins which form membrane ion channels or transporters.

1.311 Ion Channels

Ion channels are macromolecular proteins which traverse cell membranes, forming an aqueous pore. They permit ions to cross from one side of the cell membrane to the other, an action fundamental for cell-to-cell communication and in the nervous system for excitation and inhibition of neurones. Most ion channels are selectively permeable, allowing the passage of specific ions across the membrane. Expression of different ion channels with varying selectivities imparts intrinsic membrane properties to cells. The Goldman-Hodgkin-Katz (GHK) equation (see equation 1.7) can be used to determine the selectivity of a channel to a particular ion.

Ion channels can be broadly divided into two groups based on their gating properties: voltage-gated and ligand-gated ion channels.

Voltage-Gated Ion Channels

Voltage-gated ion channels open as a result of change in the membrane potential of the cell. Charged amino acid residues exist within the ion channel pore and act as voltage sensors to detect the membrane potential. Detection by the voltage-sensor of specific changes in membrane potential then permits the opening of the ion channel.

Ligand-Gated Ion Channels.

Ligand-gated ion channels are gated by the binding of a specific ligand to a receptor which is closely associated with the channel. The ligand might be a neurotransmitter, intracellular metabolite or a hormone. The nicotinic acetylcholine receptor (nAChR) ion channel is ligand-gated and opens as a result of binding acetylcholine or other agonist to the two α subunits of the receptor. Binding of these two subunits opens the associated ion channel, permitting non-specific cation flow. Ligand-gated ion channels, some of which are found at chemical synapses are critically involved in synaptic transmission. In this project an inhibitory form of synaptic transmission mediated by glycine receptor ion channels is the main focus of investigation.

1.312 Basic Electrophysiological Properties of Cell Membranes

A neurone is surrounded by a membrane which is essentially the combination of a capacitor and resistor, or conductor arranged in parallel (figure 1.4).

Resistance and Conductance

The resistance of a membrane represents the resistance to current flow and so is related to the number of open ion channels. As ion channels open, resistance reduces and its reciprocal, conductance increases. Ohm's Law (equation 1.1) relates the membrane potential of a cell to the current flowing through a given resistor:

$$V = IR \qquad \text{Equation 1.1}$$

where V is voltage in volts, I is current in amperes (A) and R is resistance in ohms (Ω).

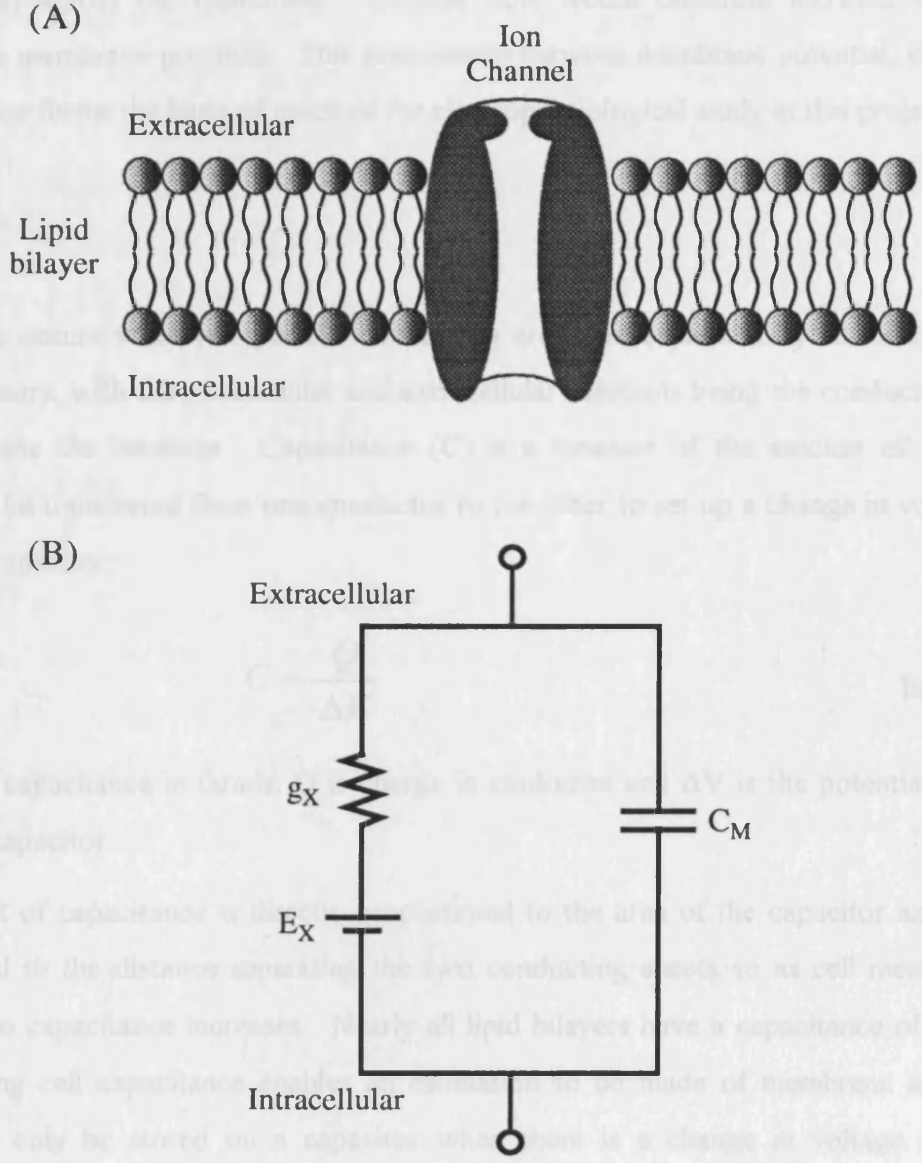

Figure 1.4 **Representation of a cell membrane**

(A) Schematic diagram of a cell membrane. The ion channel forms a resistor or conductor and is the route of passage of ions into and out of the cell. The lipid bilayer separating the intracellular and extracellular compartments forms a capacitor.

(B) Equivalent circuit of a cell membrane. The membrane comprises a capcitor (C_M) and resistor (g_X) arranged in parallel.

So, the greater the conductance of a channel at a given voltage, the greater the current flow through that channel will be. For example, if the membrane was clamped at a specified voltage, opening of ion channels would cause a reduction in resistance (and increase in conductance) across the membrane. Current flow would therefore increase in order to maintain the membrane potential. This relationship between membrane potential, current flow and resistance forms the basis of much of the electrophysiological study in this project.

Capacitance

Capacitance occurs when two parallel conducting areas are separated by an insulator. Cells form capacitors, with the intracellular and extracellular solutions being the conductors and the cell membrane the insulator. Capacitance (C) is a measure of the amount of charge (Q) required to be transferred from one conductor to the other to set up a change in voltage (ΔV) across the capacitor:

$$C = \frac{Q}{\Delta V} \qquad \text{Equation 1.2}$$

where C is capacitance in farads, Q is charge in coulombs and ΔV is the potential difference across the capacitor.

The amount of capacitance is directly proportional to the area of the capacitor and inversely proportional to the distance separating the two conducting sheets so as cell membrane area increases, so capacitance increases. Nearly all lipid bilayers have a capacitance of ~1μF/cm^2, so measuring cell capacitance enables an estimation to be made of membrane area. Since charge can only be stored on a capacitor when there is a change in voltage across that capacitor (equation 1.2), the current flow through the capacitor is proportional to the voltage change with time. Consequently, current flowing through a membrane (I_m) is the combination of current flow through the membrane resistance (I_i) and current flow through the capacitor (C) with respect to time:

$$I_m = I_i + C\frac{\delta V}{\delta t} \qquad \text{Equation 1.3}$$

Therefore, if the voltage across the membrane were to remain the same with respect to time the effects of the capacitance on the current flowing through the membrane could be ignored. However, during an electrophysiological recording when a change in membrane potential

occurs, it is necessary to compensate for the capacitance stored by the neuronal membrane since the initial current flow resulting from a change in membrane potential will be a combination of capacitance and ionic current flow.

Using a small voltage step it is possible to estimate the capacitance of the membrane. The time constant of a cell membrane (τ_m) is the product of cell capacitance (C_m) and membrane resistance (R_m). A small voltage step applied to a cell membrane will generate a transient capacitance current. Measuring the time constant of decay of this current will enable an estimation of the capacitance of the cell membrane to be made, using the following equation:

$$C_m = \frac{\tau_m I}{V} \qquad \text{Equation 1.4}$$

The Nernst Equation

All systems move toward an equilibrium, or state of balance including ions through an open channel in a cell membrane. Electrochemical gradients occur as a result of the combination of electrical and chemical gradients across a cell membrane. When an electrochemical gradient is balanced, an equilibrium is reached called the equilibrium potential. The equilibrium potential can be calculated for any ion using the Nernst equation (Nernst, 1888 (from Hille, 1992)):

$$E_x = \frac{RT}{zF} \ln \frac{[X]_o}{[X]_i} \qquad \text{Equation 1.5}$$

where, R = Gas Constant (8.314 J K^{-1} mol^{-1})

T = Absolute Temperature (K)

z = Valency of ion (e.g. Calcium = +2, Chloride = -1)

F = Faraday Constant (96500 C mol^{-1})

$[X]_o$ and $[X]_i$ = Concentration of X outside and inside the cell

E_X = Potential, in volts of inside with respect to outside the cell

At 20°C for monovalent cations, the Nernst equation can be rewritten as:

$$E_{ion} = 58 \log \frac{[ion]_o}{[ion]_i} \qquad \text{Equation 1.6}$$

The Nernst equation assumes that a membrane contains channels which are entirely selective for the given ion but this is rarely the case. However, the equation will provide information regarding the main charge carrier of the current. By comparing E_{ion}, calculated using equation 1.5 or 1.6 with the measured reversal potential of a current (see below) the main charge carrier of the current may be revealed. However, in order to determine specific ion selectivities of a channel the Goldman-Hodgkin-Katz (GHK) equation is used:

$$E_x = \frac{RT}{zF} \ln \frac{P_A[A]_o}{P_A[A]_i} + \frac{P_B[B]_o}{P_B[B]_i} \qquad \text{Equation 1.7}$$

This is the simplest form of the equation and incorporates the permeability ratios (P_A / P_B) of the two ions in question (A and B) (reviewed by Hille, 1992).

Current-Voltage Relationship

Some insight can be gained into a the properties of a membrane by studying its current-voltage relationship. For instance the reversal potential, that is the voltage at which there is no net current flow into or out of the cell can be measured. Comparison of this measurement with the calculated equilibrium potential using the Nernst or GHK equations (equations 1.5, 1.6 & 1.7) can be used to determine the charge carrier(s) of the current. The slope of the line produced in a current-voltage relationship reflects the conductance through the channel and if that conductance obeyed Ohm's law (equation 1.1) a linear current-voltage relationship would result.

1.32 Voltage-Clamp

The technique of voltage clamp was first developed by Cole (1949), Marmont (1949) and Hodgkin, Huxley & Katz (1949, 1952) for studying the squid giant axon. The method allows ions to flow across a cell membrane, whilst the voltage is held under experimental control using a feedback amplifier. The flow of ions across the cell membrane is measured as electrical current.

Since the introduction of voltage clamp the technique has been developed and is now widely used by scientists. Traditionally the method entailed the use of two separate intracellular microelectrodes, one with the role of voltage measurement and the other with the role of current passage into the cell to maintain the required holding potential. This technique is called

the two-electrode voltage-clamp technique and was also adapted to use a single microelectrode whose role alternates between recording voltage and passing current. This is called the single-electrode voltage-clamp, or switch clamp technique.

An alternative method of voltage clamp is that of the patch clamp technique and is the electrophysiological technique used throughout this thesis (see chapter *2.21*). The patch clamp technique was developed by Neher & Sakmann (1976) who studied acetylcholine receptor ion channels in frog muscle. This technique also uses a single pipette but in contrast to switch clamp, the pipette simultaneously records voltage and passes current. This technique has the advantage of being able to discern faster currents than was possible using the switch clamp technique but is also hindered by series resistance problems.

Series Resistance

Whilst voltage clamping, the membrane potential is monitored by a voltage follower. The voltage follower has a very high input resistance so it draws a negligible input current. The clamping amplifier compares the membrane potential with the command potential. It then passes current through the access resistance to control the membrane potential. The access resistance comprises both electrode and cytoplasmic resistances.

As well as the input resistance there is also a resistance in series with the membrane. The patch clamp technique uses the patch pipette to both record the voltage of the membrane and to be a path of current passage. Consequently, the access resistance in patch clamping contributes part of the series resistance. When a current flows across this resistance a discrepancy between the measured membrane potential and the true potential difference across the membrane results. Series resistance errors are enhanced when large membrane currents flow because the size of the voltage error is determined by the current size multiplied by the series resistance (from Ohm's Law, equation 1.1). Series resistance errors can be compensated for by adding a voltage signal to the command voltage of the clamping amplifier (see chapter *2.262*). This voltage signal is proportional to the membrane current and is scaled appropriately. The higher the level of compensation achieved (80-90%), the closer the actual potential difference across the membrane and the measured membrane potential will be.

1.4 Aims of this Study

This project investigates a wide range of issues involving the MSO nucleus, in the aim of developing a clearer understanding of its characteristics and synaptic inputs. The whole cell patch clamp technique in the brain stem slice preparation was used to study both inhibitory and excitatory synaptic transmission. This technique was also employed during investigations of the voltage-activated ion channels present in the MSO neuronal membrane.

Development of a clear understanding of the physiology of the superior olivary complex forms an integral part of research in this system. The characteristics of both the inhibitory and excitatory components of synaptic transmission in this system will contribute to an understanding of the method by which sound source localisation occurs.

Chapter 2 -Methods

2 Methods

2.1 Thin slice preparation

The preparation used for this study of medial superior olivary (MSO) neurones was transverse thin slices of the rat auditory brain stem. Patch clamping in the thin brain slice preparation was first used by Blanton, Lo Turco & Kriegstein (1989) and Edwards *et al.* (1989) and has been developed by our group (Forsythe, Barnes-Davies & Brew, 1995) for studying synaptic transmission in the superior olivary complex of the auditory brain stem.

The location of the superior olivary complex within the central nervous system makes *in vivo* intracellular studies of this system technically difficult. However, in order to achieve an understanding of synaptic transmission in the superior olivary complex, it is important to preserve as many physiological synaptic connections as possible. The transverse thin slice preparation is very useful for such a task since despite being an *in vitro* preparation, many of its synapses remain intact. This is the case since the axon tracts of this system lie in the same plane as the slice preparation.

2.11 Dissection

Lister Hooded rats, aged from postnatal day six to thirteen were used for all experiments. The rats were killed by decapitation using a size 4 scalpel fitted with a size 26 surgical blade (Swann Morton).

The head was placed with the ventral surface downwards, in a partially frozen bicarbonate buffered low-sodium artificial cerebrospinal fluid (ACSF) solution (appendix 1Aiii). The ACSF was maintained at 0-4°C throughout the dissection. Cold ACSF was used primarily to solidify the brain, making cutting easier but also to minimise metabolic and synaptic activity in the preparation. All solutions used were gassed with a 95%O_2, 5%CO_2 mixture which combined with the bicarbonate buffer in the ACSF maintained pH7.4.

Following decapitation, biochemical studies in the hippocampus have shown that there is a rapid drop in brain levels of ATP (Whittingham, Lust & Passonneau, 1984). The reduced availability of ATP inhibits the function of the sodium pump, leading to neuronal depolarisation which has been shown to be acutely neurotoxic. This is thought to result from the passive influx of chloride ions, which in turn causes the influx of cations, including sodium into the cell.

Sodium influx then causes water to enter the cell, leading to cell swelling and lysis (Olney *et al.*, 1986; Rothman, 1985). In order to reduce the risk of cell death resulting from water entry, bicarbonate buffered low-sodium ACSF was used in preparing the brain stem slices.

Once decapitated, the skin on the back of the head was cut in a rostro-caudal direction and the muscles across the back of the head and neck were severed. The skull was then cut in a caudo-rostral direction, from the spinal cord to the rostral end of the olfactory lobes using fine dissection scissors. Each side of the skull was then folded to either side of the head, exposing the brain. The brain was carefully teased out of the head cavity by cutting the nerves, meninges and blood vessels.

Once removed from the skull, the brain was positioned in bicarbonate buffered low-sodium ACSF with the dorsal surface downwards and a single vertical transverse cut was made just caudal to the pons, detaching the mid brain and cortex from the brain stem. Two pairs of size 5 watch makers forceps, filed to sharp points were used to detach connective tissue and blood vessels from the ventral surface of the brain stem.

2.12 Slicing

A slicing chamber (figure 2.1) was filled to just below the top of the teflon stage with bicarbonate buffered low-sodium ACSF (appendix 1Aiii). The chamber and an ice cube tray filled with bicarbonate buffered low-sodium ACSF were then placed in a -20°C freezer overnight. The frozen ACSF did not contain additional cations as freezing would cause the cations to come out of solution, forming a precipitate and altering the osmolarity of the solution on the surface of the frozen block.

Once the dissection of the rat brain was complete, the slicing chamber was removed from the freezer and the teflon stage dried of condensation. A cyanoacrylate adhesive (Permabond) was dabbed onto the top of the teflon stage and spread thinly using filter paper. The brain stem was blotted using filter paper to remove excess fluid from its surface and was placed on the teflon stage, rostral surface downwards and dorsal surface toward the front of the chamber. The brain stem was left for approximately 30 seconds to allow the glue to dry.

A carbon steel cutting blade (Campden Instruments Ltd.) was dipped in methanol and carefully wiped with a clean tissue to remove any dirt or grease from its surface. The blade was then clamped onto the vibrotome (Campden Instruments Ltd.). The slicing chamber was clamped

Figure 2.1 **Perspex slicing chamber used for the preparation of brain stem slices.**

(A) Three dimensional view and (B) cross sectional view of the slicing chamber. The chamber was filled to just below the top of the teflon stage with bicarbonate buffered low-sodium ACSF (appendix 1Aiii) and frozen overnight (no cations). The dissected brain stem was affixed to the surface of the teflon stage using a cyanoacrylate adhesive. The preparation was oriented with the dorsal surface toward the front of the chamber and the rostral surface affixed to the teflon stage. Once the glue was dry, the chamber was filled with enough bicarbonate buffered low-sodium ACSF so as to just submerge the preparation (plus 2mM $MgCl_2$ & 1mM $CaCl_2$). The whole slicing chamber was then mounted on the vibrotome (Campden Instruments Ltd.) with the ventral surface of the brain stem closest to the cutting blade.

(A)

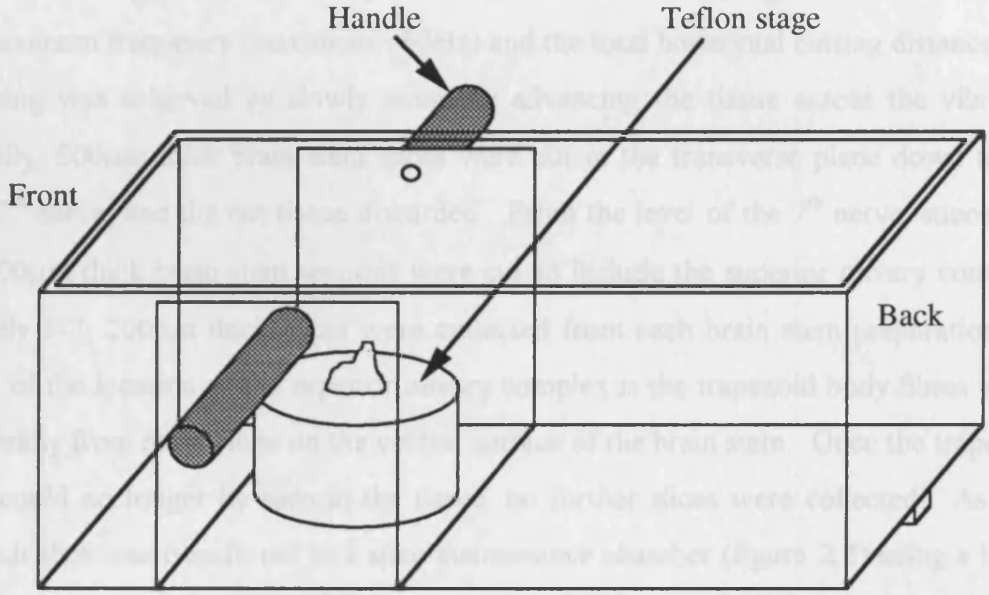
Handle
Teflon stage
Front
Back

(B)

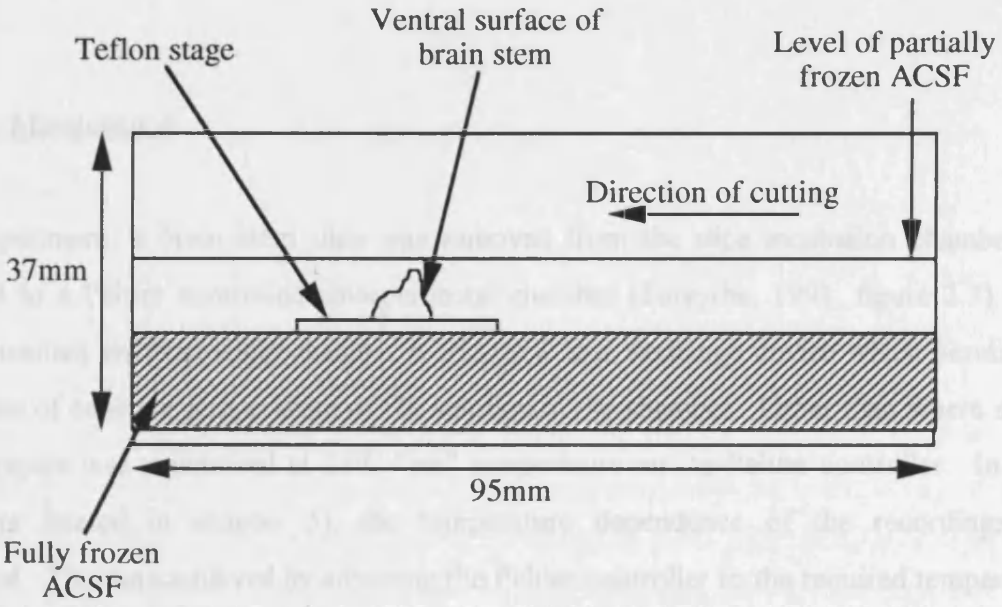
Teflon stage
Ventral surface of brain stem
Level of partially frozen ACSF
Direction of cutting
37mm
95mm
Fully frozen ACSF

to the vibrotome and enough bicarbonate buffered low-sodium ACSF was poured into the chamber to submerge the brain stem. The orientation of the chamber on the vibrotome was such that the back of the chamber was closest to the cutting blade. Consequently, the ventral surface of the brain stem was cut first when sectioning.

Throughout the cutting procedure the speed of vibration of the cutting blade was used just below the maximum frequency (maximum ~50Hz) and the total horizontal cutting distance was ~1mm. Slicing was achieved by slowly manually advancing the tissue across the vibrating blade. Initially, 500μm thick brain stem slices were cut in the transverse plane down to the level of the 7th nerve, and the cut tissue discarded. From the level of the 7th nerve, successive transverse 200μm thick brain stem sections were cut to include the superior olivary complex. Approximately 5-7, 200μm thick slices were collected from each brain stem preparation. A clear marker of the location of the superior olivary complex is the trapezoid body fibres which project bilaterally from the midline on the ventral surface of the brain stem. Once the trapezoid body fibres could no longer be seen in the tissue, no further slices were collected. As they were cut, each slice was transferred to a slice maintenance chamber (figure 2.2) using a blunt, fire polished Pasteur pipette. The slice maintenance chamber contained gassed bicarbonate buffered normal ACSF (appendix 1Aii) heated to 37°C with an osmolarity of ~320mOsM. The slices were incubated in this chamber at 37°C for an hour following sectioning. The chamber was then removed from the water bath and allowed to return to room temperature. The slices were kept in the incubation chamber until required for the experiment and were continually gassed.

2.13 Slice Maintenance

For an experiment, a brain stem slice was removed from the slice incubation chamber and transferred to a Peltier controlled environmental chamber (Forsythe, 1991, figure 2.3). The Peltier controlled environmental chamber works as a heat exchange device which permits the maintenance of constant temperature of the solution in the chamber. Other than where stated, the temperature was maintained at 25°C "set" temperature on the Peltier controller. In some experiments (stated in chapter *5*), the temperature dependence of the recordings was investigated. This was achieved by adjusting the Peltier controller to the required temperature. The "set" temperature on the Peltier controller was not always equal to the actual temperature in the bath and figure 2.4 shows the relationship between the "set" temperature and the actual

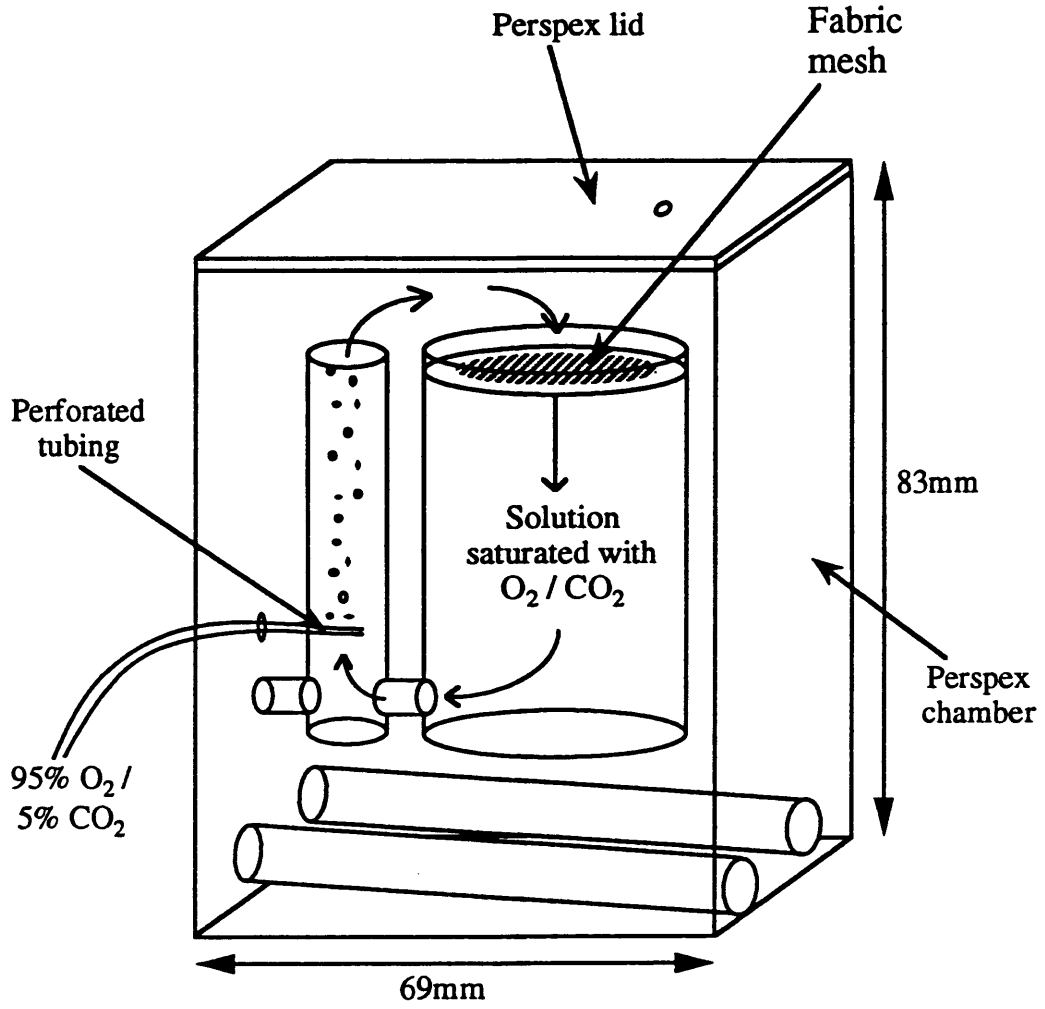

Figure 2.2 **Perspex slice maintanance chamber used for incubation of brain stem slices.**

The slice maintenance chamber was filled with bicarbonate buffered normal ACSF (appendix 1Aii) and heated to 37°C in a water bath. Freshly cut brain stem slices were transferred onto the fabric mesh of the chamber using a blunt fire polished Pasteur pipette. The slices were then incubated for one hour at 37°C. Following incubation the chamber was removed from the water bath and allowed to return to room temperature. The slices were maintained at room temperature until use. The ACSF was continually gassed with a 95% O_2 / 5% CO_2 mixture to ensure physiological pH.

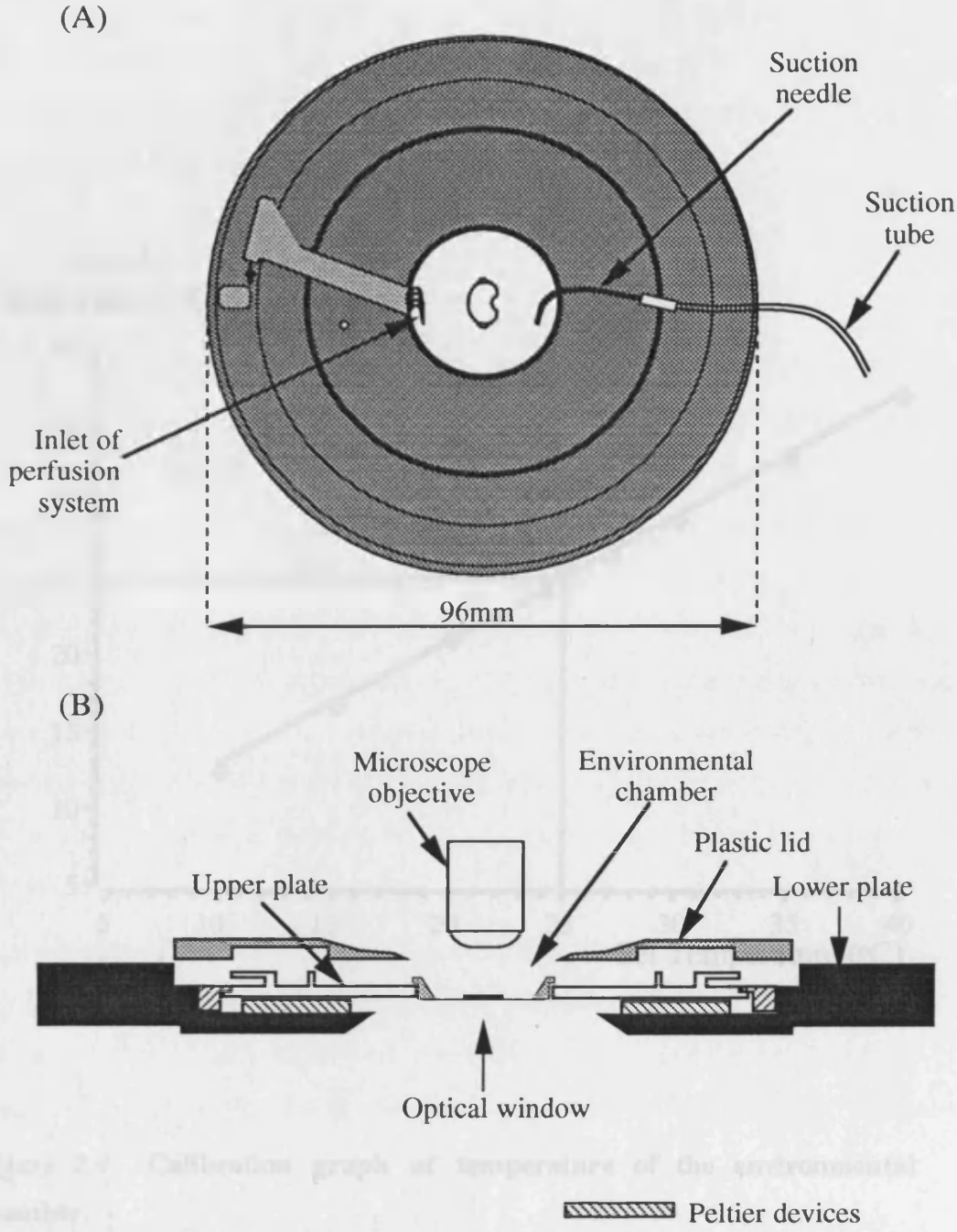

Figure 2.3 **Environmental chamber**

(A) Plan view and (B) cross sectional view of the peltier controlled environmental chamber. The solution's temperature is maintained by being circulated through tubing around the environmental chamber prior to entry into the chamber where the slice is postioned.

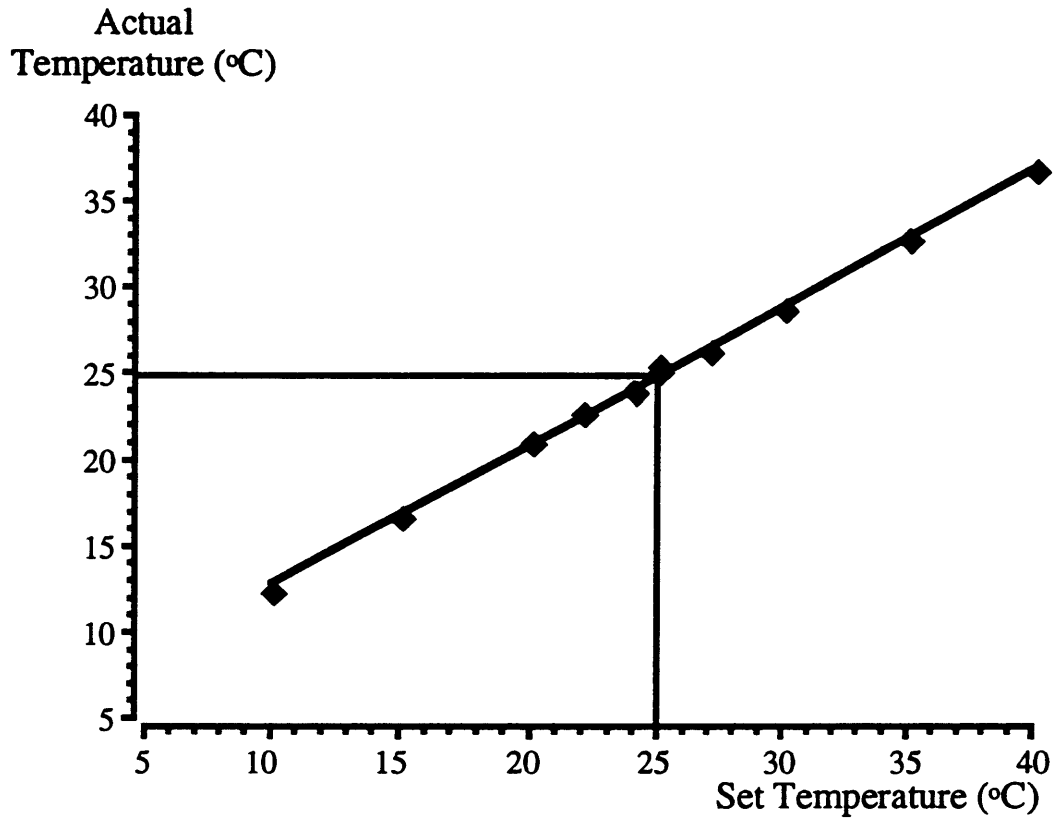

Figure 2.4 **Calibration graph of temperature of the environmental chamber.**

The environmental chamber is maintained at a constant specified temperature during experiments. The "set" temperature on the Peltier controller was not always equal to the actual temperature in the chamber as a result of heat loss or gain from the ambient environment. Most experiments were conducted at a "set" temperature of 25°C which happens to be very similar to the actual temperature of the environmental chamber.

temperature in the environmental chamber. The results given for temperature dependence experiments in chapter *5.31* are given at the actual bath temperatures.

The Peltier controlled environmental chamber was fitted to the stage of an upright M2A microscope (MicroInstruments, Ltd.) on the experimental rig. The slice was secured in position in the environmental chamber using a platinum "harp" (Edwards *et al.*, 1989). Fine nylon threads traversed the harp and secured the slice in position (figure 2.5).

2.14 Perfusion

All electrophysiological experiments were conducted in the environmental chamber which was continuously perfused at a rate of ~0.7ml/min using an eight channel peristaltic pump (Gilson, Minipuls 3). Figure 2.6 shows a flow diagram of the perfusion system used. The volume of the environmental chamber was ~300-400µl. Four perfusion lines had direct entry into the environmental chamber, minimising dead space and permitting rapid exchange between solutions. The flow of oxygenated solutions onto and away from the brain stem slice was essential for the survival of the preparation. In order to maintain a continuous flow, solution was removed from the environmental chamber using a wide gauge needle, blunted and bent to the appropriate shape so as to permit its placement in the bath. In order to maintain a constant fluid level in the environmental chamber the suction needle was designed to suck both air and fluid (figure 2.7C).

It is crucial for electrophysiological experiments that electrical noise is kept to a minimum. To achieve this, components within the Faraday cage were electrically and mechanically isolated. The contents of the Faraday cage were mechanically isolated from any vibration in the surrounding environment by being mounted on an anti-vibration table (Wentworth Laboratories Ltd.).

The perfusion system was a great potential source of electrical noise. If a continuous column of solution was permitted to enter the Faraday cage, it would readily form an aerial. To maintain electrical isolation, a continuous column of solution entering and exiting the Faraday cage was therefore avoided. This was achieved by the use of bubble traps positioned at the entry and exit points of solutions to Faraday cage (figure 2.7A, B). The bubble traps used at the entry point of the solution to the Faraday cage had a 1ml syringe and needle pierced through a bung in the top of a 5ml syringe (figure 2.7A). The 1ml syringe was drawn back to ~0.3ml and the negative pressure generated a reservoir of ~0.5ml in the 5ml syringe of the

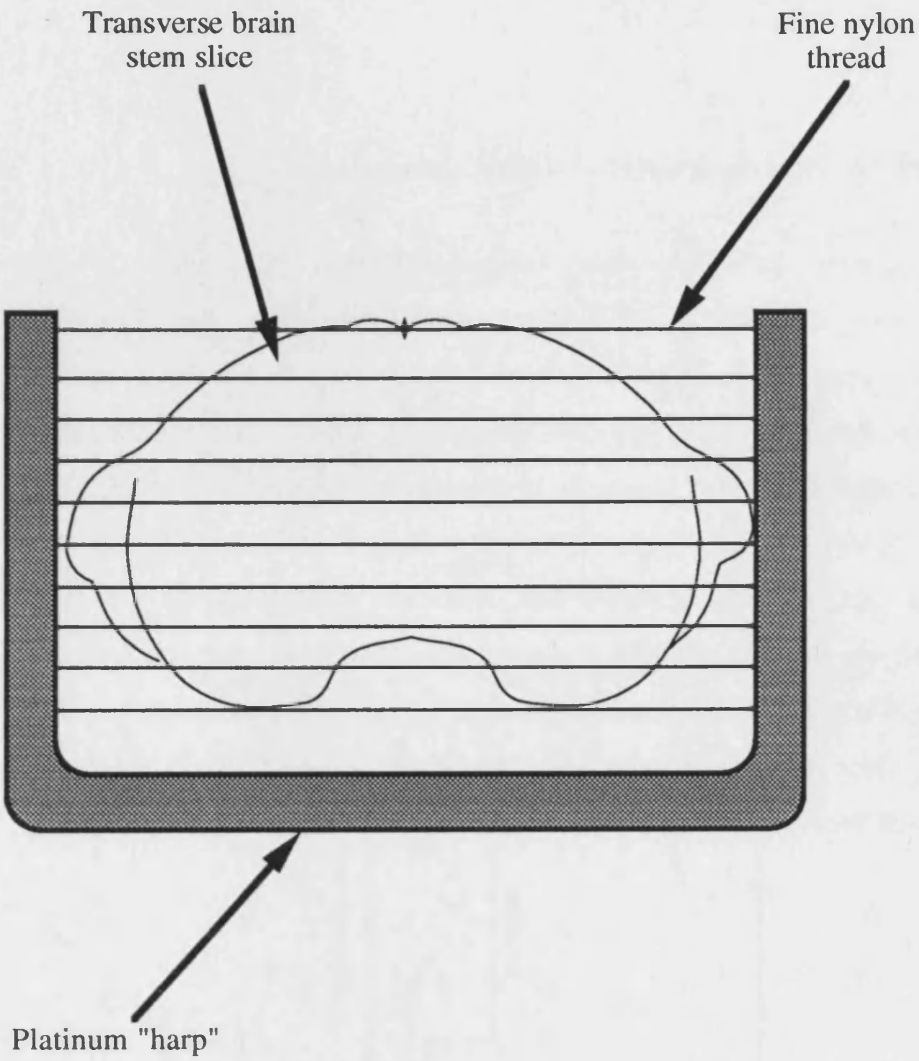

Figure 2.5 **Platinum harp.**

The platinum "harp" was positioned over the brain stem slice in order to keep it in place for electrophysiological experiments. The nylon threads traversing the harp were carefully dissected from nylon tights and attached to the lower surface of the platinum using cyanoacrylate glue. Pieces of broken coverslip glass were then also attached to the bottom of the platinum harp. The harp was positioned so that the fine nylon threads lay medio-laterally across the brain stem. The broken coverslip provided enough height so that the nylon threads did not dig into the slice but secured it in a fixed position.

Figure 2.6 **Flow diagram of perfusion system.**

An 8-channel peristaltic pump (Gilson, Minipuls 3), pumped solution around the perfusion system and up to five different inflow lines were used. The solution entered the Faraday cage where it passed through a bubble trap to electrically isolate the interior of the Faraday cage. The solution then passed through gas-impermeable tubing to the environmental chamber where its temperature was maintained using a Peltier controlled heat exchanger after which the solution entered the bath and perfused over the slice preparation. A suction needle was positioned in the chamber enabling solution to be sucked out and discarded. Just prior to the solution leaving the Faraday cage it passed through another bubble trap, improving electrical isolation of the interior of the Faraday cage. Once out of the Faraday cage the solution passed around the peristaltic pump again and was discarded in a waste bottle.

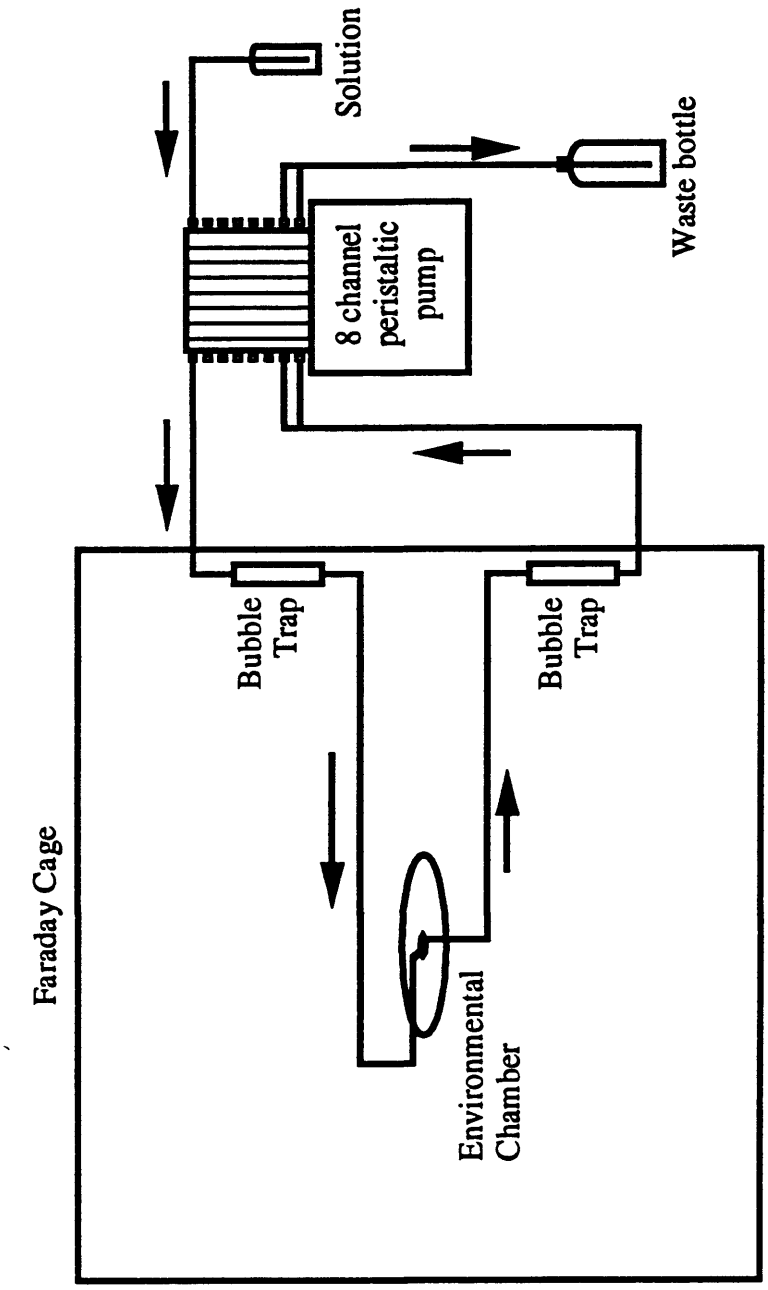
Solution
Waste bottle
8 channel peristaltic pump
Bubble Trap
Bubble Trap
Faraday Cage
Environmental Chamber

Figure 2.7 **Bubble traps and suction needle.**

(A) Entry bubble trap and (B) Exit bubble trap. Solution is circulated around the perfusion system using a peristaltic pump (Gilson, Minipuls 3). Upon entry to or exit from the Faraday cage, solution was allowed to drip into the 5ml syringe of the bubble trap. This prevented a continuous column of solution entering the Faraday cage which would have readily formed an aerial to conduct electrical noise to the electrophysiological recording.

The bubble trap positioned at the entry of the Faraday cage (A), also had a 1ml syringe and needle pierced through the bung placed in the 5ml syringe. When solution was perfused around the system, a small reservoir of solution (~0.5ml) was allowed to build up in the 5ml syringe by creating negative pressure in the syringe by drawing back the plunger on the 1ml syringe to ~0.3ml.

C) Suction needle constructed using a wide gauge needle positioned with the tip in the environmental chamber. This allows the suction of both air and solution, maintaining a constant fluid level in the environmental chamber.

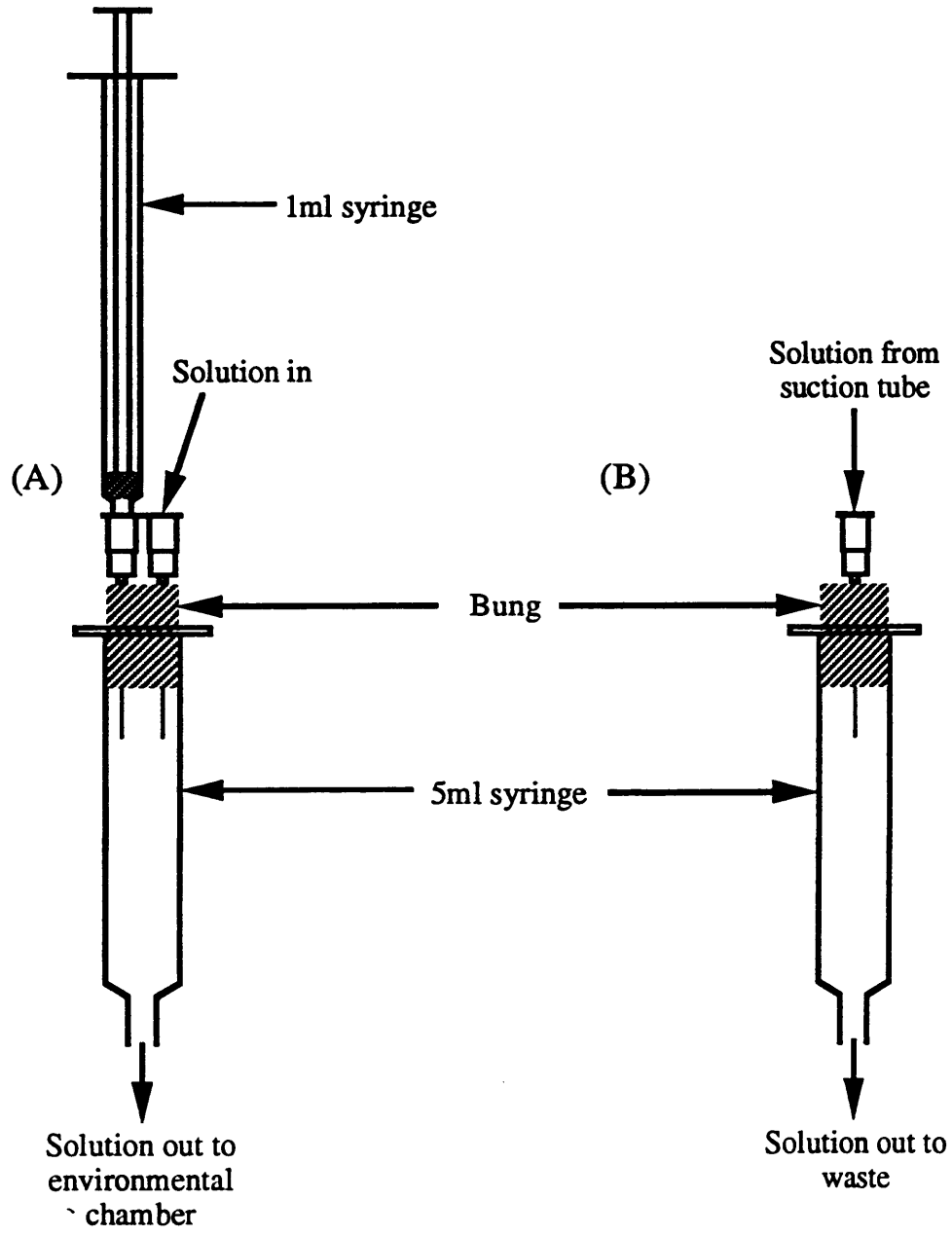
1ml syringe
Solution in
(A)
(B)
Solution from
suction tube
Bung
5ml syringe
Solution out to
environmental
chamber
Solution out to
waste

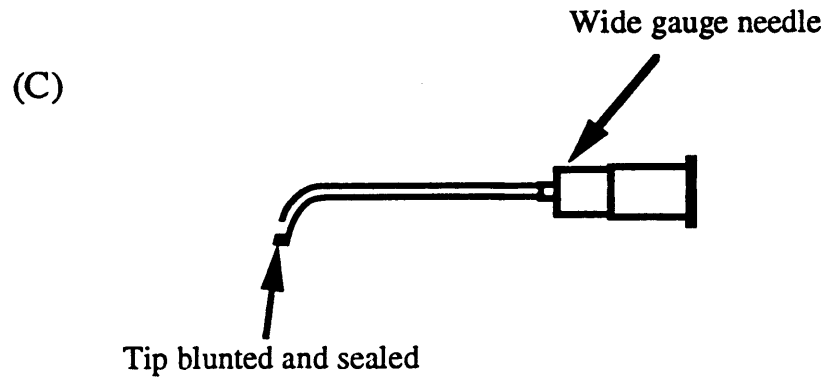
(C)
Wide gauge needle
Tip blunted and sealed

bubble trap. The reservoir prevented air bubbles entering the environmental chamber, an event which would potentially cause the destruction of an electrophysiological recording. The prevention of air bubble formation was not necessary in the suction tube exiting the environmental chamber. Consequently, the bubble trap positioned at the exit of the solution from the Faraday cage was simplified such that it consisted only of a 5ml syringe (figure 2.7B). On the morning of experimentation prior to circulating the perfusion system with appropriate solution, each line, including the bubble trap was gassed with a 95%O_2, 5%CO_2 mixture for approximately 5 minutes. All the tubing used in the experimental rig had a low gas permeability (Anachem Ltd., Cole-Parmer Instrument Company) such that the solutions were maintained in a high O_2 concentration environment even when static in the tubing for sometimes up to several hours.

2.15 Microscopy

An upright M2A microscope (MicroInstruments) was used to visualise the neurones. Low power magnification (x4 objective, Zeiss) was used to locate the area in the slice to be studied. The microscope was fitted with Universal Differential Interference Contrast (DIC), or Nomarski optics and a high magnification (x40 objective, Zeiss 0.75NA, 1.6WD) water immersion objective was used to locate individual neurones. The microscope was also fitted with a Panasonic CCD camera linked to a Panasonic WV-5340 monitor. This allowed both visualisation of the cells during recording and permitted images to be stored on a computer and analysed with NIH Image, version 1.55 Software on a Macintosh computer.

2.151 Fluorescence Microscopy

Following electrophysiological recording, the identity of the neurones was sometimes confirmed using the fluorescent dye, Lucifer Yellow CH dipotassium salt (Aldrich). Approximately 1mg/ml of Lucifer Yellow was included in the intracellular patch solution. One advantage of using Lucifer Yellow as the fluorescent indicator is its small size (MWt=457). This enabled the cell, including its extensive dendritic tree to be rapidly dialysed with the solution. Cells filled with Lucifer Yellow were visualised initially using an ultra-violet light source supplying the microscope.

Once electrophysiological study of a filled neurone was finished, the slice could be preserved for further examination. Preserving the slice entailed its fixation in 5% paraformaldehyde in phosphate buffered saline (PBS) solution overnight. The slice was then transferred to PBS solution, washing off any residual paraformaldehyde. At this stage, the slice was fixed and was ready for examination using confocal microscopy.

The slice was transferred to a glass slide (Blue Star) with a hole ground through its centre (~10mm diameter). The slide had a glass coverslip affixed to it, so that the hole through the middle of the slide formed a well in which the brain stem slice could sit. Following the transfer of a slice to the slide, a few drops of SlowFade, an antifade solution (Molecular Probes) were dropped onto the slice. The slice was then weighted down to a fixed position in the well of the microscope slide using a piece of platinum wire positioned over a piece of broken coverslip on top of the brain stem slice. A glass coverslip was then placed over the top of the weighted down slice and the preparation was then ready for examination using confocal microscopy.

Confocal microscopy was used to construct a projected image of the Lucifer Yellow filled neurones. This was done by first optically sectioning the neurone into 2μm thick transverse sections. A projected image was then reconstructed using these optical sections superimposed on top of one another. An MRC 600 confocal microscope fitted with an argon laser and fluorescence filter sets was used mounted on an inverted microscope. Nomarski optics made it possible to get an impression of the three dimensional nature of the slice by focusing up and down, however, confocal microscopy permitted the permanent visualisation of a full three dimensional image of the neurone. Examples of the structure of MSO neurones are shown in chapter *5*, figure 5.12.

2.2 **Electrophysiological Techniques**

Neher and Sakmann first developed the patch clamp technique in 1976 to study single acetylcholine activated channels in frog muscle fibres. Since then, the technique has become widely used by electrophysiologists to study ionic currents in biological membranes. The patch clamp technique entails the used of glass micropipettes pressed onto the surface of the cell membrane, forming a giga-ohm (≥10GΩ) seal and the recording of ionic currents passing through that cell membrane.

2.21 Configurations of the Patch Clamp Technique

Various forms of the patch clamp technique exist, all of which can be achieved following the formation of a giga-ohm seal onto the surface of the cell membrane:

1) Single channel ionic currents can be recorded from the membrane directly beneath the patch pipette in the cell-attached patch configuration (figure 2.8A). Extracellular solution is used as the bath perfusate and to fill the pipette.

2) A patch of membrane can be pulled from the cell by gently withdrawing the pipette from the cell forming an inside-out patch of membrane (figure 2.8B). In this configuration, the pipette is filled with extracellular solution and the bath perfused with intracellular solution. This technique permits the easy exposure of the intracellular membrane to a variety solutions.

3) From the on-cell configuration, further suction on the back of the pipette will rupture the patch of membrane beneath the pipette, resulting in the whole cell configuration (figure 2.8C). This configuration enables the study of whole-cell macroscopic currents. The pipette is filled with an intracellular solution and the bath perfused with extracellular solution.

4) Once the whole-cell patch clamp configuration is achieved, gently withdrawing the pipette from the cell will pull a patch of membrane from the cell, resulting in the outside-out configuration of patch clamping (figure 2.8D). This enables the study of single ion channels in the cell membrane. For this configuration, the pipette is filled with an internal solution and the bath perfused with an extracellular solution.

In this thesis, the whole cell configuration was used in all electrophysiological recordings.

2.22 Experimental Rig

Figure 2.9 shows a circuit diagram of the experimental rig used for the electrophysiological experiments. Current and voltage were recorded directly onto a digital audio tape (DAT) recorder (48kHz sampling frequency) (Biologic, DTR-1404). The current was then filtered (2kHz, unless otherwise stated) using an eight-pole Bessel filter (Frequency Devices) and the filtered data digitised (usually 5-20kHz) using a CED 1401 interface before being stored on a DELL 450/L personal computer.

The computer was used to control stimulation and voltage command of the List-Medical EPC 7 amplifier. A home-made pulse conditioner containing two operational amplifiers was

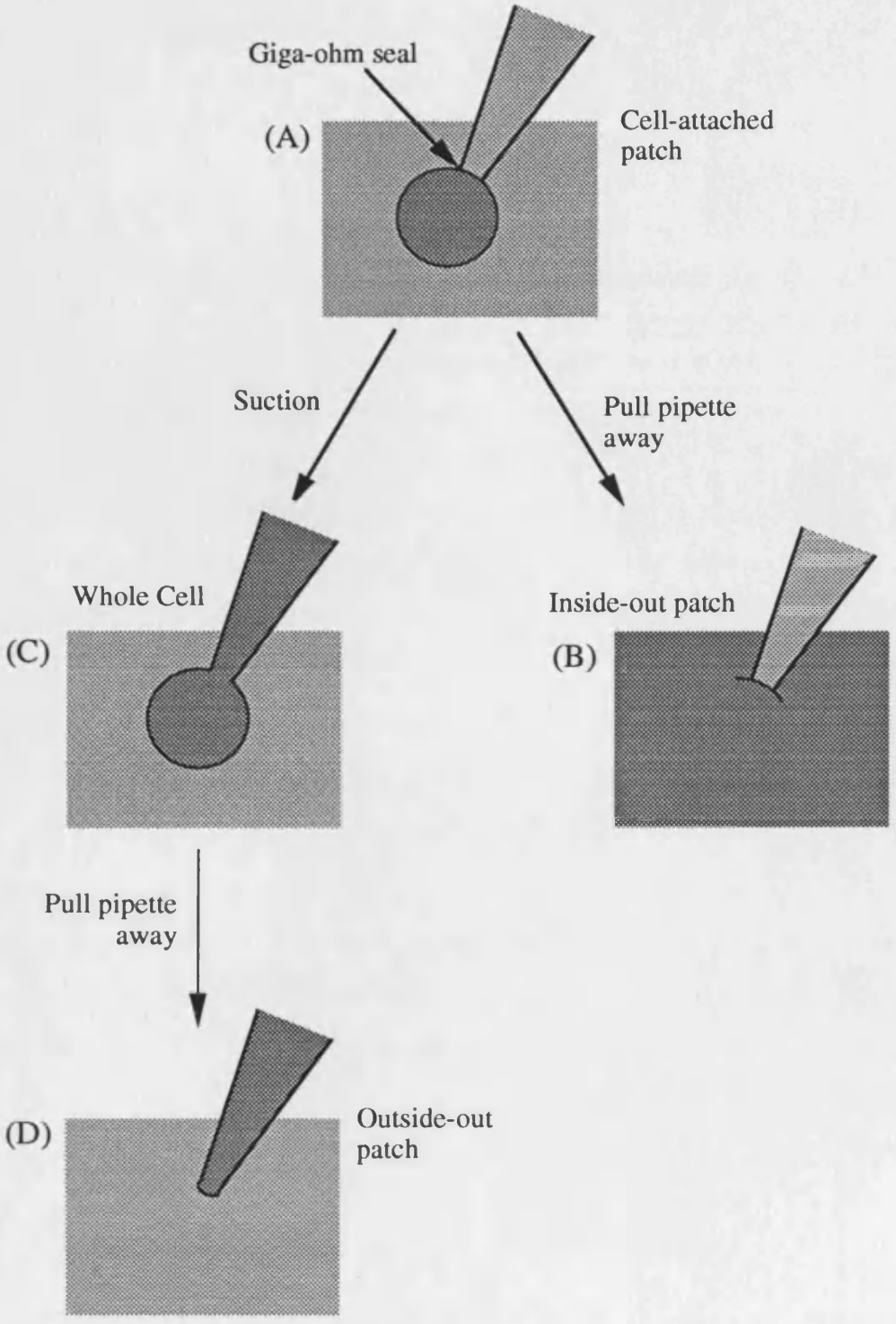

Figure 2.8 **Configurations of the patch clamp technique.**

All configurations of the patch clamp technique require the formation of a giga-ohm seal onto the surface of the cell membrane.

Darker shading indicates intracellular solution and lighter shading indicates extracellular solution.

Figure 2.9 **The experimental rig used for all electrophysiological recordings.**

A patch pipette was attached to the headstage of the EPC 7 patch clamp amplifier (figure 2.11). The current output of the EPC 7 amplifier was passed directly to channel 1 of a Biologic DTR-1404 Digital Tape Recorder (DAT recorder). The current output from the DAT recorder was monitored directly using a Gould storage oscilloscope. The current from the DAT recorder was filtered using an eight-pole Bessel filter and the output from the filter sent to a DELL 450/L personal computer via a CED 1401 analogue to digital interface.

A pulse conditioner was included in the circuit between the CED 1401 and the EPC 7 amplifier to reduce noise in the circuit (figure 2.10). A gain box was also included from the voltage monitor to the analogue to digital converter inputs on the CED 1401.

Digital outputs from the CED 1401 were sent directly to the TTL input of the DAT recorder. Using the TTL output from the DAT recorder, the stimulating electrode was triggered via a trigger delay and the voltage monitored on the oscilloscope. The oscilloscope was triggered directly from the output of the TTL pulse on the DAT recorder.

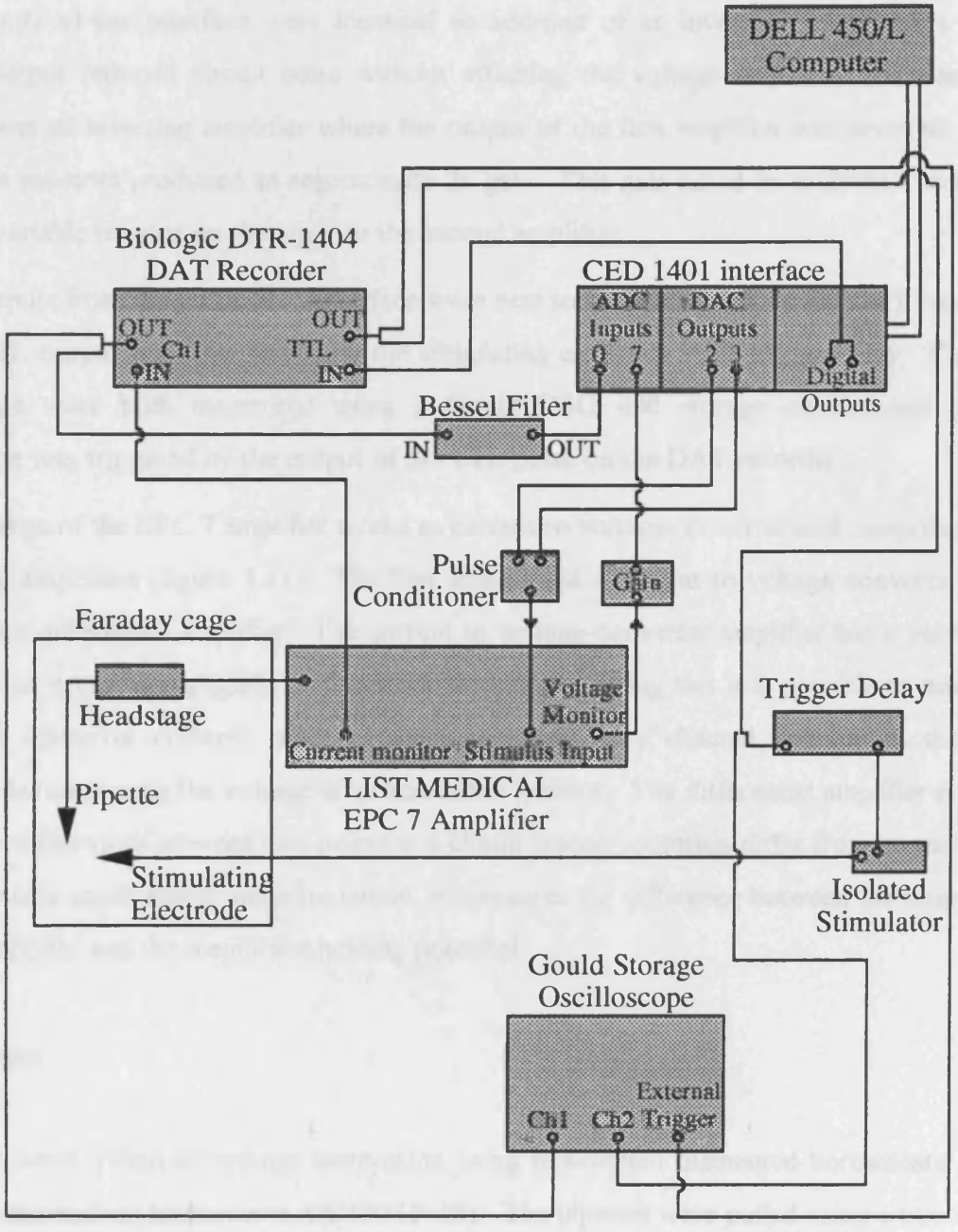
DELL 450/L
Computer
Biologic DTR-1404
DAT Recorder
OUT
Ch1
IN
OUT
TTL
IN
CED 1401 interface
ADC
Inputs
0 7
DAC
Outputs
2 1
Digital
Outputs
Bessel Filter
IN
OUT
Pulse
Conditioner
Gain
Faraday cage
Headstage
Pipette
Stimulating
Electrode
Voltage
Monitor
Current monitor
Stimulus Input
LIST MEDICAL
EPC 7 Amplifier
Trigger Delay
Isolated
Stimulator
Gould Storage
Oscilloscope
External
Ch1
Ch2 Trigger

incorporated into the circuit from the CED 1401 interface to the EPC 7 amplifier (figure 2.10) in order to eliminate noise generated by the CED 1401. The first amplifier was a summing amplifier which inverted the pulse from the CED 1401 interface (DAC output 3) and added it to the holding potential from the CED 1401 (DAC output 2). The noise output from the two DAC outputs of the interface were identical so addition of an inverted output and a non-inverted output reduced circuit noise without affecting the voltage step size. The second amplifier was an inverting amplifier where the output of the first amplifier was inverted. The ratio of the resistors produced an approximate 2x gain. This gain could be calibrated precisely using the variable resistor on the input to the second amplifier.

Digital outputs from the CED 1401 interface were sent to the TTL input on the DAT recorder and the TTL output was used to trigger the stimulating electrode via a trigger delay. Current and voltage were both monitored using a Gould DSO 400 storage oscilloscope. The oscilloscope was triggered by the output of the TTL pulse on the DAT recorder.

The headstage of the EPC 7 amplifier works as current to voltage converter and comprises two operational amplifiers (figure 2.11). The first amplifier is a current to voltage converter, and the second a differential amplifier. The current to voltage converter amplifier has a very high resistance, so it draws negligible current from the circuit. Using this it is possible to measure very small unknown currents, such as those resulting from channel opening in the cell membrane by measuring the voltage drop across the resistor. The differential amplifier is used to measure differences between two points in a circuit whose potentials differ from ground. So in the case of a patch clamp amplifier circuit, it measures the difference between the output of the first amplifier and the membrane holding potential.

2.23 Pipettes

Whole cell patch clamp recordings were made using thin-walled filamented borosilicate glass (Clark Electromedical Instruments, GC150TF-15). The pipettes were pulled using a two stage vertical puller (Narishige).

The bubble number of each pipette was measured in order to maintain a consistent pipette resistance. To do this a 10ml syringe was filled with air and attached to the unpulled end of the pipette by a piece of tubing. The pulled end of the pipette was then dipped in methanol and the plunger of the 10ml syringe depressed. The volume of air remaining in the syringe when

Figure 2.10 **Pulse conditioner circuit.**

The pulse conditioner circuit has two purposes, that of adjusting the gain so that it is appropriate for the EPC 7 amplifier and for reducing the noise of the circuit. It comprises two operational amplifiers, a summing amplifier and an inverting amplifier. The summing amplifier inverts the pulse from the CED 1401 interface (DAC output 3) and adds it to the holding potential from the CED 1401 (DAC output 2). The noise from the two DAC outputs of the interface is identical so addition of an inverted output and a non-inverted output was used to subtract the circuit noise. The output of the first amplifier was then inverted at the next amplifier and the ratio of resistors produced an approximate 2x gain. This gain could be calibrated precisely using the variable resistor on the input of the second amplifier.

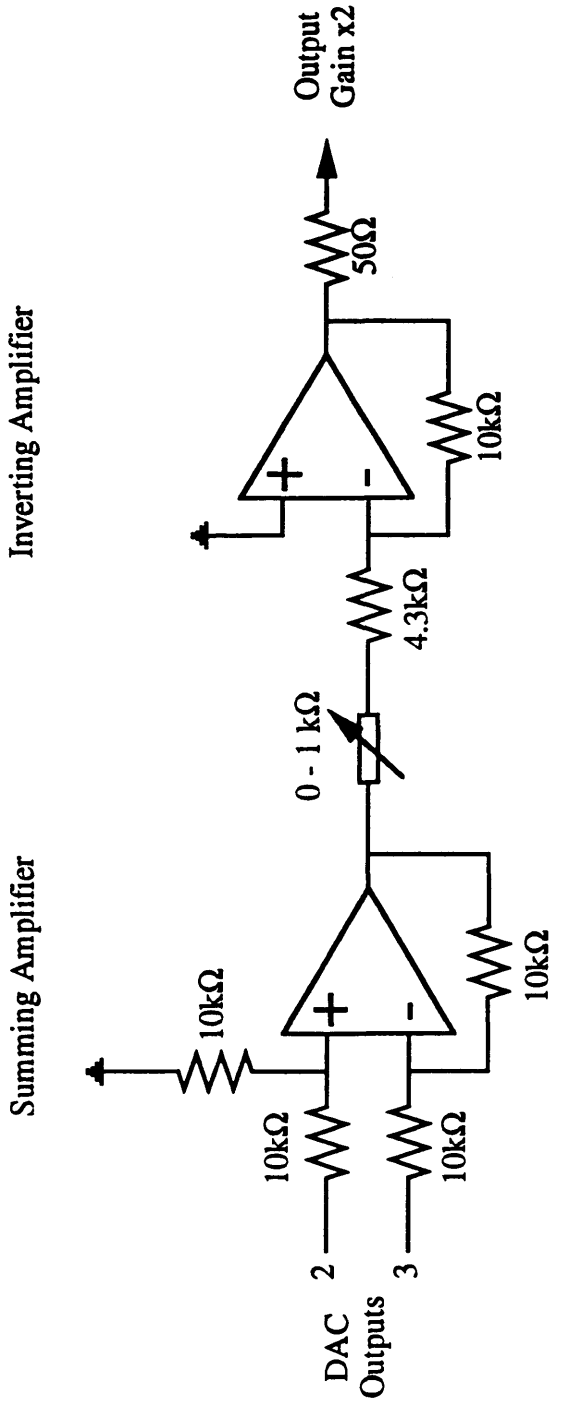
Output
Gain x2
50Ω
Inverting Amplifier
10kΩ
4.3kΩ
0 - 1 kΩ
Summing Amplifier
10kΩ
10kΩ
10kΩ
10kΩ
2
3
DAC
Outputs

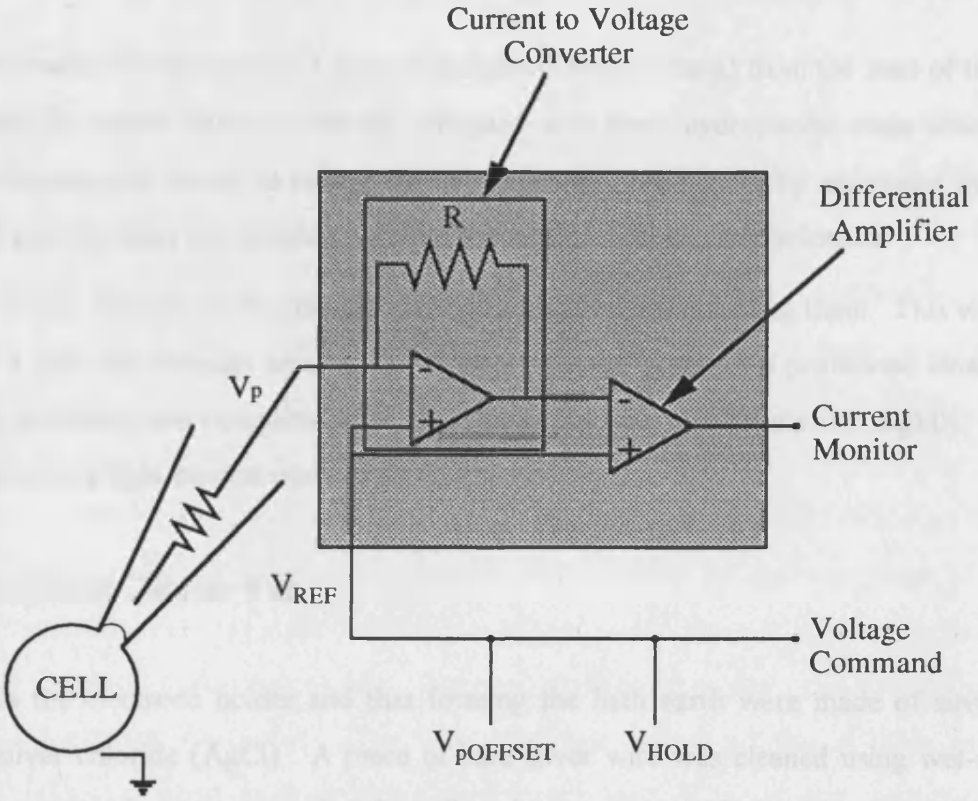

Figure 2.11 **Circuit diagram of an EPC 7 patch clamp amplifier headstage.**

The EPC 7 patch clamp amplifier headstage works essentially as a current to voltage converter and consists of two operational amplifiers. The first operational amplifier is a current to voltage converter and the second a differential amplifier. Using the current to voltage converter amplifier it is possible to measure very small unknown currents flowing through the cell membrane by comparing the voltage of the pipette (V_p) with the voltage set from the voltage command (V_{REF}). The differential amplifier is used to measure the difference between the output of the first amplifier and that from the voltage command (V_{REF}). $V_{pOFFSET}$ and V_{HOLD} are potentiometers. They can be used to alter V_{REF}, eliminating any pipette offset and to set the required holding potential.

small bubbles began to appear in the methanol from the end of the pipette provided the bubble number of that pipette. The bubble numbers of the pipettes used here ranged from 6.3 to 6.7 giving electrodes which when fire polished and filled with patch solution had a resistance of 5-6MΩ.

The pipette shanks were coated in a layer of Sylgard (Dow Corning) from the start of the taper of the pipette to within 250μm of the tip. Sylgard is an inert, hydrophobic resin which cures rapidly on heating and serves to reduce the capacitance of the pipette by increasing the width of the wall and therefore the distance between the internal and external solutions.

Just prior to use, the tips of the pipettes were smoothed by fire polishing them. This was done by heating a piece of platinum wire coated in glass with the pipette tip positioned close to the wire. Fire polishing was complete when the pipette tip was seen to narrow slightly, using a x40 objective on a light microscope.

2.24 Silver / Silver Chloride Wire

The wire in the electrode holder and that forming the bath earth were made of silver (Ag) coated in silver chloride (AgCl). A piece of bare silver wire was cleaned using wet-and-dry paper. The cleaned silver wire was then dipped in molten AgCl, coating it fully. Silver chloride coated silver wires are the most frequently used electrodes in electrophysiology. Cl^- ions react with Ag producing AgCl plus an electron (e^-). However, this is a reversible reaction so an electron can react with the AgCl to produce Ag plus Cl^-. Current is therefore carried by chloride in the following reversible reaction:

$$Cl^- + Ag \Leftrightarrow AgCl + e^-$$

The AgCl electrode is fully reversible so current will freely pass through the electrode in either direction. There is also no potential between AgCl and water so that when no current is passing, no potential is produced.

2.25 Stimulation

In order to evoke inhibitory synaptic currents in MSO neurones, the MNTB was stimulated electrically. This was done using a platinum bipolar stimulating electrode (figure 2.12) positioned over the MNTB.

Approximately 20cm of 75μm diameter teflon coated platinum wire (Advent Research Materials Ltd.) was bent in half and the two threads twisted together to form a helix. The loop at the end of the helix was cut and the resulting fork of platinum briefly passed through a flame, burning off the teflon coating and exposing the bare platinum wire beneath. This fork of bare platinum wire formed the tip of the stimulating electrode. A 1ml syringe was cut off to ~0.5ml and the twisted platinum wire passed through the 1ml syringe, leaving ~6cm of wire, including the exposed platinum fork, protruding from the 'needle' end of the syringe. The platinum wire was secured in position in the syringe using the bung from the plunger of the 1ml syringe. The teflon coated platinum wire protruding from the 1ml syringe was passed through a piece of borosilicate electrode glass and this was affixed to the syringe. The electrode glass, and the first ~2cm of syringe were then wrapped in aluminium foil, and coated in high conductivity silver paint (Acheson). The wire was then shaped so that it fitted into the environmental chamber when clamped to the microscope stage. The platinum wire and silver paint was then coated in a layer of varnish up to ~0.5cm from the tip. The stimulating electrode was then clamped to the directional manipulators and the wires coming from the back of the 1ml syringe were connected to the isolated stimulator DS2A (Digitimer). The tips of the stimulating electrode were separated just enough to allow each wire to pass over the top and bottom of a 200μm slice without digging into the slice.

The stimulating electrode was then clamped to the stage of the microscope and, while viewing under low (x4) power the directional manipulators were used to position the electrode tips either side of the brain stem slice over the MNTB ipsilateral to the MSO to be recorded from. The isolated stimulator provided a pulse of variable amplitude and width. The width was generally maintained at 0.2ms whilst the amplitude was varied between 0 and 10V using the normal or reverse polarity of stimulation. A home made trigger generator was connected to the stimulator providing the ability to generate trains or individual stimuli at various rates.

Figure 2.12 **Bipolar platinum stimulating electrode.**

(A) Complete stimulating electrode. The stimulating electrode was clamped to the microscope stage and the platinum tips of the electrode moved toward the brain stem slice using the directional manipulators. Each fork of the tip of the platinum electrode was then positioned on the upper and lower surface of the 200μm slice, directly over the MNTB. The electrode was triggered by an isolated stimulator DS2A (Digitimer).

(B) Structure of stimulating electrode.

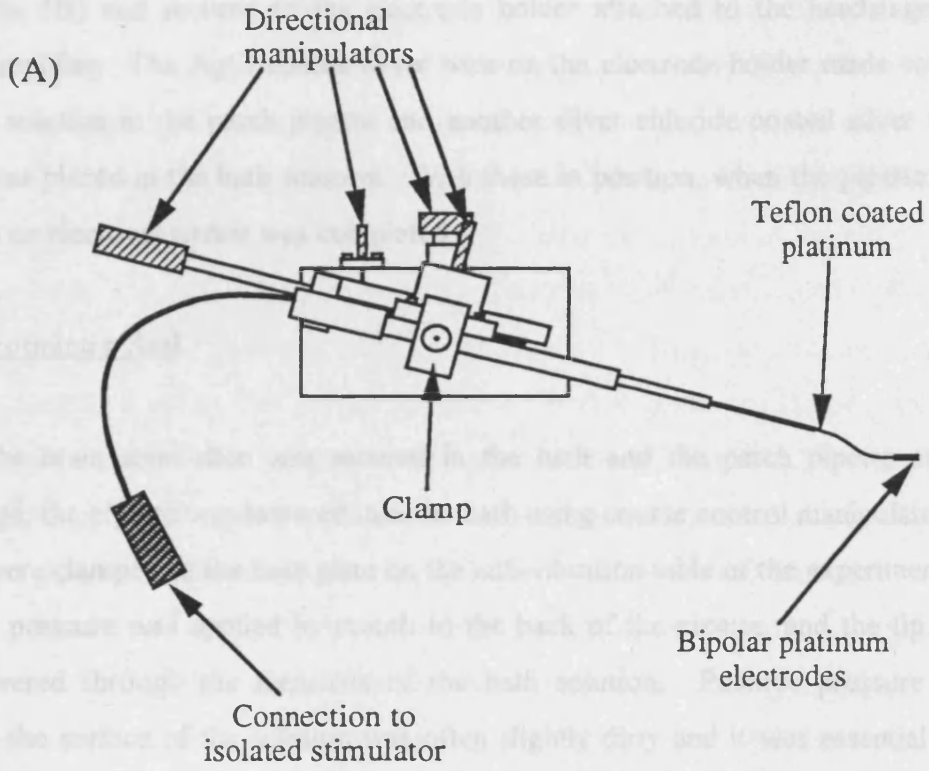
(A)
Directional manipulators
Teflon coated platinum
Clamp
Bipolar platinum electrodes
Connection to isolated stimulator

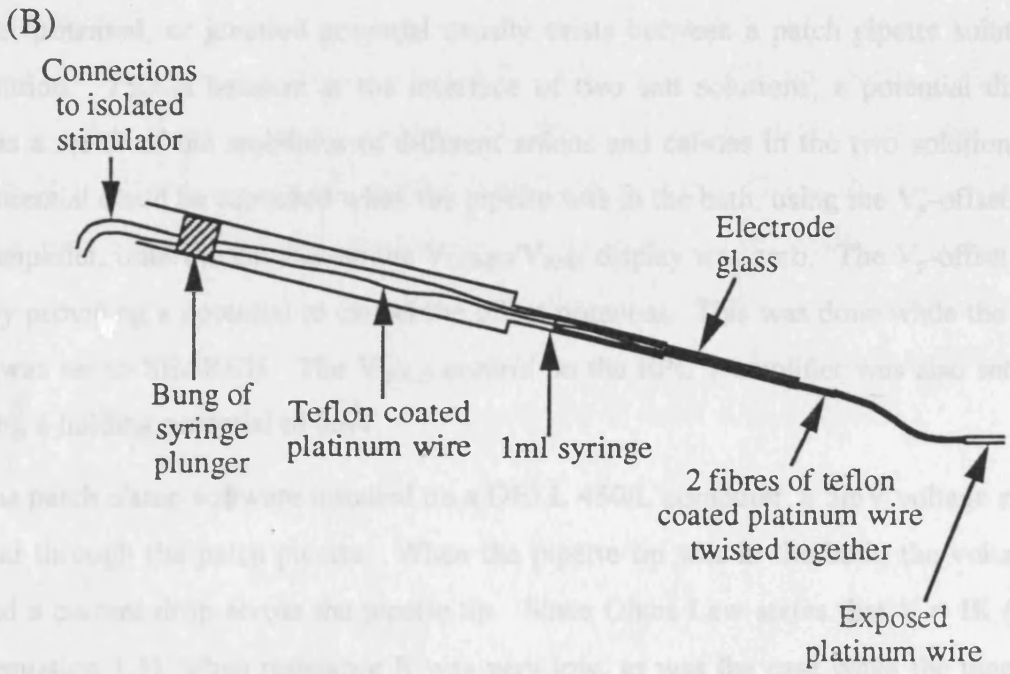
(B)
Connections to isolated stimulator
Electrode glass
Bung of syringe plunger
Teflon coated platinum wire
1ml syringe
2 fibres of teflon coated platinum wire twisted together
Exposed platinum wire

2.26 Whole Cell Patch Clamping

A sylgarded, fire polished patch pipette was filled with the appropriate internal patch solution (appendix 1B) and secured to the electrode holder attached to the headstage of the patch clamp amplifier. The AgCl coated silver wire on the electrode holder made contact with the internal solution in the patch pipette and another silver chloride coated silver wire (the bath earth) was placed in the bath solution. With these in position, when the pipette was placed in the bath an electrical circuit was completed.

2.261 Forming a Seal

When the brain stem slice was secured in the bath and the patch pipette attached to the headstage, the pipette was lowered into the bath using course control manipulators (Narishige) which were clamped to the base plate on the anti-vibration table of the experimental rig. Slight positive pressure was applied by mouth to the back of the pipette, and the tip of the pipette was lowered through the meniscus of the bath solution. Positive pressure was required because the surface of the solution was often slightly dirty and it was essential for good seal formation that the tip of the pipette was kept clear of any debris.

An offset potential, or junction potential usually exists between a patch pipette solution and bath solution. This is because at the interface of two salt solutions, a potential difference occurs as a result of the mobilities of different anions and cations in the two solutions. This offset potential could be cancelled when the pipette was in the bath, using the V_p-offset control on the amplifier, until the number on the V_{COMM}/V_{RMS} display was zero. The V_p-offset control works by providing a potential to cancel the offset potential. This was done while the MODE control was set to SEARCH. The V_{HOLD} control on the EPC 7 amplifier was also set to 5.0, producing a holding potential of 0mV.

Using the patch clamp software installed on a DELL 450/L computer, a 5mV voltage step was generated through the patch pipette. When the pipette tip was in the bath, the voltage step produced a current drop across the pipette tip. Since Ohms Law states that V = IR (chapter *1.312*, equation 1.1), when resistance R was very low, as was the case when the pipette was free in the bath, then to produce the 5mV voltage step V, current I was high.

Using the course control manipulators and the x40 water immersion objective on the microscope, the pipette was lowered toward the brain stem slice. When the tip of the

electrode was ~100μm from the surface of the slice 1-2ml of positive pressure was applied to the back of the patch pipette using a 10ml syringe. The positive pressure was maintained using a three way tap fitted to the end of the 10ml syringe. The pipette was then manoeuvred toward an identified MSO neurone using an hydraulic manipulator (Narishige). The positive pressure applied to the pipette separated the connective tissue surrounding the neurones and allowed clear access for the electrode to the neurone (Edwards *et al.*, 1989). Without application of the positive pressure the pipette would become coated in debris, reducing the likelihood of seal formation onto the neurone. Once the surface of the neurone was cleaned and the pipette was within a few microns of the cell membrane a small indentation, or bleb could be seen to form on the surface of the neurone. This bleb formed as a result of the positive pressure pushing fluid out of the pipette onto the surface of the neurone. At this time, the positive pressure was released from the pipette. As this was done, the bleb on the surface of the cell reduced in size as the membrane closed back onto the pipette tip. Gentle suction at this point assisted seal formation. As the seal was formed, the current step produced in response to the 5mV voltage step reduced as a result of the increasing resistance across the pipette. To verify that a giga-ohm seal had been formed the gain on the amplifier was increased to 20mV/pA. At this gain, a flat current trace (except for the transient capacitance currents) confirmed seal formation. Usually seal formation was rapid, after which the holding potential was set to an appropriate voltage (usually -70mV) using the V_{HOLD} control on the EPC 7 amplifier. This was done when the MODE control was set to VC. The holding potential was displayed on the V_{COMM}/V_{RMS} window. If seal formation was slow however, V_{HOLD} could be adjusted to -70mV while the seal was forming. This is thought to assist seal formation. Once a giga-ohm seal was formed between the tip of the patch pipette and the cell membrane, with the Slow Range control set on the 'Off' position, the transient capacitance currents seen on the current trace could be cancelled using the C-FAST and τ-FAST controls. These transient capacitance currents were formed as a result of capacitance of the pipette, described in the introduction.

2.262 Whole Cell

Once a giga-ohm seal had been formed on the cell membrane, slight mouth suction on the back of the pipette ruptured the patch of membrane underneath the pipette tip permitting electrical continuity between the inside of the cell and the patch pipette and resulting in the attainment of the whole cell patch clamp configuration (figure 2.8C). Upon entry into the neurone further

transient capacitance currents appeared on the current trace of the oscilloscope. Assuming complete compensation of the transient capacitance currents in the cell-attached configuration, these transient capacitance currents were entirely due to the capacitance of the cell. This capacitance was compensated for using the C-SLOW and G-SERIES controls with the Slow Range control set to 10pF for small cells or 100pF for larger cells. For cells which are largely somatic, the transient current will decay over a single exponential time course and would be relatively easy to cancel using the C-SLOW and G-SERIES controls. However, cells that are very dendritic, such as MSO neurones would have transient cell capacitance currents which do not decay with a single exponential (see chapter *3.32*, figure 3.1) and so cancellation of the transient current would not be complete. The final values of C-SLOW and G-SERIES provided estimates of the cell membrane capacitance and series conductance of the cell, the reciprocal of the latter being series resistance. Sometimes, if the series resistance was high then it was possible to suck a little more on the pipette to improve the access into the cell. Once the C-SLOW and G-SERIES controls were set, the series resistance was compensated for using the %-COMP control on the EPC 7 amplifier. Series resistance was always maintained below 25MΩ and series resistance compensation between 60 and 90% was routinely used with the RS COMP switch on the FAST mode.

Throughout the electrophysiological recording the series resistance was monitored and the G-SERIES and %-COMP controls adjusted accordingly. If the series resistance deteriorated then attempts were made to improve access by suction application to the pipette.

Prior to seal formation the V_p-offset control was used to cancel the junction potential resulting from the different ionic concentrations in the internal patch solution and the extracellular bath solution (explained above). However, once in the whole cell configuration no junction potential existed because the patch solution would have dialysed into the cell leaving no interface between the patch pipette and the intracellular solution. The corrected offset potential was therefore incorrect in the whole cell configuration.

The size of the junction potential measured by using the V_p-offset control was dependent on the ionic concentrations of the intracellular and extracellular solutions, so if either one was altered then the junction potential changed. For example, in experiments where the reversal potential of the synaptic current was measured, a change in intracellular chloride concentration was required (chapter *4.324*). This change affected the relative ionic compositions between the internal and external solutions and so for each solution, the junction potential was measured. This was done by filling a patch pipette with the internal solution used in an

experiment and attaching it to the headstage of the patch clamp amplifier. The patch pipette was then lowered into a dish containing the extracellular solution used in the experiment, and in a similar manner to when preparing for seal formation, the V_p-offset control was adjusted until the V_{COMM}/V_{RMS} display read zero. Once this was done, the patch pipette was transferred from contact with the extracellular solution into a dish containing the same intracellular solution as was in the patch pipette. The number that was then displayed on the V_{COMM}/V_{RMS} display was the junction potential which was corrected for in each situation. Appendix 1C documents the junction potentials obtained throughout this study but were only corrected for when measuring the reversal potential of the evoked inhibitory synaptic current in chapter *4.324*.

2.27 Amplifier

The amplifier used in most of the electrophysiological experiments was a List-Medical EPC 7. However for some earlier acquired data, an Axopatch 200A amplifier was used.

2.28 Sample and Filter Rates

All data were filtered using an 8-pole Bessel filter. The data were sampled and filtered appropriately so that the sample rate was always at least twice the filter frequency (most often 5kHz and 2kHz, respectively). The relative sample and filter rates is of importance otherwise a phenomenon known as aliasing may occur. Miniature current data in chapter *5* were filtered and digitised at 5kHz and 40kHz, respectively in order to make accurate estimations of the time course of the currents.

2.29 Data Acquisition and Analysis

All data were collected using a DELL 450/L computer and a Digital Tape Recorder (DTR-1404).

Except for miniature current data, all data were acquired and analysed using 'Current and Voltage Clamp' from 'Patch', version 6 (Cambridge Electronic Design).

Miniature current data in chapter *5* were acquired and analysed using a software suite written by Dr. D. Maconochie, called 'Viewmenu'.

Miniature current data in chapter *6* were acquired and analysed using 'Strathclyde Electrophysiology Software, Whole Cell Program', version 1.2. Graphs and figures were all drawn using Kaleidegraph 3.0 and Macdraw Pro on a Macintosh computer.

Chapter 3 - Results

3 **Results**

3.1 **Introduction**

In this project characteristics of the medial superior olivary (MSO) nucleus and some of the synaptic projections it receives have been investigated. In this chapter the whole cell patch clamp technique was used to study some intrinsic features of MSO neurones:

1) The resting properties of MSO neurones,

and 2) Voltage-activated channels present in MSO neuronal membranes.

Finally, a brief study of the potassium channel $K_v3.1$ transfected into murine erythroleukaemia (MEL) cells was conducted. This chapter reveals the presence of voltage-activated sodium channels and voltage-activated potassium channels, one of which may be $K_v3.1$ in MSO neuronal membranes.

3.2 **Methods**

The whole cell patch clamp technique was used throughout. Brain stem slices were prepared as described in chapter *2* and MEL cells were transfected and maintained using the method described by Shelton *et al.* (1993).

Normal bicarbonate buffered artificial cerebrospinal fluid (ACSF) containing 133.5mM chloride (appendix 1Aii) was used in all investigations of the MSO. Measurement of the capacitance of MSO neurones was made using a CsCl-based intracellular patch solution, containing 132mM chloride (appendix 1Biii). For examination of voltage-activated channels in MSO, a KCl-based intracellular patch solution containing 132mM chloride was used (appendix 1Bii). Investigations of the $K_v3.1$ ion channel transfected into MEL cells used a HEPES buffered extracellular solution (appendix 1Ai) and a potassium gluconate based intracellular patch solution (appendix 1Bi). 2mM $CaCl_2$ was added to all extracellular solutions except when investigating voltage-activated currents in MSO neurones when 0.2mM $CaCl_2$ was added in order to minimise calcium currents and calcium-activated potassium currents.

3.3 **Results**

3.31 Zero Current Potential

Prior to the use of any physiological or pharmacological tools, the zero current potential of the MSO neurone was found to be -58.3±1.1mV (SEM, n=10). This value is thought to approximate the resting membrane potential of the neurone and is similar to that of between -58 and -67mV observed in MSO principal neurones by Smith (1995). The MODE control on the EPC 7 patch clamp amplifier was set to VC and upon entry into the neurone V_{HOLD} was adjusted until the pipette current display on the amplifier was zero. The corresponding zero current potential was displayed on the V_{COMM}/V_{RMS} window of the patch clamp amplifier.

3.32 Capacitance

Estimations of the capacitance of the MSO neurone were made immediately after attaining the whole cell configuration by examining the transient capacitance currents resulting from a step in holding potential. As previously described in chapter *2*, transient capacitance currents resulting from pipette capacitance were cancelled in the cell-attached configuration. Upon entry into the neurone, a voltage step applied to the membrane produced further transient capacitance currents at the time of the beginning and end of the voltage step on the current trace (figure 3.1). This results from the transient charging of the membrane capacitance upon a change in holding potential as described in chapter *1.312*. By obtaining an estimation of cell capacitance an estimation can also be made of membrane area, since in most biological membranes, capacitance is ~1μF/cm^2.

The neurone was voltage clamped at -70mV and repeated -5mV steps were applied to the membrane and the corresponding current recorded. Measurement of the area under the transient capacitance current (figure 3.1) gave an estimation of the capacitance of the MSO neurone to be 50.1±9.5pF (SEM, n=13), using a CsCl-based intracellular patch solution. This is higher than that measured using a KCl-based intracellular patch solution (Brew, unpublished observations) but the discrepancy can be explained by the CsCl-based solution resulting in a higher membrane resistance. A higher membrane resistance allows voltage clamp of a larger region of membrane, thereby increasing the measured membrane capacitance. It should be

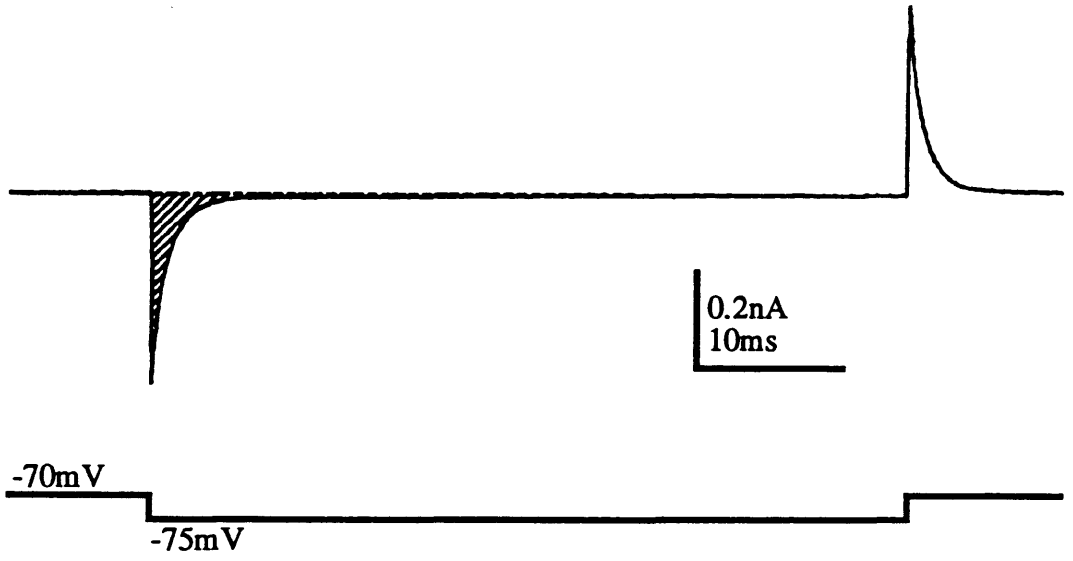

Figure 3.1 **An estimation of the capacitance of the membrane is made using transient capacitance measurements.**

A -5mV step from a holding potential of -70mV, for 50ms resulted in transient capacitance currents at the beginning and end of the voltage step.
Hatched area under the capacitance transient revealed an estimated capacitance of MSO neurones of 50.1±9.5pF (SEM, n=13)

noted that the decay time course of the transient capacitance current is fitted by a double exponential equation with mean time constants of 0.49±0.06ms and 1.55±0.10ms (SEM, n=13). This suggests the membrane capacitance to comprise two compartments, namely the somatic and dendritic compartments.

3.33 Voltage-Activated Currents in MSO Neurones

The MSO neurone was voltage clamped at -70mV and incremental +5mV steps were applied from -100mV to +20mV for 300ms (figure 3.2). Following a voltage step, the holding potential was returned to -70mV. The voltage steps were repeated at a frequency of 1Hz.

The amplitude of the slowly-inactivating outward current resulting from stepping the membrane potential was measured 10ms from the end of a 300ms voltage step (figure 3.2A•) and a leak-subtracted current-voltage relationship was constructed (figure 3.2B). Example raw data traces and voltage step protocols are shown in figure 3.2A. The current activated at around -57mV (n=12) from a holding potential of -70mV.

The amplitude of the outward current when the neurone was stepped to +20mV was 4.2±0.5nA (SEM, n=10) when measured 10ms from the end of a 300ms voltage step (figure 3.2B). Further depolarising steps would have produced greater current amplitudes, but these currents were increasingly difficult to voltage clamp.

A rapidly inactivating inward current was also observed at the beginning of the voltage step (figure 3.2A∗) which activated at around -46mV (n=14). However, the magnitude and speed of this current made it very difficult to voltage clamp.

3.331 Inactivation and Block of the Fast Inward Current

Figure 3.3 shows example raw data traces of voltage activated currents from a holding potential of -40mV. It was not possible to leak subtract this data since at -40mV some voltage-activated potassium channels are already open. Figure 3.3 demonstrates that at this holding potential the fast inward current, thought to be a voltage-activated sodium current is much reduced in amplitude (n=5). This is presumably because at -40mV, sodium channels are largely inactivated (Hodgkin & Huxley, 1952) although here a small amount of inward current is still present (figure 3.3∗).

Figure 3.2 **Current-voltage relationship of MSO neurones from -70mV holding potential revealed a rapidly inactivating inward current and a slowly-inactivating outward current.**

Neurones were clamped at -70mV and voltage steps applied for 300ms from -100mV to +20mV in +5mV incremental steps, returning to the holding potential of -70mV.

A) Example raw data traces and voltage step protocol. Early rapidly inactivating inward current (*) preceded a slowly-inactivating outward current (•).

B) Leak-subtracted current-voltage relationship corresponding to (A) of the slowly-inactivating outward current measured 10ms from the end of the 300ms voltage step (•).

The outward current activated at around -57mV (n=12).

The inward current activated at around -46mV (n=14).

The mean outward current amplitude at +20mV holding potential when measured 10ms from the end of a 300ms voltage step was 4.2±0.5nA (SEM, n=10).

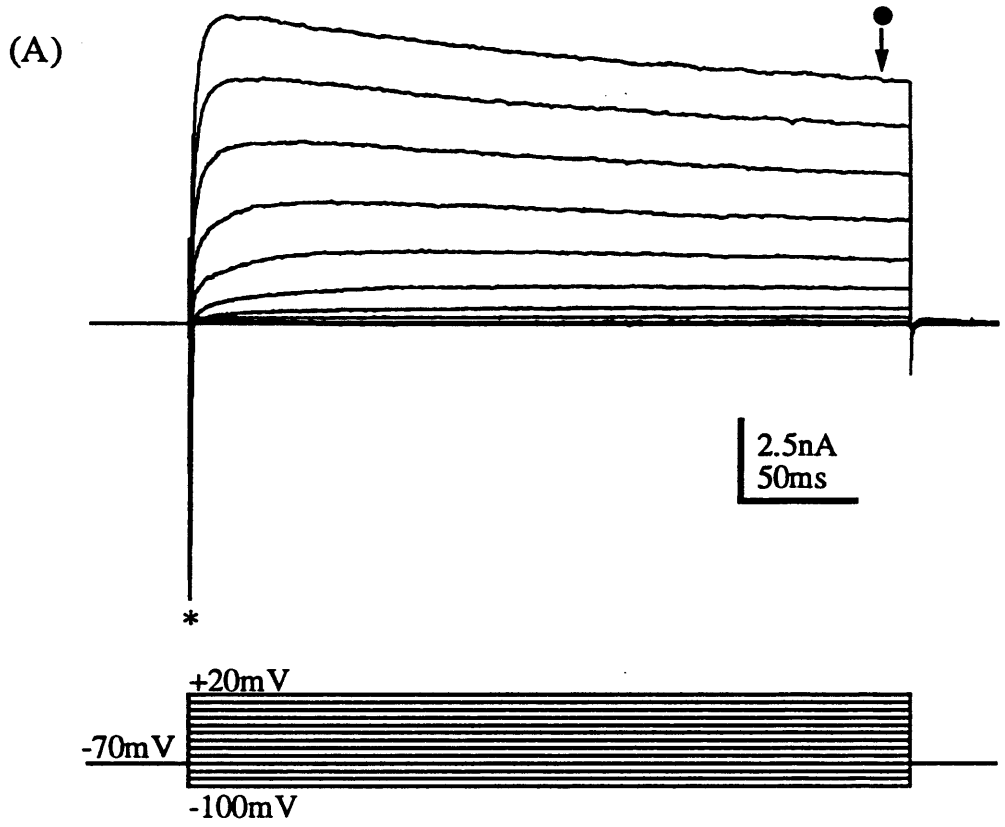
(A)
2.5nA
50ms
*
+20mV
-70mV
-100mV

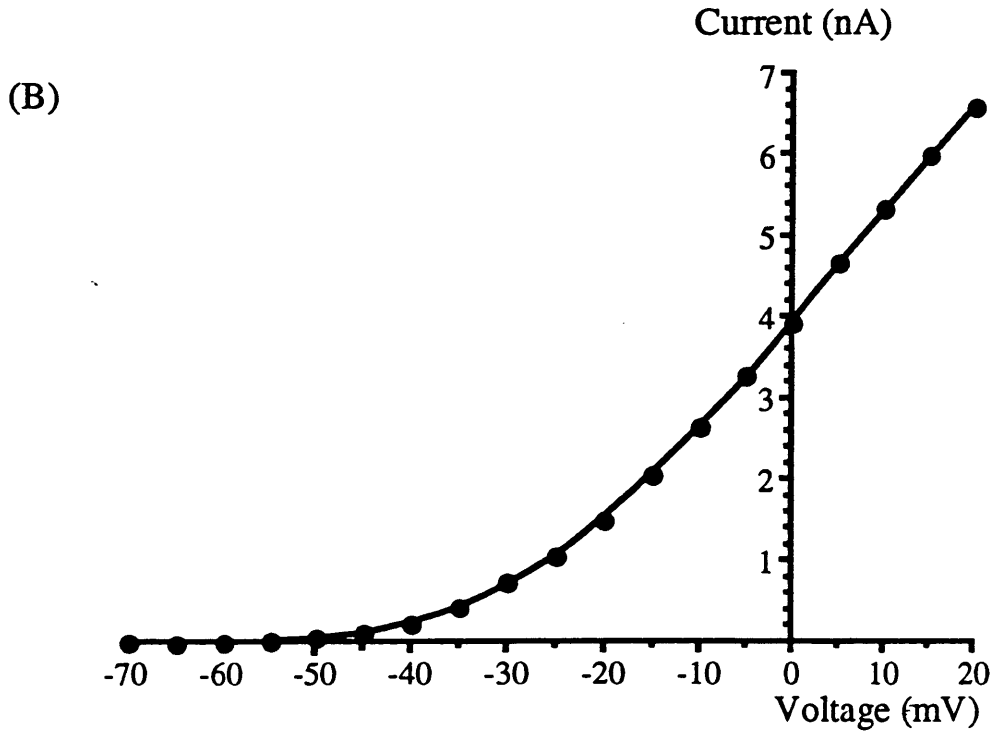
(B)
Current (nA)
7
6
5
4
3
2
1
-70
-60
-50
-40
-30
-20
-10
0
10
20
Voltage (mV)

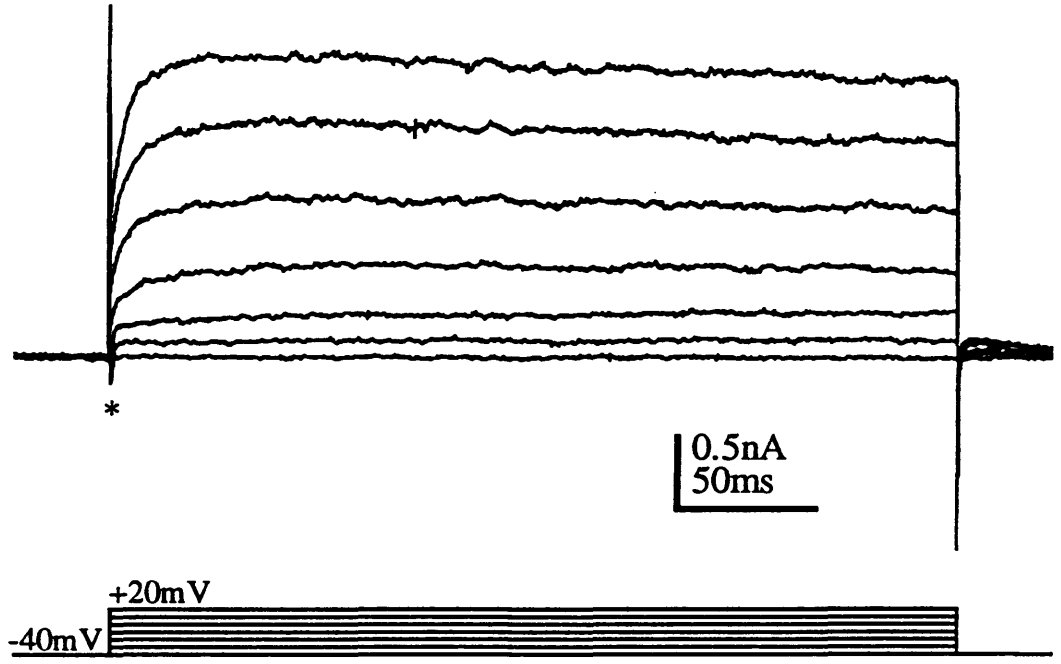

Figure 3.3 **Current - voltage relationship of MSO neurone from holding potential of -40mV.**

Neurones were clamped at -40mV and voltage steps applied for 300ms from -40mV to +20mV in 5mV incremental steps, returning to the holding potential of -40mV.

Voltage step protocol and corresponding example current traces show outward, non-inactivating current and virtual absence of rapidly inactivating inward current (n=5). A small amount of inward current however, still remains (*).

Raw data traces are non-leak subtracted.

Confirmation that the fast inward current was indeed a voltage-activated sodium current was established by examining the effect of tetrodotoxin (TTX), a voltage-activated sodium channel blocker (Narahashi, Moore & Scott, 1964) perfused onto the slice. Figure 3.4 demonstrates the reduction in amplitude of the sodium current upon application of 0.5μM TTX (n=5). Figure 3.4A shows average data traces overlaid and figure 3.4B shows each peak inward current amplitude for one neurone (indicated by •). The neurone was voltage clamped at -70mV and repeated voltage steps to -20mV were applied. The transient outward current indicated by * in figure 3.4A is a transient capacitance current, present since the data were not leak subtracted. Following application of 0.5μM TTX the sodium current appears to be outward (figure 3.4Ac). However this apparent outward current is unlikely to be real but instead results from the superimposition of the current trace with the capacitance transient (*).

Following application of 0.5μM TTX, voltage step protocols from holding potentials of -70mV (n=5), -40mV (n=2) and -100mV (n=2) showed a complete absence of sodium current (figure 3.5B). The small inward current remaining prior to TTX application when at a holding potential of -40mV (indicated by * in figure 3.3) was successfully eliminated by application of 0.5μM TTX at this same holding potential (figure 3.5Biii).

3.332 Slowly-Inactivating Outward Current

Following application of 0.5μM TTX, activation of the outward current was examined from holding potentials of -70mV, -40mV and -100mV (figure 3.5). Application of 0.5μM TTX had little apparent effect on the activation or amplitude of the outward current measured 10ms from the end of a 300ms voltage step. When the cell was voltage clamped at -70mV in the presence of 0.5μM TTX, activation of the current was around -56mV (n=5; figure 3.5A, Bii) and the amplitude using a voltage step to +20mV was 3.7nA±0.8nA (SEM, n=5). These data suggest that activation of the outward current is independent of voltage-activated sodium current activation. This would be anticipated since the sodium current time course is far shorter than the 300ms voltage step. When the neurones were voltage clamped at -100mV, the activation of outward current again seemed largely unaffected because even for only n=2, the mean activation was around -53mV (figure 3.5A, Bi).

Results of the activation protocols suggest the outward current to be that of a voltage-dependent potassium current.

Figure 3.4 **Progressive block of inward sodium current with application of 0.5μM TTX.**

MSO neurones were voltage-clamped at -70mV and repeated steps to -20mV applied. Inward sodium current is completely and rapidly blocked by 0.5μM TTX (n=5).

(A) Example overlaid average current traces of (a) no block; (b) partial block; and (c) complete block of the fast inward sodium current using bath applied 0.5μM TTX. Traces are averages of 10 events each and are non-leak subtracted. * indicates transient capacitance currents.

(B) Corresponding peak inward sodium current plotted over time. 0.5μM TTX applied at t=0.

(A)

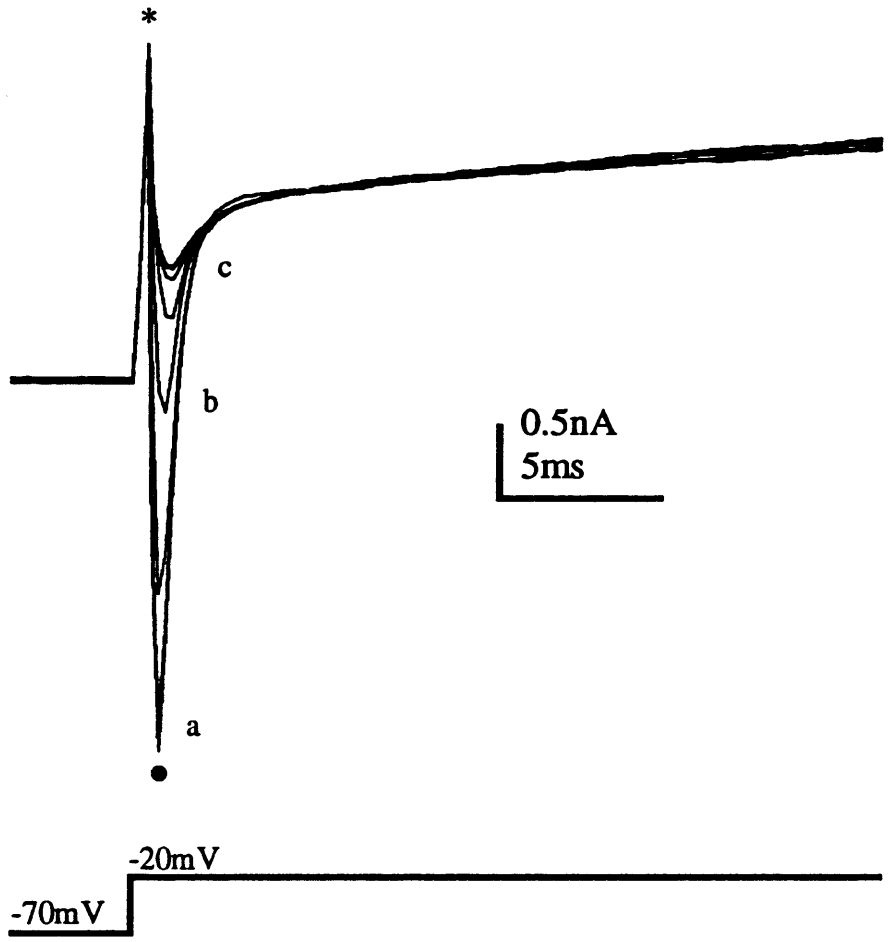
*
c
b
a
0.5nA
5ms
-20mV
-70mV

(B)

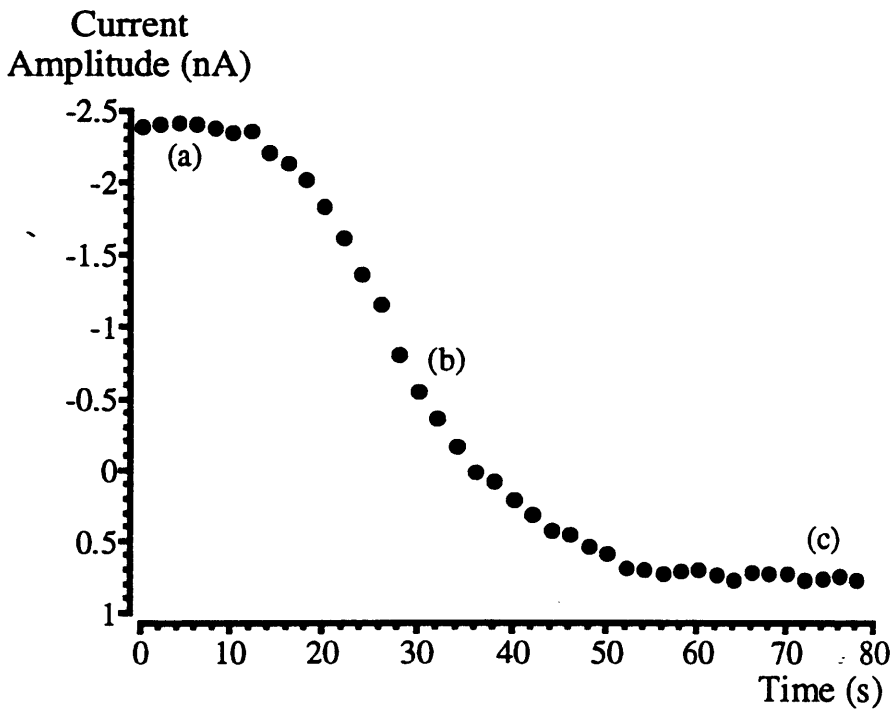
Current
Amplitude (nA)
-2.5
-2
-1.5
-1
-0.5
0
0.5
1
(a)
(b)
(c)
0
10
20
30
40
50
60
70
80
Time (s)

Figure 3.5 **Current-voltage relationship of MSO neurones from different holding potentials in the presence of 0.5μM TTX.**

(A) Non-leak subtracted current-voltage relationship of an MSO neurone from -40mV, -70mV and -100mV holding potentials.

(B) Corresponding non-leak subtracted raw data traces and voltage protocol from holding potentials of (i) -100mV; (ii) -70mV and (iii) -40mV.

Inward sodium current was eliminated in all cases by application of 0.5μM TTX. Activation and amplitude of the outward potassium current was unaffected by application of 0.5μM TTX at -70mV holding potential: Activation around -56mV (n=5). Amplitude at +20mV, 10ms from the end of a 300ms voltage step=3.7±0.8nA (SEM, n=5).

Activation of outward current from -100mV holding potential at around -53mV (n=2).

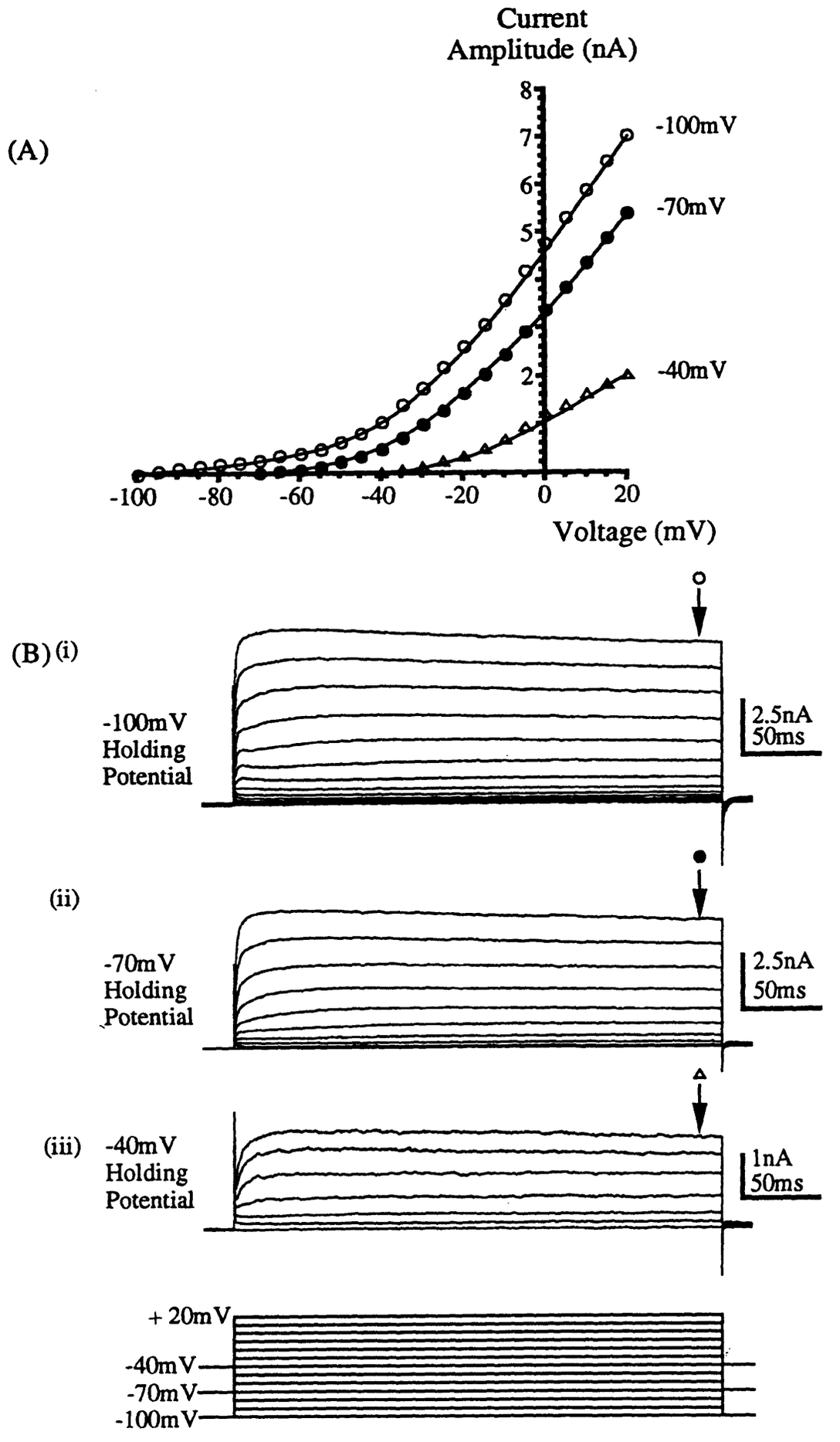
(A)
Current
Amplitude (nA)
8
7
6
5
2
-100mV
-70mV
-40mV
-100
-80
-60
-40
-20
0
20
Voltage (mV)
(B) (i)
-100mV
Holding
Potential
2.5nA
50ms
(ii)
-70mV
Holding
Potential
2.5nA
50ms
(iii)
-40mV
Holding
Potential
1nA
50ms
+ 20mV
-40mV
-70mV
-100mV

Pharmacology of Outward Current

A study of the pharmacology of the slowly-inactivating outward current was conducted by bath application of a potassium channel blocker, 1mM tetraethylammonium (TEA). The neurones were voltage clamped and voltage step protocols were conducted, as described above. In control conditions, whilst voltage clamping at -70mV, a normal current-voltage relationship was produced (figure 3.6Ai, B). 0.5μM TTX and 1mM TEA were bath applied, causing a dramatic reduction of 81.8±7.0% (SEM, n=7) of the current amplitude, measured 10ms from the end of a 300ms voltage-step (figure 3.6Aii, B). Partial wash out of the TTX and TEA was observed on one occasion (figure 3.6Aiii, B) but the recording was lost prior to washout on the remaining six occasions.

The voltage-activated sodium current present at the beginning of the voltage step is very rapid so should not affect the amplitude of the outward potassium current being measured after 10ms from the end of a 300ms voltage step (see figures 3.2 & 3.4). However, in order to ensure the potassium current was not contaminated with sodium current, 0.5μM TTX was applied prior to TEA application on three occasions. 1mM TEA was then washed on in the presence of TTX to observe the effect of TEA on the potassium current alone. The amount of block by TEA, independent of voltage-activated sodium current was 83.4±3.3% (SEM, n=3; data not shown).

The sensitivity to TEA confirmed the slowly-inactivating outward current to be that of a voltage-activated potassium current. A useful tool in identifying potassium channels is their different sensitivities to concentrations of TEA (Grissmer *et al.*, 1992). The *Shaker*- and *Shaw*-related potassium channels $K_v1.1$ and $K_v3.1$ are both highly sensitive to TEA (Grissmer *et al.*, 1992) and are thought to be present in nuclei of the superior olivary complex ($K_v1.1$: Wang *et al.*, 1994; $K_v3.1$: Perney *et al.*, 1992; Weiser *et al.*, 1994; Perney & Kaczmarek, 1997; Wang *et al.*, 1998). The potassium currents measured from MSO neurones here were both slowly-inactivating and highly sensitive to TEA, suggesting that the potassium channels $K_v1.1$ or $K_v3.1$ may be expressed in the MSO neuronal membrane. However, accurate characterisation of the potassium channels present in the MSO neuronal membrane was not conducted here so a more detailed examination of the biophysical and pharmacological characteristics of the channel would be necessary for this to be achieved.

Figure 3.6 **1mM TEA reversibly blocks slowly-inactivating outward currents in MSO neurones.**

Neurones were clamped at -70mV and voltage steps were applied for 300ms from -100mV to +20mV in +5mV incremental steps, returning to the holding potential of -70mV. Data were leak subtracted.

A) Voltage step protocol and corresponding example current traces in (i) control solution (ii) 0.5μM TTX + 1mM TEA and (iii) partial washout after 20 minutes in control solution.

B) Current-voltage relationship corresponding to (A). Measurements made 10ms from the end of a 300ms voltage step. Open circles represent current amplitude in control solution; closed circles represent current amplitude in 0.5μM TTX + 1mM TEA and triangles represent current amplitude after wash out in control solution for 20 minutes.

Mean block of slowly-inactivating outward current from control solution to 0.5μM TTX + 1mM TEA is 81.8±7.0% (SEM, n=7). Partial washout of TTX and TEA was seen on one occasion.

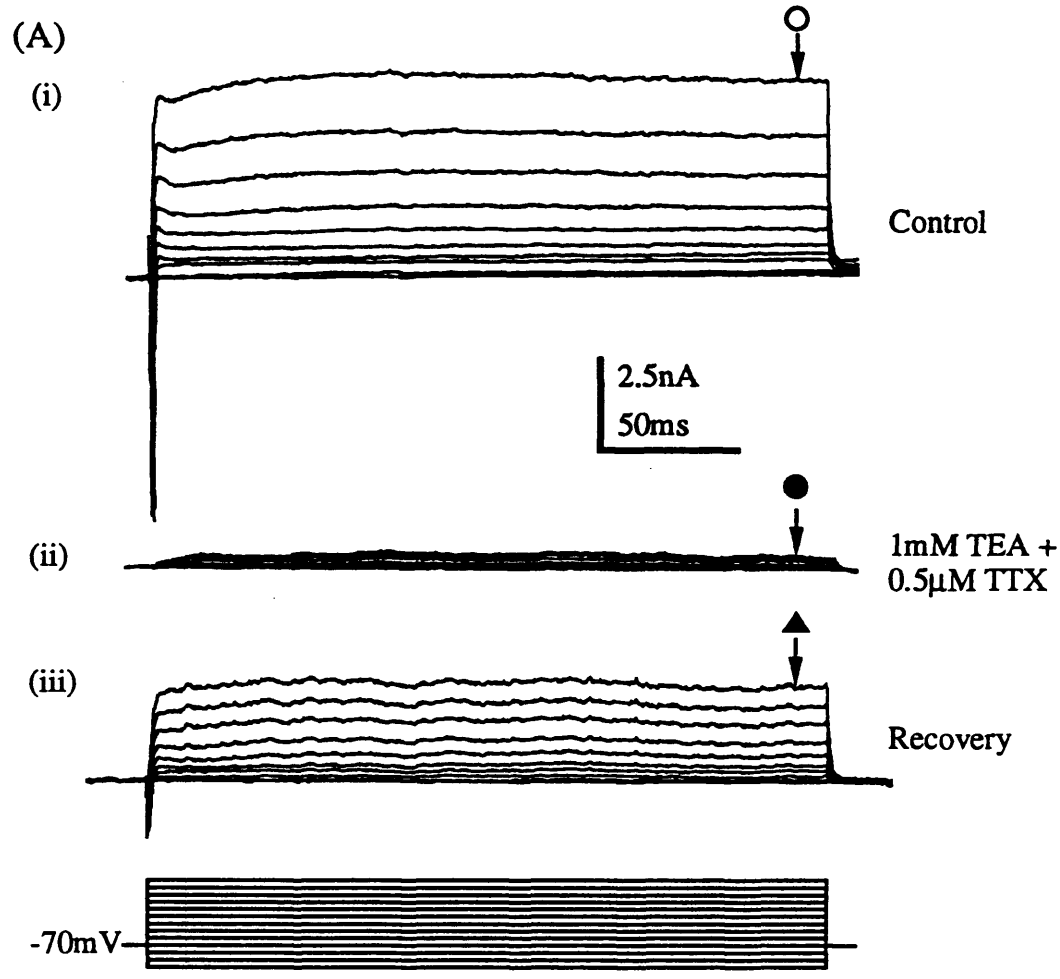
(A)
(i)
Control
2.5nA
50ms
(ii)
1mM TEA +
0.5µM TTX
(iii)
Recovery
-70mV

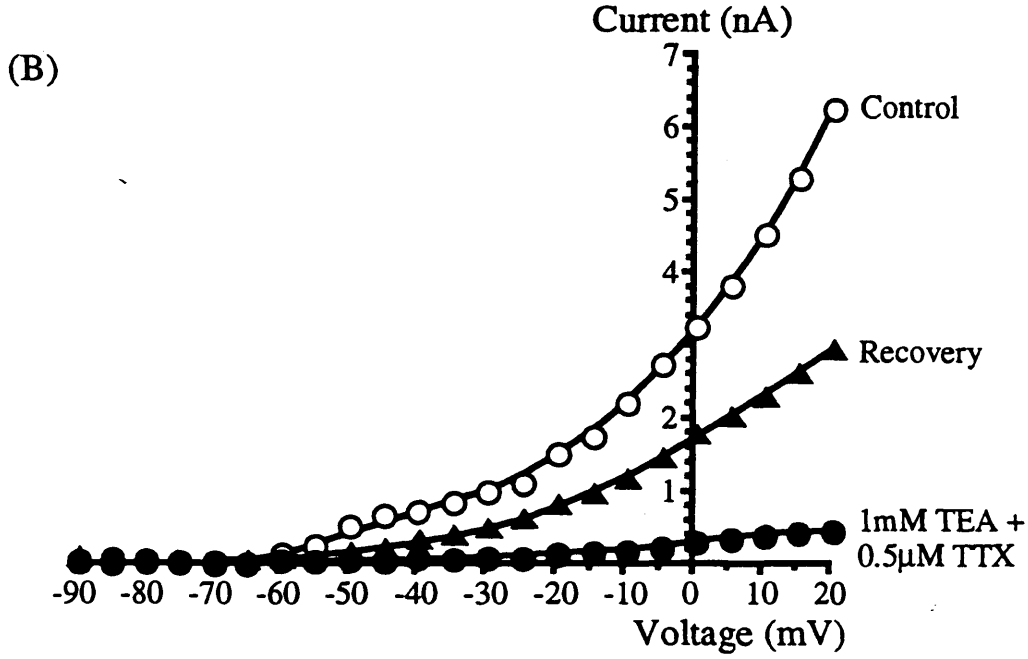
(B)
Current (nA)
7
6
5
4
2
1
Control
Recovery
1mM TEA +
0.5µM TTX
-90 -80 -70 -60 -50 -40 -30 -20 -10 0 10 20
Voltage (mV)

3.333 $K_v3.1$ Expressed in MEL Cells

A brief study was conducted of $K_v3.1$ channels transfected into MEL cells and the activation and sensitivity to TEA of these channels measured. The cells were voltage clamped at -70mV and incremental +10mV steps up to +70mV were applied to the membrane. The $K_v3.1$ channels activated at around -9mV (n=6, figure 3.7Ai, B). This activation potential is far more positive than found for the native channel in the MSO (~-57mV, see section *3.33*). However, this finding is not surprising since there are many observations of different properties of channels in different expression systems (reviewed by Robertson, 1997) for example voltage sensitivity, threshold, kinetics and blocker sensitivity.

The potassium channel $K_v3.1$ is highly sensitive to TEA (Grissmer *et al.*, 1992) and when transfected into MEL cells were found to be reversibly blocked by 3mM TEA (86.7%, n=2, figure 3.7). On one other occasion, 5mM TEA blocked the $K_v3.1$ channel by 90.8% and partial wash out was seen.

3.4 **Summary and Discussion**

Major findings of this chapter:

- The MSO neuronal membrane conducts a TTX sensitive Na^+ current.
- The MSO neuronal membrane conducts a slowly-inactivating outward K^+ current.
- The slowly-inactivating outward K^+ current is sensitive to TEA.
- A $K_v3.1$ channel expressed in MEL cells has similar characteristics to the TEA sensitive K^+ channel in the MSO neuronal membrane.

In order to fulfil the role of detection of interaural timing differences (ITDs) which has been ascribed to the MSO (reviewed by Irvine, 1986; Yin & Chan, 1988), the preservation of timing information is necessary. The MNTB securely preserves timing information in the following way. Firstly, MNTB neurones will only fire a single action potential in response to a depolarising step and secondly, the action potential is rapidly repolarised which ensures that the membrane is ready to fire another action potential very shortly after the first (Forsythe &

Figure 3.7 **Activation of $K_v3.1$ transfected into MEL cells reveals a slowly-inactivating outward current which is reversibly blocked by TEA.**

Cells were clamped at -70mV and voltage steps were applied for 350ms from -70mV to +70mV in +10mV incremental steps, returning to the holding potential of -70mV.

A) Voltage step protocol and corresponding example non-leak subtracted current traces in (i) control solution; (ii) 3mM TEA; and (iii) partial washout in control solution.

B) Non-leak subtracted current-voltage relationships corresponding to (A). Measurements made 10ms from the end of the voltage step (indicated by symbols). Open circles represent current amplitude in control solution; closed circles represent current amplitude in 3mM TEA and triangles represent current amplitude after partial wash out in control solution.

Voltage step protocol produces a slowly-inactivating outward current which activates at around -9mV (n=6).

Mean block of slowly-inactivating outward current with 3mM TEA was 86.7% (n=2) and with 5mM TEA was 90.8% (n=1). Partial washout was observed on all three occasions.

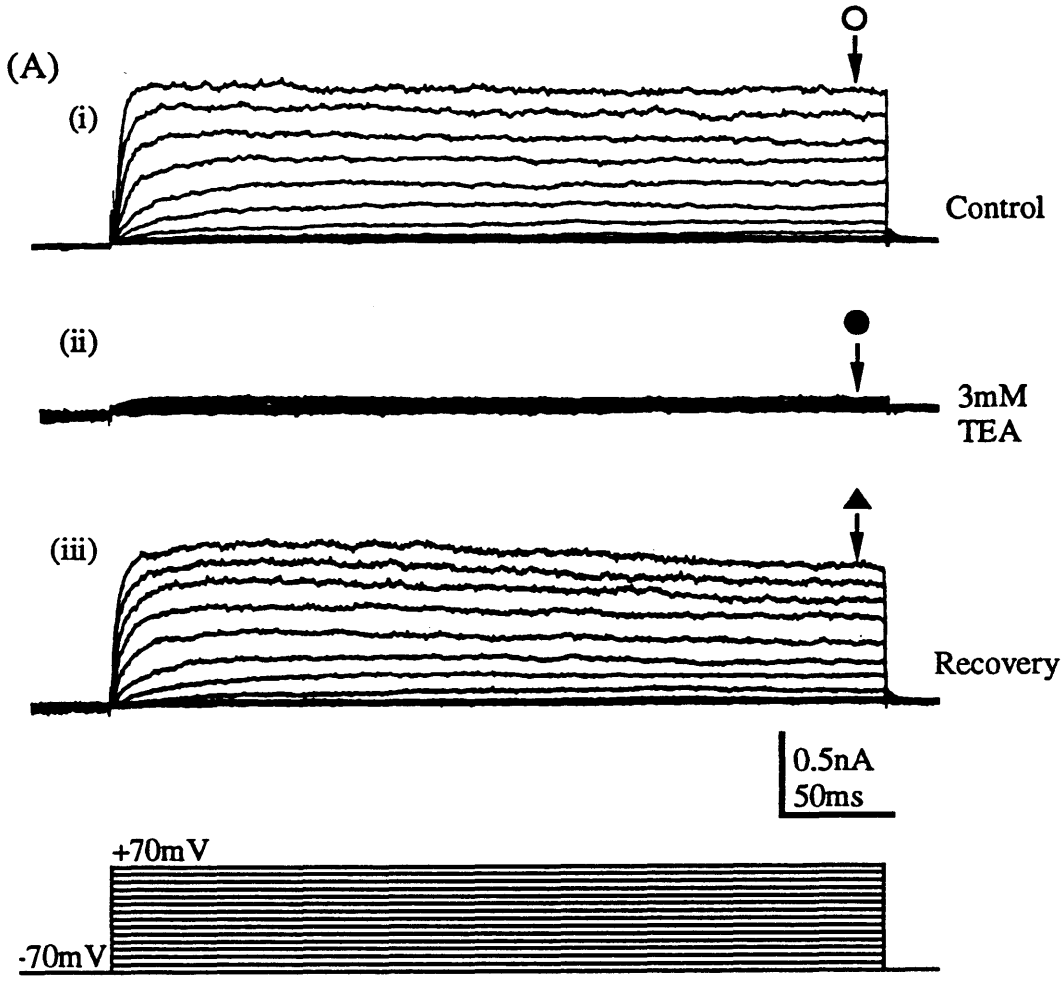
(A)
(i)
Control
(ii)
3mM
TEA
(iii)
Recovery
0.5nA
50ms
+70mV
-70mV

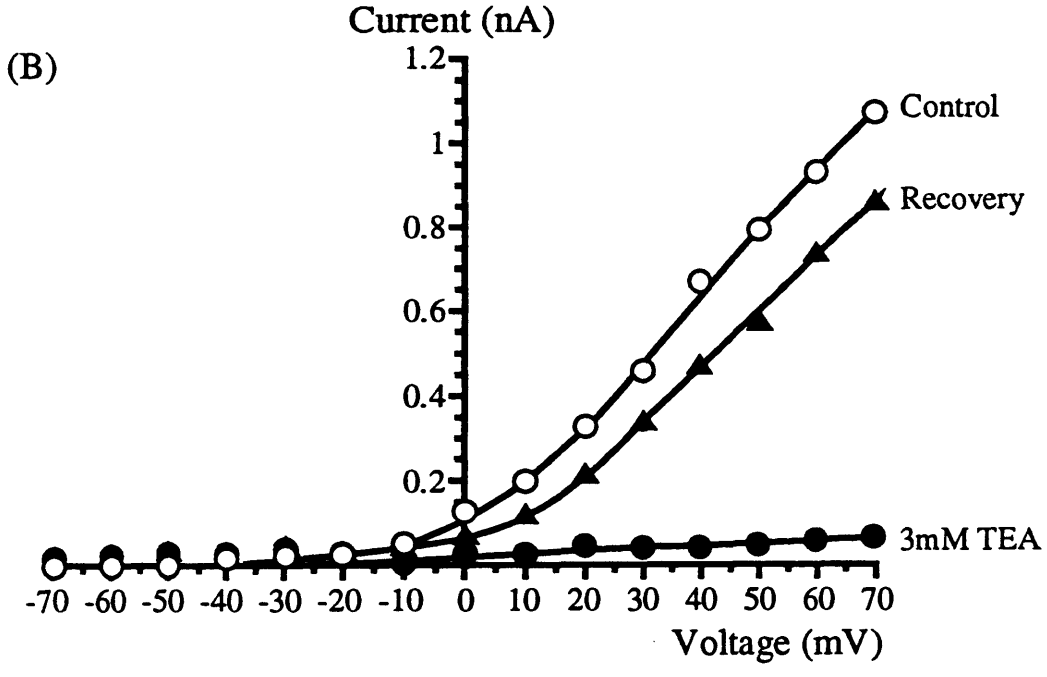
(B)
Current (nA)
1.2
1
0.8
0.6
0.4
0.2
Control
Recovery
3mM TEA
-70 -60 -50 -40 -30 -20 -10 0 10 20 30 40 50 60 70
Voltage (mV)

Barnes-Davies, 1993a; Brew & Forsythe, 1995).

The mechanisms thought to underlie this process use a combination of two potassium channel conductances. Forsythe & Barnes-Davies (1993a) blocked these conductances by applying 4-amino pyridine (4-AP) to the MNTB which broadened the action potential in response to a depolarising step and resulted in multiple action potentials being fired. Brew & Forsythe (1995) later pharmacologically isolated the potassium channel conductances responsible for the single action potential firing and found that a low voltage activated conductance which is blocked by the application of dendrotoxin-I (DTX-I) limits the membrane to firing only a single action potential in response to a depolarising step (Brew & Forsythe, 1995; Wang *et al.*, 1998). A second, TEA sensitive conductance which is a high voltage activated delayed rectifier rapidly repolarises the action potential so that the membrane is ready to fire another action potential, therefore facilitating high frequency firing (Brew & Forsythe, 1995; Wang *et al.*, 1998). This high voltage activated conductance has been recently confirmed to be the $K_v3.1$ channel since its characteristics are similar to those of the $K_v3.1$ channel expressed in the Chinese hamster ovary (CHO) cell line (Wang *et al.*, 1998).

MSO neurones have also been previously reported to produce only one or a few action potentials in response to a depolarising current clamp step (Brew & Forsythe, 1996; Smith 1995) so it is possible that the underlying conductances in MNTB and MSO neurones are similar. Smith (1995) demonstrated that application of 4-AP caused the MSO neurone to then fire multiple action potentials in response to a depolarising step, in a similar manner as was previously reported in the MNTB by Forsythe & Barnes-Davies (1993a). Preliminary investigations were made in this chapter to examine the channels responsible for the action potential firing characteristics in the MSO.

The sensitivity of the outward potassium current to TEA observed here suggests that $K_v3.1$ or $K_v1.1$ may be expressed. These voltage-gated potassium channels have been previously shown to be present in the superior olivary complex ($K_v1.1$: Wang *et al.*, 1994; $K_v3.1$: Perney *et al.*, 1992; Weiser *et al.*, 1994; Wang *et al.*, 1998; Perney & Kaczmarek, 1997) and the latter study suggested that $K_v3.1$ conductances contribute to the repolarisation of action potentials. This repolarisation would mean that when a neurone is stimulated at high frequencies, $K_v3.1$ may enhance its ability to accurately follow high frequency temporal inputs. Recently, Wang *et al.* (1998) reported that $K_v3.1$ does indeed contribute to high frequency firing in mouse MNTB neurones. It is therefore likely that the potassium conductance reported in my study is that of

the $K_v3.1$ channel. However, in contrast to reports in the MNTB, there appears to be very little contribution from a low voltage activated current.

A study was also conducted of the $K_v3.1$ channel transfected into MEL cells. These channels also showed sensitivity to TEA but the activation voltage was more positive than was observed in the natively expressed potassium channels in MSO. This finding is however unsurprising since various characteristics of channels expressed in cell lines, including activation voltage have been shown to be quite different from that of natively expressed channels (reviewed by Robertson, 1997).

Firm identification of the slowly inactivating outward potassium channels expressed in MSO neurones cannot be made from the data presented here so further examination is needed to achieve this. For example, sensitivity to 4-AP is a useful tool for indentification since $K_v3.1$ channels, as well as being sensitive to TEA have also been reported to be highly sensitive to 4-AP (Kanemasa *et al.*, 1995). Additionally, it would be useful to apply DTX-I to the preparation to see if it had any effect on the outward conductances recorded. Since there appears to be little low voltage activated conductance here it is difficult to discern the mechanism by which the neurones only fire one or a few action potentials in response to a depolarising step as was reported by Smith (1995). However, it is likely that the *Shaw*-related potassium channel $K_v3.1$ may play a role in maintaining temporal acuity in MSO neurones.

Chapter 4 - Results

4 Results

4.1 Introduction

The principle aim of this thesis was to study inhibitory synaptic transmission between the medial nucleus of the trapezoid body (MNTB) and the ipsilateral medial superior olivary (MSO) nucleus. As explained in the introduction, the MSO receives a bilateral excitatory projection from spherical bushy cells of the anterior ventral cochlear nucleus (AVCN) and a unilateral inhibitory projection from the principal neurones of the ipsilateral MNTB.

The aim of this chapter is to describe the basic physiology and pharmacology of two of these synaptic projections. Although the chapter focuses on the inhibitory MNTB to MSO projection, it was first necessary to investigate the nature of excitatory synaptic transmission from the contralateral AVCN in order to identify the pharmacological tools necessary to minimise contamination of the inhibitory synaptic current.

The chapter is therefore divided into two major sections:

1) A study of the basic physiology and pharmacology of the direct projection from the spherical bushy cells of the contralateral AVCN to the MSO;

and 2) A study of the basic physiology and pharmacology of the inhibitory synaptic projection from principal neurones of the ipsilateral MNTB to the MSO.

4.2 Methods

The whole cell patch clamp technique described in chapter *2* was used throughout. Extracellular bicarbonate buffered ACSF containing 133.5mM chloride (appendix 1Aii) with 2mM $CaCl_2$ and 1mM $MgCl_2$ added and a CsCl-based intracellular patch solution containing 132mM chloride (appendix 1Biii) were used throughout, except where stated. When measuring the reversal potential of the inhibitory synaptic current, junction potentials (appendix 1C) were corrected for.

Synaptic stimulation of the MSO was achieved using a bipolar platinum stimulating electrode (chapter *2.25*, figure 2.12) positioned over the ipsilateral MNTB. The circuitry of the superior olivary complex (SOC) (chapter *1*, figure 1.1) resulted in stimulation of this nature activating synaptic inputs both directly from the MNTB and from the contralateral AVCN by stimulating

axons passing through the MNTB to the MSO. The use of pharmacological agents to isolate the currents under study was achieved using whole bath perfusion (chapter *2.14*) of the brain stem slice.

4.3 **Results**

4.31 Excitatory Synaptic Transmission in the MSO

The excitatory component of synaptic transmission studied was that of the projection from spherical bushy cells of the contralateral AVCN to the MSO. To pharmacologically isolate the excitatory component the specific glycine receptor antagonist, 1μM strychnine and the $GABA_A$ (γ-aminobutyric acid) receptor antagonist, 10μM bicuculline were bath applied.

The neurone was voltage clamped at -60mV and the stimulus intensity increased until a reliable evoked current was observed. At -60mV this consisted of only a single inward fast synaptic current (figure 4.1A, bottom trace). The membrane was depolarised from -60mV to +60mV in +20mV incremental steps. Depolarisation caused the direction of the current to reverse from an inward to an outward direction and progressively, two components of synaptic current became apparent. At +60mV the outward current comprised two clear components, one fast and one slower, indicated by the closed and open triangles in figure 4.1A, top trace.

The current-voltage relationship and reversal potential for these two current types were determined by plotting the peak of each of the currents against the holding potential of the neurone (figure 4.1B). The fast synaptic current amplitude was easily measured as it was quite distinctive. Measurement of the slower current was more difficult because hyperpolarisation reduced its amplitude, resulting in contamination by the fast synaptic current, which in turn increased in amplitude at negative holding potentials. To estimate the amplitude of the slower synaptic current in control solution over a range of voltages, a cursor was set at its peak when the neurone was voltage clamped at +60mV. Here, the current amplitude could be measured accurately as its peak was quite distinct from that of the fast current. Current amplitude of the slow component was then measured at this time point across the range of voltages.

An example current-voltage relationship prior to pharmacological isolation of the two synaptic currents is shown in figure 4.1Bi. The fast component of the synaptic current is partially rectified at positive holding potentials (n=4) and follows a current-voltage relationship similar

Figure 4.1 **Current-voltage relationship of excitatory synaptic currents in an MSO neurone.**

Excitatory evoked synaptic currents were recorded from MSO neurones in the presence of 1μM strychnine and 10μM bicuculline.

A) Average current traces across a range of holding potentials. Triangles represent the time at which the amplitude of the synaptic current was measured.

B) Current-voltage relationship corresponding to current amplitudes measured in (A). (i) Fast evoked synaptic current rectifies at positive holding potentials. Slow evoked synaptic current rectifies at negative holding potentials. (ii) Enlargement of current-voltage relationship of slow evoked synaptic current showing negative slope conductance of current at negative holding potentials.

Current traces and points on graph are averages of 20 events each.

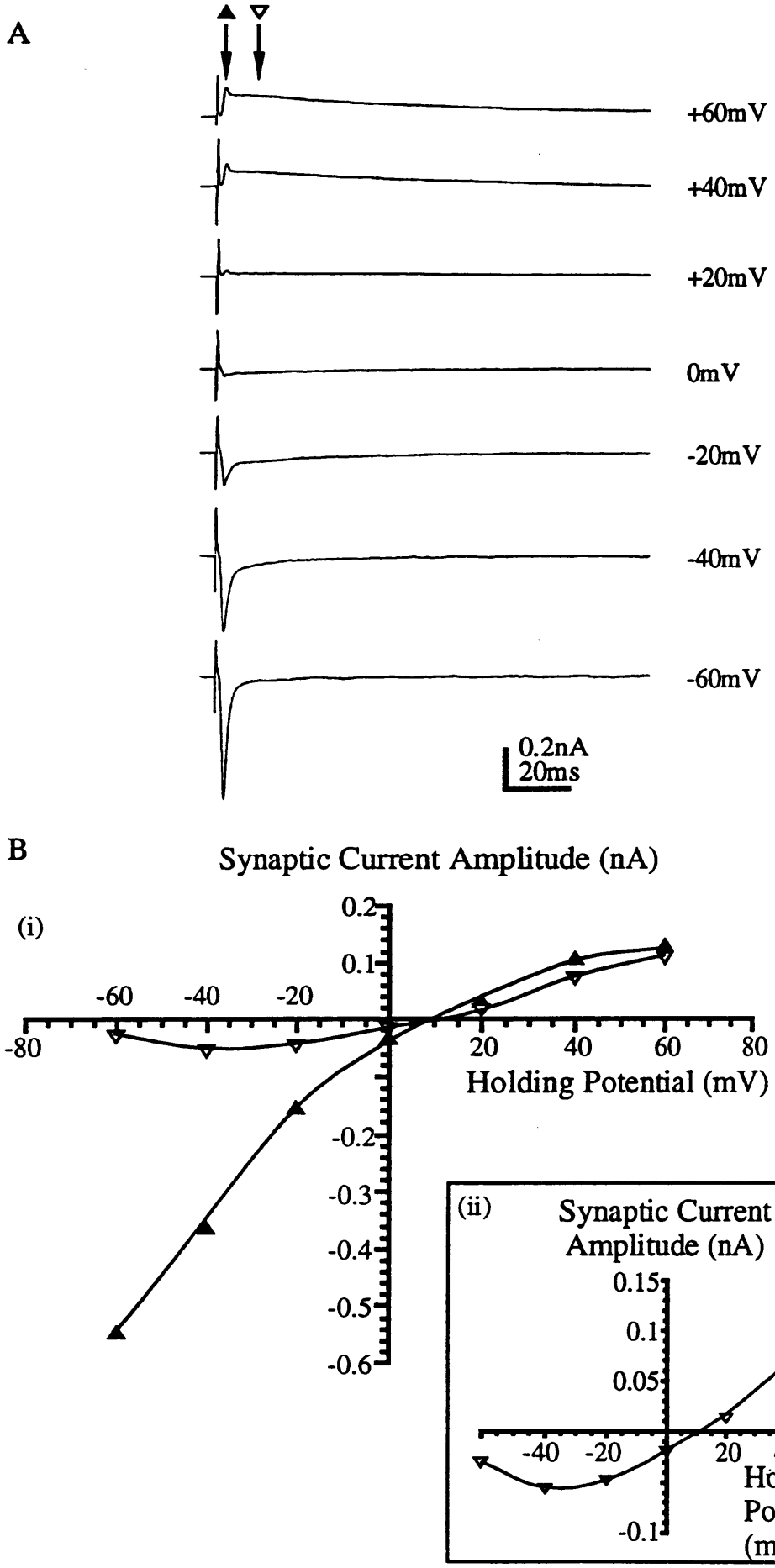
A
+60mV
+40mV
+20mV
0mV
-20mV
-40mV
-60mV
0.2nA
20ms
B
Synaptic Current Amplitude (nA)
(i)
0.2
0.1
-60
-40
-20
-80
20
40
60
80
Holding Potential (mV)
-0.2
-0.3
-0.4
-0.5
-0.6
(ii)
Synaptic Current Amplitude (nA)
0.15
0.1
0.05
-40
-20
20
40
60
Holding Potential (mV)
-0.1

to that expected of non-NMDA, AMPA (α-2-amino-3-[3-hydroxy-5-methylisoxazol-4-yl]-propanoic acid) receptors (Forsythe & Barnes-Davies, 1993b).

The slower component of the synaptic current was similar in amplitude as the fast component at positive holding potentials but was blocked at negative holding potentials (n=4). Figure 4.1Bii shows an enlarged current-voltage relationship of the slower component of the synaptic current to be similar to that of an NMDA (*N*-methyl-D-aspartate) receptor mediated synaptic current (Forsythe & Barnes-Davies, 1993b). The negative slope conductance shown at negative holding potentials results from the voltage-dependent block of the NMDA receptor by extracellular magnesium (Nowak *et al.*, 1984; Mayer, Westbrook & Guthrie, 1984).

4.311 Pharmacology of Excitatory Synaptic Currents in MSO

To study the two components of the excitatory synaptic current in MSO neurones, pharmacological isolation was necessary. The current-voltage relationships produced prior to pharmacological isolation indicated the presence of NMDA and non-NMDA receptor mediated currents (figure 4.1)

Non-NMDA Receptor Mediated Currents

Figure 4.2 shows a plot of peak synaptic current and selected corresponding average data traces at -70mV holding potential. Initially, current amplitude was measured in control solution (figure 4.2Aa,Ba). Perfusion of 1μM strychnine and 10μM bicuculline onto the slice eliminated the inhibitory current (figure 4.2Ab,Bb) leaving only excitatory currents. Inclusion of the non-NMDA receptor antagonist, 10μM CNQX (6-cyano-7-nitroquinoxaline-2,3-dione) or 10μM DNQX (6,7-dinitro-7-quinoxaline-2,3-dione) (Honoré *et al.*, 1988) to the perfusate then caused a rapid 92.3±5.7% (SEM, n=4) block of the remaining synaptic current (figure 4.2Ac,Bc). Block was reversed when CNQX was washed out (figure 4.2Ad,Bd) (n=2). On two other occasions the recording was lost prior to wash out being achieved.

The peak synaptic current in control solution shown in figure 4.2A is reducing in amplitude over time prior to antagonist application. However, the rapid reduction in amplitude of the synaptic current upon CNQX application and the reversibility of that action suggests that although some rundown may have been occurring, CNQX was also having a dramatic effect on the synaptic current amplitude.

Figure 4.2 **At -70mV holding potential the evoked peak synaptic current is blocked by 1μM strychnine, 10μM bicuculline and 10μM CNQX.**

A) Average peak synaptic current plotted over time. 1μM strychnine + 10μM bicuculline and 10μM CNQX were applied as indicated by the bars.

B) Four average current traces corresponding to (A) in the presence of (a) no antagonists, (b) 1μM strychnine + 10μM bicuculline, (c) 1μM strychnine + 10μM bicuculline + 10μM CNQX and (d) wash out in 1μM strychnine + 10μM bicuculline. Current amplitude was measured at the time indicated by the symbol •.

Inhibitory component of the peak synaptic current is blocked by 1μM strychnine + 10μM bicuculline. At -70mV holding potential the remaining synaptic current was blocked by 10μM CNQX (92.3±5.7%, SEM, n=4). Block by CNQX was washed out in the presence of 1μM strychnine + 10μM bicuculline on 2 occasions. On the remaining 2 occasions, the recording was lost prior to wash out.

Current traces and points are averages of 20 events each.

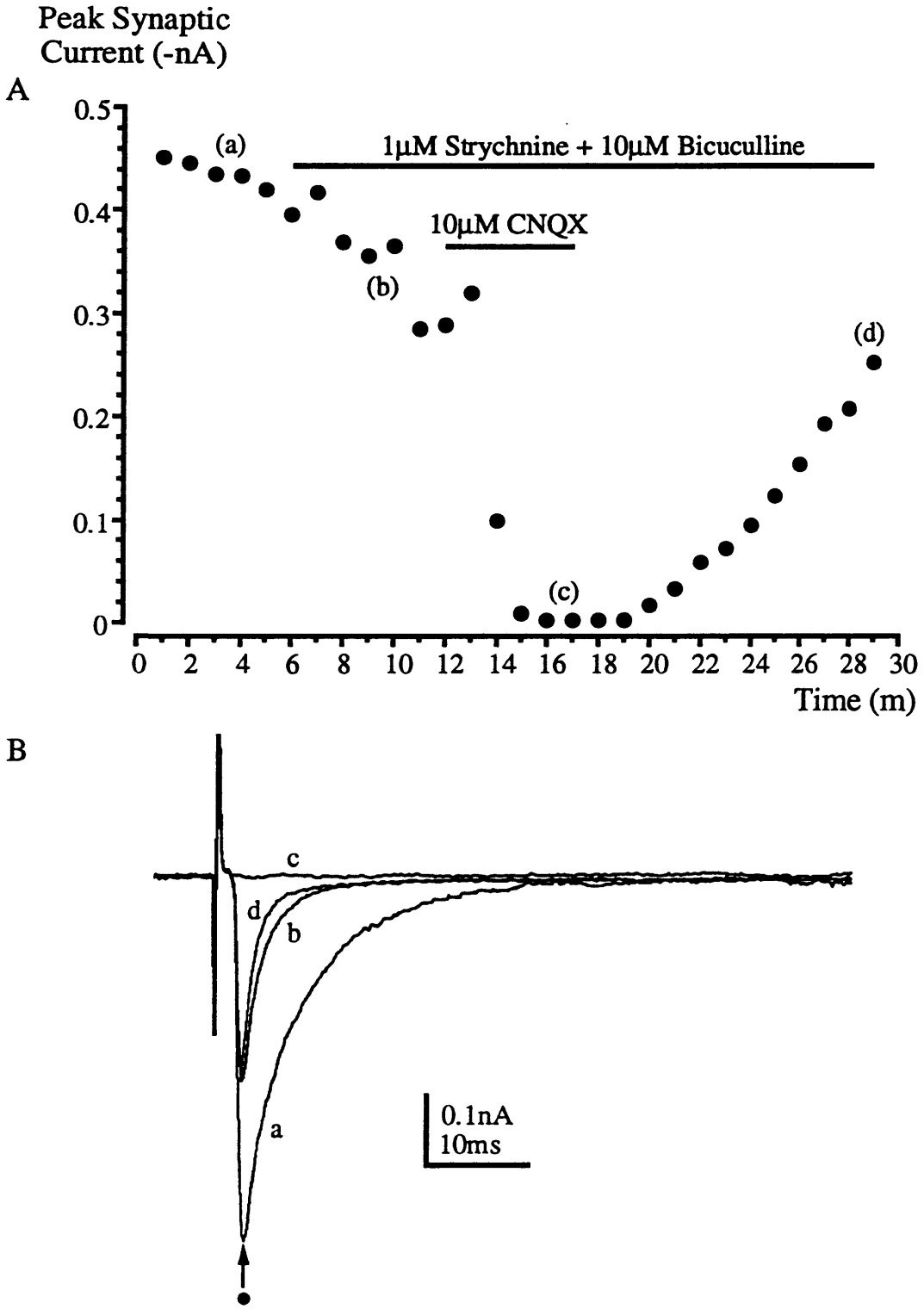
A
Peak Synaptic Current (-nA)
0.5
0.4
0.3
0.2
0.1
0
(a)
1μM Strychnine + 10μM Bicuculline
10μM CNQX
(b)
(c)
(d)
0 2 4 6 8 10 12 14 16 18 20 22 24 26 28 30
Time (m)
B
c
d
b
a
0.1nA
10ms

The voltage-dependent magnesium block of NMDA receptor ion channels resulted in a complete absence of the slower synaptic current type at -70mV holding potential following application of 1μM strychnine, 10μM bicuculline and 10μM CNQX (n=4).

NMDA Receptor Mediated Currents

Figure 4.3 shows the presence and block of NMDA receptor mediated currents at a +40mV holding potential. The voltage dependent magnesium block which NMDA receptor ion channels are subject to is relieved at positive holding potentials. In figure 4.3, 1μM strychnine and 10μM bicuculline were applied throughout. Application of 50μM DL-AP5 ((±)-2-amino-5-phosphono-pentanoic acid) reduced the peak synaptic current amplitude by 83.4±2.3% (SEM, n=3). DL-AP5 is a widely used competitive NMDA receptor antagonist (Evans *et al.*, 1982). At +40mV, the non-NMDA receptor mediated currents remained unblocked by DL-AP5 (figure 4.3Bb). However, the disparity between the time to peak of the non-NMDA and NMDA receptor mediated currents allowed clear observation of block of the NMDA receptor mediated current. Wash out of DL-AP5 was achieved on one occasion but the recording was lost on the remaining two occasions prior to wash out.

4.312 Current-Voltage Relationships

A more accurate determination of the current-voltage relationship of the non-NMDA and NMDA receptor mediated currents than was shown in figure 4.1 was done following their pharmacological isolation.

Non-NMDA Receptor Mediated Currents

The current-voltage relationship shown in figure 4.4A and the corresponding average current traces (figure 4.4B) demonstrate pharmacologically isolated non-NMDA receptor mediated currents across a range of voltages (-60mV to +60mV, in 20mV steps). The perfusate contained 1μM strychnine, 10μM bicuculline and on two occasions 50μM DL-AP5 to reduce contamination by the NMDA receptor mediated synaptic current. The peak current amplitude indicated by ▲ in figure 4.4B was plotted against the holding potential.

Figure 4.3 **The slower, NMDA receptor mediated component of the evoked synaptic current is blocked by 50μM DL-AP5.**

A) Average peak synaptic current plotted over time. 1μM strychnine + 10μM bicuculline were applied throughout. 50μM DL-AP5 was applied at the time indicated by the bar.

B) Three average current traces corresponding to (A) in the presence of (a) 1μM strychnine + 10μM bicuculline, (b) 1μM strychnine + 10μM bicuculline + 50μM DL-AP5 and (c) wash out in 1μM strychnine + 10μM bicuculline. Notice the presence of the non-NMDA receptor mediated current in (b). Current amplitude was measured at the time indicated by the symbol •.

At +40mV holding potential, 50μM DL-AP5 blocked the slower component of the synaptic current by 83.4±2.3% (SEM, n=4). Washout out of DL-AP5 was observed on one occasion but the recording was lost prior to wash out on the remaining two occasions.

Current traces and points are averages of 20 events each.

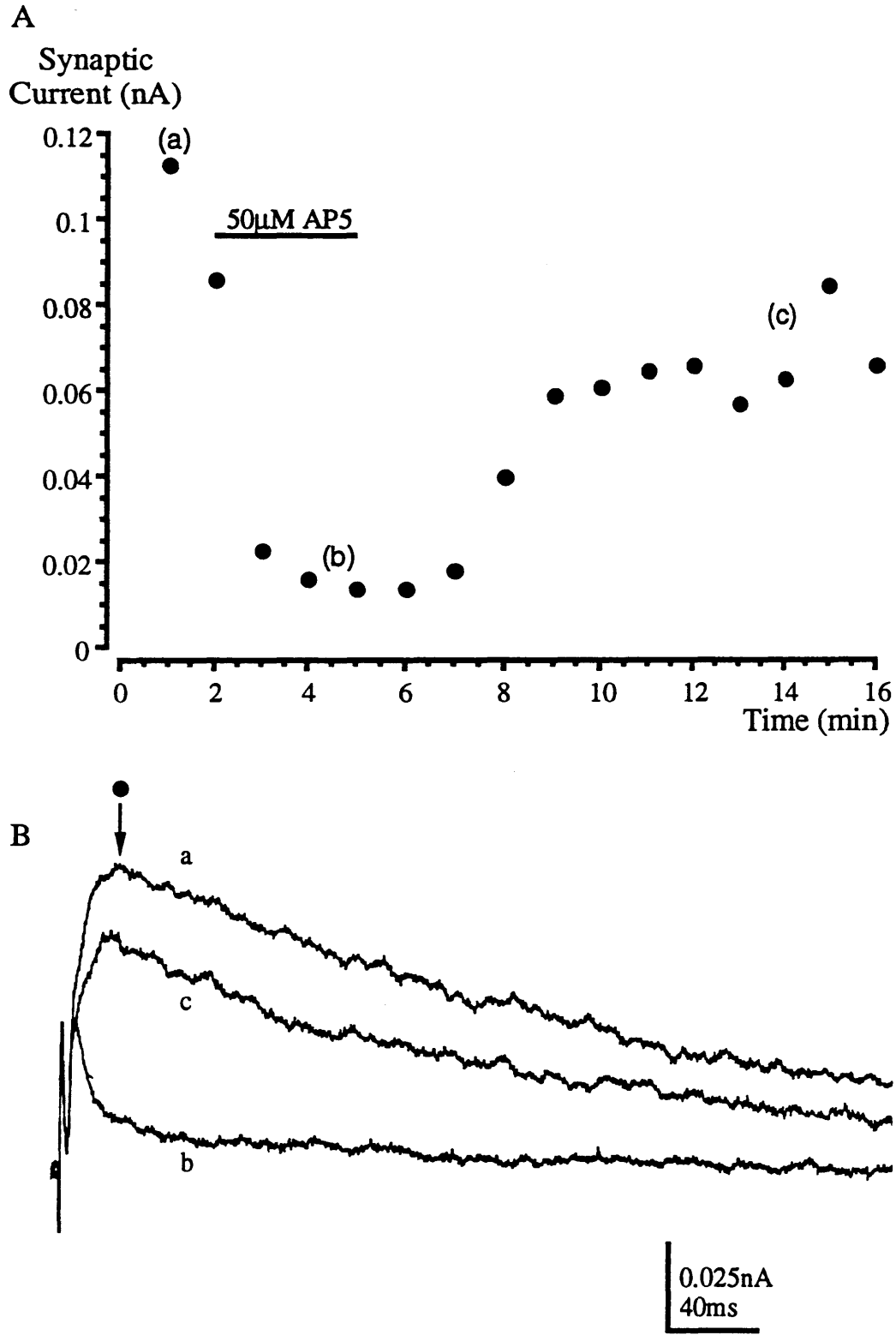
A
Synaptic
Current (nA)
0.12
0.1
0.08
0.06
0.04
0.02
0
(a)
50μM AP5
(b)
(c)
0
2
4
6
8
10
12
14
16
Time (min)
B
a
c
b
0.025nA
40ms

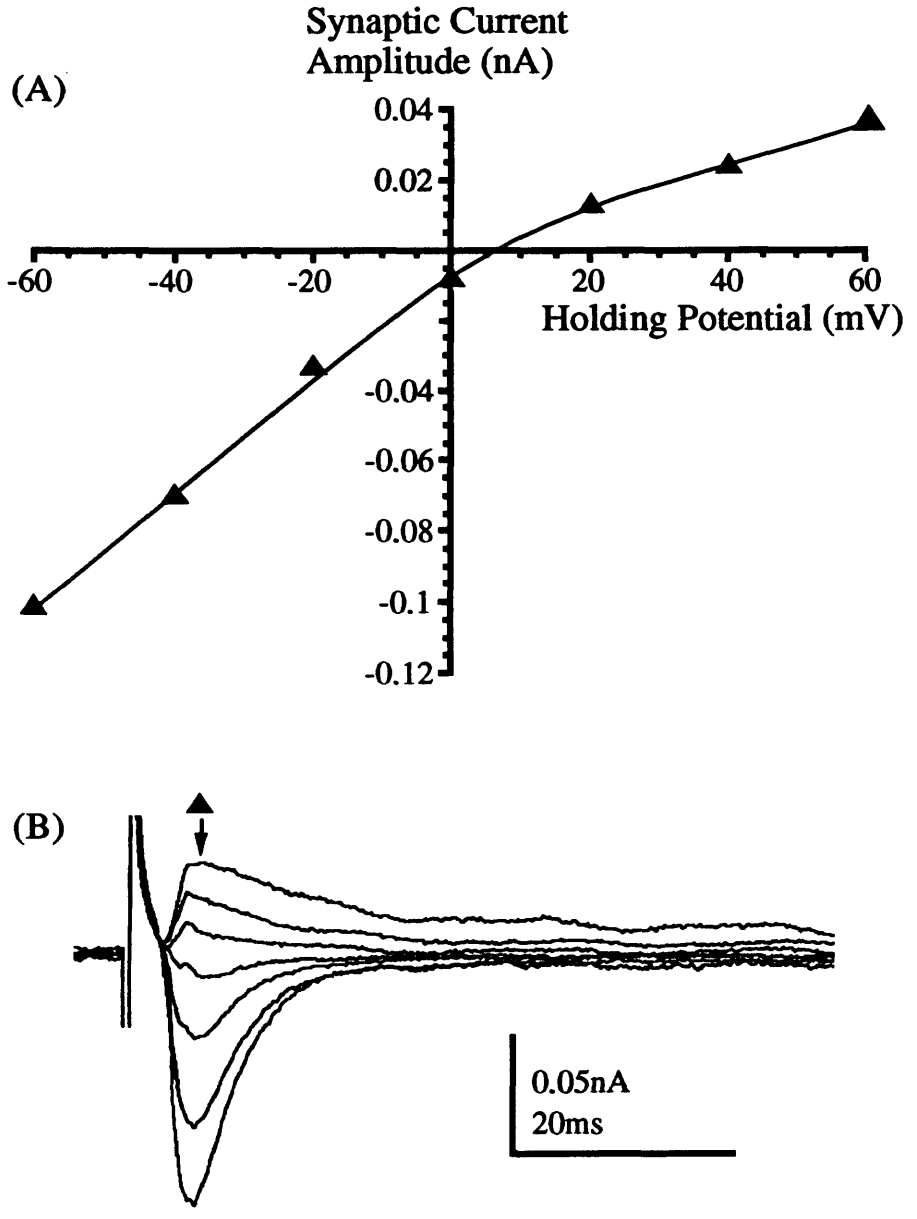

Figure 4.4 **Reversal potential of non-NMDA receptor mediated synaptic current in MSO neurones.**

(A) Plot of peak synaptic current across a range of holding potentials in the presence of 1μM strychnine and 10μM bicuculline. Mean reversal potential = +7.8±1.4mV (SEM, n=4). On 2 occasions, 50μM DL-AP5 was included in the perfusate.

(B) Corresponding average current traces to (A). Synaptic current amplitude was measured at the time indicated by▲.

Current traces and points are averages of 20 events each.

The reversal potential of this current was +7.8±1.4mV (SEM, n=4). This is similar to the reversal potential of ~+7mV of the fast excitatory postsynaptic current in reported in MNTB neurones by Forsythe & Barnes-Davies, (1993b).

NMDA-Receptor Mediated Currents

The current-voltage relationship shown in figure 4.5A and the corresponding average current traces (figure 4.5B) demonstrate the pharmacologically isolated NMDA receptor mediated component of the synaptic current. 1μM strychnine, 10μM bicuculline and 10μM CNQX were included in the perfusate. The holding potential was changed between -60mV and +60mV in +20mV steps. The peak current amplitude indicated by ∇ in figure 4.5B was plotted over this range of voltages (figure 4.5A). CNQX and less-so DNQX are not entirely specific non-NMDA receptor antagonists as they also partially block the NMDA receptor via a glycine receptor site on the channel (Birch, Grossman & Hayes, 1988). The small amplitude of the current in figure 4.5 may result through the partial inhibition of the NMDA receptor by CNQX. The mean reversal potential of the NMDA receptor mediated current was +12.3±2.3mV (SEM, n=4) in the presence of 1μM strychnine, 10μM bicuculline and on two occasions 10μM CNQX.

4.32 Inhibitory Synaptic Transmission in the MSO

Globular bushy cells of the anterior ventral cochlear nucleus (AVCN) project contralaterally to principal neurones of the MNTB where they form giant synapses called calyces of Held. The principal neurones, in turn project to the ipsilateral superior olivary nucleus, including the medial superior olivary (MSO) nucleus. In order to study this projection in detail it was first necessary to examine the nature of the synaptic projection so that the experimental procedure could be standardised in order that it did not affect the synaptic response. So the first question to be asked was whether there were single or multiple synaptic inputs. To examine this, stimulus response curves were applied to the synaptic input.

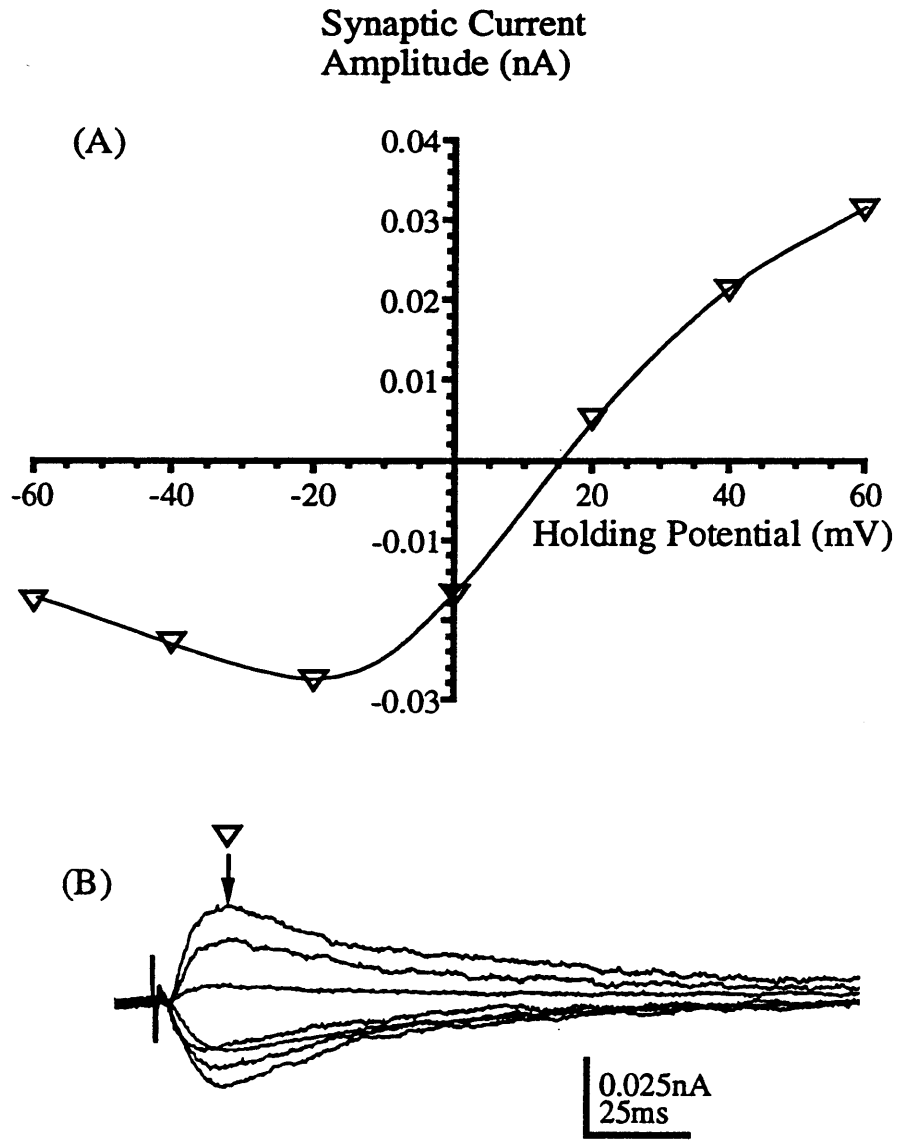

Figure 4.5 **Reversal potential of NMDA receptor mediated synaptic current in MSO neurones.**

(A) Plot of peak synaptic current across a range of holding potentials in the presence of 1μM strychnine and 10μM bicuculline. Mean reversal potential = +12.3±2.3mV (SEM, n=4). On two occasions, 10μM CNQX was included in the perfusate.

(B) Corresponding average current traces to (A). Synaptic current amplitude measured at the time indicated by ▽.

Current traces and points are averages of 20 events each.

4.321 Stimulus Response Curves

Mixed Synaptic Current

In normal bicarbonate buffered ACSF (appendix 1Aii), stimulation using a bipolar platinum stimulating electrode positioned over the MNTB produced a mixed excitatory and inhibitory synaptic response in MSO neurones. The amplitude of the response increased as the stimulus intensity was increased (figure 4.6) from 0V to 10V using an isolated stimulator DS2A (chapter *2.25*). The neuronal membrane was voltage clamped at -70mV. The increased amplitude of synaptic current with stimulus intensity probably resulted from recruitment of synaptic inputs with different thresholds of stimulation.

The mean maximum peak synaptic current amplitude was -5.7±1.6nA (SEM, n=5) and ranged from -0.8nA to -8.5nA.

Figure 4.7 demonstrates the mixed composition of the evoked synaptic current in an MSO neurone. In figure 4.2 the involvement of an inhibitory component of synaptic transmission was demonstrated as the current was partially blocked by 1μM strychnine and 10μM bicuculline. In figure 4.7a, the perfusate was initially normal bicarbonate buffered ACSF (appendix 1Aii). 1μM strychnine and 10μM bicuculline were then included, leaving only an excitatory synaptic current (figure 4.7b). Current trace (c) in figure 4.7 is the product of subtraction of trace (b) from trace (a) and represents the inhibitory component of the total synaptic current in an MSO neurone. Comparing traces (b) and (c) it is clear that the rise time and duration of the inhibitory synaptic current is much slower than that of the excitatory component. The time course of the inhibitory synaptic current is addressed in the next chapter but the relative slowness of its time course observed here is consistent with findings of others where fast excitatory synaptic responses are generally much faster than inhibitory synaptic responses (e.g. Barnes-Davies & Forsythe, 1995; Legendre, 1998).

Inhibitory Synaptic Current

Results in section *4.31* demonstrated the presence of an excitatory input into the MSO. Examination of the inhibitory synaptic current therefore required pharmacological isolation so excitatory amino acid (EAA) antagonists (10μM CNQX, 50μM DL-AP5, 5μM MK801 and 5μM 5,7-dichlorokynurenic acid) and 10μM bicuculline were included in the perfusate.

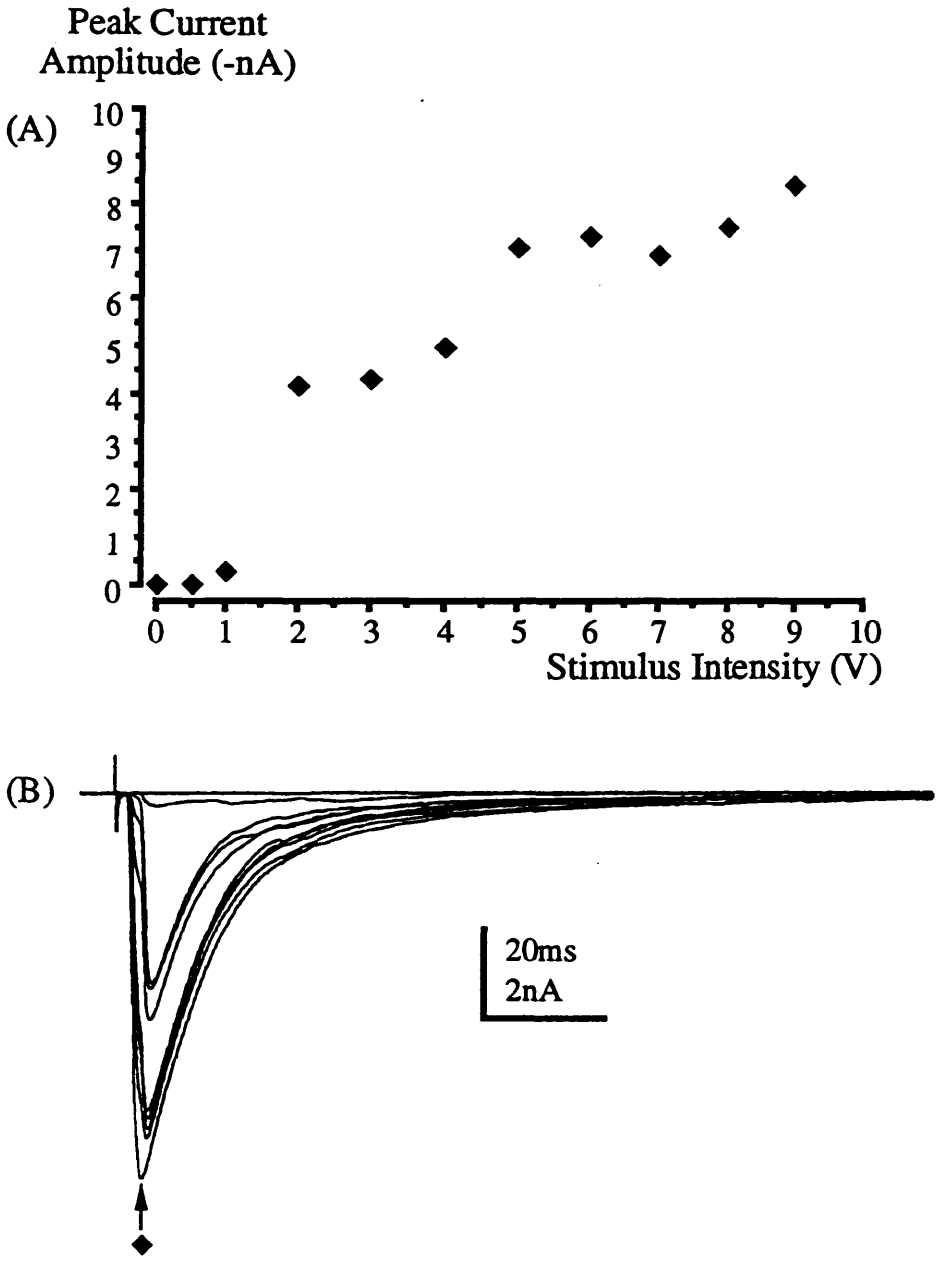

Figure 4.6 **Mixed excitatory and inhibitory synaptic currents are produced in MSO neurones as stimulus intensity is increased.**

(A) Peak synaptic current plotted against stimulus intensity and, (B) corresponding average current traces from -70mV holding potential in normal bicarbonate buffered ACSF. Synaptic current amplitude was measured at the time indicated by ♦.

As stimulus intensity was increased, larger synaptic currents resulted. Mean maximum peak synaptic current was-5.7±1.6nA (SEM, n=5).

Current traces and points are averages of 20 events each.

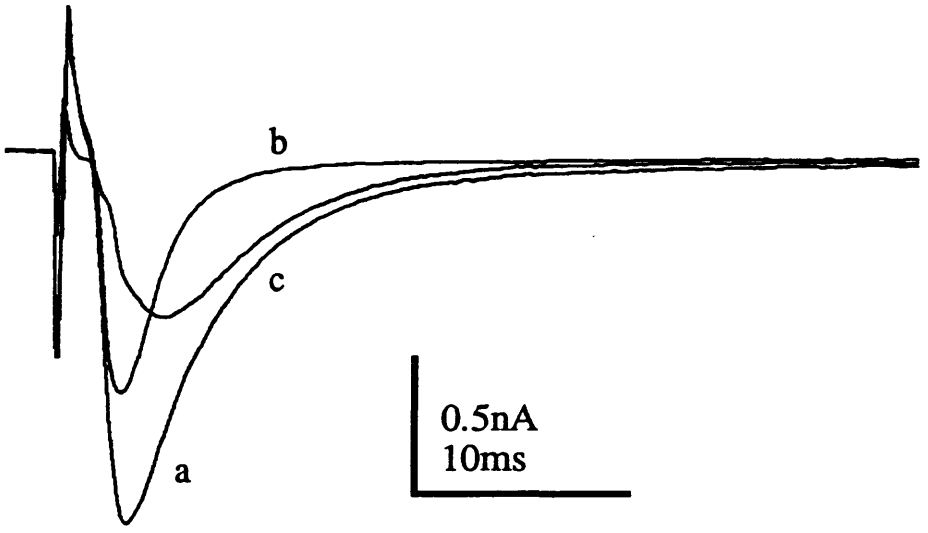

Figure 4.7 **Evoked synaptic current comprises an excitatory and inhibitory component.**

Average data traces recorded from an MSO neurone at -70mV holding potential.

(a) Perfusate is normal bicarbonate buffered ACSF, (b) Excitatory current remaining following 1μM strychnine and 10μM bicuculline application, and (c) inhibitory current remaining after subtraction of (b) from (a)

MK801 ((+)-5-methyl-10,11-dihydro-5*H*-dibenzo[*a*,*d*]cyclohepten-5,10-imine maleate, or dizocilpine) is an open channel blocker of the NMDA receptor ion channel (Wong *et al.*, 1986) and 5,7-dichlorokynurenic acid is an antagonist at the NMDA receptor glycine site (Baron *et al.*, 1990). It was necessary to include so many EAA antagonists in order to maximise pharmacological isolation of the inhibitory synaptic current (see section *4.322*).

Figure 4.8A shows the relationship between stimulus intensity applied to the MNTB and the peak amplitude of synaptic currents produced in an MSO neurone in the presence of EAA antagonists and bicuculline. The corresponding average current traces are shown in figure 4.8B. As stimulus intensity was increased so the peak synaptic current amplitude increased (n=5) when measured at the time indicated by ◆. Again, this probably resulted from recruitment of synaptic inputs with different stimulation thresholds. The mean maximum peak synaptic current at -70mV holding potential was -0.8±0.2nA (SEM, n=8) and ranged from -0.2nA to -1.6nA.

Why is an Inhibitory Current Inward?

Inhibitory currents generally proceed in an outward direction at the resting membrane potential and hyperpolarise the membrane therefore reducing the likelihood of action potential generation. It should be noted however, that the inhibitory synaptic current here is inward when voltage clamping at -70mV (e.g. figure 4.8). This apparent anomaly can be explained by the relative chloride concentrations of the extracellular and intracellular solutions where the equilibrium potential is positive to the holding potential of the neurone.

The physiological intracellular chloride concentration was reported to be ~6.6mM by Forsythe & Redman (1988) and is generally accepted to be around this concentration. However, Kandler & Friauf (1995) also suggested that $[Cl^-]_i$ varies with age since they found that strychnine sensitive postsynaptic potentials changed from being depolarising to hyperpolarising during early postnatal development (E18-P0 to P10). Using low intracellular- and a high extracellular chloride concentrations of ~6mM and ~130mM, respectively synaptic stimulation would result in inward chloride ion movement, or outward current flow at -70mV holding potential. The results shown in figure 4.8 were however obtained with extra- and intracellular concentrations of chloride being almost the same at 133.5mM and 132mM, respectively (appendix 1Aii, 1Biii). Synaptic stimulation in these circumstances caused an outward flow of chloride ions at -70mV holding potential, resulting in an inward synaptic current.

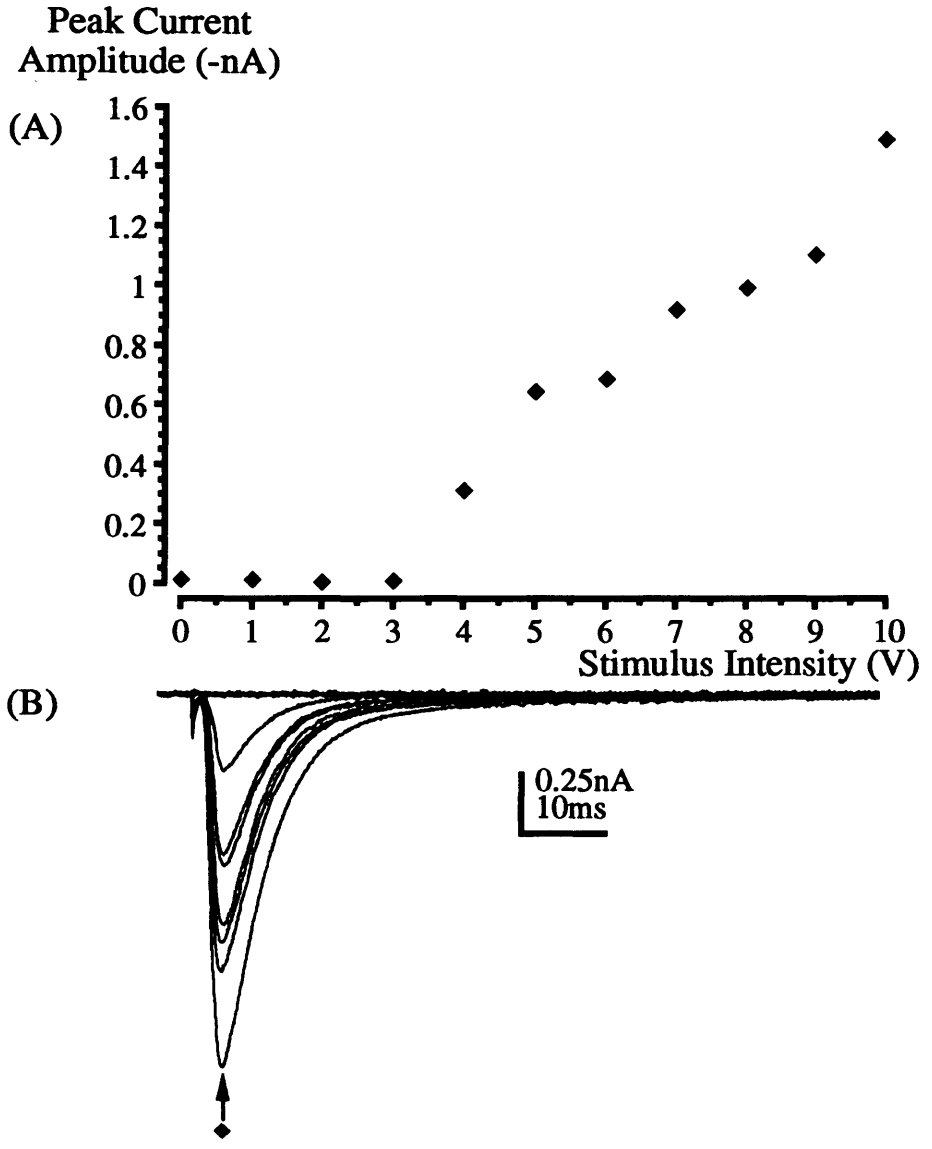

Figure 4.8 **Synaptic current amplitude increases in MSO neurones as presynaptic MNTB stimulation in increases.**

(A) Peak synaptic current plotted against stimulus intensity and, (B) corresponding average current traces from -70mV holding potential. Synaptic current amplitude was measured at the time indicated by ♦.

MNTB neurones were stimulated in the presence of 10μM CNQX, 50μM DL-AP5, 5μM MK801 and 5μM 5,7-dichlorokynurenic acid to block excitatory responses. 10μM bicuculline was also included in the perfusate to block $GABA_A$ mediated synaptic current.

At -70mV holding potential the mean maximum peak synaptic current was 0.8±0.2nA (SEM, n=8).

Current traces and points are averages of 20 events.

Stimulus Intensity

The observed recruitment of synaptic inputs with increasing stimulus intensity posed the question of what stimulus intensity to use when studying the physiology and pharmacology of the synaptic response. Initially, minimal stimulation was attempted, using the bipolar platinum stimulating electrode to attain responses from single synaptic inputs. However, this proved to be difficult because at the low stimulus intensities required, activation of the synaptic response was not guaranteed, resulting in many 'failures' of synaptic transmission.

A different method of stimulation of individual MNTB neurones was then tried. An electrode, similar to the patch recording electrode was positioned on an MNTB neurone which was stimulated whilst recording from a postsynaptic MSO neurone. The presynaptic electrode was moved between MNTB neurones in an attempt to stimulate a neurone which was synaptically connected to the MSO neurone being recorded from. However, this procedure was difficult to achieve since there were a lot of MNTB neurones to choose from. One aid to locating an MNTB neurone synaptically connected to the MSO neurone was pressure ejection of the intracellular patch solution from the presynaptic electrode. The presynaptic electrode was filled with a KCl-based solution (appendix 1Bii), a small amount of which was forced out of the electrode when positive pressure was applied to the back of the pipette. When positioned in certain regions of the MNTB, pressure ejection of the KCl-based patch solution from the stimulating electrode resulted in synaptic activity of the postsynaptic MSO neurone (figure 4.9) suggesting that neurones close by the tip of the stimulating electrode were synaptically connected to the MSO neurone. However, despite this additional aid, the exact location of MNTB neurones synaptically connected to the MSO neurone being recorded from was never determined and return to the gross stimulation method using the bipolar platinum stimulating electrode was necessary.

Since minimal stimulation using the bipolar stimulating electrode was not possible, a designated stimulus intensity was attempted. This also was found to be not suitable because responses from neurone to neurone were too variable. For example, a 10V stimulus produced a very small current amplitude in one neurone and a current too large to ensure reliable voltage clamp in another. Consequently, the stimulus intensity used was specific to an individual neurone such that a reliable response (~1nA) was produced.

The variability of synaptic response between neurones may originate from the variable number of synaptic connections remaining intact following sectioning. Also, MNTB neurones lying

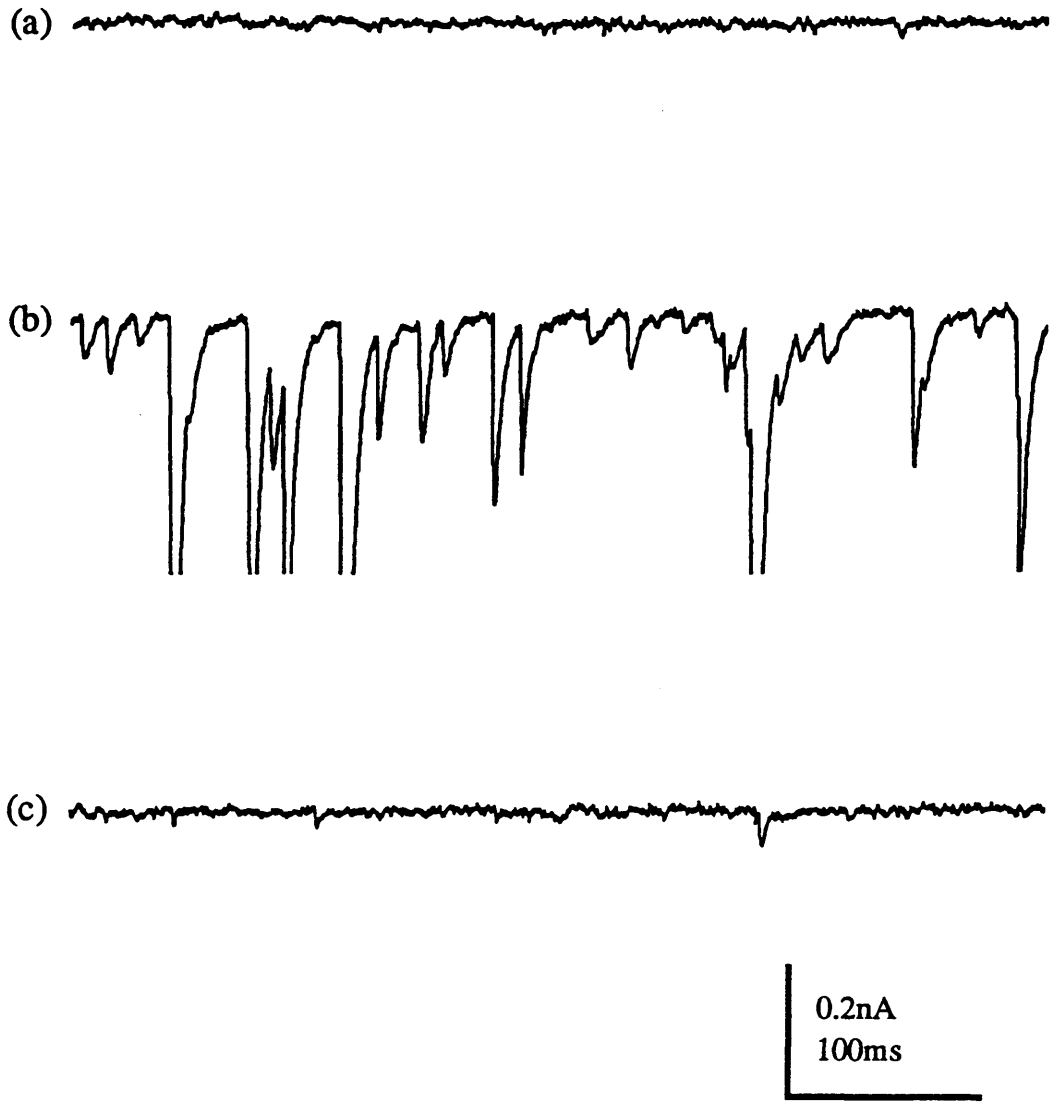

Figure 4.9 **Pressure ejection of KCl onto the MNTB produces synaptic activity in an MSO neurone.**

Raw data traces from an MSO neurone (a) in normal bicarbonate buffered ACSF, (b) after pressure ejection application of KCl on MNTB neurones and (c) after wash off of KCl from the MNTB neurones.

physically close to the stimulating electrode will respond to stimulation more readily than neurones deeper in the slice.

4.322 Pharmacology of the Inhibitory Synaptic Current in MSO

Isolation of the Inhibitory Synaptic Current

Shown in figures 4.1 to 4.8, excitatory and inhibitory synaptic inputs are both stimulated in MSO with the bipolar platinum stimulating electrode positioned over the ipsilateral MNTB. In order to study inhibitory synaptic transmission between the MNTB and MSO, isolation of this synaptic pathway was necessary.

Figures 4.1 to 4.5 demonstrate that the excitatory input to the MSO is mediated by non-NMDA and NMDA receptors. GABA has also been reported in the superior olivary complex (SOC) and Smith (1995) reported that although ipsilateral stimulation of the trapezoid body produced mainly glycine mediated synaptic potentials in the MSO there was also some pharmacological evidence for a $GABA_A$ mediated component. Immunocytochemical evidence has also revealed the presence of GABAergic terminals on MSO dendrites (Vater, 1995; Adams & Mugnaini, 1990). Consequently, its involvement in inhibitory synaptic transmission here needed to be addressed. However, despite the possibility that GABA may play some role, glycine is implicated as the major neurotransmitter involved in synaptic transmission between MNTB and MSO (chapter *1.114*, e.g. Smith, 1995, Grothe & Sanes, 1993, 1994, Smith & Forsythe, 1996, 1997).

Figure 4.10B shows average data traces recorded from an MSO neurone before, during and after application of 5μM DNQX, 20μM DL-AP5, 10μM bicuculline and 1μM strychnine. Figure 4.10A shows the corresponding amplitude of the peak synaptic current plotted over time. Initially, normal bicarbonate buffered ACSF (appendix 1Aii) was used. A stable baseline was established (figure 4.10Aa,Ba), following which, 5μM DNQX and 20μM DL-AP5 were included in the perfusate to antagonise non-NMDA and NMDA receptor mediated currents. DNQX and DL-AP5 caused a reduction in the peak current amplitude (figure4.10Ab,Bb) measured at the time indicated by • in figure 4.10B. 10μM bicuculline was then also included in the perfusate and little or no further reduction in current amplitude was observed (n=6; figure4.10Ac,Bc). This suggests that there is little or no involvement of $GABA_A$ receptors in this synaptic current. However, in light of the proposed involvement of $GABA_A$ receptors in

Figure 4.10 **Synaptic current is almost completely blocked by application of 5μM DNQX, 20μM DL-AP5, 10μM bicuculline and 1μM strychnine.**

(A) Peak synaptic current plotted over time and, (B) corresponding average peak synaptic current traces at -70mV holding potential: (a) No antagonists were included in the perfusate so a mixed synaptic response was seen, (b) 5μM DNQX and 20μM DL-AP5 were added to the perfusate, reducing the current amplitude; (c) Application of 10μM bicuculline did not further reduce the current amplitude; (d) Inclusion of 1μM strychnine almost completely blocked the remaining current. Small remaining current magnified in inset following application of above antagonists.

Data traces are averages of 20 events and points on graph are peak current amplitudes of individual data traces.

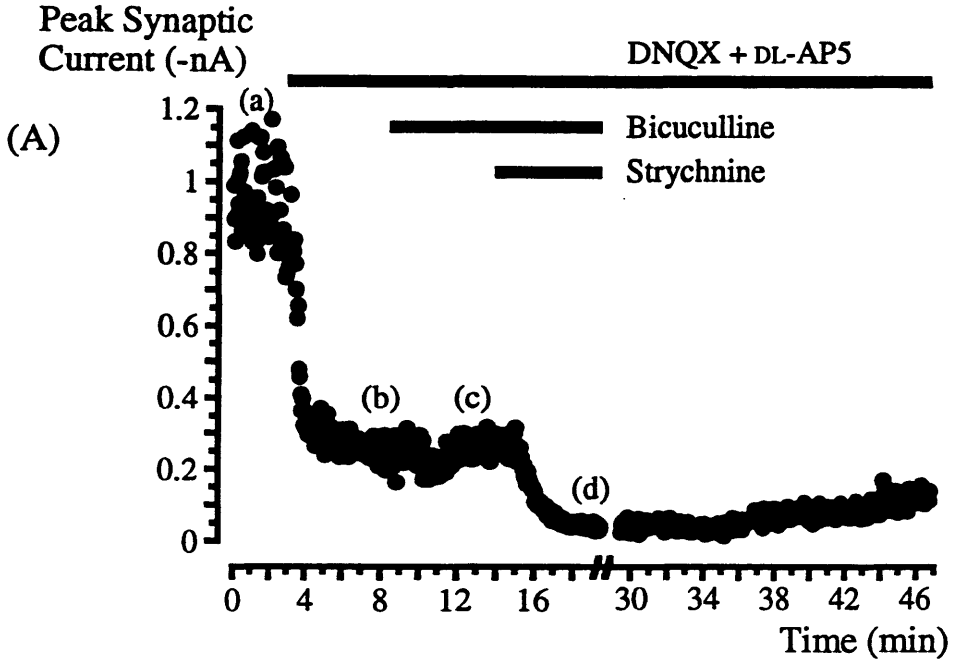
Peak Synaptic
Current (-nA)
(A)
DNQX + DL-AP5
Bicuculline
Strychnine
(a)
(b)
(c)
(d)
1.2
1
0.8
0.6
0.4
0.2
0
0 4 8 12 16 30 34 38 42 46
Time (min)

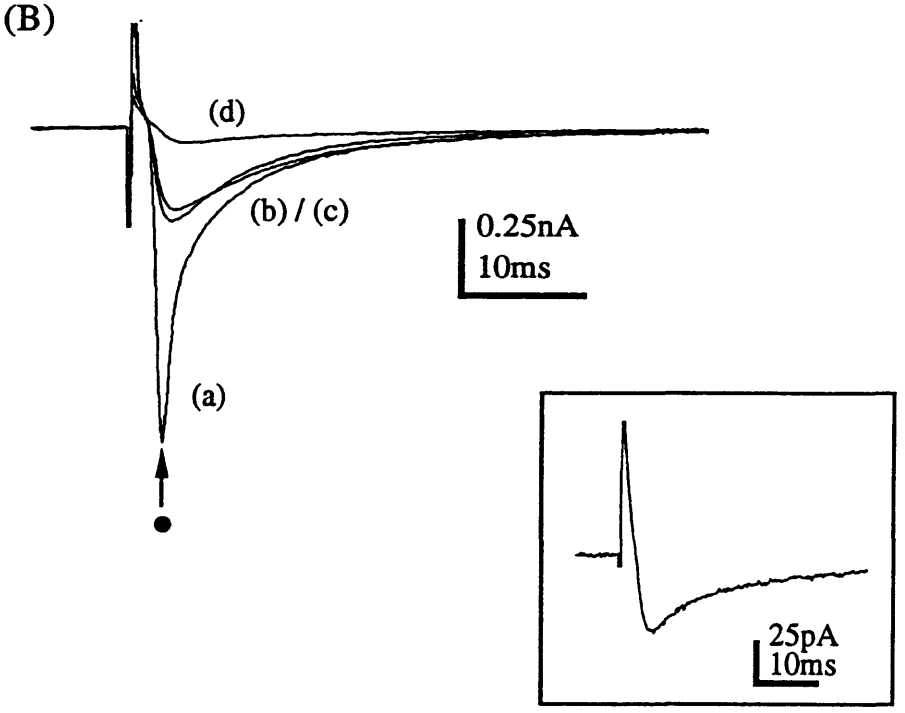
(B)
(d)
(b) / (c)
(a)
0.25nA
10ms
25pA
10ms

this synaptic pathway, mentioned above and the observation that $GABA_B$ receptors are located at this synapse (chapter *6.31*), subsequent experiments included bicuculline in the perfusate to ensure complete isolation of the glycine mediated inhibitory synaptic current.

The specific glycine receptor antagonist, 1μM strychnine was then also included in the perfusate resulting in a dramatic further reduction in evoked current amplitude (n=13; figure 4.10Ad,Bd). This supports the idea that glycine is the neurotransmitter active at this synapse since strychnine sensitivity is indicative of the presence of glycine receptors (Barron & Guth, 1987; Curtis *et al*, 1968; Curtis, Duggan & Johnston, 1971; Ryall, Piercey & Polosa, 1972; Davidoff, Aprison & Werman, 1969).

The inset in figure 4.10B demonstrates that even with inclusion of DNQX, DL-AP5, bicuculline and strychnine to the perfusate, a small amount of synaptic current remained (n=4). For further study of the glycine receptor mediated current, elimination of this small current was necessary. The current may have resulted from some non-amino acid transmitter release but before venturing down this avenue, other amino acid receptor antagonists (5μM MK801, 5μM 5,7-dichlorokynurenic acid) were also applied. Additional application of these antagonists and 1μM strychnine almost completely blocked the synaptic response from MSO neurones (figure 4.11, n=7). Henceforth, both 10μM bicuculline and EAA antagonists of the following concentrations were included in the perfusate: 50μM DL-AP5, 10μM CNQX, 5μM MK801, 5μM 5,7-dichlorokynurenic acid.

Strychnine Sensitivity

Since strychnine is a specific blocker of glycine receptors it can be used as a method of glycine receptor identification. Following EAA antagonist and bicuculline application, block of the synaptic current by strychnine in figures 4.10 and 4.11, demonstrated that synaptic transmission between MNTB and MSO neurones is likely to be mediated by glycine receptors.

In the introduction, the developmental heterogeneity of glycine receptors was described. Briefly, the neonatal (α_2) and adult (α_1) isoforms of the glycine receptor can be partly identified by their different sensitivities to strychnine in that the neonatal isoform has a lower affinity for strychnine than the adult isoform (Akagi & Miledi, 1988; Becker, Hoch & Betz, 1988). From birth until around 3 weeks post partum there in a gradual developmental change of glycine receptor expression from neonatal to adult form (Friauf, Hammerschmidt & Kirsch, 1997, Takahashi *et al.*, 1992). This change is characterised by an increase in sensitivity to

Figure 4.11 **Synaptic current is more completely blocked by application of 50μM DL-AP5, 10μM CNQX, 5μM MK801, 5μM 5,7-dichlorokynurenic acid, 10μM bicuculline and 1μM strychnine.**

(A) Peak synaptic current plotted over time and, (B) corresponding average peak synaptic current traces at -70mV holding potential: (a) No antagonists included in perfusate; (b) 50μM DL-AP5, 10μM CNQX, 5μM MK801, 5μM 5,7-dichlorokynurenic acid and 10μM bicuculline included in the perfusate, leaving strychnine sensitive current which is completely blocked by 1μM strychnine (c). Synaptic current amplitude was measured at the time indicated by ● in B.

Data traces are averages of 15 events and points on graph are peak current amplitudes of individual data traces.

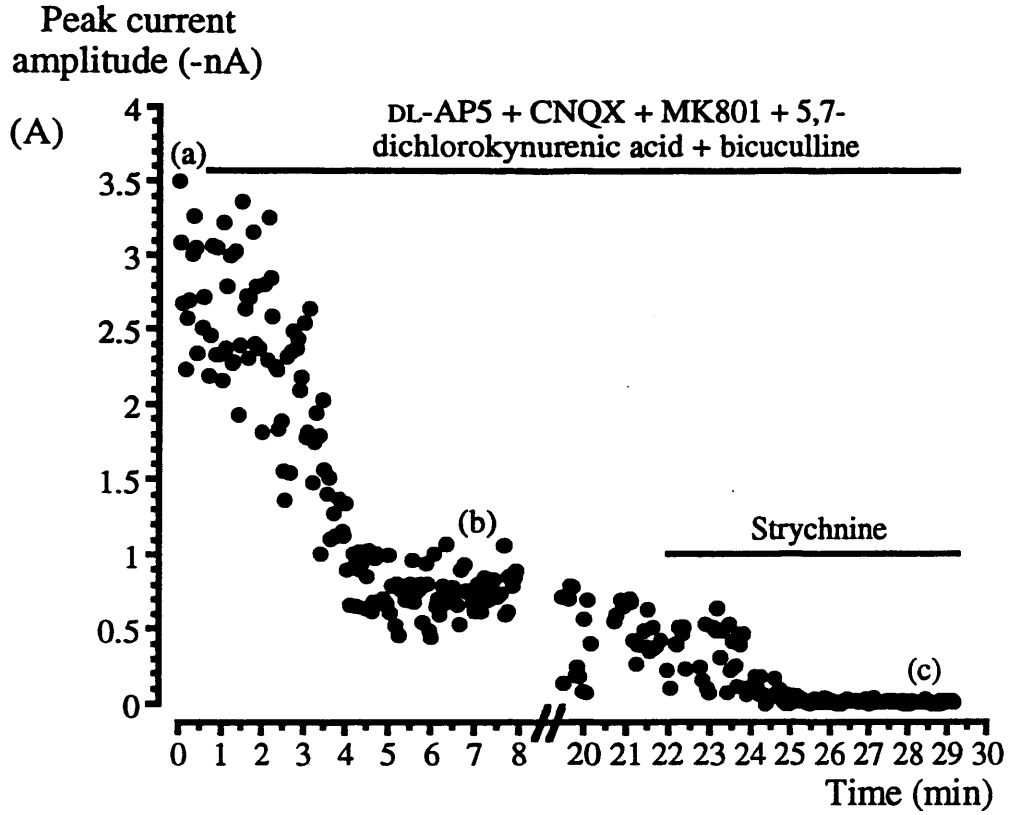
Peak current amplitude (-nA)
(A)
DL-AP5 + CNQX + MK801 + 5,7-dichlorokynurenic acid + bicuculline
(a)
(b)
Strychnine
(c)
4
3.5
3
2.5
2
1.5
1
0.5
0
0 1 2 3 4 5 6 7 8 20 21 22 23 24 25 26 27 28 29 30
Time (min)

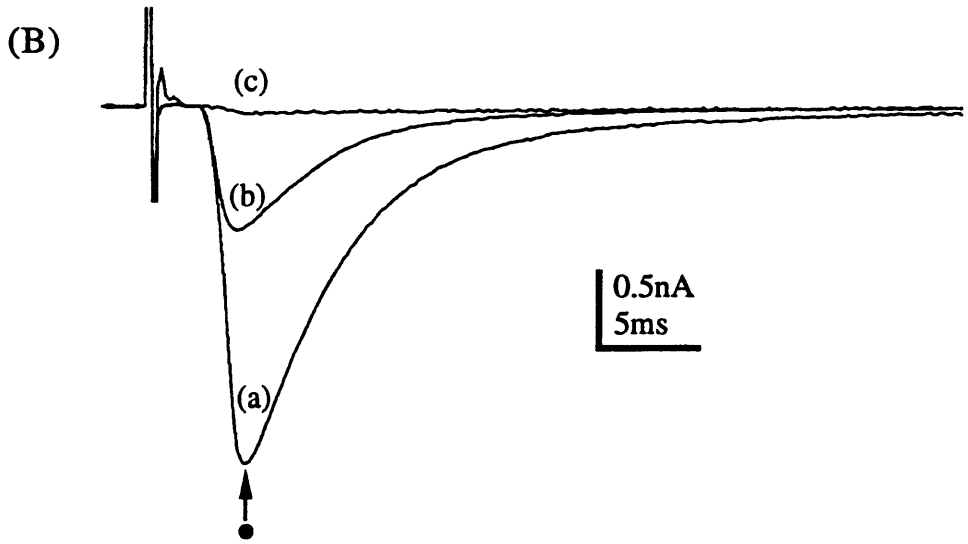
(B)
(c)
(b)
(a)
0.5nA
5ms

strychnine (Becker, Hoch & Betz, 1988) and by a shortening of the decay time constant and single channel open time (Takahashi *et al.* 1992; Krupp, Larmet & Feltz, 1994) of the glycine receptor ion channel. The change is concurrent with change in binding of monoclonal antibodies to those specific for the adult glycine receptor isoform (Friauf, Hammerschmidt & Kirsch, 1997, Becker, Hoch & Betz, 1988, Pfeiffer *et al.*, 1984).

The age of animals used in this project (6-13 days) spans the age across which this change over occurs. In order to ensure that the strychnine dose was supramaximal and in an initial attempt to identify the nature of glycine receptors present, the sensitivity of the inhibitory synaptic current to strychnine was examined. In figure 4.12 the neurone was voltage clamped at -70mV and the peak synaptic current was measured in the presence of EAA antagonists and bicuculline at the time indicated by ● in (B). The range of concentrations of strychnine applied were: 5nM, 10nM, 50nM, 100nM and 500nM. Initially, application of the EAA antagonists and bicuculline caused a rapid reduction in synaptic current amplitude. After approximately 4 minutes this reduction in amplitude slowed but did not cease, possibly resulting from further equilibration of the antagonists in the slice, or perhaps due to rundown of the synaptic current. Application of 5nM and 10nM strychnine had no additive effect on the reducing synaptic current amplitude. Application of 50nM strychnine and above further reduced the synaptic current amplitude and complete block was achieved with 500nM strychnine (n=2). The animals used on these two occasions were 9 and 10 days old. On one other occasion, using a 7 day old rat, concentrations of strychnine used were 3nM, 10nM, 30nM, 100nM, 300nM and 1μM and complete block was achieved upon 1μM strychnine application. These data confirm that the concentration of strychnine used to block the response (figure 4.10 & 4.11) was supramaximal. However, construction of a dose response curve in this preparation was difficult since equilibration of the respective strychnine concentrations into the brain slice was not possible over a reasonable time period. Difficulties in achieving equilibration of strychnine in this brain stem slice preparation meant that the sensitivity of the current to strychnine was not further investigated.

Figure 4.12 **Strychnine dose response.**

(A) Peak synaptic current amplitude and, (B) some corresponding average current traces with increasing concentrations of strychnine application. 50μM DL-AP5, 10μM CNQX, 5μM MK801, 5μM 5,7-dichlorokynurenic acid and 10μM bicuculline were applied throughout. Concentrations of strychnine included in the perfusate were: (a) None, (b) 5nM, (c) 10nM, (d) 50nM, (e) 100nM & (f) 500nM. Synaptic current amplitude was measured at the time indicated by ● in (B).

Partial block by strychnine was first observed upon application of 50nM strychnine and complete block was achieved with 500nM strychnine.

Points on graph are peak synaptic current amplitudes of individual current traces and traces are averages of 20 events each.

(A)

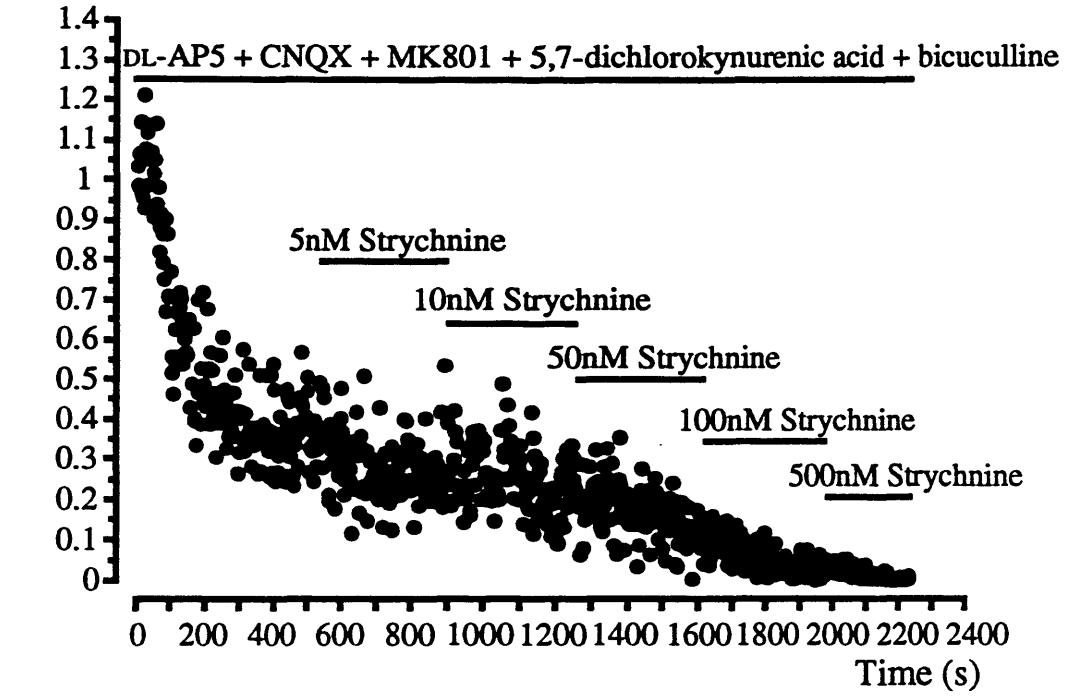
Peak Synaptic Current (-nA)
1.4
1.3
1.2
1.1
1
0.9
0.8
0.7
0.6
0.5
0.4
0.3
0.2
0.1
0
DL-AP5 + CNQX + MK801 + 5,7-dichlorokynurenic acid + bicuculline
5nM Strychnine
10nM Strychnine
50nM Strychnine
100nM Strychnine
500nM Strychnine
0 200 400 600 800 1000 1200 1400 1600 1800 2000 2200 2400
Time (s)

(B)

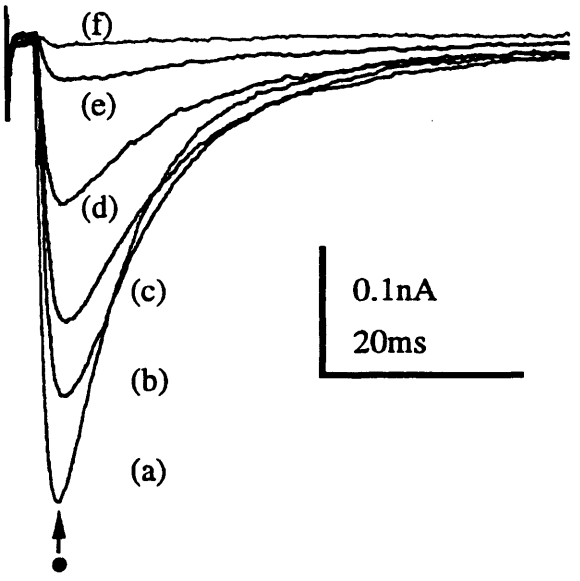
(f)
(e)
(d)
(c)
(b)
(a)
0.1nA
20ms

4.323 Block of Synaptic Transmission

At -70mV holding potential, 0.5μM tetrodotoxin (TTX) was shown to be effective at blocking the sodium current present in MSO neurones in figures 3.4 & 3.5. TTX is a voltage-activated sodium channel blocker which will block synaptic transmission (Narahashi, Moore & Scott, 1964) by preventing action potential propagation into the presynaptic terminal. Figure 4.13 shows that application of 0.5μM TTX to this preparation will block synaptic transmission between the MNTB and MSO (n=14). On all but 3 occasions EAA antagonists and bicuculline were previously included in the perfusate, blocking all but the strychnine sensitive component of synaptic transmission. Synaptic transmission on the remaining 3 occasions was also completely blocked by 0.5μM TTX without prior application of EAA antagonists and bicuculline (data not shown).

Spontaneous and Miniature Currents

Synaptic currents can be broadly divided into three categories:
1) Evoked postsynaptic currents which are generated by activation of the presynaptic neurone;
2) Spontaneous postsynaptic currents which result from the spontaneous propagation of action potentials into the presynaptic terminal; and
3) Miniature postsynaptic currents which are independent of action potential propagation into the presynaptic terminal but instead result from spontaneous release of neurotransmitter from the presynaptic terminal. Presynaptic vesicles are thought to contain a discrete quantity of neurotransmitter (Katz, 1969; del Castillo & Katz, 1954; reviewed by Korn & Faber, 1991) which when released, bind to postsynaptic receptors. Current flow resulting from this reflects the release of these discrete packets of transmitter.

So far, all the data shown in this chapter are those of evoked synaptic currents in the MSO. These currents have been blocked by various means, including the use of TTX to block voltage-activated sodium channels. Spontaneous and miniature inhibitory postsynaptic currents have also been recorded.

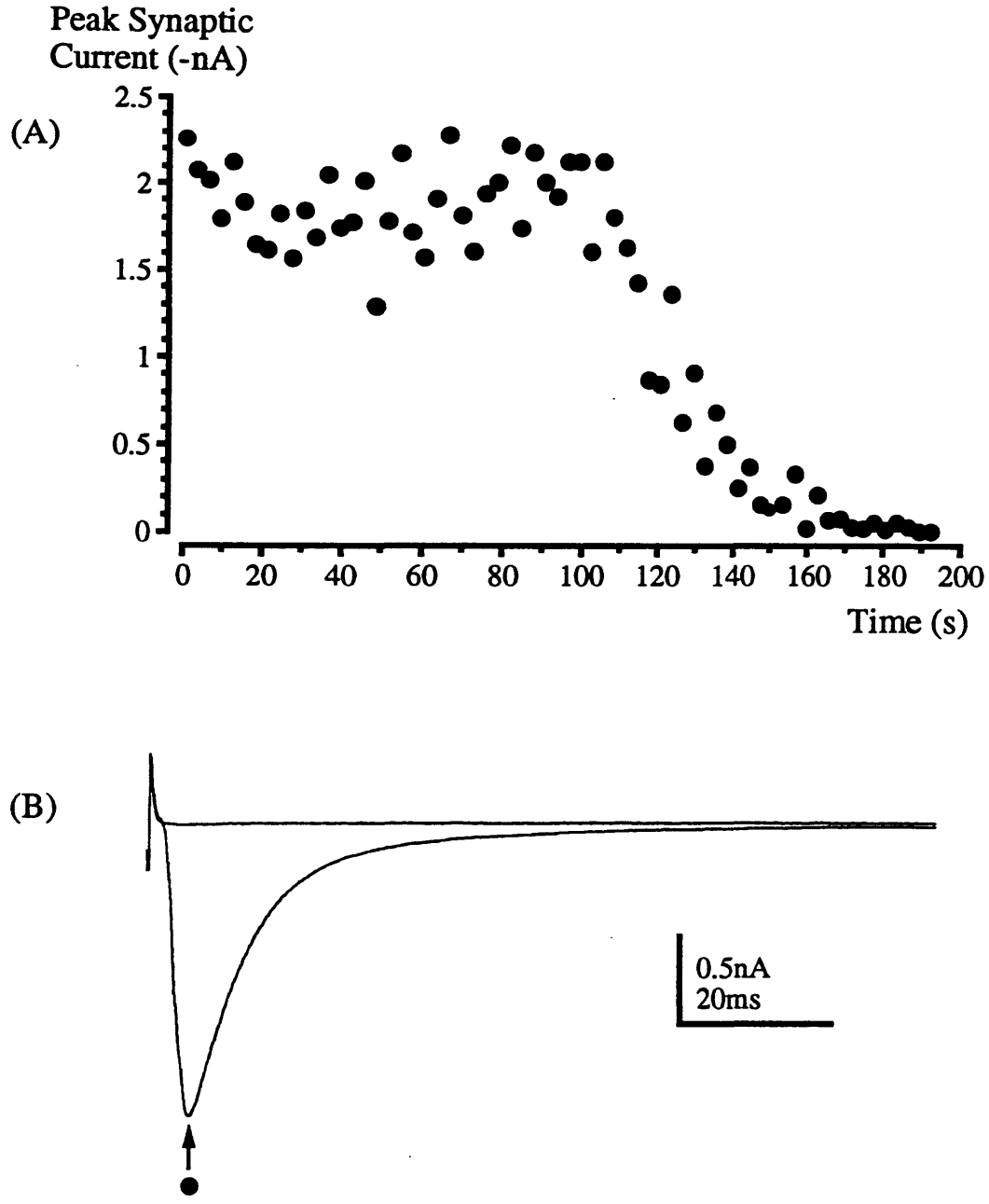

Figure 4.13 **0.5μM TTX abolishes evoked synaptic current**

(A) Peak synaptic current amplitude and , (B) two average current traces before and after inclusion of 0.5μM TTX in the perfusate. EAA antagonists and bicuculline were applied throughout. Synaptic current amplitude was measured at the time indicated by ● in (B).

Complete block of the synaptic current occured following 0.5μM TTX application. Points on graph (A) are peak synaptic current amplitudes of individual current traces and traces in (B) are averages of 10 events each.

(i) Spontaneous Inhibitory Postsynaptic Currents

The upper traces of figure 4.14 show spontaneous postsynaptic currents recorded from an MSO neurone. EAA antagonists and bicuculline were equilibrated in the slice throughout and the absence of TTX from the perfusate permitted presynaptic action potential propagation. 1μM strychnine application caused synaptic activity to reduce over time (lower traces of figure 4.14), thereby confirming a strychnine sensitive synaptic input to the MSO. Notice that many of the spontaneous events in the upper traces are as large as the evoked currents previously seen.

(ii) Miniature Inhibitory Postsynaptic Currents

The block of synaptic transmission by TTX was demonstrated in figure 4.13. In figure 4.15 all miniature postsynaptic currents were recorded in the presence of EAA antagonists and bicuculline, ensuring strychnine sensitive, glycine receptor mediated currents to be all that remained. Figure 4.15A shows four example raw data traces recorded from an MSO neurone following equilibration in EAA antagonists, bicuculline and TTX. The miniature postsynaptic currents are smaller than spontaneous currents and are also blocked by application of 1μM strychnine (figure 4.15B, n=3) offering further confirmation that the MSO receives a glycine receptor mediated inhibitory synaptic input.

The Role of Calcium in Synaptic Transmission

The involvement of the voltage-activated sodium channels in synaptic transmission is shown in figure 4.13. Their role is important but not critical because if the presynaptic neurone were to be depolarised by some other means such as regenerative calcium currents, synaptic transmission would still occur. On the other hand, transmitter release is critically dependent on calcium current activation (reviewed by Katz 1969). The involvement of calcium is shown in figure 4.16 because when $[Ca^{2+}]_o$ was lowered from 2mM to 0.1mM, synaptic transmission was abolished (n=2). Calcium influx is generated by action potentials which depolarise the presynaptic terminal, open voltage-gated calcium channels and so permit calcium entry. The increase in intracellular calcium concentration then triggers vesicle release (Borst & Sakmann, 1996).

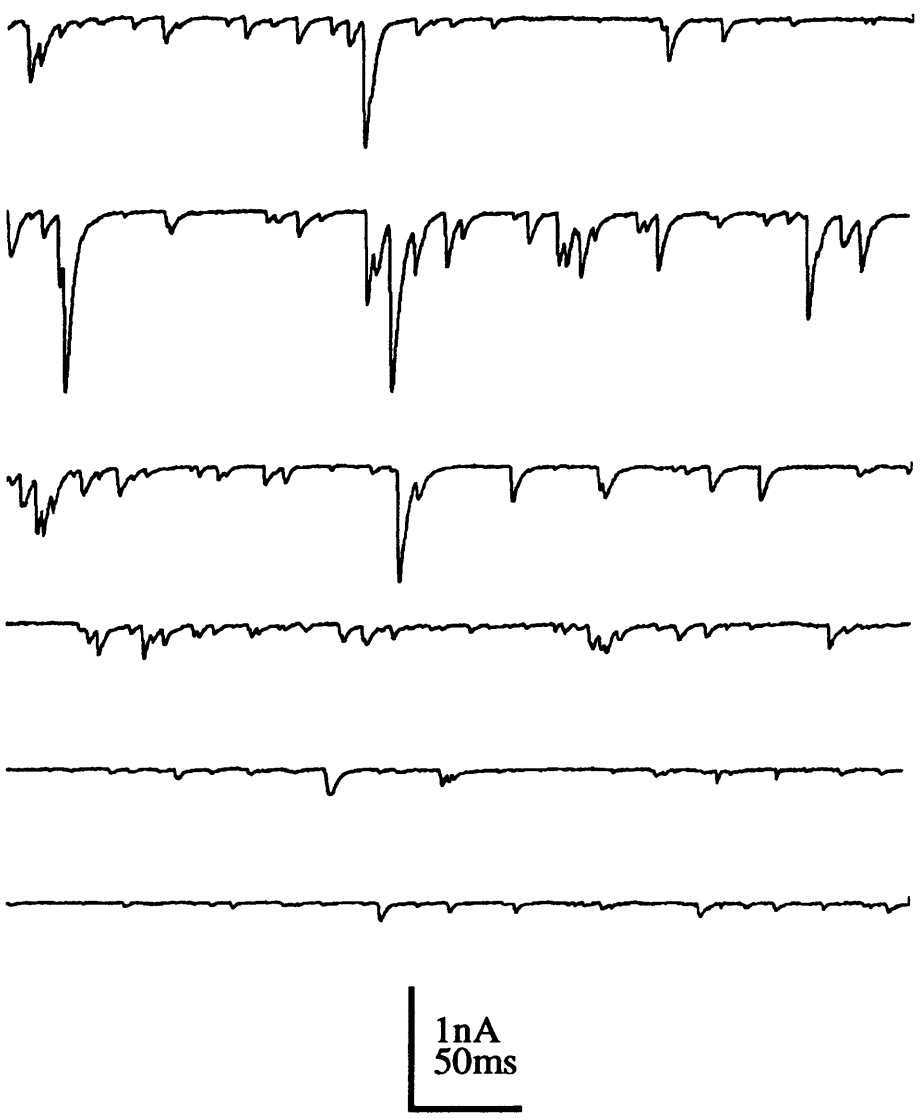

Figure 4.14 **Spontaneous inhibitory synaptic currents are blocked by 1μM strychnine**

Spontaneous inhibitory post synaptic currents (upper traces) are large in amplitude and result from spontaneous presynaptic action potential propagation. The spontaneous inhibitory postsynaptic currents are progressively blocked by 1μM strychnine (lower traces).

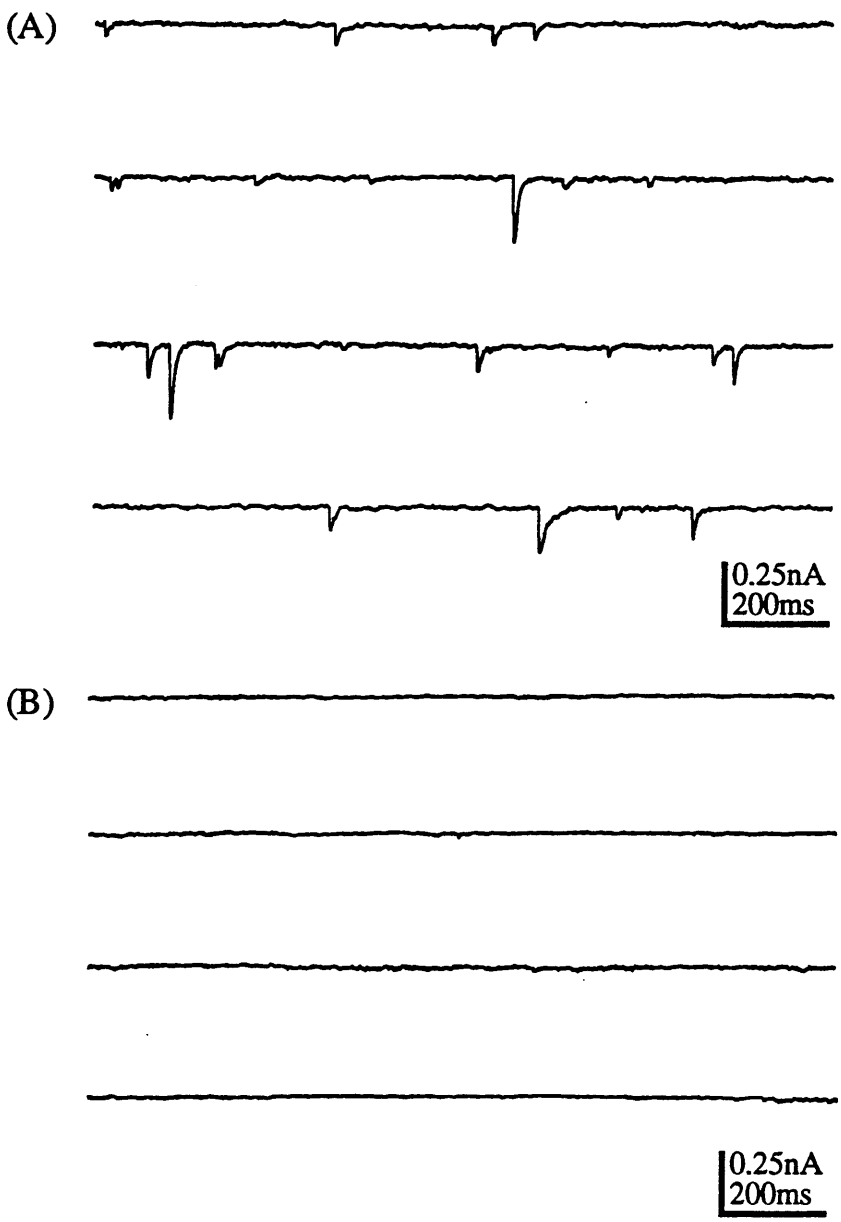

Figure 4.15 **Miniature synaptic currents are blocked by 1μM strychnine**

(A) Example raw data traces of miniature inhibitory postsynaptic currents from an MSO neurone in the presence of EAA antagonists, bicuculline and TTX.

(B) Example raw data traces following strychnine application in the presence of EAA antagonists, bicuculline and TTX.

Miniature inhibitory postsynaptic currents are blocked by 1μM strychnine.

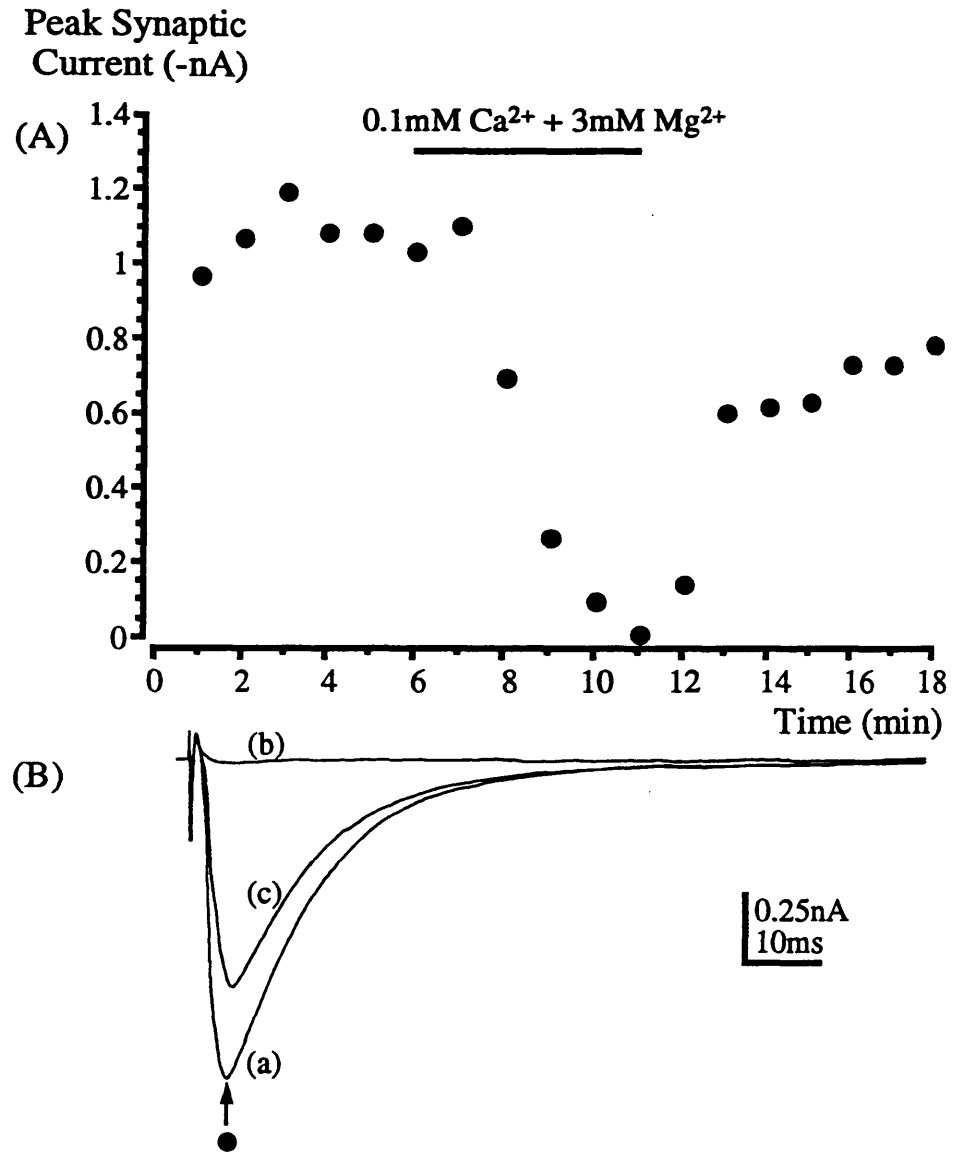

Figure 4.16 **Inhibitory postsynaptic currents are critically dependent on extracellular calcium**

(A) Average peak synaptic current plotted over time, and (B) selected corresponding mean current traces measured at the time indicated by ●: (a) in normal bicarbonate buffered ACSF containing 2mM $[Ca^{2+}]_o$ + 1mM $[Mg^{2+}]_o$, (b) in 0.1mM $[Ca^{2+}]_o$ + 3mM $[Mg^{2+}]_o$, and (c) wash out in normal ACSF containing 2mM $[Ca^{2+}]_o$ + 1mM $[Mg^{2+}]_o$.

EAA antagonists and bicuculline were included throughout. Inclusion of low calcium in the perfusate caused a reversible reduction in peak synaptic current amplitude.

Data traces and points are averages of 20 events each.

4.324 Reversal Potential

The evidence shown so far suggests that MSO neurones receive an inhibitory synaptic projection from the MNTB. The insensitivity of this current to EAA antagonists and bicuculline and its sensitivity to strychnine strongly suggest that the inhibitory synaptic current is generated by activation of glycine receptor ion channels.

Glycine receptor ion channels are anion selective and most permeable to chloride ions (Coombs, Eccles & Fatt, 1955; Bormann, Hamill & Sakmann, 1987). Measurement of the reversal potential of the miniature and evoked currents here demonstrates the dominant charge carrier of this synaptic current. When measuring the reversal potential of the synaptic current, normal bicarbonate buffered extracellular solution containing 133.5mM chloride was used throughout (appendix 1Aiii). The intracellular patch solution used when measuring the reversal potential of the miniature currents contained 132mM chloride. This concentration and two others of 34.5mM and 5.9mM chloride were used to measure the reversal potential of the evoked synaptic current. Different proportions of solutions documented in appendix 1Biii & 1Biv were used to achieve these intracellular chloride concentrations. Junction potentials (appendix 1C) were accounted for in all reversal potential calculations of the evoked inhibitory synaptic current.

The reversal potential of the miniature synaptic currents was difficult to discern as their small amplitude meant that at holding potentials near the reversal potential, the currents were indistinguishable from the noise of the trace (figure 4.17). However, the estimated reversal potential using almost equal amounts of intracellular and extracellular chloride lay between -10mV and +20mV (n=1).

A more accurate determination of the reversal potential of the evoked synaptic current was possible and was found to be +1.6±0.7mV (SEM, n=11) when $[Cl^-]_i$ was 132mM and $[Cl^-]_o$ was 133.5mM. The reversal potential when using $[Cl^-]_i$ of 5.9mM was -71.8±2.5mV (SEM, n=4), and using 34.5mM was -37.9±2.5mV (SEM, n=5). The Nernst equation (chapter *1.312*, equation 1.5 & 1.6) is used to determine the equilibrium potential of a current assuming it is carried by a single ion type. Figure 4.18B shows a semi-logarithmic plot of the measured reversal potential of the evoked synaptic currents using different intracellular chloride concentrations (points ± SEM). On the same plot, the line demonstrates the equilibrium potential calculated using the Nernst equation assuming chloride to be the only charge carrier. Figure 4.18A shows some example average evoked current traces produced using different

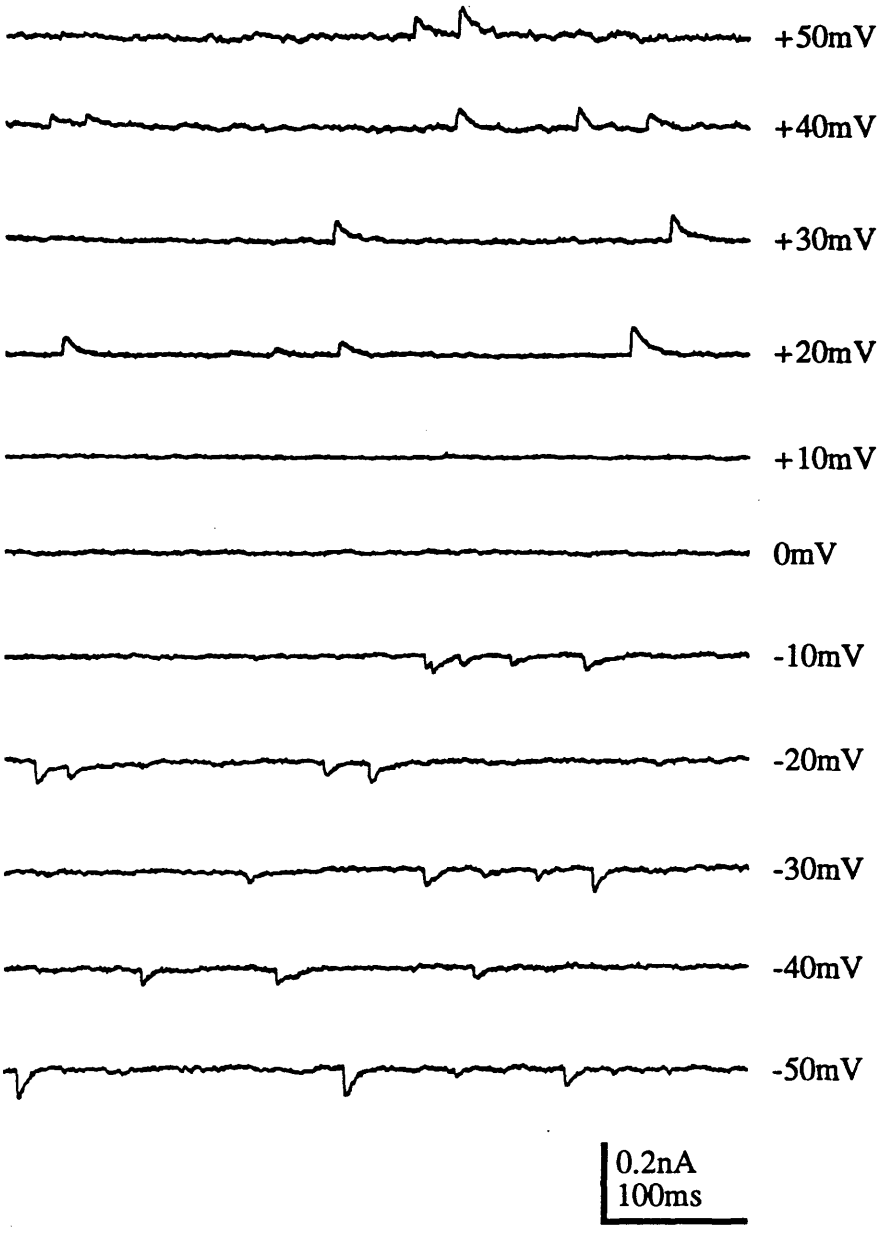

Figure 4.17 **Reversal potential of miniature inhibitory postsynaptic currents.**

Raw current traces recorded from an MSO neurone in the presence of EAA antagonists, bicuculline and TTX. Neurone was voltage clamped across a range of holding potentials and reversed between -10mV and +20mV (n=1).

Figure 4.18 **Evoked synaptic current reverses around the chloride equilibrium potential.**

(A) Average current traces recorded from an MSO neurone in different $[Cl^-]_i$ at various holding potentials, and (B) semi-logarithmic plot demonstrating the average reversal potential using three different $[Cl^-]_i$ (points ± SEM) and the chloride equilibrium potential (line).

$[Cl^-]_o$ was maintained at 133.5mM and EAA antagonists and bicuculline were included in the perfusate throughout. Reversal potential when $[Cl^-]_i$ was: 5.9mM was -71.8±2.5mV (SEM, n=4); 34.5mM was -37.9±2.5mV (SEM, n=5); 134.5mM was +1.6±0.7mV (SEM, n=11).

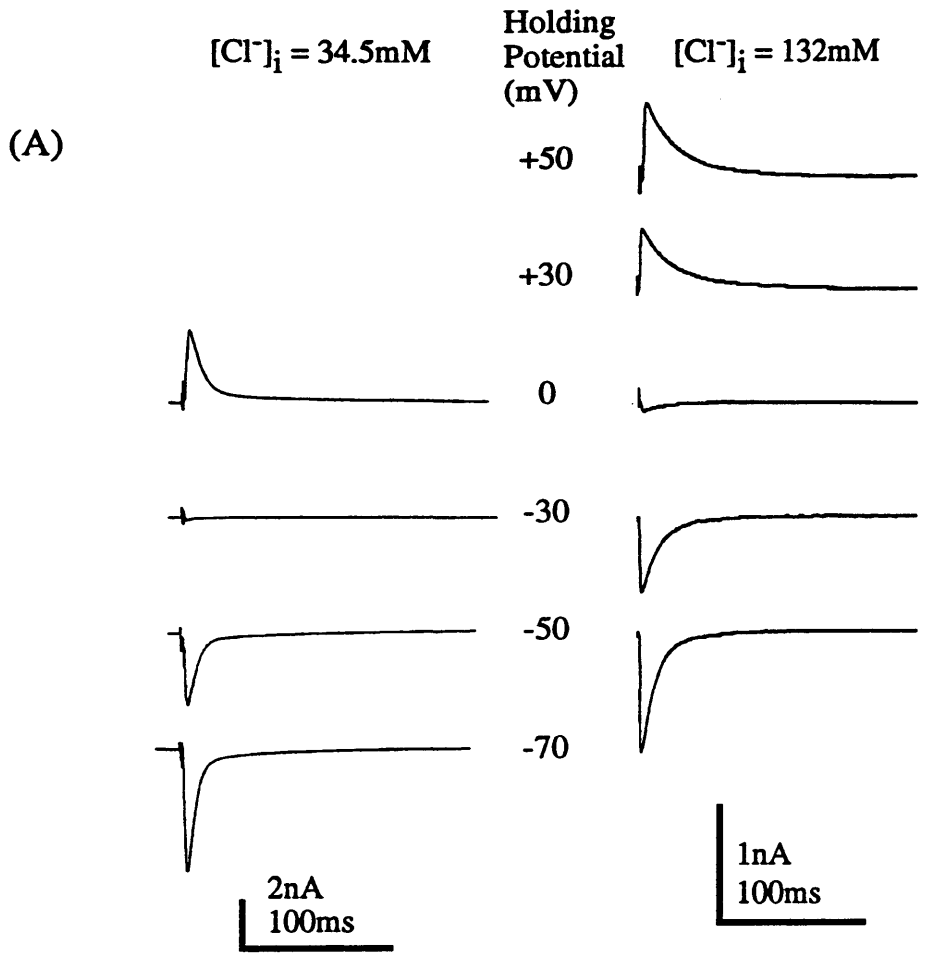
(A)
$[Cl^-]_i$ = 34.5mM
Holding Potential (mV)
$[Cl^-]_i$ = 132mM
+50
+30
0
-30
-50
-70
2nA
100ms
1nA
100ms

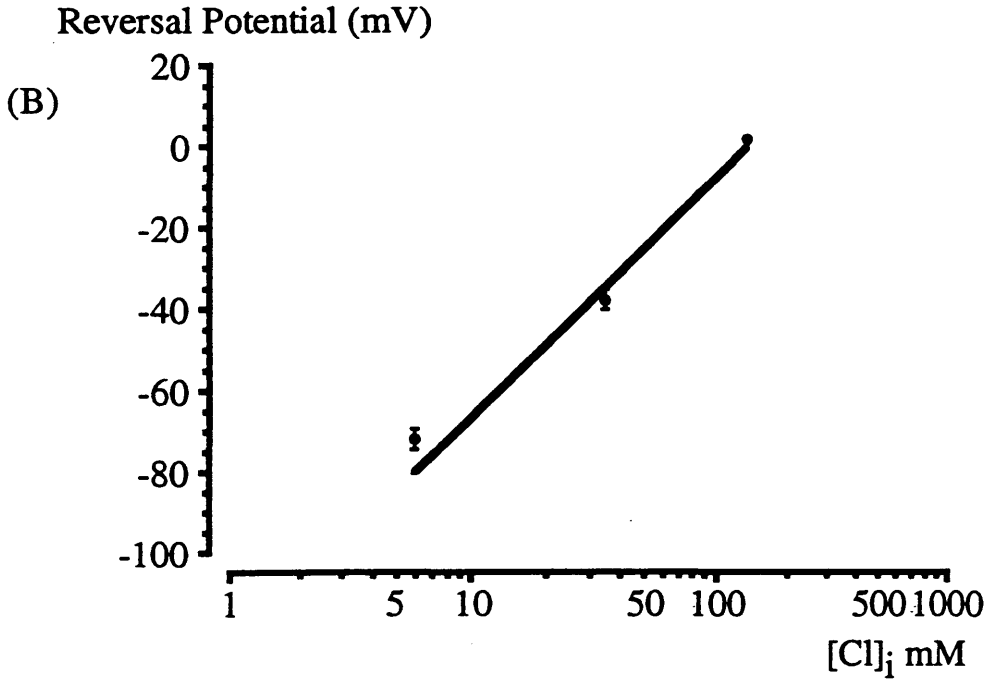
(B)
Reversal Potential (mV)
20
0
-20
-40
-60
-80
-100
1
5
10
50
100
500
1000
$[Cl]_i$ mM

intracellular chloride concentrations. The measured reversal potentials are very similar to the equilibrium potential calculated using the Nernst equation, confirming chloride to be the dominant charge carrier of this synaptic current.

4.4 Summary and Discussion

Major findings of this chapter:

- The MSO nucleus receives an excitatory synaptic projection which is mediated by NMDA and non-NMDA receptors.
- The non-NMDA receptors have similar characteristics to Ca^{2+} permeable AMPA receptors reported elsewhere.
- The MSO receives an inhibitory synaptic projection from the ipsilateral MNTB.
- The inhibitory synaptic current is blocked by strychnine and reverses around the chloride equilibrium potential so is likely to be mediated by glycine receptors.

Bilateral excitatory and unilateral inhibitory synaptic inputs to the MSO are well established but extensive intracellular study of these has not been done. This chapter has gone some way into investigating some of the characteristics of two of these response types, namely the inhibitory input from the ipsilateral MNTB and the excitatory input from the contralateral AVCN. This was achieved by making whole cell patch clamp recordings from MSO neurones whilst stimulating the ipsilateral MNTB using a bipolar platinum stimulating electrode (chapter *2.25*). The circuitry of the auditory brain stem means that gross stimulation of this nature resulted in excitatory and inhibitory synaptic current generation. . The excitatory input was found to be mediated by NMDA and non-NMDA receptors and the inhibitory input was mediated by glycine receptors.

This demonstration of excitatory and inhibitory synaptic inputs to the MSO supports the long established contribution this nucleus makes to sound source localisation. Much evidence has been documented that the MSO receives a bilateral excitatory input which contributes greatly to the establishment of delay lines in its role of detecting interaural time differences (ITDs) (e.g. Jeffress, 1948; Crow *et al.*, 1978; Goldberg & Brown 1969). The involvement of the inhibitory synaptic input is less well documented but the data presented here clearly

demonstrate its existence, suggesting it too may play an important role in sound source localisation.

4.41 Synaptic Transmission

Excitatory and inhibitory synaptic transmission share some common characteristics. Application of the voltage activated sodium channel blocker, 0.5μM TTX (Narahashi, Moore & Scott, 1964) was found to block synaptic transmission in this preparation. This occurred since block of voltage activated sodium currents prevents generation of an action potential and propagation into the synapse. However, depolarisation by some other means, such as regenerative calcium currents could permit action potential propagation despite the presence of TTX. So, whilst activation of voltage-gated sodium channels are important for action potential propagation, they are only indirectly essential for exocytosis.

Comparatively, calcium current entry into the presynaptic terminal is essential for transmitter release, and therefore synaptic transmission. Action potential propagation in the presynaptic terminal causes depolarisation which results in the opening of voltage-gated calcium channels. This then allows calcium entry into the presynaptic terminal, which in turn triggers neurotransmitter release (Borst & Sakmann, 1996; reviewed by Katz, 1969). The importance of extracellular calcium was demonstrated here where it was observed that lowering extracellular calcium from 2mM to 0.1mM abolished synaptic transmission.

4.42 Excitatory Synaptic Transmission

Pharmacological isolation of the excitatory component was achieved by application of the glycine receptor antagonist, strychnine and the $GABA_A$ receptor antagonist, bicuculline. The current voltage relationship then revealed two components of excitatory synaptic transmission. One component was very similar to that of a non-NMDA receptor mediated current and the other to that of an NMDA receptor mediated current (Forsythe & Barnes-Davies, 1993b, Mayer, Westbrook & Guthrie, 1984). Each was pharmacologically isolated and its physiological characteristics examined.

4.421 Non-NMDA Receptor Mediated Excitatory Synaptic Transmission

Examination of the non-NMDA receptor mediated current suggests the presence of Ca^{2+} permeable AMPA receptors. The lines of evidence supporting this are as follows. If the channel were only and equally permeable to monovalent cations, the reversal potential would be expected to be around 0mV. Instead it was found to be relatively positive (+7.8±1.4mV, SEM, n=4) and was very similar to that reported in MNTB neurones (Forsythe & Barnes-Davies, 1993b). Sensitivity to polyamines and the relatively positive reversal potential of the current has led to the suggestion of Ca^{2+} permeable AMPA receptors mediating part of the excitatory synaptic current in MNTB neurones (Barnes-Davies & Forsythe, 1996). Intracellular polyamines (e.g. spermine, spermidine, putrescine) are known to block Ca^{2+} permeable AMPA receptors at positive holding potentials (reviewed by Forsythe, 1995) and in the MSO here, the non-NMDA receptor mediated current also showed some rectification at positive holding potentials (figures 4.1 & 4.4). The rectification may have resulted from polyamines which are present intracellularly in free concentrations ranging from 10-100μM (reviewed by Forsythe, 1995). However, polyamines were not included in the intracellular patch solution so would not be expected to have an effect here. A possible explanation for this could be the presence of dendritically located Ca^{2+} permeable AMPA receptors where complete dialysis of the neurone may not have been achieved. Since excitatory inputs to the MSO have been shown to occur at the dendritic tree, this explanation is possible. Confirmation of calcium permeability was not conducted in this study although an examination of the effect of changing $[Ca^{2+}]_o$ on the reversal potential of the synaptic current would demonstrate its involvement.

AMPA receptor ion channels are pentameric structures and their kinetics are determined by the relative expression of the flip and flop versions GluRA, B, C or D. AMPA receptors with the fastest kinetics express high levels of the GluRD subunit. GluRB subunits in their edited form at the Q/R site on transmembrane segment II are widely expressed throughout the CNS. Inclusion of the edited form of the GluRB subunit to the AMPA receptor confers calcium impermeability to the channel. However, in some places in the CNS, GluRB is either undetectable or present in small concentrations. In this situation, the AMPA receptors are Ca^{2+} permeable. So, the level of expression of the GluRB subunit determines the calcium permeability of the AMPA receptor (reviewed by Seeburg, 1993).

Conventionally, the fast kinetic nature of AMPA receptors was thought to confer lack of calcium permeability, thereby preventing the initiation of any long term biochemical changes occurring. Although impermeability of AMPA receptors to calcium is most common in the CNS, the mammalian and avian auditory pathways as well as a few other pathways in the CNS (e.g. cerebellar Bergman glial cells) express high levels of Ca^{2+} permeable AMPA receptors (mammalian: Barnes-Davies & Forsythe, 1996; Wang *et al.*, 1998; Geiger *et al.*, 1995; avian: Otis, Raman & Trussell, 1995). The question therefore remains of what they may be doing in the auditory system? In the MNTB, AMPA receptors underlie large rapidly decaying EPSPs (Forsythe & Barnes-Davies, 1993b) which in turn cause the secure generation of a single action potential (Forsythe & Barnes-Davies, 1993b, Brew & Forsythe, 1995; Wang *et al.*, 1998). This security in single action potential generation then contributes to the high reliability and temporal fidelity in this pathway. MSO neurones have been shown to have a similar single action potential generation as MNTB neurones (Smith, 1995; Brew & Forsythe, 1996) and so AMPA receptors could be performing the same function here. The calcium permeability of the AMPA receptors present in the auditory pathway may be contributing to temporal fidelity in this system at least in part by facilitating the termination of the excitatory postsynaptic potential through activation of calcium dependent potassium channels (Geiger *et al.*, 1995).

Elevated intracellular Ca^{2+} has also been implicated in long term potentiation (LTP) and excitotoxicity. So, the combination of Ca^{2+} permeable AMPA receptors and NMDA receptors (which are Ca^{2+} permeable and are implicated in LTP and excitotoxicity) may provide a route for calcium entry allowing pathological or physiological changes to occur.

4.422 NMDA Receptor Mediated Excitatory Synaptic Transmission

The NMDA-receptor mediated synaptic current displayed characteristics very similar to those previously reported in the MNTB (Forsythe & Barnes-Davies, 1993b) and was found to reverse at +12.3±2.3mV (SEM, n=4). This relatively positive reversal potential again probably results from the NMDA receptor ion channel complex being a relatively non-selective cation channel allowing Na^+ and Ca^{2+} ion influx and K^+ ion efflux (reviewed by Ascher & Johnson, 1994).

The NMDA receptor possesses several unique features. As shown in figure 4.5, it is subject to a voltage dependent magnesium block such that at negative holding potentials, there is a marked rectification of current flow. So, activation of non-NMDA receptors will depolarise

the membrane thereby relieving the voltage dependent magnesium block that NMDA receptors are subject to. In addition, NMDA receptors are activated by polyamines. For example spermine has been shown to enhance NMDA receptor mediated responses in cultured striatal neurones (Sprosen & Woodruff, 1990). The NMDA receptor also possesses a glycine binding site whose binding is both a necessity for activation of the NMDA receptor (Kleckner & Dingledine, 1988) and whose occupancy enhances NMDA receptor mediated responses (Johnson & Ascher, 1987). This glycine binding site is distinct from that mediating inhibitory responses since it is insensitive to strychnine. Calcium permeability of NMDA receptor ion channels is a particularly important feature of these channels and is thought to underlie their role in synaptic plasticity and excitotoxicity (reviewed by Collingridge & Watkins, 1994).

4.43 Inhibitory Synaptic Transmission

Pharmacological isolation of the strychnine sensitive inhibitory synaptic current was achieved through application of EAA antagonists (50μM DL-AP5, 10μM CNQX, 5μM MK801, 5μM 5,7-dichlorokynurenic acid) and the $GABA_A$ receptor antagonist, 10μM bicuculline. Other than for examination of the reversal potential of the synaptic current the intracellular patch solution contained 132mM chloride (appendix 1Biii) and the extracellular solution contained 133.5mM chloride (appendix 1Aii). When voltage clamping at -70mV, the inhibitory synaptic current using these solutions was inward. It was found that with increasing stimulus intensity, recruitment of synaptic inputs occurred as a result of the gross method of stimulation used. Alternative techniques were tried by both attempting to stimulate individual presynaptic MNTB neurones with a glass electrode and by using minimal stimulation with the bipolar platinum stimulating electrode. Both methods were problematic so gross stimulation using the bipolar platinum stimulating electrode such that the synaptic currents were ~1nA amplitude were used throughout.

Following application of EAA antagonists and bicuculline, stimulation of the MNTB resulted in a synaptic current which was abolished by application of the glycine receptor specific antagonist, 1μM strychnine. This finding suggested it to be a glycine mediated synaptic current, consistent with observations previously reported (e.g. Smith, 1995; Grothe & Sanes, 1993, 1994; Smith & Forsythe, 1996, 1997). Further experiments confirmed this finding since the reversal potential using different intracellular chloride concentrations was very similar to the equilibrium potential predicted by the Nernst equation when assuming chloride to be the

only charge carrier. Since glycine receptor ion channels are primarily selective for chloride ions, this finding supports chloride to be the dominant charge carrier of the inhibitory synaptic current. Slight deviation of the reversal potential from the equilibrium potential can be observed, suggesting that other charge carriers may be minimally contributing to the synaptic current. This observation warrants further investigation but is unsurprising since most ion channels are at least in part, permeable to more than one ion. It is likely that in addition to permeability to chloride, this ion channel is also permeable to other anions such as bicarbonate (Coombs, Eccles Fatt, 1955; Bormann, Hamill & Sakmann, 1987).

4.431 Physiological Implications of Inhibitory Synaptic Transmission to the MSO

The MSO clearly receives an inhibitory synaptic input from the MNTB which is largely mediated by glycine receptor ion channels. As mentioned previously, the MSO forms a part of the binaural pathway and is involved in sound source localisation. However, traditional and even more recent models of sound source localisation do not necessitate an inhibitory synaptic input so its role in coincidence detection and sound source localisation is not well established. The question of what role this inhibitory input may be playing must therefore be addressed.

Two possible roles for the inhibitory input involve it acting by some form of surround inhibition to fine tune an excitatory response. Firstly, according to Jeffress (1948) sound source localisation requires the detection of coincidence of excitatory synaptic inputs. Thus, when a sound arrives at the two ears, neurones responding within the auditory pathway will respond optimally to particular interaural time differences (ITDs) and will fire an action potential. Yin & Chan (1990) proposed the first mammalian map of these ITDs in the MSO such that the anterior pole responded to very small ITDs (~0μs) and the dorsal pole will respond optimally to longer ITDs. Although each neurone responded optimally to a particular ITD they found that surrounding neurones would also respond but to a lesser extent and that they too would have their own optimal ITD. In other words a peak ITD response curves exists for the MSO. From this Yin & Chan (1990) proposed that the inhibitory input sharpens the ITD response curve by hyperpolarising neurones surrounding the neurone responding maximally to a particular ITD. The second possible role involving surround inhibition in the MSO is its action on the response of neurones to different frequencies of sound. It is established that the projection from the MNTB to the MSO is tonotopically organised (Guinan, Norris & Guinan, 1972, Kuwabara & Zook, 1992) such that MNTB neurones responding

optimally to low frequency sounds project to specific low frequency regions of the MSO. Similarly, the excitatory inputs are also tonotopically organised (reviewed by Cant, 1991). However, despite this tonotopic organisation it is possible that inhibitory and excitatory inputs have different characteristic frequencies. This could mean that in addition to reducing a neurone's response to ITDs other than its optimal ITD, the inhibitory input may be reducing the likelihood of a neurone firing an action potential at a frequency other than its characteristic frequency. Essentially, the inhibitory input may be fine tuning and sharpening the synaptic integration of the excitatory response. Indeed, such a role for the unilateral $GABA_A$ receptor mediated inhibitory input to the chick nucleus laminaris has been postulated by Funabiki, Koyano & Ohmori (1998) where the decay time course of excitatory synaptic inputs were found to accelerate upon GABA application such that the window of coincidence detection was sharpened. Such a function of the inhibitory response is not incorporated into most biophysical models of the MSO. Colburn, Han & Culotta (1990) did however acknowledge that whilst in their model inhibitory inputs were not essential for coincidence detection, that they are present in the physiological system and may be somehow involved in temporal processing and function to modulate the excitatory synaptic pathway. Further modelling work by Han & Colburn (1993) supported this idea by suggesting that the inhibitory input provides relatively slow (tenths of seconds), long term adjustments to the excitatory input, a function which could be useful in tuning the cell population to particular directions, frequencies or levels. Brughera *et al.* (1996) more recently incorporated inhibitory inputs to their model of MSO function but failed to prescribe a role to the inhibition. However they did suggest it to be involved in localisation of transient stimuli rather than steady state tones.

An additional role of the inhibitory synaptic input to the MSO is its involvement in the maintenance of high fidelity transmission of auditory timing information. As mentioned in chapter *3*, this maintenance is highly dependent on the generation of a single action potential in response to a depolarising current pulse. The role of the basic membrane properties is discussed in that chapter but the inhibitory input may also play a part in this process. Excitatory synaptic transmission has a faster time course than inhibitory synaptic transmission (see chapter *5*). If the excitatory response occurs before the inhibitory response *in vivo*, the neurone will be left for a period of time in a relatively hyperpolarised state following excitatory input. This will then act to reduce the likelihood of further action potential generation in the MSO neurone limiting the rate of arrival of localisation information and so improving temporal fidelity of the system.

This inhibitory input may also play a developmental role in the auditory system. Kandler & Friauf (1995) found that during early development, the strychnine sensitive glycine mediated current was depolarising and became hyperpolarising upon maturation. The glycine induced depolarisations could be activating voltage activated calcium channels previously reported in early postnatal LSO (Schmanns & Friauf, 1994), thereby increasing intracellular calcium concentrations. The pathway between the MNTB and LSO may therefore be transiently acting in an excitatory manner and therefore be using some Ca^{2+}-dependent cellular mechanisms known to be involved in strengthening and reshaping excitatory connections (Malenka, 1994). No such investigation was conducted here but a similar feature may occur and be contributing to the developmental status of the neurones.

An interesting demonstration of the involvement of the inhibitory input to the MSO in coincidence detection was proposed by Grothe & Sanes (1993, 1994) who proposed that in addition to coincidence of excitatory synaptic transmission, synaptic inhibition is also important in the functioning of the MSO as a coincidence detector. They found at low stimulus amplitudes synaptic inhibition did not play a role but at higher stimulus intensities, synaptic inhibition was recruited. They found inhibitory inputs at high stimulus intensities to prolong the refractory period following the first of two pulses, limiting the rate of action potential generation to high frequency stimulation. It is possible that response to ITDs is somewhat level dependent because in human psychoacoustic experiments ITD, sensitivity has been shown to be partially dependent on stimulus level such that humans perform less precisely at low sound levels but between 50 and 90dB their resolution was better (Zwislocki & Feldman, 1956; Hershkowitz & Durlach, 1969).

Finally it must also be mentioned that the inhibitory input may not be playing a role in temporal coding of auditory information but may serve some other function. For example, Grothe *et al.*, (1992) reported a largely monaural excitatory and inhibitory input to MSO of the mustached bat which may contribute to its high frequency echolocating abilities.

.....

In summary, whilst the involvement of excitatory synaptic inputs to the MSO and its role in detection of ITDs is well established, the involvement of the inhibitory input is complicated and not yet clearly understood. Since the involvement of the MSO in sound source localisation relies heavily on precise timing of the inputs, *in vitro* experiments are subject to a fundamental

flaw in that the combination of the timing of excitatory and inhibitory synaptic inputs cannot be examined since the precise time of their activation *in vivo* is unknown. Consequently, a clear role for the inhibitory input has not yet been established. To achieve this, intracellular *in vivo* experiments need to be conducted in order to examine the response of MSO neurones to the combination of excitatory and inhibitory inputs.

Chapter 5 - Results

5 Results

5.1 Introduction

Chapters 3 and 4 provided some detail of the basic physiology and pharmacology of the MSO nucleus and the synaptic inputs it receives. This chapter focuses on the inhibitory synaptic current resulting from activation of principal neurones of the ipsilateral MNTB.

The chapter begins by documenting some basic characteristics of the decay of the evoked inhibitory synaptic current, including its double exponential time course and the relative contributions made by the fast and slow components of that time course. Voltage and temperature dependencies of the decay time course are also investigated.

The decay time course is noted to show a great deal of variability between neurones so the remainder of the chapter examines possible explanations for this variability. Particular attention is paid to any age dependent change which may occur because as described in chapter *1.22*, until around 3 weeks post partum there is a developmental change in glycine receptor subunit expression from the neonatal, α_2 to the adult, α_1 subunit. In addition to pharmacological and immunohistochemical evidence of change over during this period (Friauf, Hammerschmidt & Kirsch, 1997; Akagi & Miledi, 1988; Becker, Hoch & Betz, 1988) the single channel open time of glycine receptor ion channels and the decay time course of evoked glycine mediated synaptic currents have also been demonstrated to decrease (Takahashi *et al.*, 1992; Krupp, Larmet & Feltz, 1994).

Investigations were also conducted to determine if differential location of synaptic inputs was responsible for the observed variability of the decay time course by examining any correlation between rise time and half width and the speed with which the evoked synaptic current switches off. Further examination was also conducted of miniature currents which underlie the evoked synaptic current to see if they revealed distinct synaptic receptor locations.

5.2 **Methods**

The whole cell patch clamp technique and brain stem slice preparation described in chapter 2 were used throughout. To isolate the strychnine-sensitive component of the synaptic response, EAA antagonists (50μM DL-AP5, 10μM CNQX, 5μM 5,7-dichlorokynurenic acid and 5μM MK801) and 10μM bicuculline were included in the perfusate throughout. A bipolar platinum stimulating electrode (chapter *2.25*, figure 2.12) was used to evoke synaptic currents and a CsCl-based intracellular patch solution containing 132mM Cl^- (appendix 1Biii) and bicarbonate buffered extracellular solution containing 133.5mM Cl^- (appendix 1Aii) were used throughout.

Evoked synaptic current data were acquired and filtered as described in chapter *2*. Miniature currents were initially recorded onto a Digital Tape Recorder (DTR-1404) and were later filtered and digitised at 5kHz and 40kHz, respectively. Miniature data were acquired and analysed using a suite of software called 'Viewmenu', written by Dr. D. Maconochie.

5.3 **Results**

5.31 Characteristics of the Decay Time Course of the Evoked Synaptic Current.

Decay Time Course of the Evoked Synaptic Current

The decay of the evoked synaptic current was fitted by a double exponential function ($F_n=A + Be^{(-t/C)} + De^{(-t/E)}$) (e.g. figure 5.1A). At -70mV holding potential the fast and slow components of the double exponential were fitted with mean time constants of 8.54±0.44ms and 41.50±1.84ms, respectively (SEM, n=81).

The Decay Time Course Shows Some Variability Between Neurones

The decay time constants of the evoked synaptic current were very variable between neurones. Figure 5.1Bi & ii shows 2 example average data traces and their corresponding fits from a holding potential of -70mV. The neurone in figure 5.1Bi was fitted by time constants of 21.1ms and 57.8ms whilst the neurone in figure 5.1Bii was fitted by time constants of 5.5ms and 74.6ms. The range of time constants by which the fast component decayed was between

Figure 5.1 **The inhibitory evoked synaptic current decays over a double exponential time course.**

(A) An example evoked inhibitory synaptic current, the decay of which was fitted by a double exponential function: $F_n=A + Be^{(-t/C)} + De^{(-t/E)}$, where A = base line amplitude, B = amplitude of the first component, C = time course of the first component, D = amplitude of the second component, E = time course of the second component.

(B) Two different example average data traces fitted by double exponential functions. Decay time constants were variable between neurones such that at -70mV holding potential the fast time constant varied from 2.62 to 29.09ms (n=81) and the slow time constant ranged from 10.63 to 99.97ms (n=81). (i) and (ii) represent two extremes of decay time course. The current trace in (i) was fitted with a fast decay time constant of 21.1ms and a slow decay time constant of 57.8ms. The current trace in (ii) was fitted with a fast decay time constant of 5.5ms and a slow decay time constant of 74.6ms.

The mean time constants of the fast and slow components were 8.54±0.44ms and 41.50±1.84ms, respectively (SEM, n=81).

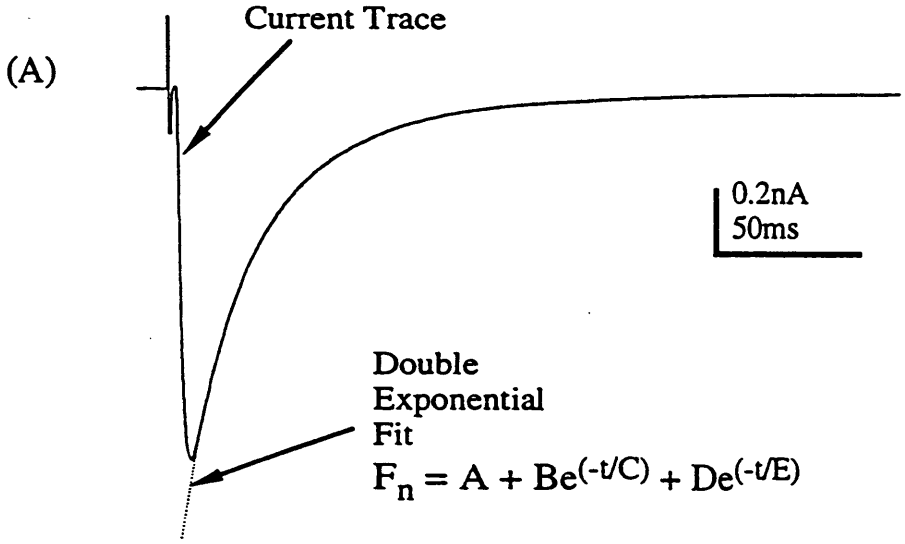
(A)
Current Trace
0.2nA
50ms
Double
Exponential
Fit
$F_n = A + Be^{(-t/C)} + De^{(-t/E)}$

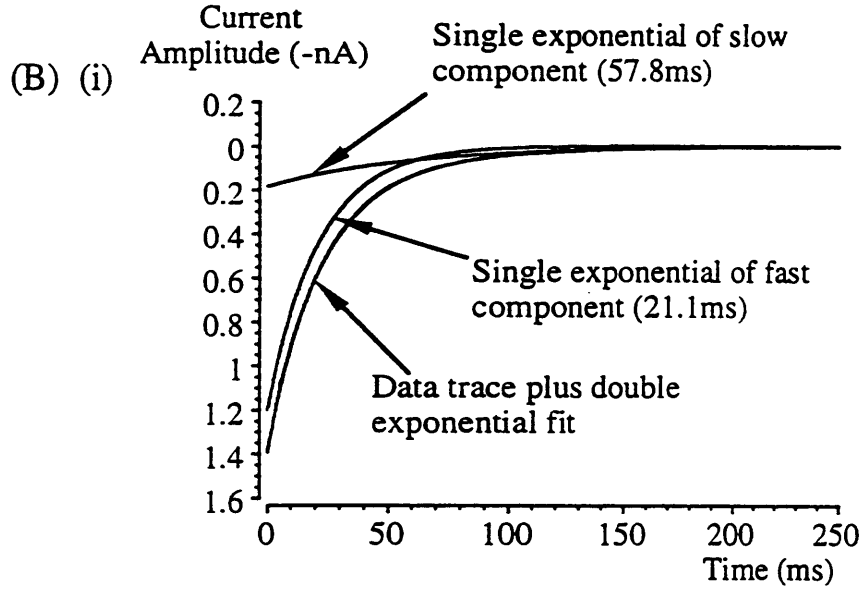
(B) (i)
Current
Amplitude (-nA)
Single exponential of slow
component (57.8ms)
Single exponential of fast
component (21.1ms)
Data trace plus double
exponential fit
0.2
0
0.2
0.4
0.6
0.8
1
1.2
1.4
1.6
0
50
100
150
200
250
Time (ms)

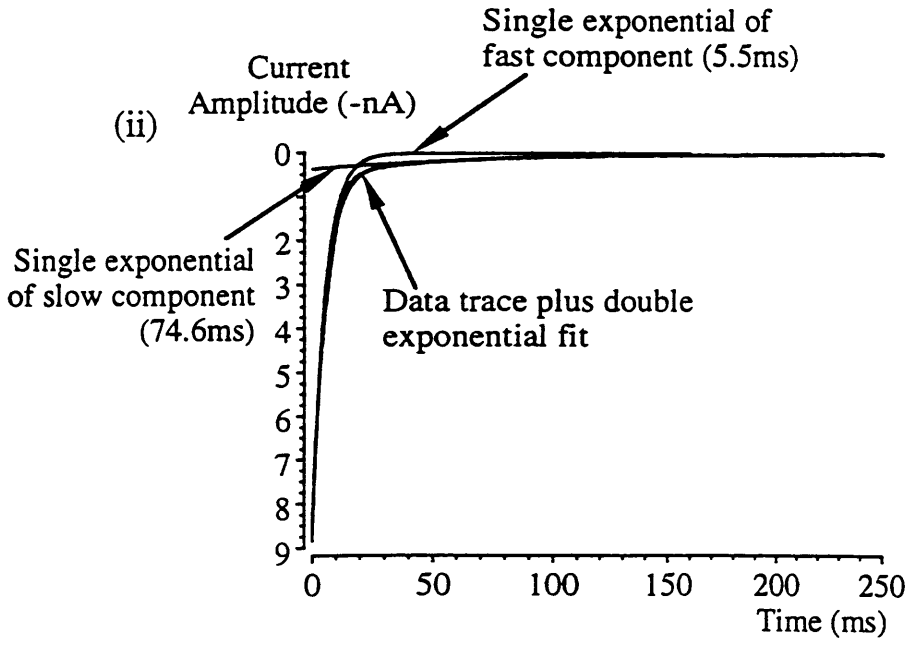
(ii)
Current
Amplitude (-nA)
Single exponential of
fast component (5.5ms)
Single exponential
of slow component
(74.6ms)
Data trace plus double
exponential fit
0
2
3
4
5
6
7
8
9
0
50
100
150
200
250
Time (ms)

2.62 and 29.09ms (n=81). An even larger variability was observed for the slow component of the synaptic current where the time constant lay between 10.63 and 99.97ms (n=81).

The Evoked Synaptic Current is Voltage Clamped Throughout the Length of its Decay

To determine if the slow component of decay was real or resulted from poor voltage control of the dendritic compartment of the neurone, a protocol described by Pearce (1993) was employed. The purpose of the protocol was to check that the synaptic current was voltage clamped and that the ion channels were open throughout the time course of the synaptic current. Pharmacological isolation of the inhibitory synaptic current was first achieved and its reversal potential determined (~0mV, see chapter *4.324*). The neurone was then voltage clamped at -70mV relative to the reversal potential (~-70mV) and a synaptic current generated by stimulation of the MNTB. The neurone was next voltage clamped at the reversal potential and the same synaptic input stimulated. No synaptic current was observed at the reversal potential since no net current flows through the ion channels at this potential, despite them being open by synaptic activation. Whilst alternating between the presence and absence of synaptic stimulation the holding potential was then stepped briefly to -70mV at various time points during the time course of the evoked synaptic current (figure 5.2). The two data sets (with and without synaptic stimulation) were averaged and then subtracted to eliminate transient capacitance currents from the traces. The peak amplitude of the synaptic current generated when stepping away from the reversal potential (to -70mV) was then measured from this subtracted data. Although no net current flow occurs at the reversal potential, the ion channels responsible for the synaptic current were expected to be open so that a step away from the reversal potential results in current flow. Assuming good voltage clamp, the peak amplitude of this current was expected to follow exactly the amplitude of the evoked synaptic response generated when voltage clamping at -70mV, throughout its time course. Figure 5.2 shows an example of such data where the ion channels have remained open for the duration of the observed synaptic current (n=4). These data suggest that both decay components are real and that the slow component does not result from inadequate voltage clamp of the neurone, but that the channels are indeed open and voltage clamped throughout the decay time course of the evoked synaptic current.

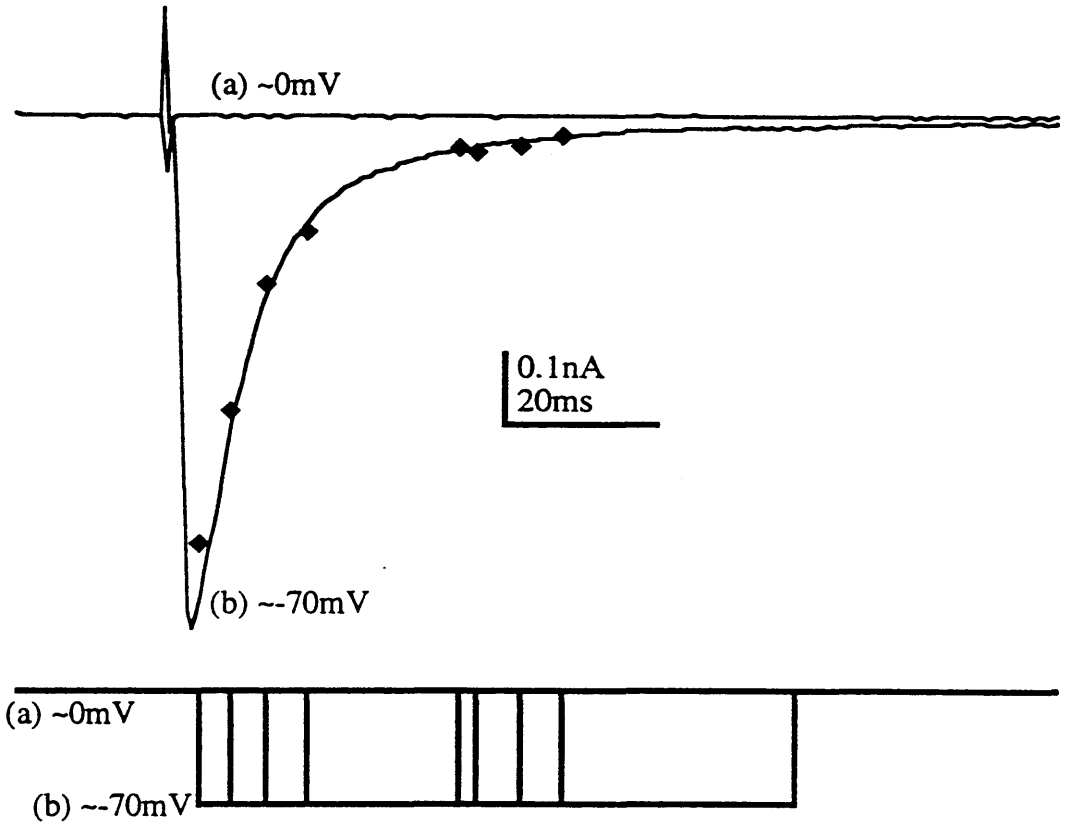

Figure 5.2 **The dual decay time course is not due to voltage clamp errors.**

Superimposed average current traces recorded from an MSO neurone at (a) the reversal potential (~0mV) and (b) 70mV negative to the reversal potential (~-70mV).

The neurone was voltage clamped at the reversal potential and stepped back to -70mV at different time points throughout the duration of the synaptic current. The symbols (◆) represent the peak synaptic current flow during the voltage step.

The peaks of the synaptic currents (◆) follows closely the time course of the evoked synaptic current recorded at -70mV, indicating that the ion channels are open throughout the duration of the synaptic current.

Data traces are averages of 20 events each.

The Fast Component of Decay of the Evoked Synaptic Current is the Dominant Component

The average amplitude of each component of decay at -70mV holding potential was -0.90±0.08nA and -0.10±0.01nA (SEM, n=81) such that the fast component constituted 89.9±0.9% (SEM, n=81) of the overall current amplitude. Similar observations of the contribution the fast component made to the synaptic current amplitude were made across a range of voltages (table 5.1) and ages of animal (see figure 5.9B) although with increasing age the fast component appears to be increasingly dominant. The combination of small amplitude and length of the slow component of decay of the synaptic current made it's time course difficult to accurately quantify, a feature which may at least in part explain the extent of its variability. So, despite being able to voltage clamp the evoked synaptic current throughout its duration (figure 5.2), much of the remaining study of the decay time course of the evoked synaptic current was focused on the more readily quantified fast component.

The Decay Time Course Shows Some Voltage Dependence

The fast component of the decay time course of the evoked synaptic current displayed a small voltage dependence such that depolarisation resulted in a lengthening of the time course of the current (figures 5.3 & 5.4).

Figure 5.3A shows some example average data traces recorded across a range of holding potentials from -70mV to +50mV. It is clear from this data set that the time course of the synaptic current changes across this voltage range, suggesting a voltage dependent change in the evoked synaptic current. Figure 5.3B & C demonstrates this voltage dependence and that although there is a variability in fast decay time constant at specified voltages between neurones (figure 5.3B), the change of the fast decay time constant with voltage observed in each neurone is consistent between neurones (figure 5.3C). This is demonstrated in figure 5.3C since the slopes of the fits to each line are similar between neurones.

The slope of the line fitted to the points in figure 5.4A shows the mean voltage dependence of the fast decay time constant plotted on a logarithmic scale, where an e-fold change in decay time constant required a ~159mV change in holding potential (n=4-10). The data in figure 5.4B lists the mean fast decay time constants (±SEM) at each holding potential, corresponding to the points on the graph in figure 5.4A.

Holding Potential (mV)	n=?	% Fast Component
-70	81	89.9±0.9
-60	8	86.8±2.6
-50	8	88.4±2.3
-40	10	87.4±2.1
-30	10	88.0±2.2
-20	10	87.4±2.1
-10	10	87.4±2.8
0	-	-
+10	10	88.4±2.4
+20	9	79.5±4.9
+30	10	83.9±2.9
+40	8	71.5±4.8
+50	6	75.9±6.9

Table 5.1

The contribution of the fast component of the decay time constant remains consistently high across a range of holding potentials.

Figure 5.3 **The decay time course of inhibitory synaptic current shows some voltage dependence.**

(A) Example mean inhibitory current traces recorded from an MSO neurone across a range of holding potentials (-70mV to +50mV). The decay time course slows at more positive holding potentials.

(B) A plot of the fast decay time constant of the inhibitory synaptic current against the holding potential in 10 MSO neurones. Each symbol represents the mean fast decay time constant recorded across a range of holding potentials from one neurone. Between neurones a variability in the decay time constant at each holding potential is apparent.

(C) A semi-logarithmic plot of the fast decay time constant against the holding potential for the corresponding data shown in (B). The slope of the lines represent the voltage dependence of the decay time constants for each neurone which are clearly similar between neurones.

All traces and points are averages of 20 events each.

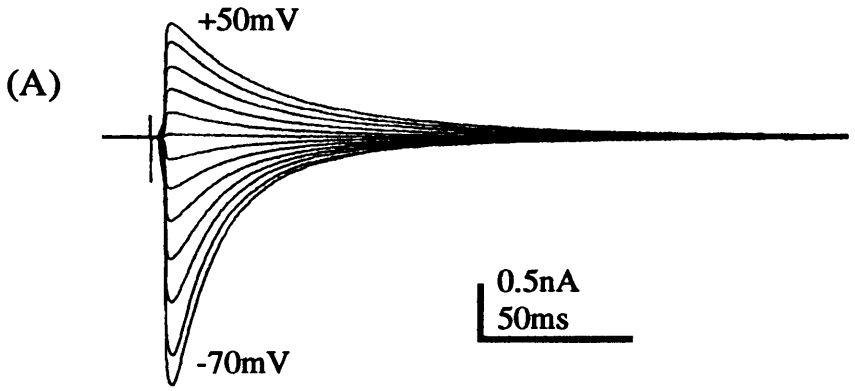
(A)
+50mV
-70mV
0.5nA
50ms

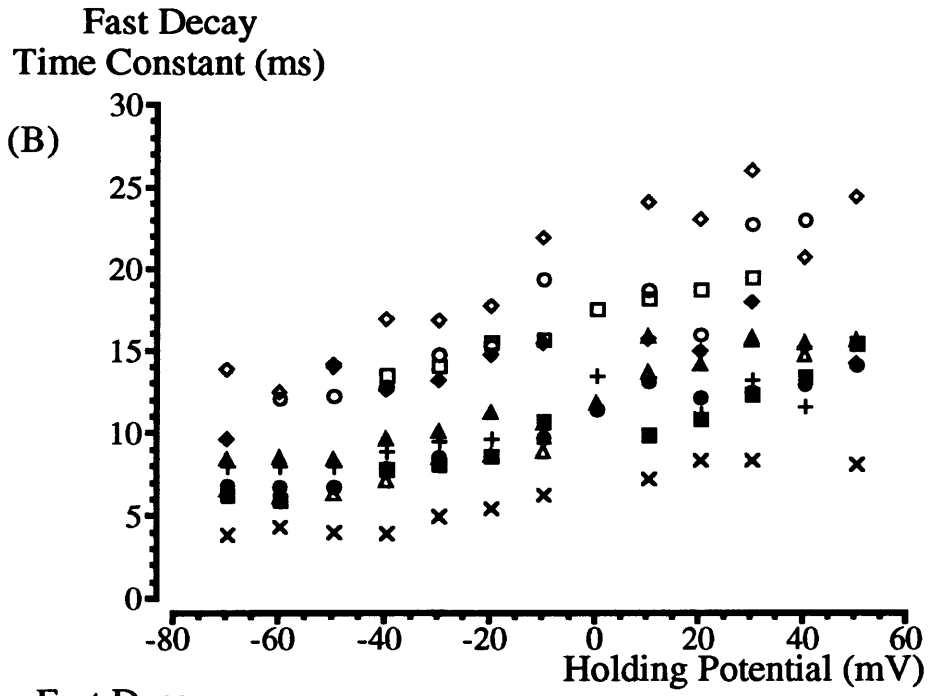
Fast Decay
Time Constant (ms)
(B)
30
25
20
15
10
5
0
-80
-60
-40
-20
0
20
40
60
Holding Potential (mV)

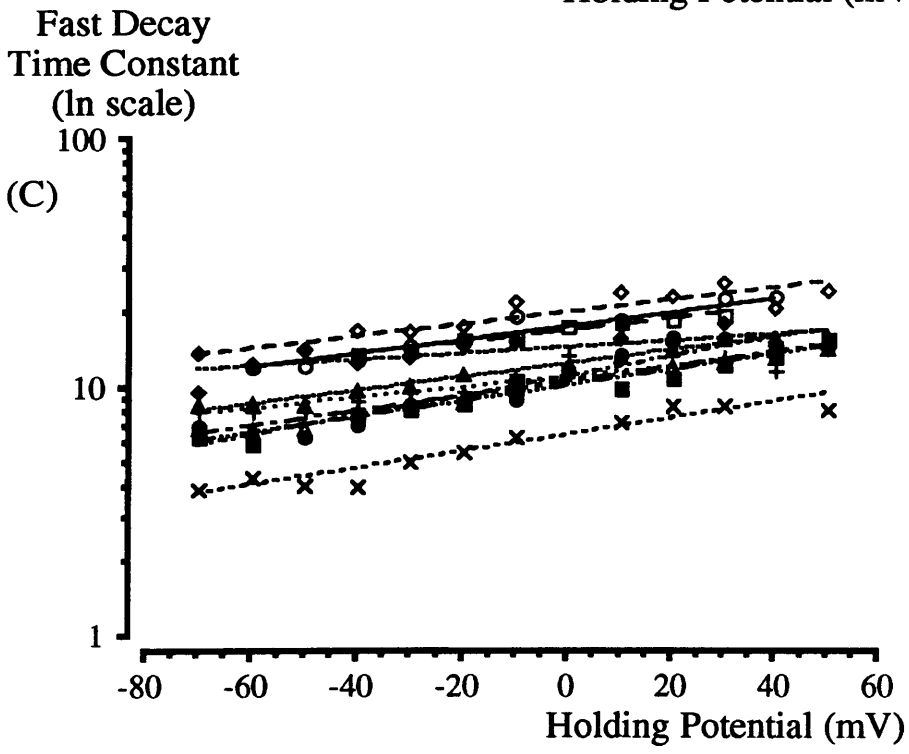
Fast Decay
Time Constant
(ln scale)
(C)
100
10
1
-80
-60
-40
-20
0
20
40
60
Holding Potential (mV)

(A)

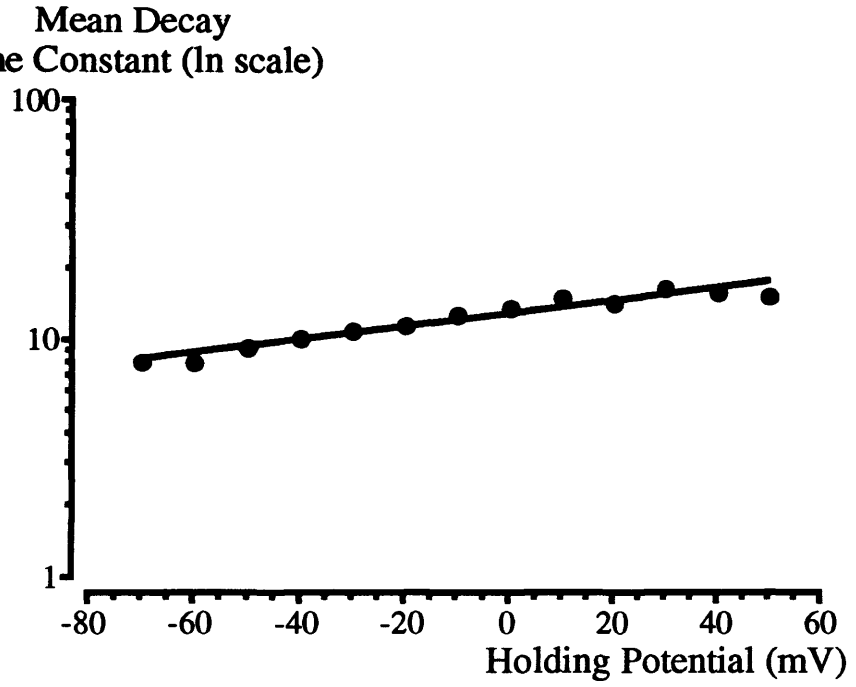

(B)

Holding Potential (mV)	Mean Fast Tau (ms)	SEM	n=?
-70.0	8.0616	1.0227	8
-60.0	8.1197	1.0336	8
-50.0	9.3398	1.3369	8
-40.0	10.216	1.1995	10
-30.0	10.971	1.1570	10
-20.0	11.651	1.2565	10
-10.0	12.920	1.5935	10
0.0	13.664	1.3845	4
+10.0	15.097	1.4957	10
+20.0	14.506	1.4880	9
+30.0	16.512	1.6717	10
+40.0	15.988	1.3877	8
+50.0	15.439	2.1323	6

Figure 5.4 **Mean voltage dependence of the fast decay of the evoked inhibitory synaptic current.**

(A) Semi-logarithmic plot and, (B) table of holding potential and mean fast decay time constant.

Voltage dependence calculated from slope of the fit to the mean decay time constants using a linear regression fit. For an e-fold change in decay time constant, a ~159mV change in holding potential is required.

The Decay Time Course Shows Some Temperature Dependence

Stuart & Redman (1990) reported that population inhibitory postsynaptic currents recorded *in vivo* in cat spinal motoneurones decayed over an exponential time course of ~1.0ms. Clearly this is much faster than reported here at 25°C, so the temperature dependence of the synaptic current was examined to see if this factor was responsible for the discrepancy. The inhibitory synaptic current was recorded across a range of temperatures (22°C-37°C) and the fast decay time course of the current was found to accelerate with increased temperature. Figure 5.5 demonstrates the temperature dependence where a Q_{10} of 2.08±0.23 (SEM, n=4) for the decay time course was calculated using the following equation:

$$Q_{10} = \left(\frac{X_2}{X_1}\right)^{\frac{10}{(T_2-T_1)}} \qquad \text{Equation 5.1}$$

At 37°C the mean fast decay time course was 3.54±0.58ms (SEM, n=4). This change with temperature appears independent of the amplitude of the synaptic current which remained constant throughout the temperature change (figure 5.6, n=4). Temperature dependence of the slow component of decay of the synaptic current was not examined since at 37°C the fast component comprised 98.1±0.9% (SEM, n=4) of the total current amplitude.

5.32 What is Causing the Variability in Decay Time Course?

The above data establishes that the evoked synaptic current decays over a double exponential time course which is both voltage and temperature dependent and shows a large variability between neurones. So what is causing this variability in decay time course? A number of possible sources of the variability were examined:

Series Resistance?

One possible explanation for the variability in decay time course between neurones is the effect that series resistance would have on the current. As series resistance increases, the ability to voltage clamp the neuronal membrane reduces. Consequently, one would expect the time course of the synaptic current to increase with series resistance.

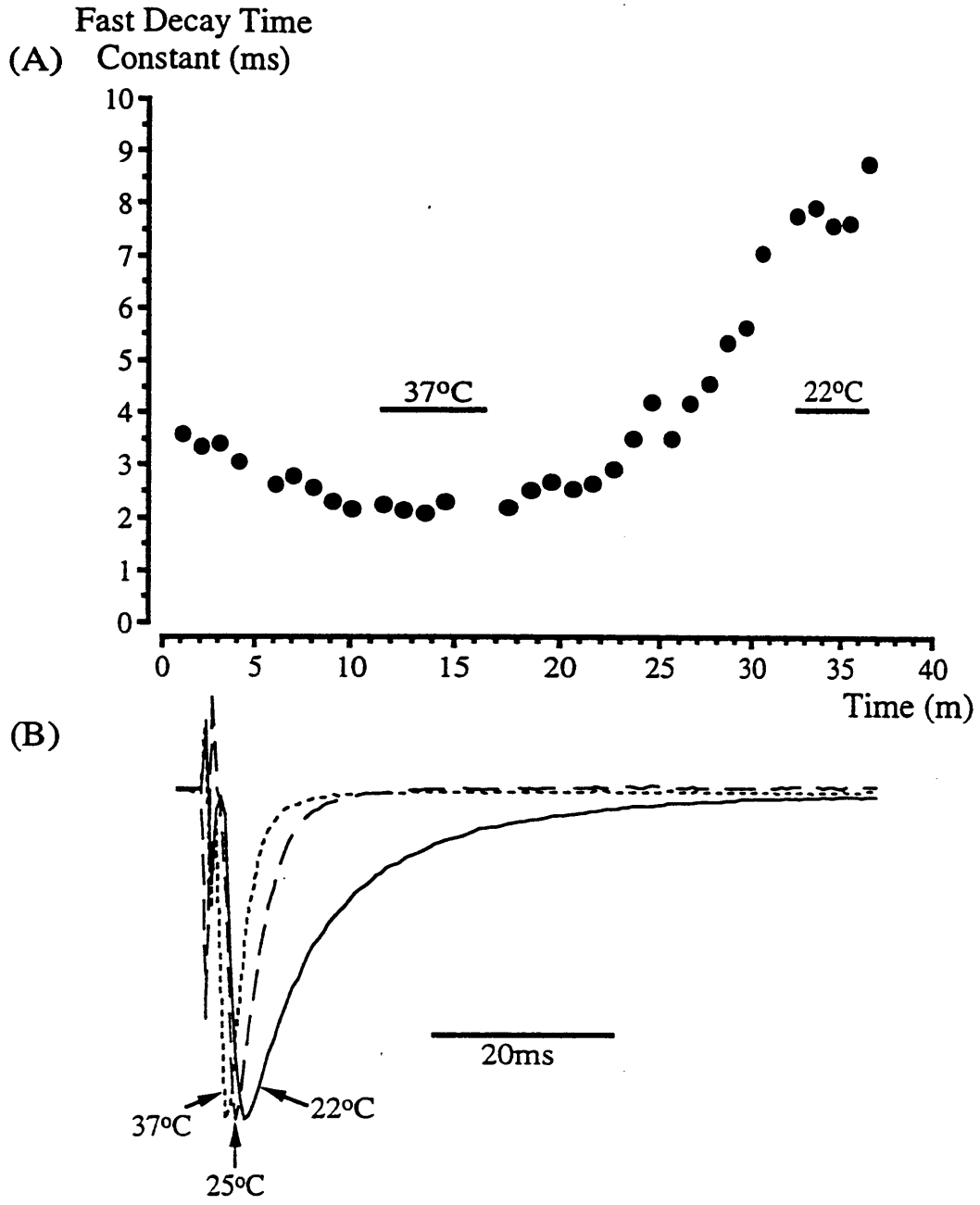

Figure 5.5 **Inhibitory postsynaptic current time course accelerates with increasing temperature.**

(A) Plot of fast decay time constant of inhibitory synaptic current over time with changing temperature, starting at 25°C, increasing to 37°C and reducing to 22°C.

(B) Average current traces normalised to their peak amplitudes at three different temperatures of 22°C (solid line), 25°C (long dashes) and 37°C (short dashes). Q_{10} calculated as 2.08±0.23 (SEM, n=4). Mean fast decay time constant at 37°C was 3.54±0.58ms (SEM, n=4).

Points and traces are averages of 20 events each.

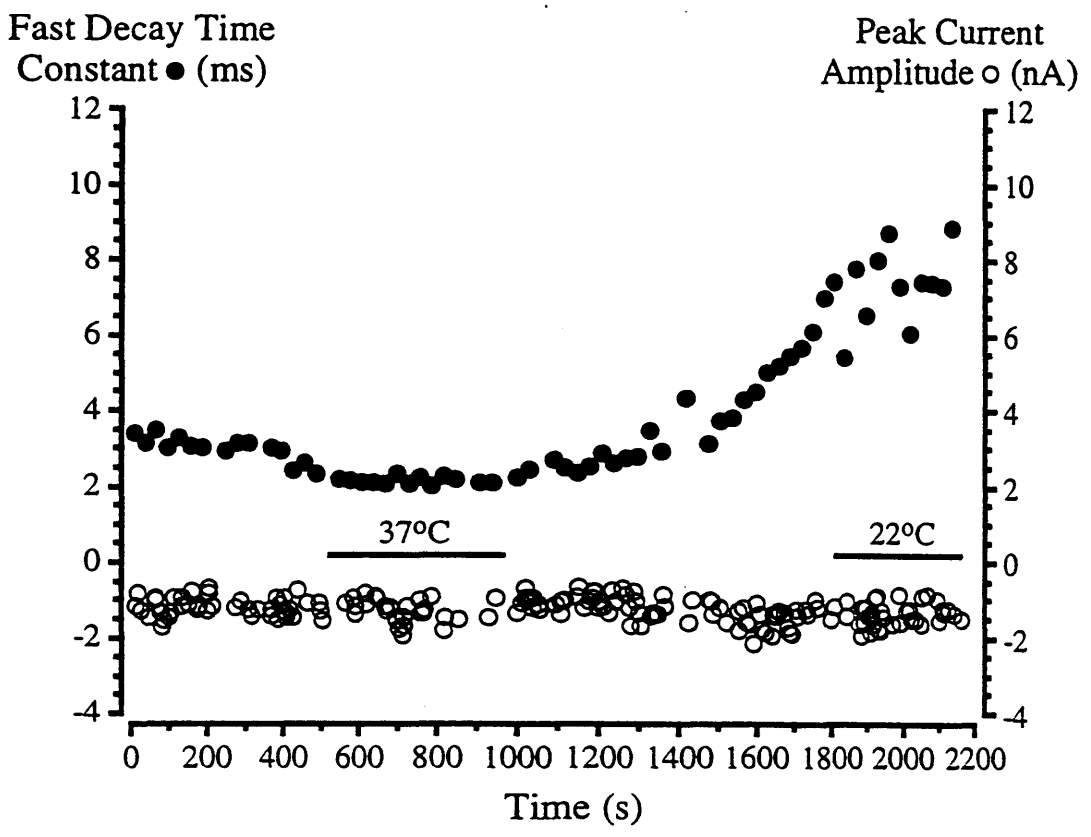

Figure 5.6 **Change in decay time course with temperature is independent of current amplitude.**

Plot of mean fast decay time constant and peak synaptic current amplitude against time. Initial temperature is 25°C, increasing to 37°C and reducing to 22°C. As the decay time constant changes with changing temperature, the current amplitude remains constant (n=4).

Points are averages of 10 events each.

Figure 5.7 shows two plots of the series resistance against fast and slow decay time constants of the current and their respective linear regression fits. Despite the great variability in decay time constant between neurones, very little correlation with series resistance was observed (R=0.030, fast decay time constant; R=0.015, slow decay time constant). However, in order to minimise the risk of series resistance affecting voltage clamp of the synaptic current, recordings were made only when the series resistance was at a maximum of 25MΩ (Mean=11.8 ±0.5MΩ; SEM, n=79) and was compensated by at least 60%. Therefore it is unlikely that the variability in decay time course of the evoked synaptic current results from errors in voltage clamp as a result of high or poorly compensated series resistance.

Age of Animal?

The age of animals used in this study were between 6 and 13 days old but as already mentioned, glycine receptor isoform expression changes over this developmental period (see chapter *1.22*). It is therefore likely that the glycine receptor mediated currents recorded here result from activation of different proportions of neonatal (α_2) and adult (α_1) glycine receptor isoforms. With this in mind, differential expression of these isoforms could explain the observed variability in the decay time course of the evoked synaptic current. This is quite possible since the single channel open time of glycine receptors comprising the neonatal isoform (α_2) is longer than that of glycine receptors comprising the adult isoform (α_1) (Takahashi *et al.*, 1992). Previous reports have demonstrated that glycine mediated synaptic currents decay over a faster time course with increasing age (Takahashi *et al.*, 1992; Krupp, Larmet & Feltz, 1994) a feature which has been attributed to the changing single channel open time with age. Attempts were therefore made to determine whether this was the case in the MSO by examining if there was any correlation between the age of the animal used and the decay time constant of the evoked synaptic current.

Figure 5.8 plots each component of the fit to the double exponential decay time constant against the age of the animal. Figure 5.8A shows each decay time constant of the fast component and figure 5.8B of the slow component of the double exponential. The lines fitted to each data set generated R values for the fast and slow decay time constants of 0.145 and 0.178, respectively suggesting little correlation between age and decay time constant although the time constants are decreasing slightly with age. Clearly at each age of animal there is a

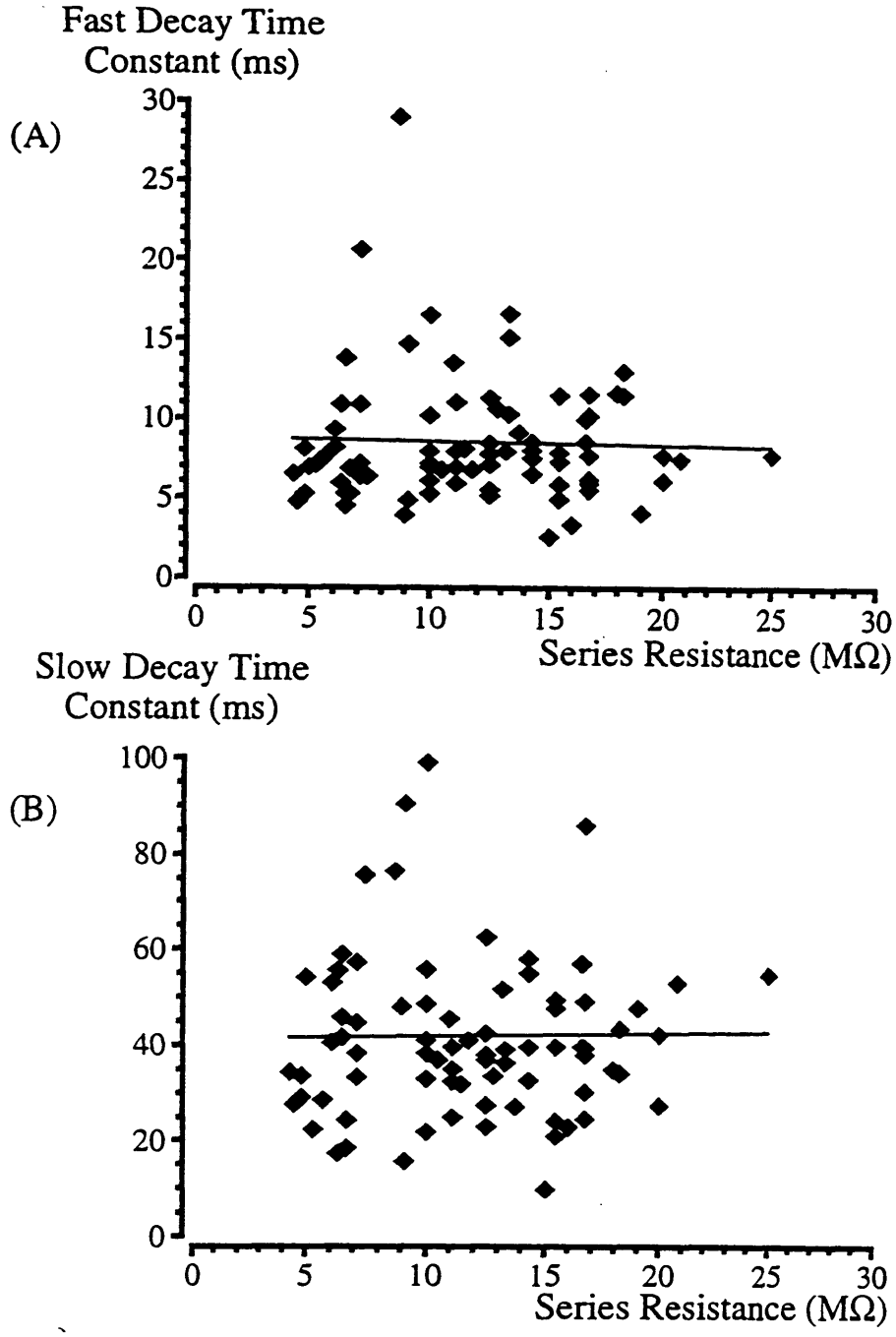

Figure 5.7 **Decay time constant is not correlated with series resistance.**

(A) Fast decay time constant plotted against series resistance. The points were fitted using the linear regression equation: Y = M0 + M1*X, generating an R value of 0.030.

(B) Slow decay time constant plotted against series resistance. The points were fitted using the linear regression equation: Y = M0 + M1*X, generating an R value of 0.015.

Both data sets show no correlation between series resistance and decay time constant. Mean series resistance was 11.8±0.5MΩ (SEM, n=79).

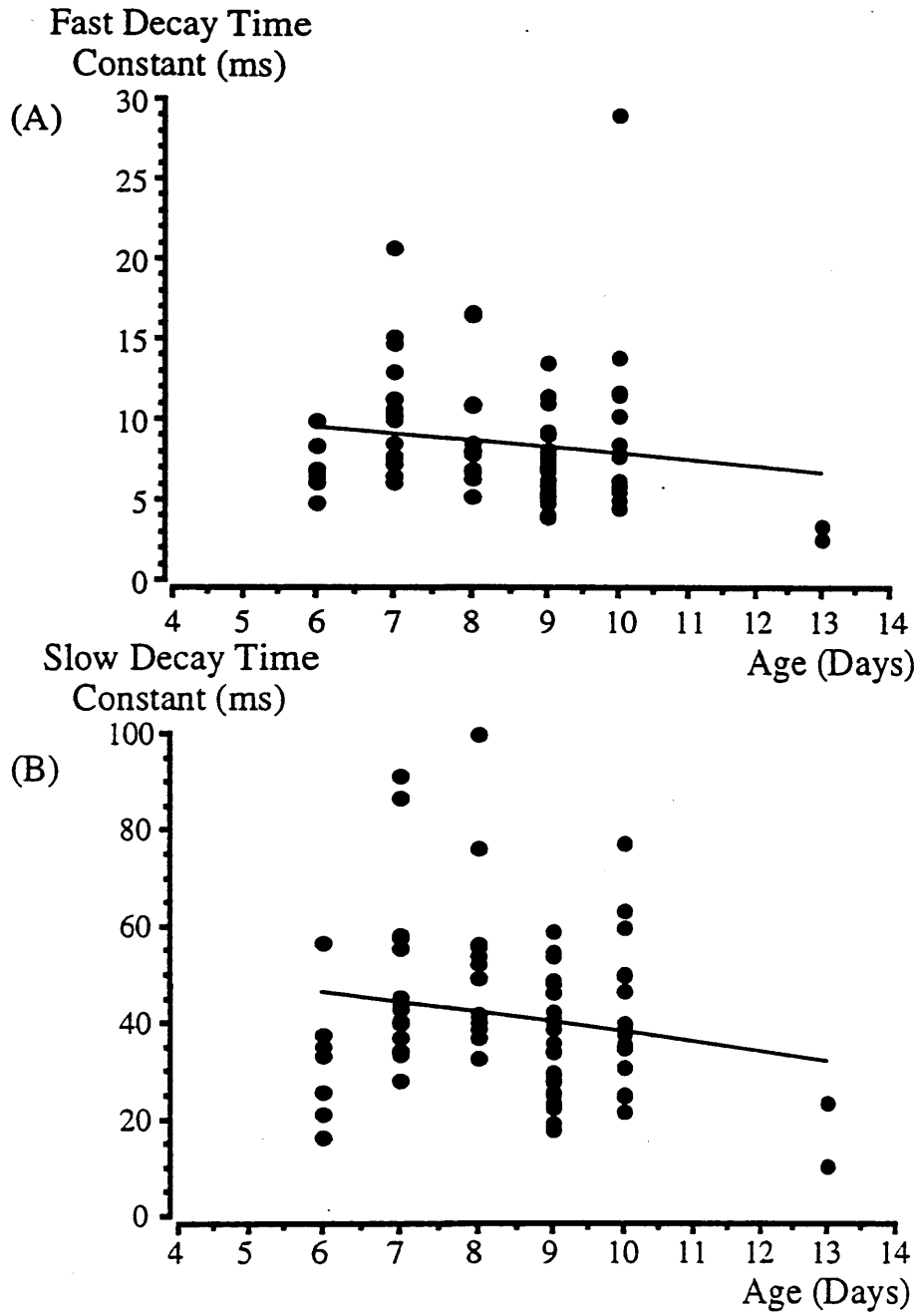

Figure 5.8 **Decay time constants plotted against age of animal.**

(A) Fast decay time constant plotted against age of animal. The points were fitted using the linear regression equation: Y = M0 + M1*X and generated an R value of 0.145.

(B) Slow decay time constant plotted against age of animal. The points were fitted using the linear regression equation: Y = M0 + M1*X and generated an R value of 0.178.

Both data sets demonstrate little correlation between time course and age of animal and that there is a great variability of the decay time constants when recording from animals of the same age.

wide distribution of decay time constant for both fast and slow component of the decay time course.

Figure 5.9A represents some of the data shown in the table in figure 5.9B, where the mean decay time constants (±SEM) are plotted against the age of animal. The open symbols (O) represent the slow component and the closed symbols (•) the fast component of the decay time constant of the current. The lines drawn on each data set are the fits to the individual data points displayed in figure 5.8 which generated the R values mentioned above. Figure 5.9B also displays the % contribution of the fast component of the decay time constant to the overall synaptic current at different ages of animal. Again, the fast component of the double exponential consistently contributed >80% of the overall current amplitude. However, it also appears that there may be a slight reduction in the contribution of the slow decay time constant to the overall synaptic current with increasing age.

A further demonstration of the poor correlation between decay time course and age is shown in figure 5.10 where evoked synaptic currents were recorded from more than one neurone in individual animals. A disparity between these decay time constants was observed such that up to 21.32ms variation in the fast decay time constants and up to 46.34ms variation in the slow decay time constants occurred when recording from more than one neurone in a particular animal. Statistical demonstration of this variance was not possible since the number of multiple recordings achieved from one animal was too small. However, the results suggest that within one animal there is a great variability in decay time constant of the evoked inhibitory synaptic current.

Different Glycine Receptor Isoforms Based on Pharmacology?

Despite the inability to demonstrate any correlation between age and decay time course of the evoked synaptic current, it is likely that recordings from MSO neurones in this project were done from animals expressing different proportions of the neonatal (α_2) and adult (α_1) glycine receptor isoforms. In order to decide whether the variability in decay time course stemmed from this differential expression, it would be ideal to record from neurones expressing exclusively one or other isoform. Since the use of young animals was necessary in this project, resulting in mixed expression of glycine receptor isoform, pharmacological isolation of one or other isoform was necessary. To this end the α_1 glycine receptor subtype selective blocker,

(A)

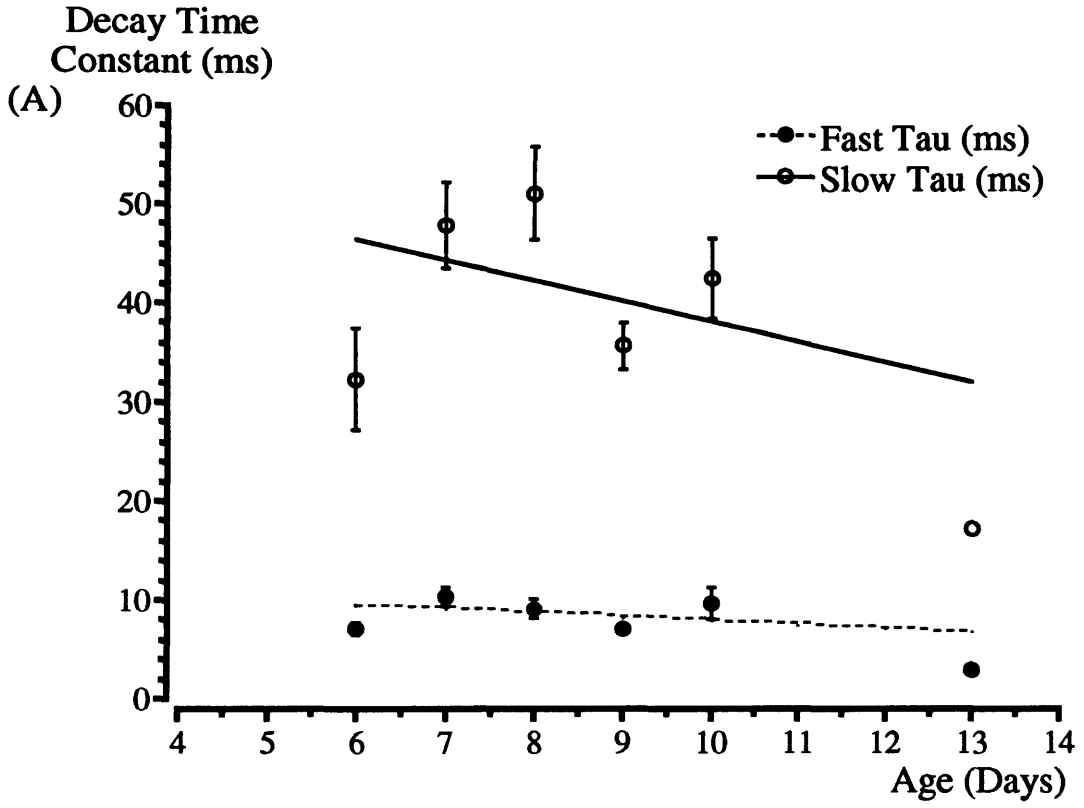

(B)

Age (Days)	n=?	Fast Tau (ms)	Slow Tau (ms)	% Contribution of Fast Component
6	7	7.08±0.62	32.33±5.03	82.9±5.9%
7	17	10.3±0.92	47.91±4.29	88.8±1.3%
8	14	9.23±0.93	51.22±4.80	92.9±1.3%
9	26	7.17±0.45	35.77±2.31	90.4±1.4%
10	15	9.68±1.57	42.59±4.03	89.9±2.3%
13	2	3.00	17.21	96.4%
N/A Mean	81	8.54±0.44	41.50±1.84	89.9±0.9%

Figure 5.9 **Mean decay time constants of evoked synaptic current with respect to age of the animal.**

(A) Mean decay time constants (±SEM) plotted against animal age. Open symbols (o) represent slow decay time constant and closed symbols (•) represent fast decay time constant. R values generated of 0.178 and 0.145, respectively.

(B) Table of decay time constants with repect to animal age. The % contribution of the fast component of the synaptic current remains consistently high across the age range of animals used.

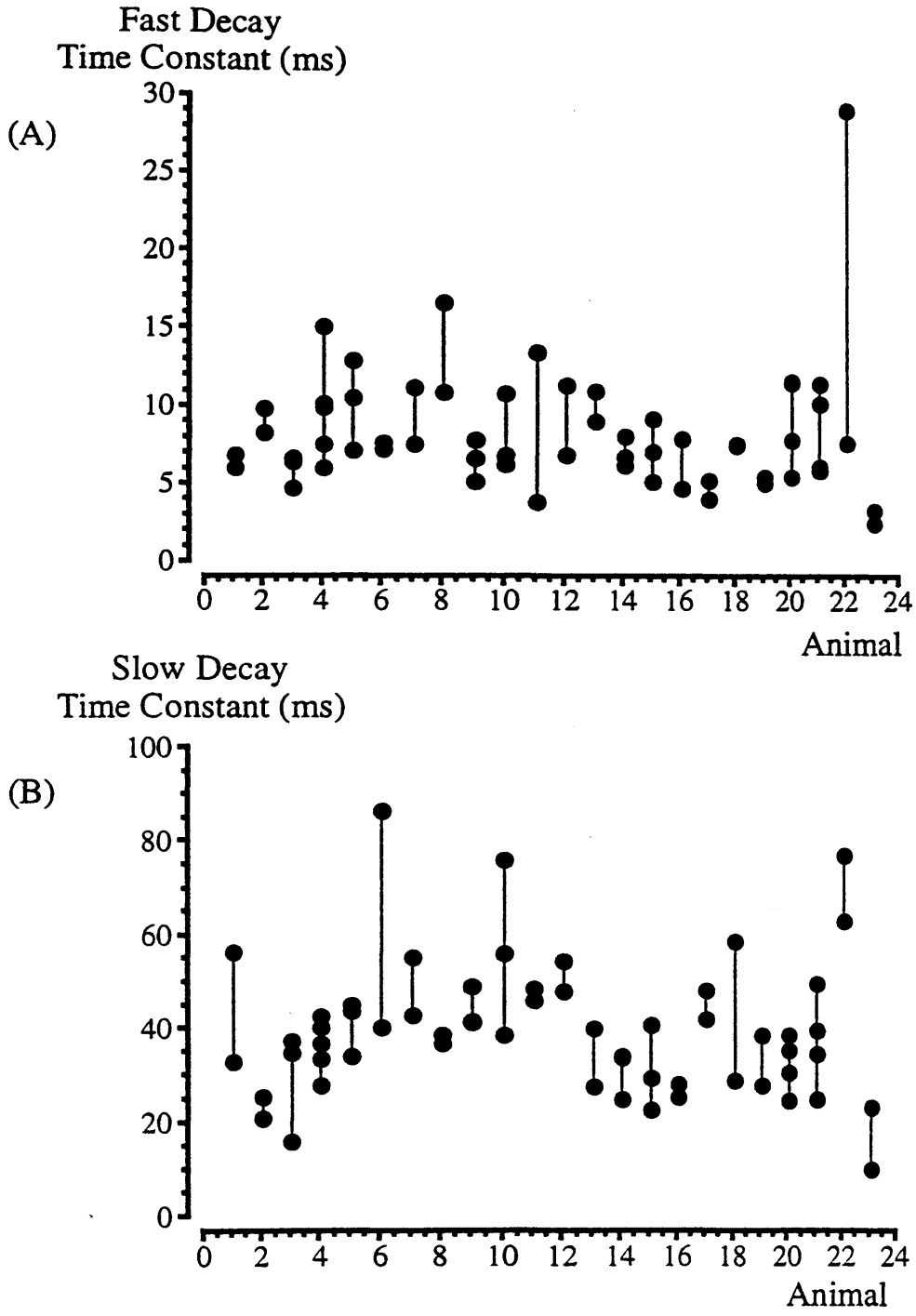

Figure 5.10 **Multiple recordings from the same animal generate a range of decay time constants.**

(A) and (B) show the range of fast and slow decay time constants fitted to currents recorded from individual animals (1-23). The disparity of decay time course of the fast component in one animal was up to 21.32ms and that of the slow decay time constant was up to 46.34ms.

cyanotriphenylborate (CTB) (Rundström *et al.* 1994) was included in the perfusate to eliminate its contribution to the inhibitory synaptic current.

CTB was perfused onto the preparation on four occasions, using one 10-day and three 9-day old animals. On one occasion 20μM CTB reversibly reduced the peak current amplitude by 25.8% (Figure 5.11). However, on three remaining occasions 20μM CTB had no effect on the amplitude of the synaptic current (data not shown). It was therefore concluded that at this concentration, CTB had little effect of the evoked synaptic current in this preparation. A higher concentration was not used since this would have produced toxic effects resulting in an increased risk of membrane breakdown (D. Langosch, personal communication).

5.321 Are the Synaptic Inputs Differentially Located on the MSO Neurones?

The above results suggest that the variability in decay time course of the evoked synaptic current is neither resulting from series resistance problems nor age dependent changes resulting from differential expression of glycine receptor isoforms. An alternative explanation for the variability may be different locations of glycine receptors on the MSO neurones. The location of synaptic inputs on a neurone is important when examining the time course of synaptic currents. If the synaptic inputs are electrotonically distant from the recording site, the current detected by the recording pipette will have been subject to dendritic filtering and will be longer and smaller than the current at its origin. MSO neurones are distinctly bipolar and the dendrites projecting from the cell soma are large and far reaching (up to several hundred μm; Kiss & Majorossy, 1983; Smith, 1995) (figure 5.12). If the inputs from the principal neurones of the MNTB synapse are on these dendritic processes the resulting synaptic currents will have been subject to electrotonic filtering, a process which will slow the time course and reduce the amplitude of the current. Using immunohistochemical and electrophysiological techniques it was therefore necessary to investigate the location of the inhibitory synaptic inputs onto the MSO neurones. It is thought, as described in the chapter *1.114*, that inhibitory terminals synapse somatically or within a short distance from the soma on MSO neurones (Clark, 1969; Oliver, Beckius & Schneiderman, 1995; Brunso-Bechtold, Henkel & Linville, 1990; Kuwabara & Zook, 1992). The effect of synaptic location on the time course of the synaptic current however warranted further investigation here.

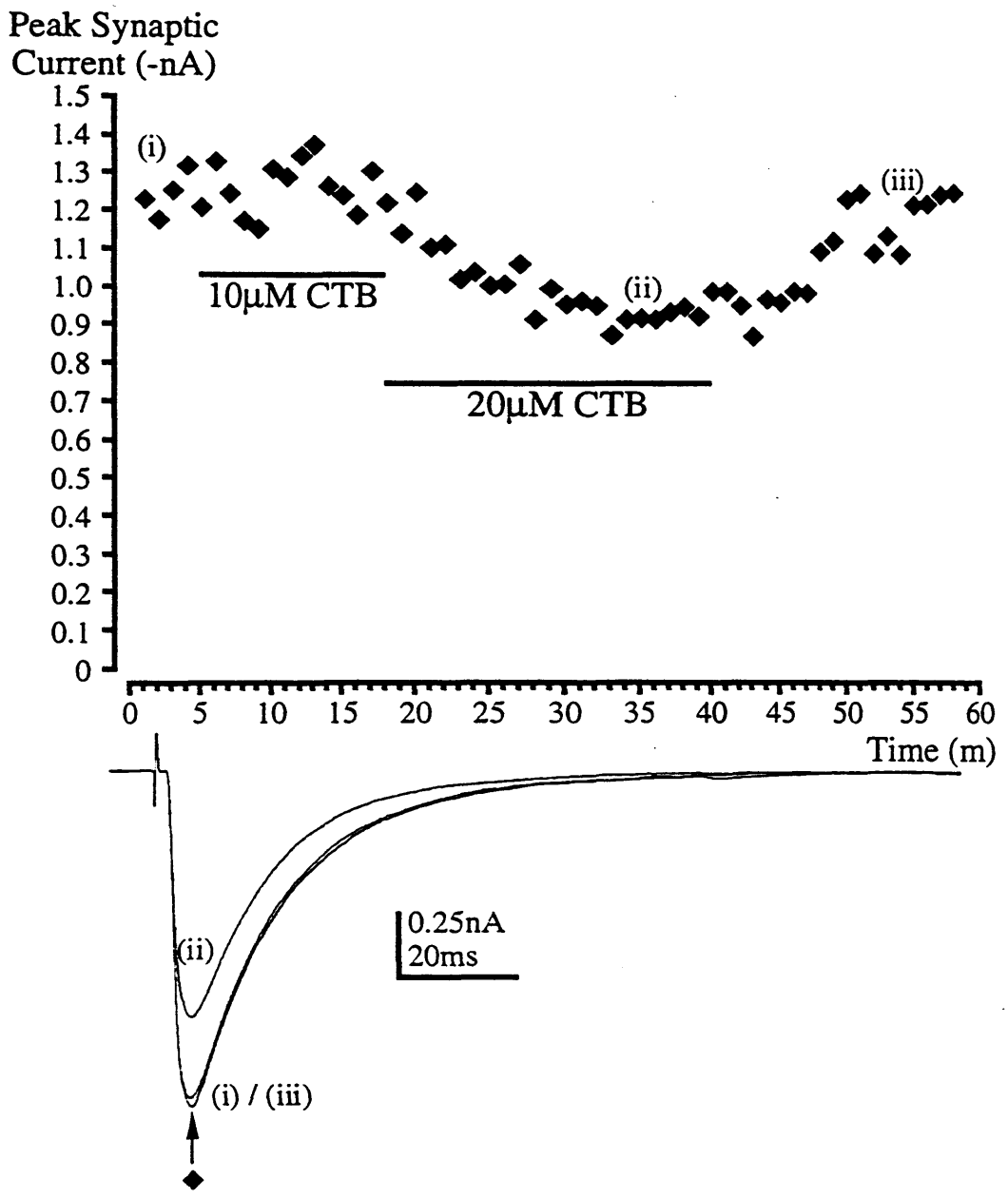

Figure 5.11 **Action of cyanotriphenylborate (CTB) on evoked inhibitory synaptic current.**

On one occasion 20 μM CTB reversibly blocked the evoked inhibitory synaptic current by 25.8% but on three other occasions (not shown) no block was observed.

(A) Plot of average peak synaptic current upon application of 10μM and 20μM CTB.

(B) Corresponding average current traces from (A), (i) before application; (ii) during application; and (iii) following wash off of 20μM CTB. Amplitude of synaptic current measured at the time indicated by ◆.

Data points and traces are averages of 20 events each.

Figure 5.12 **Confocal images of MSO neurones filled with lucifer yellow.**

(A) An MSO neurone filled with the fluorescent dye lucifer yellow shows its bipolar dendritic organisation. The image was constructed using a confocal microscope and has been digitally recoloured. The axon is projecting from the lateral primary dendrite ~13μm from the soma. Bar=20μm.

(B) Stereo image of an MSO neurone filled with lucifer yellow and reconstructed using a confocal microscope. Merging of the two images by eye will produce a 3-dimensional appearance of the neurone.

These images were constructed on the confocal microscope by Mr. Stuart Johnson as a part of his final year Biological Sciences degree project from material provided by myself, Dr. Ian Forsythe and Dr. Helen Brew.

(A)

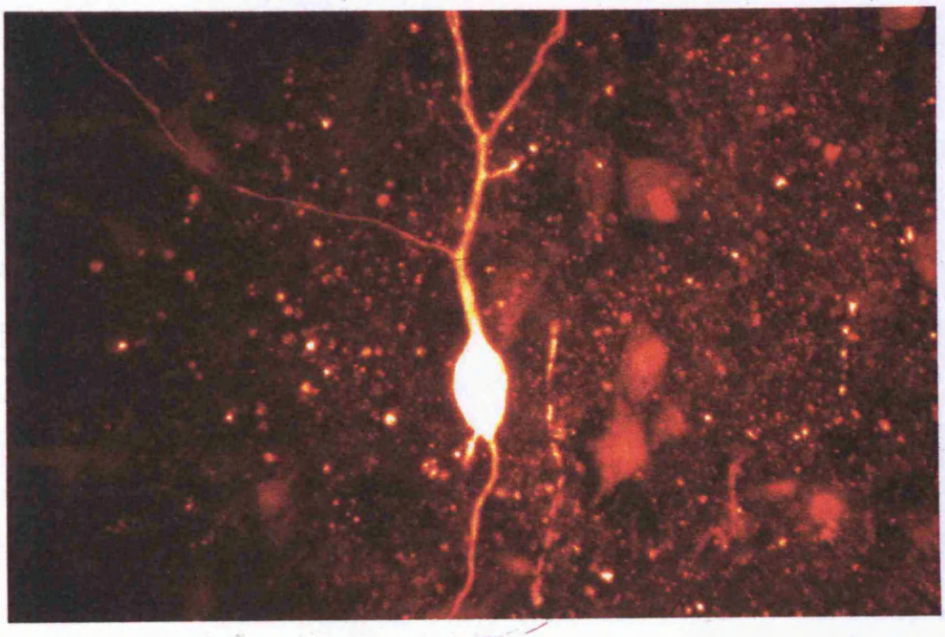

(B)

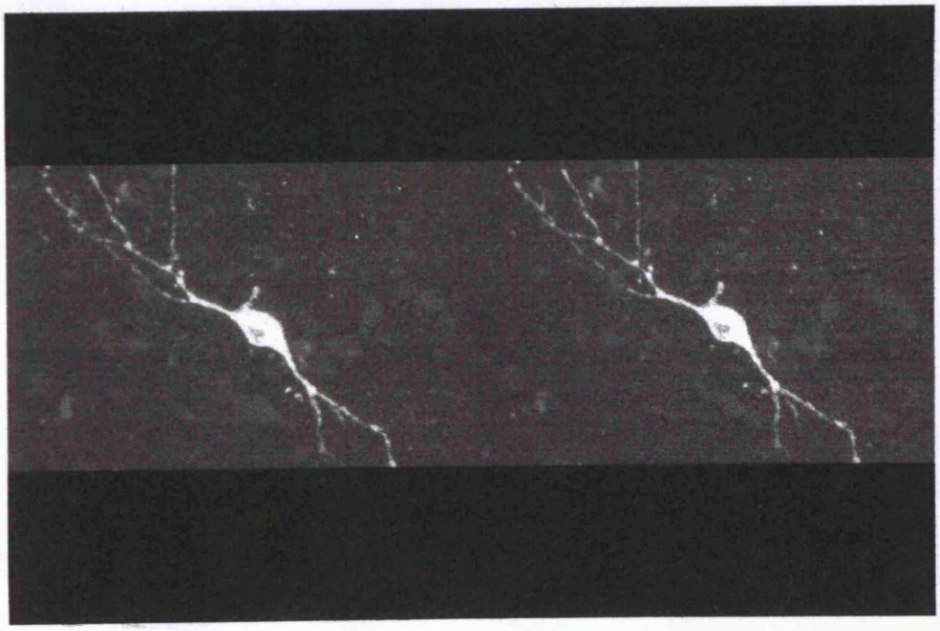

(A) Immunohistochemistry

In an attempt to identify the location of the inhibitory synaptic input onto MSO neurones, immunohistochemical techniques based on those described by Pfeiffer *et al.* (1984) and Schröder *et al.* (1991) were employed. Julie Turner and Ian Brooks, technicians in my laboratory used immunohistochemical agents applied to thin (20μm) transverse sections of the auditory brain stem. The monoclonal antibody, MAb4a attaches to any currently known glycine receptor α-subunit variant and so can be used to identify the presence of glycine receptors, neonatal or adult. Difficulties with this technique arose in maximising the contrast between the labelled receptors and that of the background. However, after much trial and error, it became apparent that MSO principal neurones were labelled with the MAb4a. Previous reports (Adams and Mugnaini, 1990; Helfert *et al.*, 1989; Friauf, Hammerschmidt & Kirsch, 1997) have shown MSO neurones to be surrounded by terminal puncta which react positively to glycine antibodies. Punctate staining indicates a dense inhibitory input and although some punctate staining was apparent here (figure 5.13, arrows) it was difficult to confirm the location of the synaptic inputs to the MSO. In figure 5.13A & B some punctate labelling of the cell body of an MSO neurone with mAb4a is apparent and there is also a hint of punctate staining along the dendrite in figure 5.13A.

Immunohistochemistry failed to reveal with certainty the location of the inhibitory synaptic inputs to the MSO so electrophysiological techniques were also employed.

Figure 5.13 **Punctate labelling of an MSO neurone using the monoclonal antibody, mAb4a.**

An MSO neurone in a 20μm thin section labelled with the monoclonal antibody, mAb4a which selectively labels all known glycine receptor α subunits.

(A) MSO neurone at 20x gain shows some punctate antibody staining (arrows). Bar=20μm.

(B) MSO neurone corrsponding to labelled neurone in (A) at 40x gain. Some punctate labelling is apparent (arrows). Bar=20μm.

Brain stem sectioning and monoclonal antibody staining were conducted by Mr. Ian Brooks.

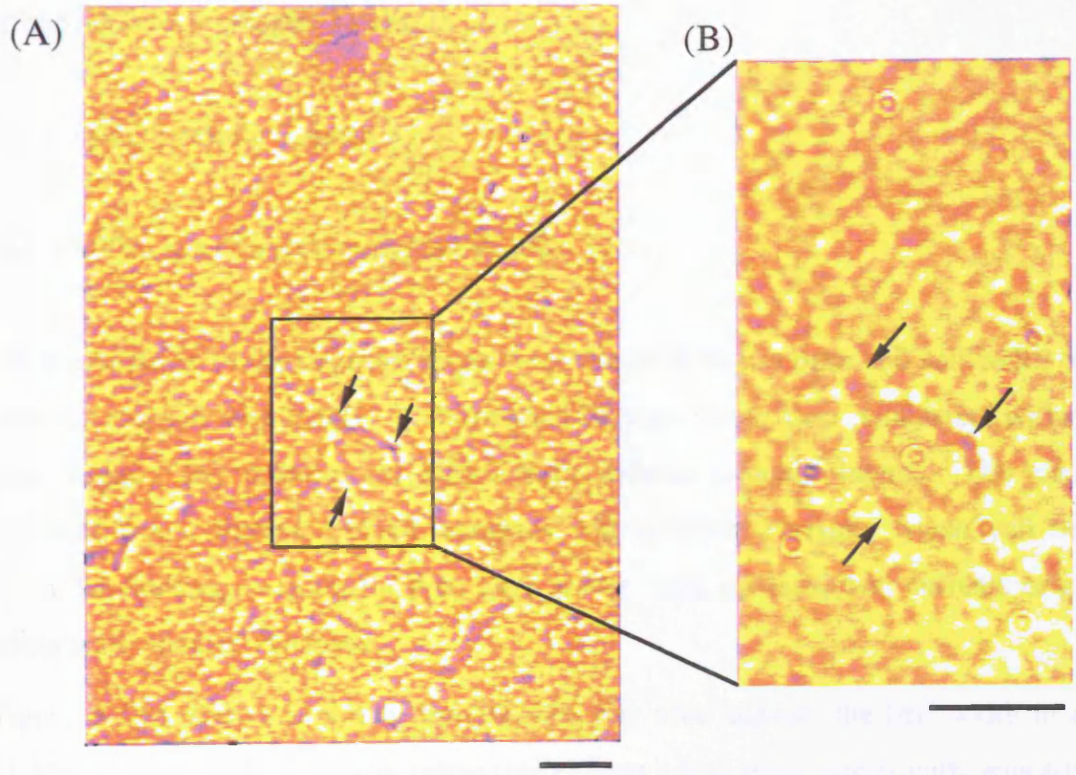
(A)
(B)

(B) Electrophysiology

The following section documents the results of electrophysiological investigations conducted on the evoked synaptic and miniature currents in an attempt to answer the question of location of the inhibitory synaptic inputs.

(i) Evoked Synaptic Current

(a) 10-90% Rise Time Versus Half Width

An examination of the relationship between the 10-90% rise time and half width of the evoked synaptic current was made. A correlation between these two parameters within a neurone, may suggest the presence of differentially located synaptic inputs. This occurs because electrotonically distant located synapses will generate currents which will be subject to dendritic filtering, causing them to have slower time courses than currents originating from somatically located synapses.

Figure 5.14A shows a plot of the 10-90% rise time against the half width in one neurone (1.16±0.05ms & 5.87±0.10ms, respectively) from which there consistently appeared to be little correlation between these two parameters when recorded from an individual neurone (R=0.190±0.071, SEM, n=9). Figure 5.14B shows a plot of the mean 10-90% rise time against mean half width (0.71±0.12ms & 8.16±0.72ms, respectively, SEM, n=9) across a population of neurones where some correlation was observed (R=0.436, n=9). The table in figure 5.14C displays the R values for correlation between mean 10-90% rise time and mean half width with each of peak current amplitude, series resistance, and age. Mean 10-90% rise time and mean half width each appeared to show no correlation with peak current amplitude (rise time: R=0.049; half width: R=0.047) but some correlation was observed with series resistance (rise time: R=0.509; half width: R=0.399) and age (rise time: R=0.703; half width: R=0.463). However, less correlation was observed between age and decay time course of the evoked synaptic current (figures 5.8 & 5.9) and almost no correlation was observed between series resistance and decay time constant (figure 5.7). These data suggest that within individual neurones there was no great distribution of synaptic inputs but that across a population of neurones, some evidence of variability was apparent (see section *5.42*).

Figure 5.14 **10-90% rise time and half width of the evoked synaptic current shows no correlation within a neurone but some correlation in a population of neurones.**

(A) Plot of half width against 10-90% rise time of individual postsynaptic currents recorded from one neurone. Little correlation between 10-90% rise time and half width was seen in any response (R=0.190±0.071, SEM, n=9).

(B) Plot of mean 10-90% rise time against mean half width (±SEM) across a population of MSO neurones. Some correlation observed across the population where R=0.436, n=9.

(C) Table showing R values of the mean 10-90% rise time and mean half width correlated with each of animal age, peak current amplitude and series resistance. No correlation with peak current amplitude was observed but some correlation with both series resistance and age was observed across the population.

(A)

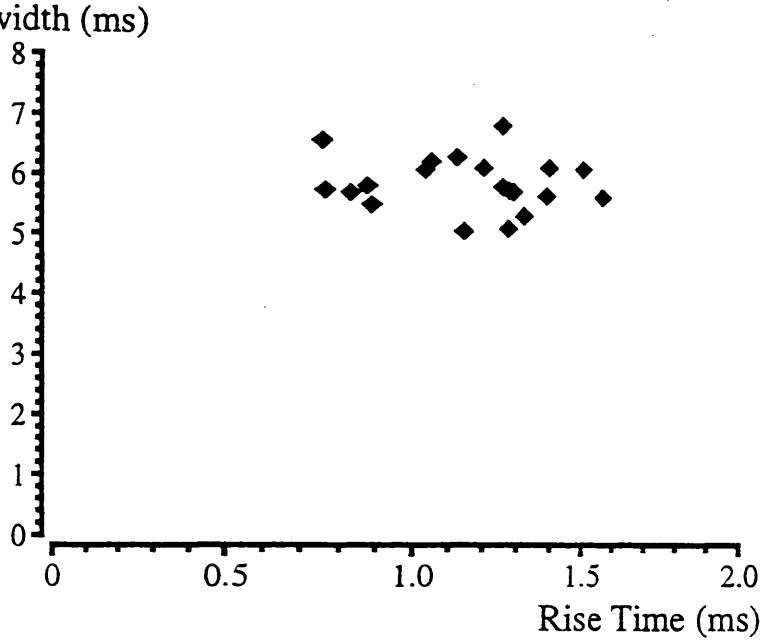

(B)

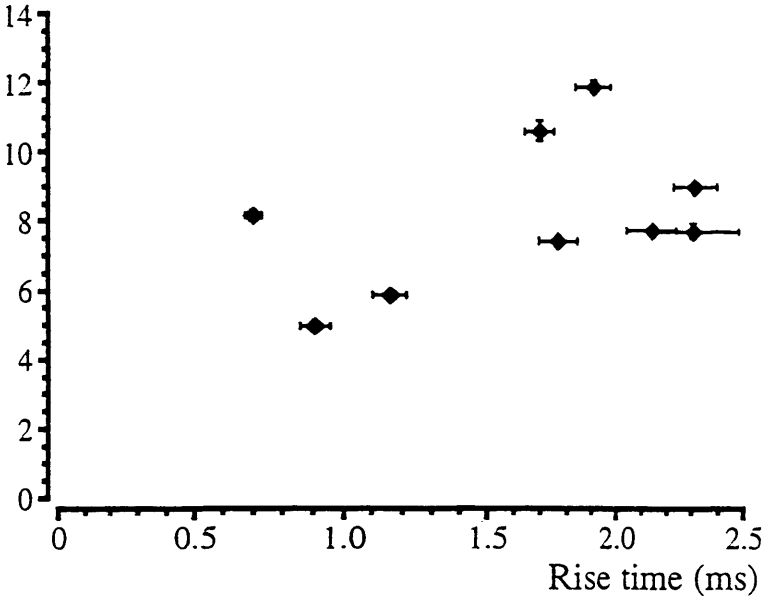

(C)

	Age	Peak Current	Series Resistance
Half Width	0.463	0.047	0.399
Rise Time	0.703	0.049	0.509

(b) "Switch off" of the Synaptic Current

A protocol similar to that described by Isaacson & Walmsley (1995a) was used in an attempt to identify the location of the inhibitory synaptic inputs onto the MSO neurones. The inhibitory evoked synaptic current was pharmacologically isolated and the reversal potential determined (~0mV, see chapter *4.324*). The holding potential was then stepped +40mV relative to the reversal potential, resulting in an outward synaptic current. During the decay of this synaptic current the holding potential was then stepped back to the reversal potential where there is no net current flow. This step was done in the presence and absence of synaptic stimulation and averages of the two data sets were subtracted in order to eliminate transient capacitance currents generated by the voltage step. Once subtracted the time course of switch off of the current was measured and a typical result, demonstrating this switch off is shown in figure 5.15. Switch off of the synaptic current here was not instantaneous but instead occurred over a double exponential time course (figure 5.15) with time constants of 0.63±0.26ms and 2.7±0.5ms (n=4, SEM), the former of which contributed 67.2±9.8% (SEM, n=4) of the total.

Isaacson & Walmsley (1995a) reported that in stellate cells of the AVCN the NMDA receptor mediated excitatory postsynaptic currents switched off over a time course of 2.9±1.0ms and proposed that this reflected the synaptic inputs being somewhat distal to the recording pipette. They also reported that in bushy cells the switch off was almost instantaneous, decaying over a submillisecond time course (50-100μs). This is consistent with the membrane being under very good voltage control, suggesting that the synaptic inputs are somatically located.

The combination of a submillisecond time course component of switch off (0.63±0.26ms) and the long 2.7±0.5ms time course component observed in the MSO here may reflect multiple synaptic inputs to the MSO at both the cell soma and elsewhere on the dendritic processes, respectively. However, it is also possible that this is not the case but that the synaptic input is entirely of somatic origin and the slower time course of switch off results from somatic current which has flowed into the dendrites, re-invading the soma when the membrane is stepped to the reversal potential. So, using this protocol, the location of the synaptic inputs cannot be stated with certainty but there is good evidence of a large somatic input and the possibility of a much smaller dendritic input.

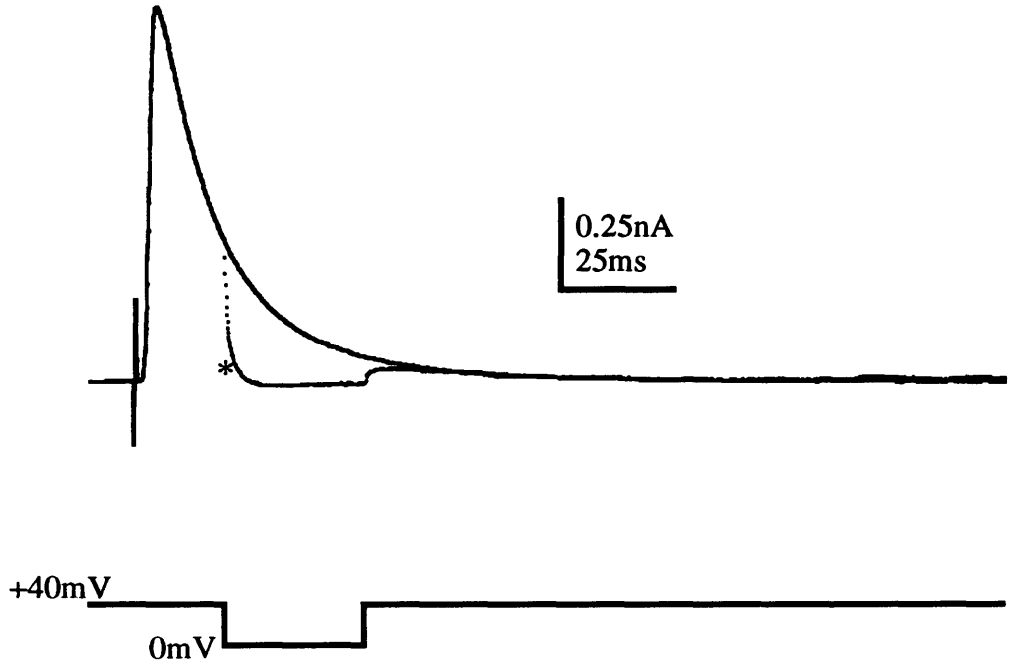

Figure 5.15 **Switch off of the inhibitory synaptic current in an MSO neurone is not instantaneous.**

Current traces were receorded from an MSO neurone at +40mV. A voltage step to the reversal potential (0mV) was applied to the membrane with and without synaptic stimulation. The transient capacitance currents were subtracted from the evoked current trace and the time course of the switch off of the synaptic current (*) was measured.

The switch off of the current was not instantaneous but decayed over a double exponential time course with time constants of 0.63±0.26ms and 2.7±0.5ms, the fast component contributing 67.2±9.8% of the total magnitude (SEM, n=4).

(ii) Miniature Currents

The evidence shown so far has only tentatively suggested differential location of synaptic input to be responsible for the variability in decay of the evoked synaptic current between neurones. Further information regarding synaptic location can be gleaned from analysis of miniature currents underlying the evoked response. As previously mentioned (chapter *4.323*) miniature currents are thought to occur as a result of discrete quantities, or packets of neurotransmitter being released from the presynaptic terminal (reviewed by Korn & Faber, 1991). Current flow resulting from activation of postsynaptic receptors then reflects release of these packets of transmitter. In experiments examining miniature currents, 0.5μM TTX was also included in the perfusate throughout.

(a) Do Miniature Currents Underlie the Evoked Synaptic Currents?

In order to make any interpretation regarding the location of the inhibitory synaptic input based on miniature current analysis it was first necessary to determine if the miniature currents underlie the evoked synaptic current. To do this the time course of the miniature currents was examined.

In four neurones examined 42.7±6.2% (SEM, n=4) of the miniature currents were fitted by a single exponential function ($F_n=A + Be^{(-t/C)}$) and the remainder were fitted by a double exponential function ($F_n=A + Be^{(-t/C)} + De^{(-t/E)}$). The mean decay time constant of miniature currents decaying over a single exponential time course was 6.34±0.42ms (SEM, n=4). Those miniature currents fitted by a double exponential time constant had fast and slow components of 3.56±0.20ms (SEM, n=4) and 22.92±1.28ms (SEM, n=4), respectively and the faster component contributed 65.99±5.06% (SEM, n=4) of the total miniature current amplitude. The mean decay time constants for each neurone are shown in table 5.2.

The miniature currents which decayed over a double exponential time course had time constants which were similar, although a little faster than those of the evoked synaptic current (fast: 8.54±0.44ms, SEM, n=81; slow: 41.50±1.84ms, SEM, n=81, see chapter *5.31*). Several factors may explain this difference and are discussed later in section *5.34*.

Cell	1	2	3	4	Mean (n=4)
Mean single exponential decay time constant (ms)	6.10±0.16 (98)	7.22±0.13 (305)	6.77±0.25 (58)	5.29±0.16 (106)	6.35±0.42
Mean fast double exponential decay time constant (ms)	3.18±0.16 (132)	4.04±0.16 (250)	3.72±0.13 (166)	3.32±0.15 (118)	3.57±0.20
Mean slow double exponential decay time constant (ms)	23.42±0.04 (132)	22.03±0.89 (250)	26.16±1.09 (166)	20.07±1.40 (118)	22.92±1.28
Mean rise time constant (ms)[1]	0.50±0.05 (98)	0.93±0.03 (305)	0.79±0.05 (58)	0.58±0.06 (106)	0.7±0.10
Mean rise time constant (ms)[2]	0.50±0.04 (132)	0.98±0.03 (250)	0.94±0.02 (166)	0.44±0.032 (118)	0.72±0.14
R value, rise vs decay[2]	0.158	0.164	0.338	0.195	0.214±0.042

Table 5.2 **Mean exponential rise and decay time constants fitted to miniature currents recorded from MSO.**

In each neurone, some miniature currents decayed over a single and some over a double exponential time course. All miniature current rise times were fitted by a single exponential time course.

R values show a small correlation between rise and decay time constants in miniature currents recorded from individual neurones. R value shows good correlation between mean rise and mean decay time constants fitted to miniature currents across a population of neurones since R=0.933 (n=4).

1 = corresponds to currents fitted by a single exponential decay time constant.

2 = corresponds to currents fitted by a double exponential decay time constant. R value calculated from rise time constant and fast component of double exponential decay time constant.

Numbers in parentheses are miniature current n values

In chapter *4.323*, figure 4.15 it was shown that application of 1μM strychnine in combination with 0.5μM TTX, EAA antagonists and bicuculline completely abolished miniature currents in the MSO.

The combination of the similar decay time course of the miniature currents and evoked synaptic currents, and the fact that both are blocked by application of 1μM strychnine suggests that the miniature currents recorded here do underlie the evoked synaptic current.

(b) Do the Miniature Currents Provide any Evidence for Distinct Locations?

Since the results above suggest that miniature currents underlie the evoked synaptic current, investigations were conducted to determine if the miniature currents provided evidence for the location of the inhibitory synaptic inputs. The lack of correlation between the 10-90% rise time and half width of the evoked synaptic current in individual neurones (see above) provided no direct evidence for distinct synaptic inputs. However, the data did suggest possible differences across the population of neurones, a factor which may also be linked to age and/or receptor subtype (see above). This technique has been taken further here by examining the relationship between the rise and decay time constants of the miniature currents. First however, the rise and decay time courses of the miniature currents and their amplitudes are documented.

Time Course of the Miniature Currents.

As mentioned above, analysis of the time course of the miniature currents in four neurones revealed that 42.7±6.2% (SEM, n=4) decayed over a single exponential time course (6.34±0.42ms, SEM, n=4) and the remainder over a double exponential time course (fast: 3.56±0.20ms, SEM, n=4; slow: 22.92±1.28ms; SEM, n=4). Using an unpaired t-test (all data were normally distributed), the single exponential decay time course was found to be significantly longer than the fast component of the double decay time course of the miniature currents recorded from the same neurone ($P<0.0001$, n=4) although the variance of decay time constant within these two groups was not significantly different on 3 of the 4 occasions (for example see figure 5.16A, bin width=0.5ms). Initial interpretation of these two groups of data recorded from individual neurones was that each may represent distinct populations of miniature currents differentially located, one which decayed over a single exponential time

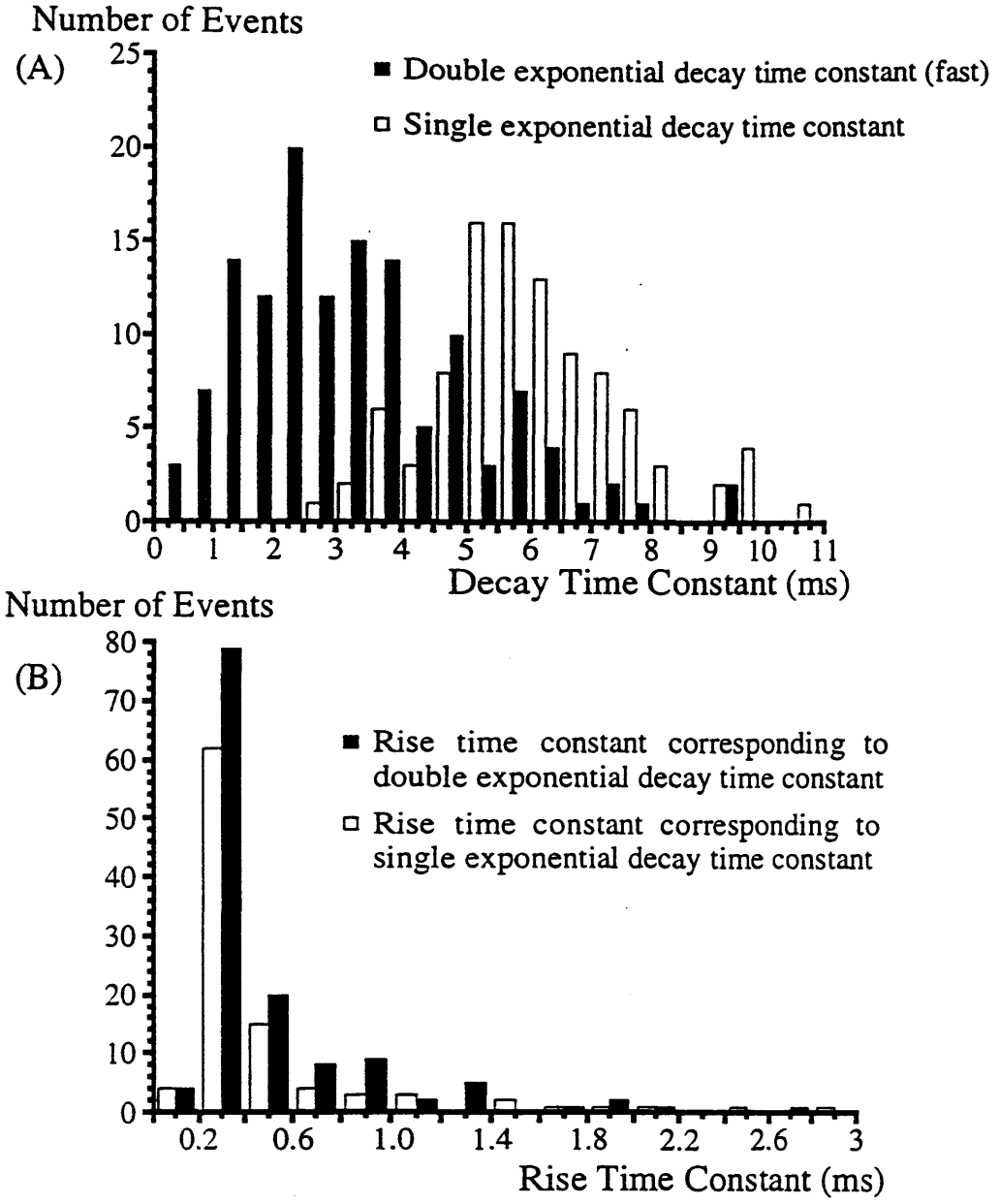

Figure 5.16 **Histograms of miniature current rise and decay time constants.**

(A) Histogram of single and double exponential decay time constants recorded from one neurone (bin width = 0.5ms). Mean single exponential decay time course was significantly longer than mean fast double exponential decay time course in miniatures recorded from the same neurone ($P<0.0001$, $n=4$).

(B) Histogram of single exponential rise time constants recorded from corresponding miniature currents in (A) (bin width = 0.2ms). Black columns represent rise time constants fitted to currents which decay over a double exponential time course; open columns represent rise time constants fitted to currents which decay over a single exponential time course. In 2 neurones no significant difference in rise time course was observed, but in 2 neurones a significant difference was observed.

course and another which decayed over a double exponential time course. From this, an investigation to determine if this distinction was also present in the rise time constant was conducted but no corresponding significant difference was observed in 2 of the 4 neurones tested (for example see figure 5.16B, bin width=0.2ms) suggesting that distinct locations of synaptic inputs could not be detected based on their rise time constants.

The poor ability to fit long decay time courses of miniature currents described above may provide an explanation for a portion of miniature currents decaying over a single exponential time course whilst the remainder decay over a double exponential time course. What may be happening is that all the miniature currents do infact decay over a double exponential time course, and those fitted by a single exponential function have a second decay component which is too long and small to be fitted accurately, forcing the fitting routine to fit a single exponential to a double exponential decay. On this assumption, the investigation of the relationship between rise and decay time constants used to discern the location of the synaptic inputs (see below) only incorporated those currents decaying over a double exponential time course (fast decay component only).

Amplitude of the Miniature Currents.

The amplitude of miniature currents was also examined in four neurones to see if this provided any evidence of two populations of miniature currents. Figure 5.17 shows amplitude histograms (bin width=20pA) along with mean and modal amplitudes of miniature currents recorded from 4 neurones. Once more there is no clear suggestion of different populations of miniature currents based on their amplitudes.

It can be noted however that the amplitude of the miniature currents is large compared to other reports for $GABA_A$ receptor mediated currents (e.g. Edwards, Konnerth & Sakmann 1990; Frerking, Borges & Wilson, 1995) but is similar to those reported by Legendre (1998) of glycine mediated miniature currents. The amplitude histograms also have quite a broad and skewed distribution, particularly in 2 of the 4 neurones examined (figure 5.17C & D) which may suggest multiquantal release of transmitter, a possibility which is discussed below.

Figure 5.17 **Histograms of miniature current amplitudes.**

Histograms of miniature current amplitudes recorded from 4 MSO neurones (bin width=20pA) and each corresponding mean and modal amplitude. No distinct miniature current populations can be detected within each neurone based on their amplitude although their amplitude is large and some difference in the distribution of amplitudes between neurones is apparent.

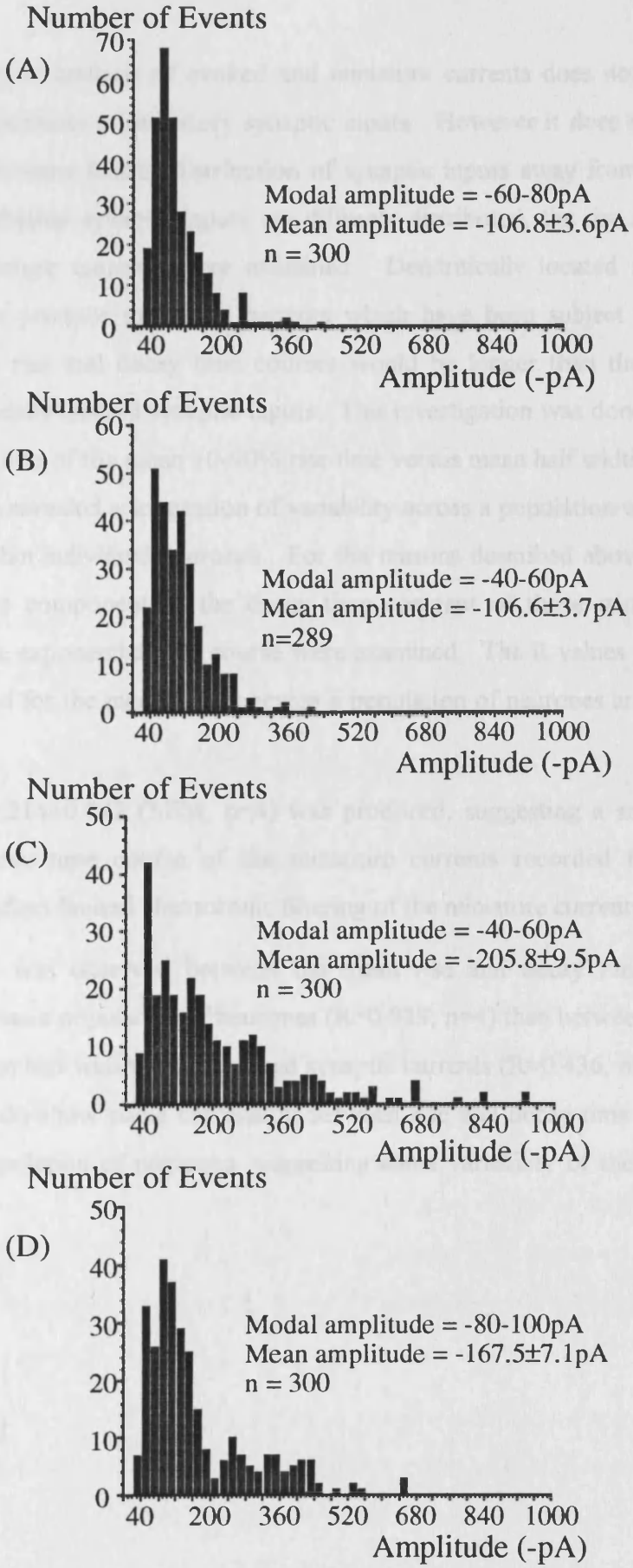
Number of Events
(A)
70
60
50
40
30
20
10
0
Modal amplitude = -60-80pA
Mean amplitude = -106.8±3.6pA
n = 300
40 200 360 520 680 840 1000
Amplitude (-pA)
Number of Events
(B)
60
50
40
30
20
10
0
Modal amplitude = -40-60pA
Mean amplitude = -106.6±3.7pA
n=289
40 200 360 520 680 840 1000
Amplitude (-pA)
Number of Events
(C)
50
40
30
20
10
0
Modal amplitude = -40-60pA
Mean amplitude = -205.8±9.5pA
n = 300
40 200 360 520 680 840 1000
Amplitude (-pA)
Number of Events
(D)
50
40
30
20
10
0
Modal amplitude = -80-100pA
Mean amplitude = -167.5±7.1pA
n = 300
40 200 360 520 680 840 1000
Amplitude (-pA)

Rise Time Constant Versus Decay Time Constant of the Miniature Currents.

Evidence shown so far of analysis of evoked and miniature currents does not provide good evidence for distinct locations of inhibitory synaptic inputs. However it does not exclude the possibility that there is some limited distribution of synaptic inputs away from the soma. In order to investigate whether synaptic inputs are diffusely distributed, the rise and decay time constants of the miniature currents were examined. Dendritically located synaptic inputs would be expected to produce miniature currents which have been subject to electrotonic filtering such that the rise and decay time courses would be longer than those of currents generated from somatically located synaptic inputs. This investigation was done in light of the results of the investigation of the mean 10-90% rise time versus mean half width of the evoked synaptic current which revealed a suggestion of variability across a population of neurones, but no such variability within individual neurones. For the reasons described above, only the rise time constant and fast component of the decay time constant of those miniature currents decaying over a double exponential time course were examined. The R values generated from individual neurones and for the mean values across a population of neurones are given in table 5.2.

A mean R value of 0.214±0.042 (SEM, n=4) was produced, suggesting a small correlation between rise and decay time course of the miniature currents recorded from individual neurones. This may reflect limited electrotonic filtering of the miniature currents.

A greater correlation was observed between the mean rise and decay time constants of miniature currents across a population of neurones (R=0.933, n=4) than between the mean 10-90% rise time and mean half width of the evoked synaptic currents (R=0.436, n=9). However, together these values do show some correlation between rise and decay time constant when recording across a population of neurones, suggesting some variability of the synaptic input between neurones.

5.4 Summary and Discussion

Major findings of this chapter:

- The decay of the inhibitory synaptic current recorded from MSO neurones was fitted by a double exponential function.
- The decay time course of the fast and slow components of the exponential fit were 8.54±0.44ms and 41.50±1.84ms, respectively (SEM, n=81) and the fast component dominated the decay.
- The decay time course is both voltage and temperature dependent.
- The decay time course is very variable between neurones, a finding which shows little correlation with age or series resistance.
- Electrophysiological study of both the evoked inhibitory synaptic current and corresponding miniature currents suggests that the synaptic input is largely somatically located.

5.41 Characteristics of the Decay Time Course of the Evoked Synaptic Current

5.411 Double Exponential Decay Time Constant

The evoked inhibitory synaptic current recorded from MSO neurones decays over a double exponential time course (8.54±0.44ms and 41.50±1.84ms, respectively; SEM, n=81.) where the fast component contributes ~90% of the overall amplitude. The time course of decay is very slow compared to that reported at fast excitatory synapses elsewhere in the auditory pathway (e.g. Barnes-Davies & Forsythe, 1995: τ_{fast}<1ms, τ_{slow}<4ms; Isaacson & Walmsley, 1995a, b: τ<1ms; Zhang & Trussell, 1994: τ<1ms) or some reports at inhibitory synapses (Stuart & Redman, 1990: τ~1ms). The decay time course was however similar to that reported of glycine mediated synaptic transmission in Mauthner cells of zebrafish larvae by Legendre (1998: τ_{fast}~5ms, τ_{slow}~40ms).

In order to determine if the slow decay of the evoked synaptic current was real or if it resulted from poor voltage control of the dendritic compartment, a protocol described by Pearce (1993) was conducted. Results from this experimental procedure suggested that the slow component was real and that the synaptic current was adequately voltage clamped throughout it's time

course. In addition, there was no correlation between the length of the decay time course and series resistance and in any case, to limit this possibility, series resistance was maintained below 25MΩ and series resistance compensation from 60-90% was routinely used.

5.412 What is Responsible for the Decay Rate of the Evoked Synaptic Current?

On the basis that the double exponential time course of decay of the synaptic current was real and did not result from poor voltage clamp, the question now arose as to what mechanisms underlie that decay rate? Rate of transmitter clearance from the synaptic cleft, receptor desensitisation and kinetics of channel deactivation are all thought to be factors which may be involved in determining the time course of synaptic currents (reviewed by Mayer *et al.*, 1995; Clements, 1996). The origin of the decay time course of the inhibitory synaptic currents recorded here is uncertain although any of these factors may be involved.

(A) Transmitter Clearance Rate

There is evidence to suggest at excitatory synapses in the CNS that transmitter time course in the synaptic cleft is very short and the average clearance rate is estimated at <200μs (reviewed by Clements, 1996). Transmitter clearance rates at central synapses are determined by a number of factors including reuptake mechanisms and transmitter diffusion rates. Since glutamate (excitatory neurotransmitter) and glycine (neurotransmitter at this synapse) are both amino acids and both have reuptake transporters it is likely that their respective timecourses in the synaptic cleft are similar. For this reason it is possible to draw parallels between transmitter clearance rates at excitatory and inhibitory synapses. With this in mind the average clearance rate of <200μs at excitatory synapses is clearly much shorter than the time course of the synaptic currents recorded here, suggesting that rate of transmitter clearance does not dictate the time course of the synaptic events.

(B) Desensitisation

Since most receptors including glycine receptors (Aoshima, *et al.*, 1992) are susceptible to desensitisation, the contribution that this mechanism made to the decay rate of the synaptic current could have been investigated. To do this, rapid iontophoretic application of paired

pulses of glycine would have been required. However, this was not done since a rapid application perfusion system was not available to me and the technique would ideally have required excised patches of membrane containing glycine receptor ion channels. Had this been done however, the results would inevitably have been complicated since iontophoretic application would have activated extrasynaptic receptors which may have different characteristics from subsynaptic receptors. However, Legendre (1998) conducted a similar investigation of glycine receptors expressed in Mauthner cells of the zebrafish larvae and did not observe any desensitisation of the glycine receptor mediated current.

An alternative technique could have been to examine the effects of rapid paired pulse synaptic stimulation. This however assumes that each stimulation results in the delivery of a supramaximal concentration of transmitter, a phenomenon which is widely accepted at excitatory synapses (reviewed by Clements, 1996). This technique was attempted but difficulties arose since the method of gross stimulation resulted in multiple axonal stimulation, each axon of which would have different activation thresholds. Consequently, postsynaptic receptor activation resulting from synaptic stimulation would not be constant between each synaptic input, making interpretation of the results difficult. In addition, this technique does not incorporate autoreceptor activation, a phenomenon which would inevitably alter the current flow in response to the second stimulus.

Further examination of the role of desensitisation could be done by reducing the probability of transmitter release and observing the effect this has on the synaptic current time course. However, this is not foolproof as it depends on the degree of saturation of the postsynaptic receptors. Although lowering extracellular calcium would reduce the probability of transmitter release, any release that did occur would be likely to saturate the postsynaptic receptors, so receptor desensitisation would still occur.

Receptor desensitisation may play a role in the decay time course, as has been demonstrated of EPSCs in bushy cells and IPSCs in MNTB neurones in the auditory pathway (Zhang & Trussell, 1994; Kungel & Friauf, 1997). In a similar manner to MSO neurones, bushy cells and MNTB neurones also need to follow high frequency inputs to maintain temporal fidelity of transmission, a process to which desensitisation may contribute. A mechanism by which receptor desensitisation may contribute to the maintenance of high fidelity firing is the cycling of receptor activation such that all receptors are not active, and therefore not desensitised at the same time.

(C) Channel Kinetics

The role of channel kinetics in determining current time course was addressed recently by Legendre (1998) who demonstrated that a glycine receptor mediated current recorded from Mauthner cells of zebrafish larvae decays over a double exponential time course. He proposed that the second slow component of decay results from a reluctant gating mode of the glycine receptor and not from receptor desensitisation.

Alternatively, Akaike & Kaneda (1989) who also demonstrated glycine receptor mediated currents decaying over a double exponential time course, proposed that the two decay phases represent different glycine receptor isoforms which operate individual chloride channels with different single channel conductances. Takahashi *et al.* (1992) supported this suggestion and proposed that the different receptor isoforms resulted from the developmental change from neonatal (α_2) to adult (α_1) isoforms of the glycine receptor. They found that with increasing age the decay time course of glycine mediated synaptic currents in spinal neurones speeded up (E20 mean=27ms; P16 mean=5.9ms). They then examined the single channel open time of each of α_1 and α_2 homomeric glycine receptors expressed in *Xenopus* oocytes and compared the open times with those of natively expressed channels. The results of their investigation demonstrated that the single channel open time of neonatal (α_2) glycine receptors is longer than that of adult (α_1) glycine receptors (*Xenopus*: α_1=2.38ms, α_2=174ms; native: P16=2.01ms, E20=39.9ms). From this they proposed that the single channel open time of the channels underlies the time course of the synaptic current. Although the mean single channel open time of the α_2 channels homomerically expressed in *Xenopus* oocytes was significantly longer than the native embryonic glycine receptors, they proposed that the difference resulted from the fact that even early on in development, at least some α_1 subunits are already expressed. A similar explanation of mixed isoform expression may underlie the reason why the decay time course of the evoked synaptic current in my study showed no clear age dependence. It is possible therefore that an age dependent change in glycine receptor expression may at least in part account for the decay rate of the synaptic current, an observation made by Krupp, Larmet & Feltz (1994) and an issue which is discussed in more detail later.

(D) Asynchronous Release

Another observation from these results was that the mean double exponential decay time course of the evoked synaptic current (τ_{fast}=8.54±0.44ms, τ_{slow}=41.50±1.84ms, SEM, n=81) was longer than that of the miniature currents (τ_{fast}=3.56±0.20ms, τ_{slow}=22.92±1.28ms, SEM, n=4). This difference could be accounted for by the fact that miniature and evoked currents were not recorded from the same neurones. However, a more likely explanation of the disparity could be the asynchronous release of transmitter slowing the time course of the evoked currents. Issacson & Walmsley (1995b) and Diamond & Jahr (1995) demonstrated at excitatory synapses that the asynchronous release of neurotransmitter at least in part determines the decay time course of evoked synaptic currents which they found to be longer than that of miniature currents. A similar observation was made by Stuart & Redman (1990) at an inhibitory, glycine receptor mediated synapse where population IPSCs had longer rise and decay time courses than unitary IPSCs. They accounted for this by the temporal dispersion of neurotransmitter release upon synaptic stimulation.

5.413 Voltage Dependence of the Decay Time Course

Another feature of the decay time course of the evoked synaptic current which is common to other ligand gated ion channels was it's voltage dependence where depolarisation resulted in a lengthening of the time course. The nicotinic acetylcholine receptor was reported by Magleby & Stevens (1972) to show some voltage dependence but depolarisation there caused a reduction of the decay time course of the current. Other reports have demonstrated that the decay time course of glycine mediated currents also have some voltage dependence (e.g. Akaike & Kaneda 1989; Legendre, 1998; Stuart & Redman, 1990; Krupp, Larmet & Feltz, 1994). Voltage dependence of ligand-gated ion channels could be explained by a change in single channel conductance, a change in frequency of channel openings or a change in single channel lifetime with voltage. The latter of these three mechanisms was proposed by Gundersen, Miledi & Parker, (1986) from their investigations of single channel currents of human glycine receptors expressed in *Xenopus* oocytes. They found that depolarisation resulted in rectification of current amplitude and using single channel analysis they found that the mean channel open time reduced at hyperpolarised potentials. Akaike & Kaneda (1989) also observed that in addition to a voltage dependence of decay time course where the time constant gradually increased with depolarisation, that current amplitude was also voltage

dependent. Stuart & Redman (1990) demonstrated that depolaristion lengthened the time course of decay of inhibitory currents in spinal motoneurones. They attributed this voltage dependence to a voltage dependence of channel opening on the basis that if the decay rate reflects channel open time, then a voltage dependence of the decay rate results from a voltage dependence of the channel open time.

Irrespective of the mechanism underlying the voltage dependence, it is potentially an important feature of the inhibitory synaptic input to the MSO. Although only a small voltage dependence was observed, as the membrane potential is depolarised toward threshold, so the contribution of the inhibitory synaptic input increases. So, what ever role the inhibitory synaptic input to the MSO is playing, it will be enhanced upon depolarisation.

5.414 Temperature Dependence of the Decay Time Course

In addition to demonstrating the voltage dependence of an *in vivo* glycine receptor mediated inhibitory current, Stuart & Redman (1990) also demonstrated that the decay time course of the inhibitory synaptic current was much faster than observed here (~1ms). However, their investigations were conducted *in vivo* at 37°C in cat, so the temperature dependence of the time course in my preparation was investigated and revealed a Q_{10} of 2.08±0.23 (SEM, n=4). The fact that my experiments were conducted at 25°C will at least in part account for the slow decay time course of the evoked synaptic current because at 37°C, the mean decay time course was ~3.5ms. Increased asynchrony of transmitter release at low temperatures may also contribute to the time course of current decay (Issacson & Walmsley, 1995b; Diamond & Jahr, 1995). Temperature dependence of glycine mediated currents was also observed in sympathetic preganglionic neurones by Krupp, Larmet & Feltz (1994). However, since the decay time course at 37°C is still substantially longer in my preparation than that reported by Stuart & Redman (1990), temperature cannot entirely account it's slowness and does in no way explain the great variability between neurones that I have observed.

5.42 What is Causing the Variability in Decay Time Course?

Apart from the observation of the long length of the decay time course of the evoked synaptic current and the mechanisms underlying the time course, a puzzling question arose regarding the clear observation that this decay is also very variable between neurones, even when

recorded from the same animal. As described above, more than one mechanism could underlie the rate of decay of the synaptic current. The known developmental change in expression of glycine receptor isoforms and the corresponding change in single channel kinetics (Friauf, Hammerschmidt & Kirsch, 1997; Akagi & Miledi, 1988; Becker, Hoch & Betz, 1988; Takahashi *et al.*, 1992) makes it entirely possible that the decay time course and its variability between neurones observed here is a consequence of developmental glycine receptor changes. Many of the experiments conducted in this chapter have therefore been done in an attempt to determine if this is the case.

5.421 Series Resistance

An obvious factor which may explain both the length and variability of the decay time course of the evoked synaptic current is high series resistance. This would result in poor voltage clamp and slowing of the synaptic current. However, this explanation is unlikely because there was no obvious correlation between decay time course and series resistance.

5.422 Age Dependent Changes

An examination to see if there was any correlation between age and decay time course was conducted but little correlation was apparent so developmental changes did not immediately explain the variability in time course. This contrasts with the findings of Krupp, Larmet & Feltz (1994) and Takahashi *et al.* (1992) who found that the decay time course of glycine mediated synaptic currents reduced with age.

Use of the α_1 glycine receptor isoform specific antagonist, cyanotriphenylborate (CTB) (Rundström *et al.*, 1994) did not reveal differential glycine receptor isoform expression between different neurones so this cannot account for the wide variability in decay time course. The lack of any action of CTB in this study contrasts with observations of Kungel & Friauf (1997) who demonstrated that CTB significantly reduced current amplitude of a glycine mediated current recorded from MNTB neurones in animals older than 7 days, whilst they observed no effect of CTB in animals younger than this. They attributed this differential action of CTB to an age dependent change in expression of glycine receptor isoform. Clearly a difference in the observed action of CTB exists between the results shown here and those of Kungel & Friauf (1997). In my study, low concentrations of CTB were used (20μM) in order

to minimise the risk of toxic effects and membrane breakdown which might occur at high doses (D. Langosch, personal communication). Kungel & Friauf (1997) iontophoretically applied 100mM glycine and applied 10mM CTB by local pressure ejection. They proposed that these application techniques required concentrations 1000-fold higher in order to reach the required concentration at the synapse. However, the difference between the results could also be explained by the site of action of the ligands in the two methods. Whilst the currents in this study resulted from activation of subsynaptic glycine receptors, iontophoretic application of glycine is likely to additionally activate extrasynaptic glycine receptors. The difference between our results may therefore stem from differential sensitivity of subsynaptic and extrasynaptic glycine receptors to CTB. In addition, although CTB is reported as an α_1 subunit specific antagonist (Rundström *et al.*, 1994), it lacks specificity as it also blocks α_2/β heteroligomers (D. Langosch, personal communication). The use of CTB was therefore not thought to be a reliable indicator of α_1 glycine receptor isoform expression.

Together, the results shown here suggest that the variability in decay time constant is not a function of age of the animal. Even time constants measured from neurones from within the same animal show a great deal of variability. However, the lack of correlation may at least in part result from experimental limitations. For example, animals develop at different rates so whilst there is a developmental change in expression in the glycine receptor isoform, this change is not going to occur at the same developmental time in each animal. Similarly, within an individual animal, cells will develop at different rates such that each neurone may express different proportions of neonatal and adult glycine receptor isoforms at any one time. A similar explanation was postulated by Takahashi *et al.* (1992) to explain the disparity they observed between the mean single channel open time of α_2 homooligomers expressed in *Xenopus* oocytes and that of embryonic (E20) native glycine receptor mediated currents in the spinal cord. Native receptors, even during embryonic development will express a certain proportion of the adult (α_1) isoform of the glycine receptor, shortening the mean single channel open time.

The ability to use a wider range of animals to observe any correlation may have been beneficial. However, it was necessary in this study to use such young animals because upon maturation the brain stem becomes densely myelinated, making visualisation of individual neurones very difficult. It is for this reason that there are relatively few records from animals over 10 days old. Future developmental study of this will require a more satisfactory method of monitoring

development, perhaps incorporating the weight of the animal as an additional index of its developmental status.

It should also be noted however that despite the above results not supporting age dependent changes to be responsible for differences in the decay time course, there is some suggestion that the fast component of decay appears to have a greater contribution to the overall current amplitude as age increases. This is quite plausible because if for example the second, slow component of decay of the evoked synaptic current results from activation of the α_2 subtype, which has a longer open time than the α_1 subtype, then as expression of α_2 declines with age, so its contribution to the synaptic current reduces. In addition, Kandler & Friauf (1995) noticed some reduction in duration of synaptic responses in the LSO between E18 and P17 which they partly attributed to a decrease in membrane time constant.

5.423 Synaptic Location

An alternative hypothesis explaining the variability in decay time course could be differences in the location of synaptic inputs. The MSO is known to receive excitatory inputs to its dendritic trees (Cant & Casseday 1986; Warr, 1966; Clark, 1969; Lindsey, 1975; Stotler, 1953) whilst the inhibitory inputs are thought to be somatically located (Clark, 1969; Oliver, Beckius & Schneiderman, 1995; Brunso-Bechtold, Henkel & Linville, 1990; Kuwabara & Zook, 1992). However, if the inhibitory inputs were more diffusely located this would affect the time course of the synaptic current slowing it's rise and decay rates. So, confirmation of the location of the inhibitory synaptic inputs was investigated here using immunohistochemical and electrophysiological techniques.

(A) Immunohistochemistry

Problems were encountered with the immunohistochemical investigations in maximising the contrast of labelling. Precise location of the inhibitory synaptic inputs using this technique was therefore not revealed although some suggestion of punctate glycine antibody labelling was observed. Further work using glycine specific antibodies needs to be conducted to fulfil this aim and eventually to identify the proportions of glycine receptor isoform present. However, this extends beyond the scope of this thesis and is not discussed any further but is a potential source of further information about the synaptic inputs the MSO receives.

(B) Electrophysiology

Several electrophysiological investigations were then conducted in an aim to identify the location of the inhibitory synaptic inputs to the MSO. Initially experiments were limited to evoked synaptic currents but later, further investigations of miniature currents were conducted.

(i) Evoked Synaptic Currents

(a) 10-90% Rise Time Versus Half Width

Examination of the 10-90% rise time and half width of the evoked synaptic current was conducted to determine if the variability in decay time course resulted from some cells having somatically located- and other cells having dendritically located synaptic receptors. Results of this investigation suggested that within individual neurones there was no great range of distribution of synaptic receptors but that across a population of neurones, some evidence of variability was apparent. This evidence did however show a small correlation with series resistance and a larger (but still small) correlation with age of animal.

Since there was little correlation between the 10-90% rise time and half width of the evoked synaptic current in individual neurones it suggests that each neurone does not have diffusely located synaptic receptors. However, the small correlation between these two parameters across a population of neurones suggests that the synaptic receptors are not necessarily consistent across a population of neurones. This inconsistency across a range of neurones may be related to the age of the animal, but this interpretation is very tentative since there is also a small correlation with series resistance, a factor which may affect the time course of the current substantially. Takahashi *et al.* (1992) found no correlation between rise and decay time constants of evoked inhibitory synaptic currents in the spinal cord, suggesting decay is independent of synaptic location. Barnes-Davies & Forsythe (1995) observed similar results to myself in the MNTB where no correlation between half width and rise time of the EPSCs was observed in individual neurones, but some correlation was observed across the population studied. Since the MNTB receives a giant calyceal synaptic input, it s location is not under question. Their interpretation of the correlation they observed between rise time and half width at this synapse between neurones was that it resulted from differential isoform expression or modulation of receptor subunits in individual MNTB neurones. This explanation

may hold true for the MSO, particularly in light of the aforementioned developmental change in expression. However before reaching this conclusion, further experiments were first conducted in an attempt to elucidate the location of the synaptic receptors.

(b) "Switch off" of the Synaptic Current

Another indication of the synaptic location of inhibitory inputs to MSO neurones was hoped to be achieved by examining the rate of switch off of the synaptic current. The rate of current switch off was determined by stepping the holding potential of a neurone to the current's reversal potential during the decay phase of an evoked synaptic current and measuring the time course over which the synaptic current disappeared, or "switched off". Isaacson & Walmsley (1995a) have previously reported the rate of switch off of a synaptic current to be indicative of synaptic location. Based on their interpretation, results presented here suggest that the synaptic input is mainly somatic, with a minor dendritic input. However, arrival at this conclusion must be treated with caution because the results could be interpreted in one of two ways. Firstly, the rate of switch off could reflect the synaptic location, as proposed by Isaacson & Walmsley (1995a) or secondly, the slower component of the current switch off rate could result from the dendrites acting as a current sink. In this second scenario it is possible that the currents are all generated somatically and that the current distributes along the dendrites so when the holding potential is stepped to the reversal potential, the now dendritic current re-invades the soma, resulting in the current switch off occurring over a slower decay time course.

Results from this investigation are therefore not clear cut so the demonstration of a double exponential switch off of synaptic current does not necessarily confirm a dendritic synaptic input although the results are consistent with a largely somatic synaptic input.

(ii) Miniature Currents

An examination of miniature currents recorded from MSO neurones was conducted in an attempt to elucidate underlying features of the evoked synaptic currents, the cause of the double exponential decay time course and the location of the synaptic receptors whose activation underlies the synaptic current. Miniature currents are interpreted as current flow through a postsynaptic ion channel resulting from the release of a presynaptic vesicle of

transmitter. Early investigations of the neuromuscular junction (Katz, 1969; del Castillo & Katz, 1954) revealed that presynaptic vesicles contain a discrete amount of transmitter, a characteristic which was later included in theories of the mechanisms underlying CNS synaptic currents (reviewed by Korn & Faber, 1991).

(a) Amplitude Distribution

On the basis that presynaptic vesicles contain a discrete quantity of neurotransmitter and are released individually, one would anticipate that analysis of miniature current amplitude would reveal a single population of miniature current amplitudes which followed a Gaussian distribution which was narrowly distributed around the mean. However, results of this study demonstrated miniature currents which were both large in amplitude and had both broad and skewed amplitude distributions (figure 5.17). The large amplitude was observed in all four data sets and the wide distribution of amplitudes and skewness of that distribution was particularly apparent in two of the data sets (figure 5.17C & D). Similar observations to this have been previously reported and have been implicated to represent multiquantal release (e.g. Edwards, Konnerth & Sakmann 1990; reviewed by Walmsley, 1991). Legendre (1997) provided pharmacological evidence that two types of postsynaptic glycine receptor in Mauthner cells of zebrafish larvae account for the broad distribution of miniature current amplitudes in that preparation, but no such pharmacological evidence has been provided here. It is also possible that each presynaptic vesicle does not contain a constant amount of neurotransmitter (Frerking, Borges & Wilson, 1995), a phenomenon which may account for the variability in miniature current amplitude. Frerking, Borges & Wilson (1997) later investigated the mechanism underlying multiquantal release in the anticipation that it results from spontaneous entry of calcium into the presynaptic terminal which in turn causes the synchronous release of transmitter from a particular terminal containing multiple release sites. However, on investigation, they found this not to be the case because even when calcium concentrations were buffered, a wide and skewed distribution of miniature amplitudes remained. The mechanism underlying multiquantal release in the CNS therefore remains unresolved at this time.

Irrespective of the origin of the large amplitude miniature currents and the skewed and wide distribution of those amplitudes, one finding that did emerge was that miniature current amplitude analysis did not obviously reflect the existence of more than one population of

miniature currents in each neurone. Combined with the observation of different variances of amplitudes between neurones this data once again supports the idea that within individual MSO neurones there is no distinct difference in expression of glycine receptor, either spatially or developmentally. However, the data may hint at differences in expression across a population of neurones.

(b) Time Course

The analysis of miniature current time courses and their sensitivity to strychnine (chapter *4.322*) revealed that the miniature currents are likely to underlie the evoked synaptic current. When examining the decay time course of the miniature currents some were found to decay over a single exponential time course and others over a double exponential time course. Various reasons could explain this. Firstly, the small mean amplitude of the miniature currents compared to the evoked synaptic currents made the ability to fit their time courses less precise. Consequently, consistent good fitting was more difficult to achieve of the miniature currents, making the measured time course less accurate. Secondly, the frequency of the miniature currents limited the time over which they could be fitted (~50ms). Since the decay time course of the evoked synaptic current is quite long and assuming that these miniature currents underlie the evoked synaptic current, one would anticipate that the miniature currents would decay over a similarly long time course. Therefore, the limiting the period over which the miniature currents could be fitted would have inevitably reduced the ability to fit those currents decaying over a long time course. Combined with the observation that the rise time constants of the miniature currents were not similarly grouped by their time courses, the conclusion was drawn that the decay of all the miniature currents would ideally be fitted by a double exponential function, so those fitted by single exponentials were excluded from further analysis.

From this assumption, it is clear the decay time course of the miniature currents is very similar to that of the evoked synaptic current, if a little faster (evoked: τ_{fast}=8.54±0.44ms, τ_{slow}=41.50±1.84ms, SEM, n=81; miniature: τ_{fast}=3.56±0.20ms, τ_{slow}=22.92±1.28ms, SEM, n=4). This disparity can be partly explained by the difficulties described above in fitting small currents accurately and by the limited time period over which the currents could be fitted. In addition the asynchrony of release of the neurotransmitter generating the evoked synaptic currents is likely to have slowed its time course. A similar disparity was observed by Stuart & Redman (1990) where population IPSCs rose and decayed over a slower time course than

corresponding unitary IPSCs in spinal cord motoneurones. They accounted for this difference by proposing that it resulted from the temporal dispersion of neurotransmitter release in spinal motoneurones. Otis & Trussell (1996) also proposed that decay time course is dependent on the absolute number of quanta released, such that the EPSCs they were recording from bushy cells in the chick auditory pathway slowed with increasing quantal content.

Rise Time Course Versus Decay Time Course

In a similar experimental procedure as was used for the evoked synaptic currents to determine if there was evidence for distinct location of synaptic inputs, the rise and decay time constants of miniature currents were measured. Electrotonically distant synaptic inputs would be expected to produce miniature currents with rise and decay time courses longer than somatically located synaptic inputs.

A small correlation (R=0.214±0.042, SEM, n=4) was observed between rise and decay time constants of the miniature currents recorded from individual neurones which may reflect limited electrotonic filtering of the miniature currents. However, a much greater correlation was observed between the mean rise and decay time constants across a population of neurones (R=0.933, n=4). Both of these correlations are bigger than the corresponding results of the evoked synaptic current where R=0.190±0.071 (SEM, n=9, individual neurones) and R=0.436 (n=9, population), respectively. Together, the R values from both the evoked synaptic and miniature currents demonstrate little variation of the synaptic input within individual neurones but suggest some variability of synaptic input across a population. This variability may however be accounted for by differential glycine receptor expression or receptor properties as a result of age dependent changes

5.43 Overview

Taken together, the results of this chapter imply that the MSO receives a largely somatic inhibitory synaptic input with the hint of more distally located inputs. Within individual neurones this seems a reasonably secure intepretation, based on evidence of the relationship between the rise and decay time constants of miniature currents and of the 10-90% rise time and half width of the evoked synaptic current. Although immunohistologically there was limited evidence to support this finding, the results are consistent with those previously

reported, which suggest that inhibitory synaptic inputs to the MSO are largely somatic (Clark, 1969; Oliver, Beckius & Schneiderman, 1995, Brunso-Bechtold, Henkel & Linville, 1990; Kuwabara & Zook, 1992). Despite this evidence within individual neurones there is some evidence to suggest differences in synaptic inputs or receptor properties between neurones. This evidence is based on the findings of the correlation between the mean rise and decay time constants of the miniature currents and the mean half width and mean 10-90% rise time of the evoked synaptic currents across a population of neurones. Barnes-Davies & Forsythe (1995) had similar findings in the MNTB and interpreted this as a possible difference between the modulation and receptor subtype expression between neurones. It may be possible to draw such a conclusion here since there is evidence from others to suggest a developmental change in glycine receptor isoform expression (Friauf, Hammerschmidt & Kirsch, 1997; Akagi & Miledi, 1988; Becker, Hoch & Betz, 1988; Takahashi *et al.*, 1992; Krupp, Larmet & Feltz, 1994) which would alter the decay time course of the synaptic current.

It is likely from the results presented here, combined with previous reports of others, that the slow decay rate of the inhibitory synaptic current and the variability of that decay rate results from a differential expression of different glycine receptor isoforms. It is likely that the expression is mainly limited to the soma of MSO neurones although there may also be a small non-somatic inhibitory synaptic input.

Chapter 6 - Results

6 Results

6.1 Introduction

The results presented so far describe in some detail the physiology and pharmacology of the MSO and the synaptic inputs it receives, in particular that of the inhibitory synaptic input from the ipsilateral MNTB. This chapter will go on to describe some of the preliminary observations that have been made regarding modulation of that inhibitory synaptic current.

The central nervous system has an intricate circuitry so descriptions of the central auditory pathway given thus far are likely to grossly underestimate the complexity of the circuitry. In addition to the basic excitatory and inhibitory synaptic inputs to the MSO from the AVCN and MNTB respectively, there are likely to be other inputs which will play a role in the action of the MSO. For example, in addition to glycine receptor immunoreactivity, previous reports have also demonstrated sparse GABAergic terminals in the MSO (Vater, 1995; Adams & Mugnaini, 1990). Glycine receptor immunoreactivity can be accounted for because of the strong glycine mediated input the MSO receives from the ipsilateral MNTB (chapters *4* & *5*). However, as was shown in chapter *4*, the $GABA_A$ receptor antagonist, bicuculline had no effect on the evoked synaptic current. So why is GABA in the MSO if it is not involved in the synaptic pathways? GABA could be acting at the G-protein-linked $GABA_B$ receptor in an action which will modulate synaptic transmission. Modulation of this nature has been demonstrated previously in the mammalian central auditory system (Barnes-Davies & Forsythe, 1995) and it is here that this chapter begins. It then goes on to explore other possible modulatory pathways including those using metabotropic glutamate receptors or 5-hydroxy tryptamine receptors. Further, more probing experiments including investigations of miniature currents need to be conducted regarding modulation of this inhibitory synaptic current, the results of which may assist in the exploration of the MSO and the synaptic inputs it receives.

6.2 Methods

The whole cell patch clamp technique and brain stem slice preparation described in chapter *2* were used throughout. The intracellular solution was a CsCl-based patch solution containing 132mM Cl^- (appendix 1Biii), and the extracellular solution was a normal bicarbonate buffered ACSF containing 133.5mM Cl^- (appendix 1Aii). EAA antagonists (50μM DL-AP5, 10μM

CNQX, 5μM 5,7-dichlorokynurenic acid and 5μM MK801) and 10μM bicuculline were included in the perfusate throughout in order to isolate the strychnine-sensitive component of the synaptic response. Miniature current recordings were made in the presence of 0.5μM TTX. A bipolar platinum stimulating electrode, described in chapter *2.25* (figure 2.12) was used to evoke synaptic currents and solutions were applied to the preparation via the bath perfusion system.

Evoked synaptic current data were acquired and filtered as described in chapter *2*. Miniature currents were initially recorded onto a Digital Tape Recorder (DTR-1404) and were later filtered and digitised at 2kHz and 5kHz, respectively. Miniature current data analysis was done using 'Strathclyde Electrophysiology Software, Whole Cell Program', version 1.2.

6.3 **Results**

6.31 $GABA_B$ Receptors

6.311 Evoked Synaptic Current

The inhibitory synaptic current generated upon stimulation of the ipsilateral MNTB when recording from the MSO is subject to modulation by the $GABA_B$ receptor agonist, baclofen. Figure 6.1 demonstrates that application of 5μM baclofen reduces the evoked peak synaptic current amplitude by 88.5±1.9% (SEM, n=4), an action which is partially reversible.

Further investigation of the role $GABA_B$ receptors play in this synaptic pathway was then conducted. The $GABA_B$ receptor antagonist, 500μM 2-hydroxy saclofen was included in the perfusate to see if there was any basal level of activity of $GABA_B$ receptors. If this were the case, the peak synaptic current would be expected to increase in amplitude. However, 500μM 2-hydroxy saclofen was found to reduce the amplitude of the evoked synaptic current by 68.3% (n=2) (figure 6.2), suggesting that it has partial agonist properties, an observation consistent with that of Kombian, Zidichouski & Pittman (1996). Kabashima *et al.* (1997) did not encounter such problems in rat supraoptic nucleus where they observed that 2-hydroxy saclofen increased the frequency of spontaneous inhibitory and excitatory currents without affecting their amplitude.

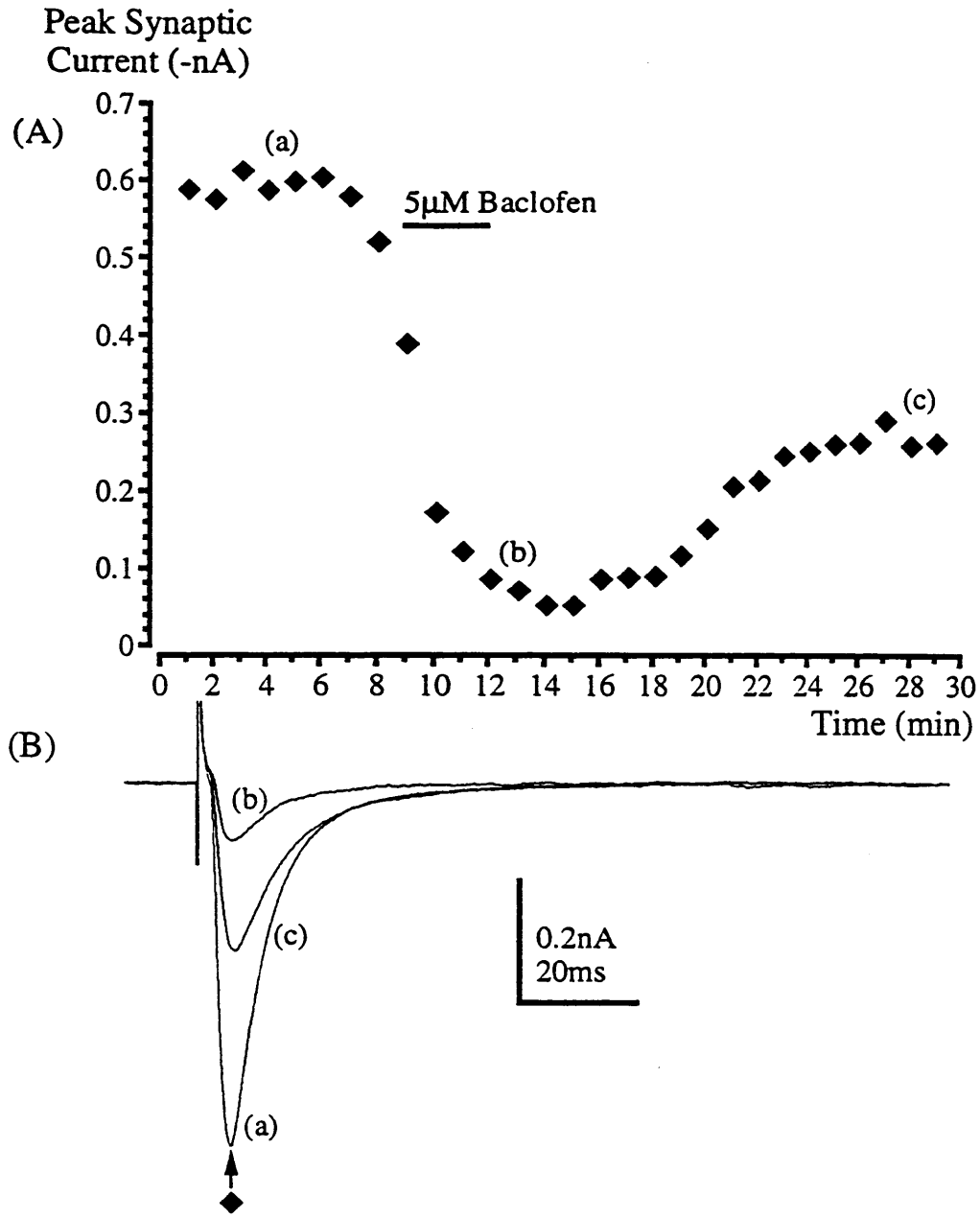

Figure 6.1 **The $GABA_B$ receptor agonist, baclofen modulates the inhibitory postsynaptic current.**

(A) Plot of mean peak inhibitory synaptic current recorded from an MSO neurone before and during application of and after wash off of 5µM baclofen.

(B) Selected mean current traces corresponding to (A) recorded from an MSO neurone (a) before, (b) during and (c) following wash off of 5µM baclofen.

The mean peak synaptic current amplitude was reduced by 88.5±1.9% (SEM, n=4) but the time course of decay of the synaptic current remained unaltered. The effect of 5µM baclofen was partially reversible.

Points and traces are averages of 20 events each.

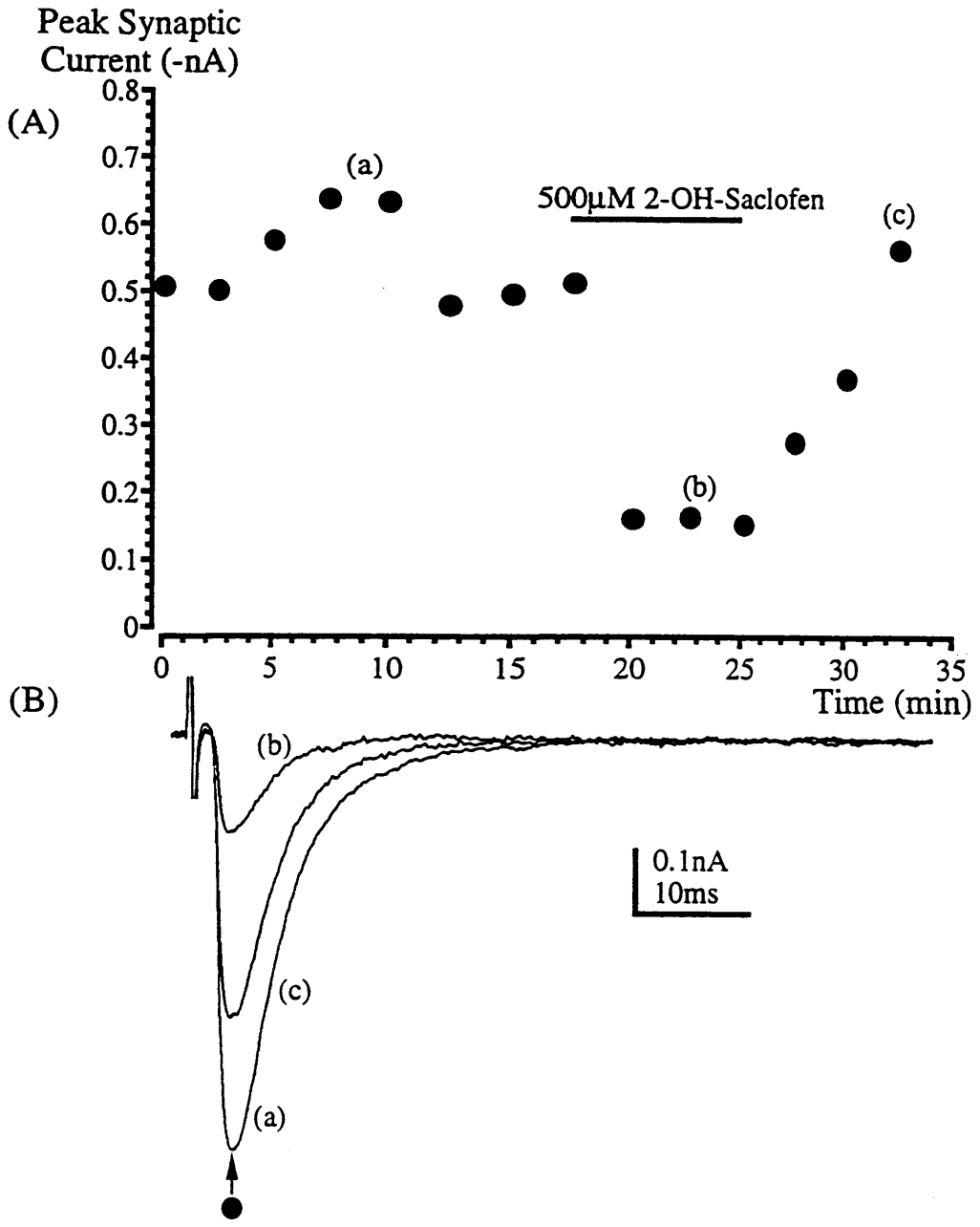

Figure 6.2 **The $GABA_B$ receptor antagonist, 2-hydroxy saclofen shows partial agonist properties.**

(A) Plot of mean peak inhibitory synaptic current reorded from an MSO neurone before and during application of and after wash off of 500µM 2-hydroxy saclofen.

(B) Selected mean current traces corresponding to (A) recorded from an MSO neurone (a) before, (b) during and (c) following wash off of 500µM 2-hydroxy saclofen.

500µM 2-hydroxy saclofen reduced the mean peak synaptic current amplitude was reduced by 68.3% (n=2).

Points and traces are averages of 10 events each. EAA antagonists and bicuculline were applied throughout

In light of the potential partial agonist properties of 2-hydroxy saclofen, its co-application with baclofen was not conducted since interpretation of the results would have been complex. Instead, a reportedly more specific (Kombian, Zidichouski & Pittman, 1996) $GABA_B$ receptor antagonist, CGP 36742 was used. Application of 50μM CGP 36742 alone was found to have no effect on the amplitude of the peak synaptic current (figure 6.3, n=2) suggesting no basal $GABA_B$ receptor activity. However, when co-applied with 5μM baclofen, 50μM CGP 36742 did not inhibit the reduction in peak synaptic current amplitude induced by baclofen (figure 6.3, n=1) suggesting a high enough concentration was not used.

500μM CGP36742 was then applied alone and was found to reduce the peak synaptic current amplitude (n=1). When co-applied at this concentration with 5μM baclofen, their actions combined to reduce the current amplitude dramatically (figure 6.4, n=1) suggesting that CGP 36742 also has partial agonist properties.

6.312 Miniature Inhibitory Postsynaptic Currents (mIPSCs)

Further information can be gleaned regarding the site of action of baclofen on the evoked synaptic response by examination of its action on the miniature current amplitude and frequency, recorded from the MSO. It is known that if a compound is acting at a presynaptic site, the miniature currents it is affecting will remain of constant amplitude but their frequency will change. Once more, as explained in chapter *5.423*, miniature currents are thought to occur as a result of the release of a discrete quantity of transmitter from the presynaptic terminal activating postsynaptic receptors (Katz, 1969; del Castillo & Katz, 1954; reviewed by Korn & Faber, 1991). So, assuming that every vesicle contains a discrete quantity of neurotransmitter, any change affecting the release of those vesicles will affect the frequency of miniature currents. It is possible that each presynaptic vesicle does not contain a constant amount of neurotransmitter, a phenomenon which may explain the variability in miniature current amplitude in chapter *5.321* and was proposed by Frerking, Borges & Wilson (1995). However, even if this were case, any presynaptic change would still be reflected by a change in miniature current frequency. If a compound is acting at a postsynaptic site, a change in miniature current amplitude would be anticipated, although interpretation of this is more complex. Previous studies have proposed that baclofen acts presynaptically in the brain stem auditory pathway (Barnes-Davies & Forsythe, 1995; Otis & Trussell, 1996) so it was expected to have a similar action here.

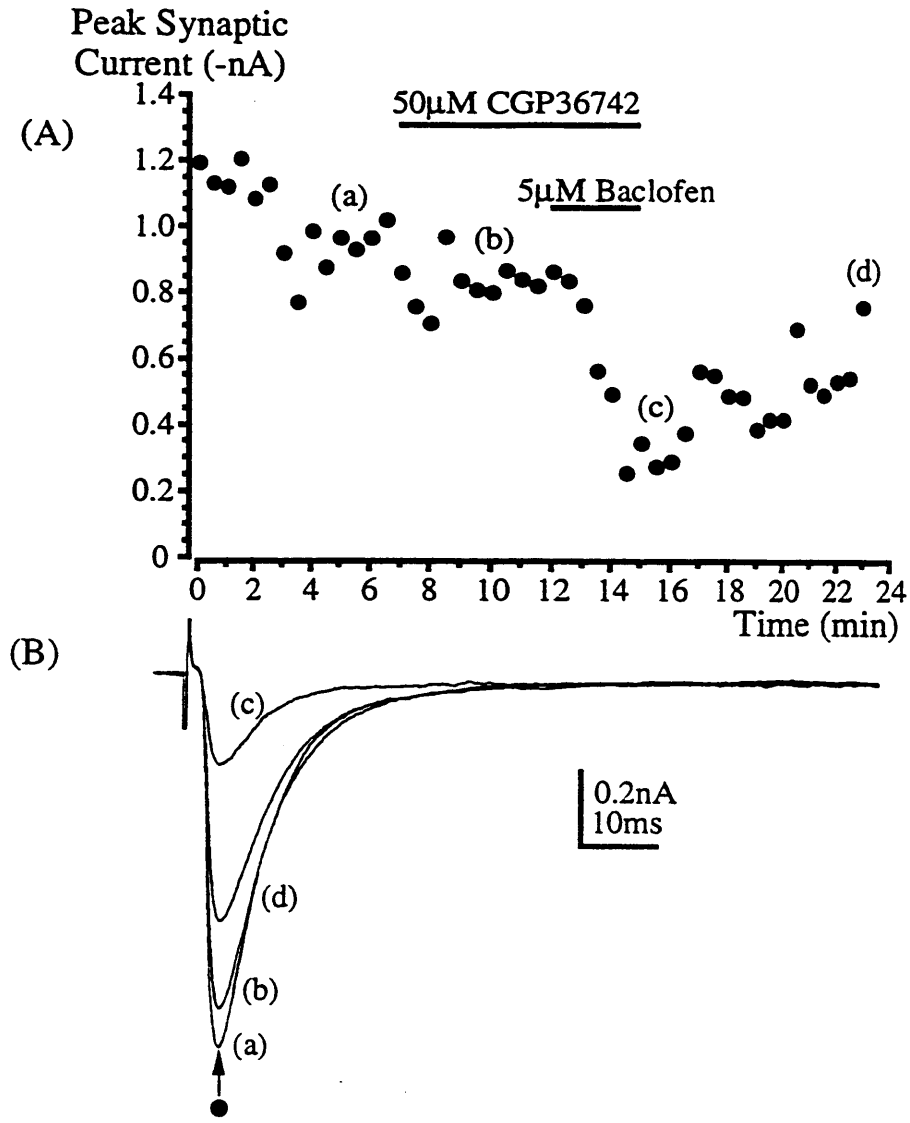

Figure 6.3 **50µM CGP36742 does not block the action of 5µM baclofen.**

(A) Plot of mean peak inhibitory synaptic current recorded from an MSO neurone before and during application of and after wash off of 50µM CGP36742 and 5µM baclofen.

(B) Selected mean current traces corresponding to (A) recorded from an MSO neurone (a) before and (b) during application of 50µM CGP36742, (c) during application of 50µM CGP36742 and 5µM baclofen and (d) after wash off of both substances.

50µM CGP36742 had no direct action on the peak synaptic current amplitude (n=2) and did not appear to block the action of 5µM baclofen (n=1). The block observed with baclofen was partially reversible.

Points and traces are averages of 10 events each. EAA antagonists and bicuculline were applied throughout.

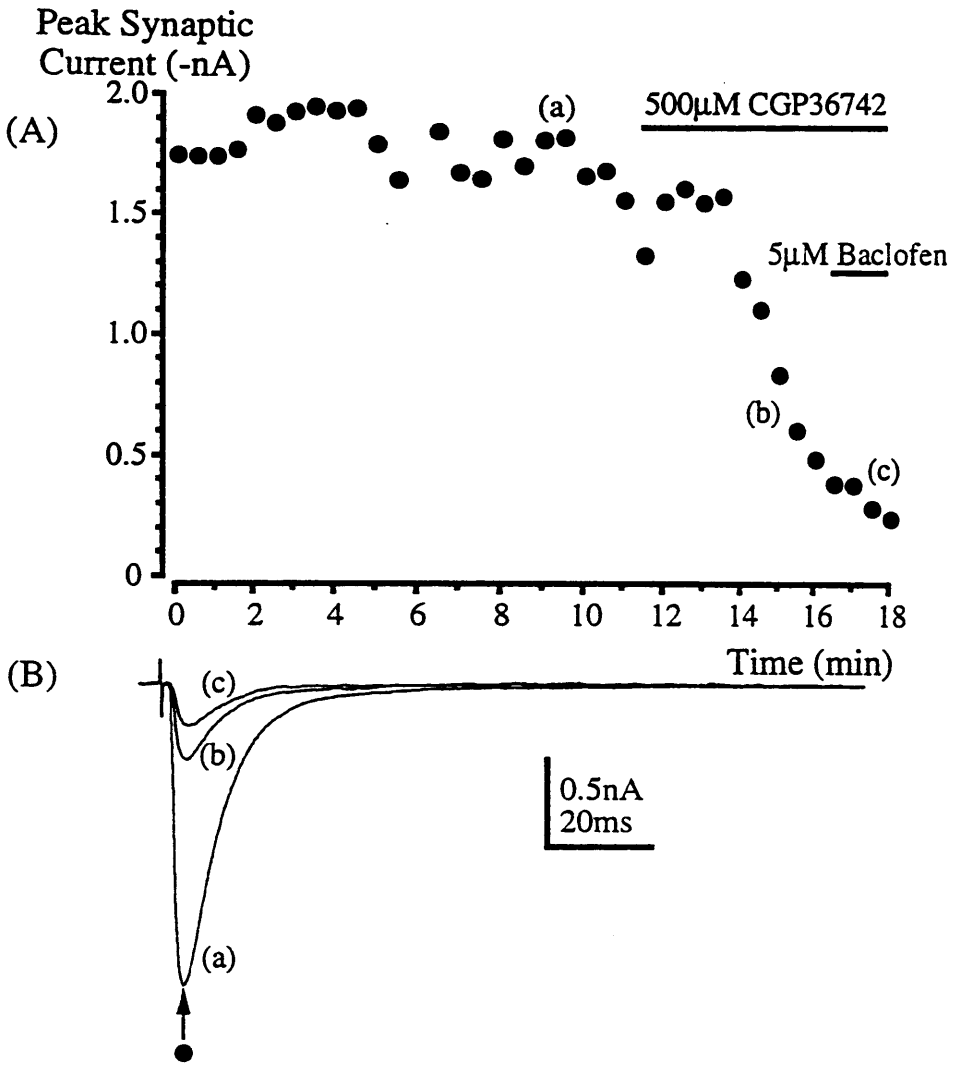

Figure 6.4 **500µM CGP36742 shows partial agonist properties at $GABA_B$ receptors.**

(A) Plot of mean peak inhibitory synaptic current recorded from an MSO neurone before and during application of 500µM CGP36742 and 5µM baclofen.

(B) Selected mean current traces corresponding to (A) recorded from an MSO neurone (a) before and (b) during application of 500µM CGP36742 and (c) during application of 500µM CGP36742 and 5µM baclofen.

500µM CGP36742 reduced the peak inhibitory synaptic current amplitude (n=1) suggesting partial agonist properties at this concentration. Application of 5µM baclofen futher reduced the peak synaptic current amplitude. No wash off was achieved on this occasion.

Points and traces are averages of 10 events each. EAA antagonists and bicuculline were applied throughout.

Cumulative probability histograms were constructed of the amplitude and frequency (interminiature interval) of miniature currents in control conditions and following application of 5μM baclofen (figure 6.5). The 50% cumulative probability points in each condition are plotted in figure 6.6A & B. Corresponding 50% cumulative probability points are tabulated in figure 6.6C. In two neurones (◆ and ▼) the interminiature interval was found to increase upon application of baclofen whilst the miniature amplitude remained relatively unaffected. In one other neurone (Δ), baclofen appeared to have very little action on either the amplitude or frequency of miniature currents.

Using Kolmogorov-Smirnov statistics neither miniature current amplitude or interminiature interval followed a Gaussian distribution (n=3) so the non-parametric Mann-Whitney U test was used examine the statistical significance of the action of baclofen on the miniature currents. Results of the statistical analysis were complex such that on one occasion (figure 6.5) baclofen significantly increased the interminiature interval ($P<0.0001$) but did not significantly alter the amplitude of the miniature currents ($P=0.177$), clearly suggesting baclofen to be acting presynaptically. On another occasion baclofen significantly increased the interminiature interval ($P=0.0298$) but also significantly reduced the miniature amplitude ($P<0.0001$). On the third occasion, baclofen did not significantly alter the interminiature interval ($P=0.7$) or the miniature amplitude ($P=0.66$) suggesting baclofen to have had no action on this occasion. Baclofen was not washed out on any occasion whilst recording miniature currents. Its action of reducing miniature current frequency dictates a long recording period. Since baclofen is difficult to wash out of the preparation (only partial washout was achieved for the evoked currents, figure 6.1) the longer recording period required in baclofen makes wash out even more difficult to achieve.

6.32 Metabotropic Glutamate Receptors (mGluRs)

Metabotropic glutamate receptors (mGluRs) have been shown to be present on presynaptic terminals elsewhere in the auditory system (Barnes-Davies & Forsythe, 1995) and their presence was investigated here. Application of mGluR agonists, 50μM 1*S*,3*S*-ACPD (1*S*,3*S*-1-aminocyclopentane-1,3-dicarboxylic acid) and 50μM L-AP4 (L(+)-2-amino-4-phosphonobutyric acid) were found to reversibly reduce the evoked inhibitory postsynaptic current amplitude by 82.5±5.7% (SEM, n=5) and 65.8% (n=1), respectively (figures 6.7 & 6.8). Once more, its site of action whether pre- or postsynaptic cannot be deduced from

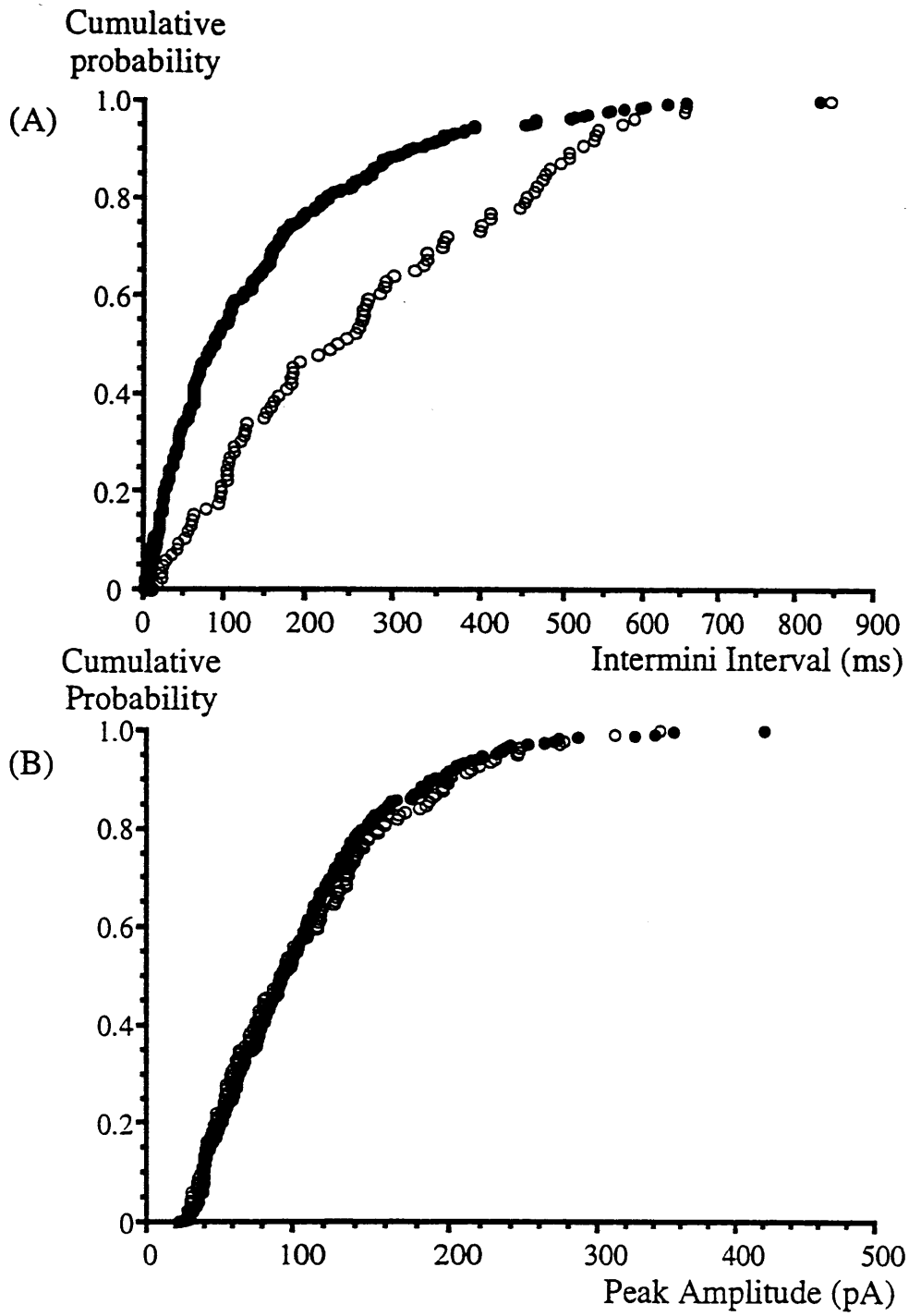

Figure 6.5 **Action of baclofen on miniature current cumulative probability histograms.**

(A) Cumulative probability histogram demonstrates that interminiature interval increases on application of 5μM baclofen.

(B) Cumulative probability histogram demonstrates that miniature current amplitude remains unaltered upon application of 5μM baclofen.
Closed symbols (•) = control solution. Open symbols (o) = 5μM baclofen.
Statistical analysis revealed complex interpretation - see text.

Figure 6.6 **50% cumulative probability positions in control solution and after application of 5μM baclofen.**

(A) 50% cumulative probability positions of miniature current amplitude before and during application of 5μM baclofen.

(B) 50% cumulative probability positions of interminiature interval before and during application of 5μM baclofen.

(C) Tabulated data corresponding to (A) and (B) with respective % changes.

Based on the 50% cumulative probability positions the following results were observed: neurone (◆) displayed a marked increase in interminiature interval but no effect on miniature current amplitude; neurone (▼) displayed an increase in interminiature interval and in addition a small reduction in miniature current amplitude; neurone (Δ) displayed very little change in both miniature current amplitude and interminiature interval.

(A)

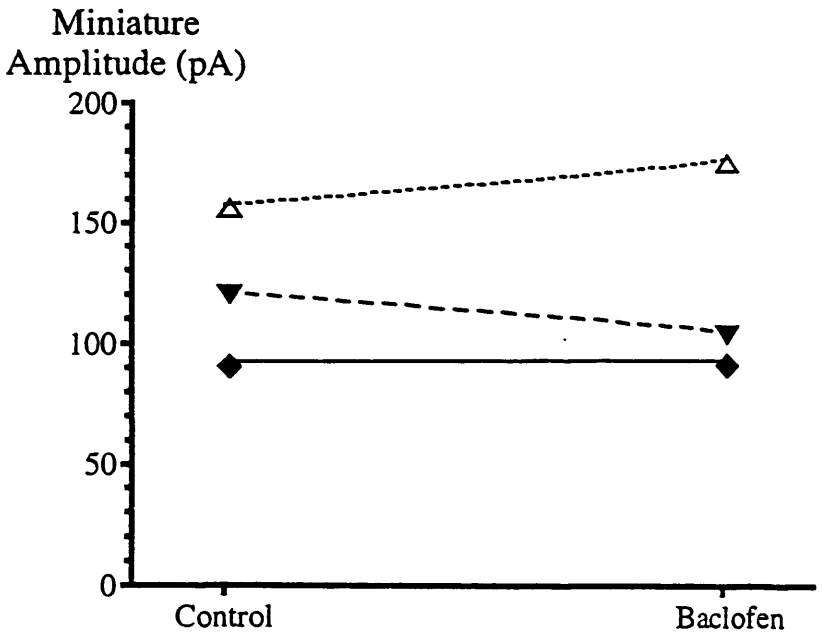

(B)

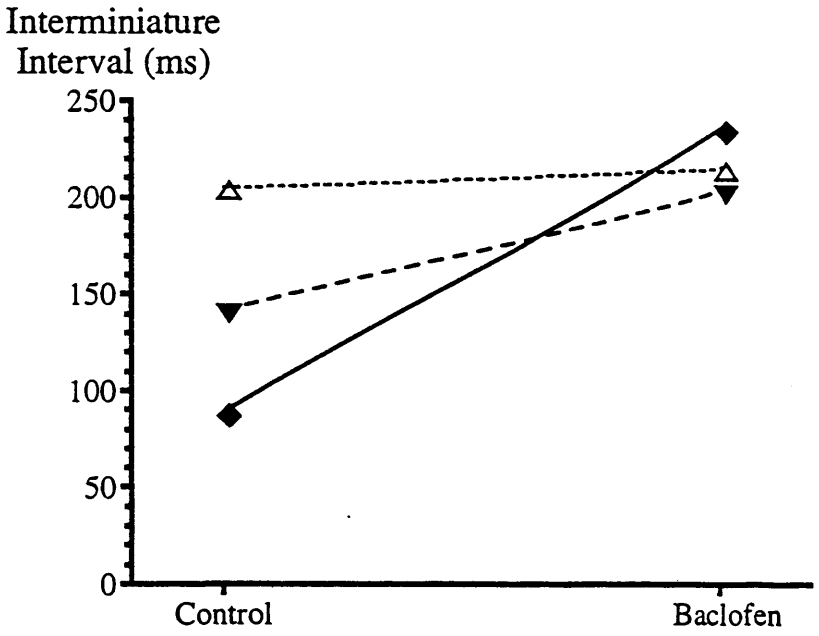

(C)

Cell	1(◆)	2(▼)	3(△)
Control 50% miniature amplitude (pA)	92.80	122.10	157.47
Baclofen 50% miniature amplitude (pA)	94.00	106.20	177.00
% change in amplitude	+1.30%	-13.02%	+12.40%
Control 50% intermini interval (ms)	89.50	141.50	205.50
Baclofen 50% intermini interval (ms)	237.00	204.00	216.00
% change in intermini interval	+164.80%	+44.17%	+5.11%

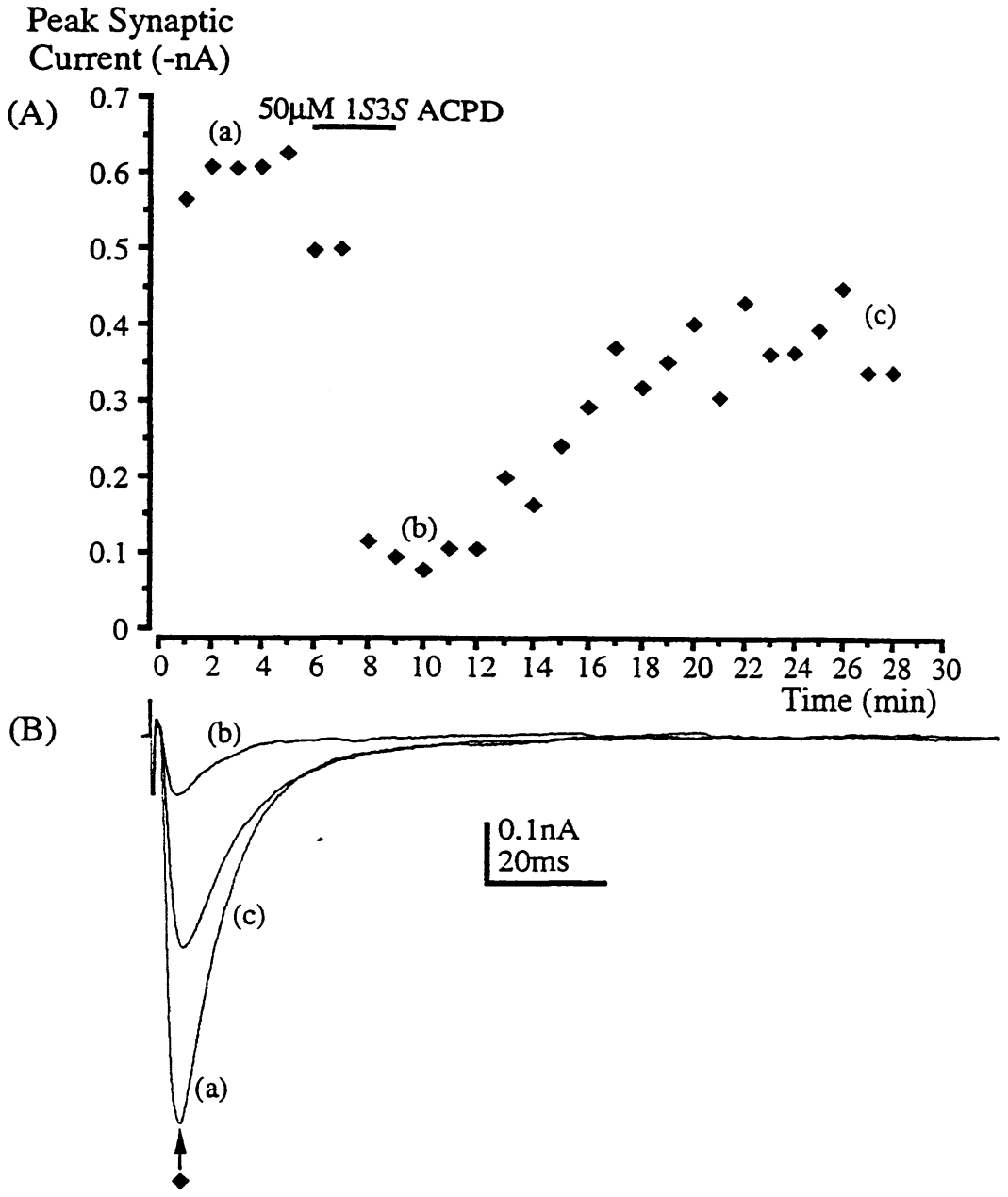

Figure 6.7 **50μM 1*S*3*S* ACPD reversibly blocks the inhibitory postsynaptic current.**

(A) Plot of mean peak inhibitory synaptic current recorded from an MSO neurone before and during application of and after wash off of 50μM 1*S*3*S* ACPD.

(B) Selected mean current traces corresponding to (A) recorded from an MSO neurone (a) before, (b) during and (c) following wash off of 50μM 1*S*3*S* ACPD. The mean peak synaptic current was reduced by 82.5±5.7% (n=5, SEM) and the effect of 1*S*3*S* ACPD was partially reversed on 3 occasions.

Points and traces are averages of 10 events each. EAA antagonists and bicuculline were applied throughout.

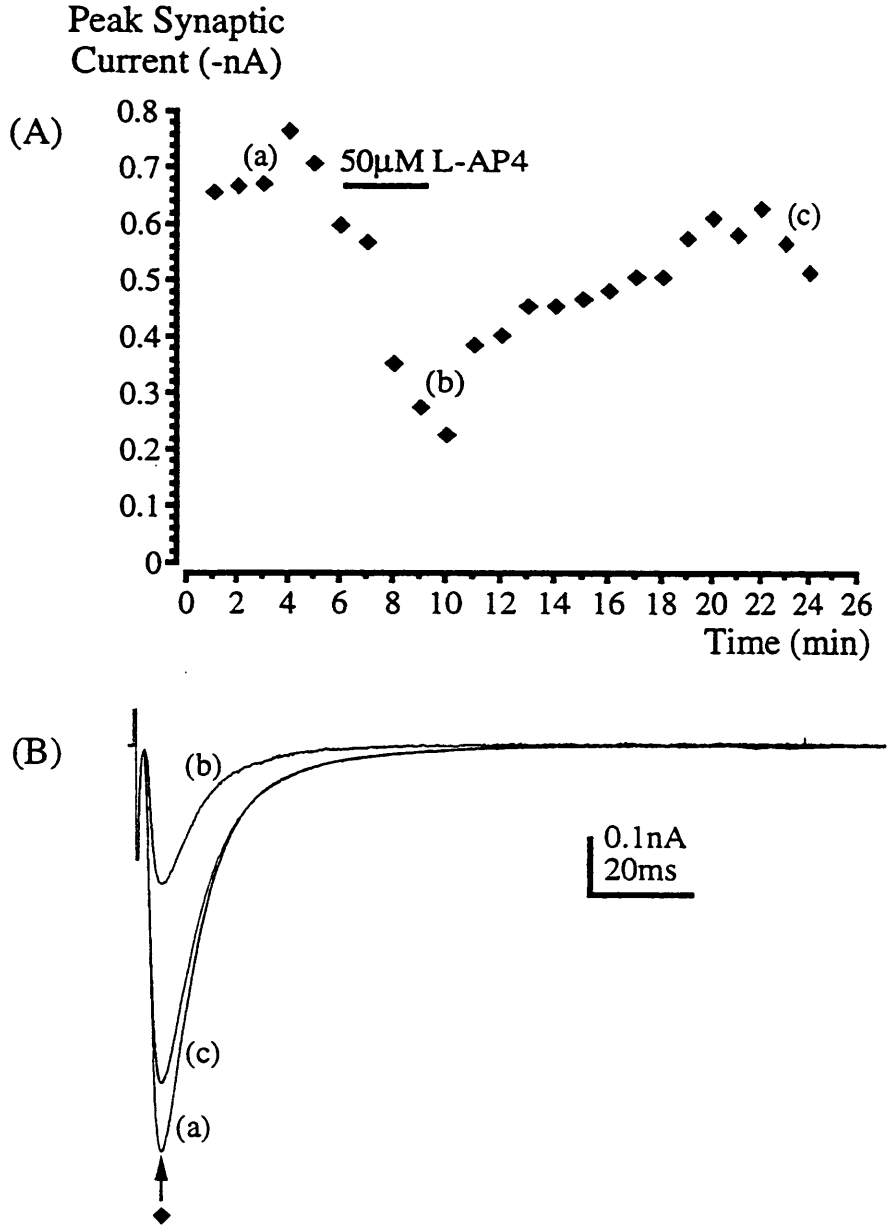

Figure 6.8 **50µM L-AP4 reversibly blocks the inhibitory postsynaptic current.**

(A) Plot of peak inhibitory synaptic current recorded from an MSO neurone before and during application of and after wash off of 50µM L-AP4.

(B) Selected mean current traces recorded from an MSO neurone (a) before, (b) during and (c) following wash off of 50µM L-AP4.

The mean peak synaptic current was reduced by 65.8% (n=1) and the effect of L-AP4 was partially reversible.

Points and traces are averages of 10 events each. EAA antagonists and bicuculline were applied throughout.

examination alone of the evoked synaptic response. Further experiments examining the action of these mGluR antagonists on miniature currents needs to be conducted.

6.33 5-Hydroxy tryptamine (5HT) Receptors

In addition to examination of the modulatory action of $GABA_B$ and mGlu receptor activation, the action of 5-hydroxy tryptamine (5HT) receptor activation was also investigated and found to modulate the inhibitory synaptic current. Application of 10μM 5HT caused a 60.3±8.4% (n=3, SEM) reduction in the inhibitory synaptic current amplitude, an action which was at least in part reversible (figure 6.9). No investigations were conducted to determine either the site of action of 5HT or the subtype of receptor involved in this modulation.

6.4 **Summary and Discussion**

Major findings of this chapter:

- The evoked inhibitory synaptic current was modulated by 5μM baclofen acting at a $GABA_B$ receptor.
- Miniature current analysis suggested that baclofen was acting at a presynaptic site since baclofen application reduced miniature current frequency but did not affect miniature current amplitude.
- The evoked inhibitory synaptic current was modulated by 50μM 1*S*3*S*-ACPD and 50μM L-AP4 acting on mGluRs.
- The evoked inhibitory synaptic current was modulated by 10μM 5HT.

Modulation of excitatory synaptic pathways has long been a focus of attention since it is thought to be important in long term physiological or pathological changes. In contrast to excitatory pathways, the role of the inhibitory synaptic input to the MSO is not clearly defined, so the role of modulation of this input can be at best speculative. However, the evoked inhibitory synaptic current is clearly subject to modulation by a number of compounds and analysis of the action of baclofen on miniature currents recorded here suggests a presynaptic site of action.

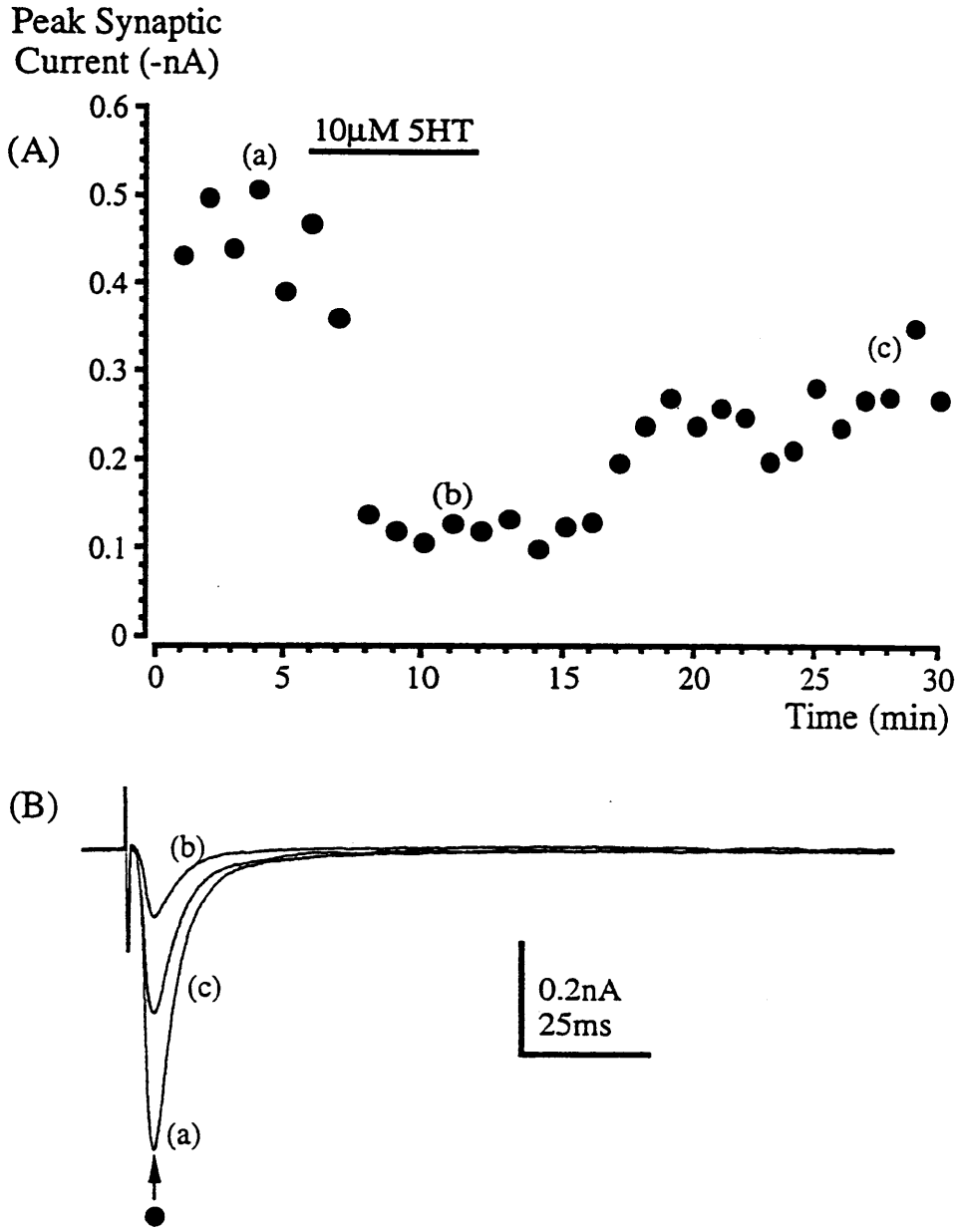

Figure 6.9 **10μM 5HT reversibly blocks the inhibitory postsynaptic current.**

(A) Plot of mean peak inhibitory synaptic current recorded from an MSO neurone before and during application of and after wash off of 10μM 5HT.

(B) Selected mean current traces corresponding to (A) recorded from an MSO neurone (a) before, (b) during and (c) following wash off of 10μM 5HT.

The mean peak synaptic current amplitude was reduced by 60.3±8.4% (n=3, SEM) and the effect of 5HT was partially reversible.

Points and traces are averages of 20 events each. EAA antagonists and bicuculline were applied throughout.

6.41 Modulation via $GABA_B$ Receptors

Baclofen, a $GABA_B$ receptor agonist was found to substantially reduce the amplitude of the evoked synaptic current but unlike the findings of Otis & Trussell (1996) in the chick nucleus magnocellularis, baclofen had no effect on the time course of the synaptic current. Otis & Trussell (1996) found that baclofen both converted paired pulse depression to facilitation and reduced the time course of the synaptic current, findings which led them to conclude that baclofen was acting presynaptically to reduce transmitter release. Consistent with this, baclofen is also likely to be acting at a presynaptic $GABA_B$ receptor site at this synapse, although this was not decipherable from its action on the evoked synaptic current alone. Instead, the action of baclofen on miniature currents recorded from MSO neurones was examined, the results of which suggested that baclofen was acting on presynaptic $GABA_B$ receptors. Although the results of miniature current analysis were not conclusive in their own right, the results are consistent with other reports in the brain stem auditory pathway (Barnes-Davies & Forsythe, 1995; Otis & Trussell, 1996). It is likely that the presynaptic activity of $GABA_B$ receptors works by reducing presynaptic calcium current entry, thereby reducing the probability of transmitter release. The observation of any action on miniature currents at least confirmed that $GABA_B$ receptor activation was occurring directly at the synapse since the inclusion of TTX eliminates the possibility of interneurone $GABA_B$ receptor activation being the cause of the modulatory effect.

Assuming that $GABA_B$ receptor activation occurs at a presynaptic site, its role in this pathway is still however undetermined. In a recent report by Brenowitz, David & Trussell (1998) presynaptic $GABA_B$ receptor activation was observed to act in a frequency dependent manner. They recorded excitatory postsynaptic potentials (EPSPs) from nucleus magnocellularis (NM) neurones and found that at high frequency stimulation (e.g. 200Hz) baclofen was excitatory but at low frequency stimulation (e.g. 20Hz) baclofen was inhibitory, respectively causing an enhancement and weakening of synaptic strength. In control conditions, high frequency stimulation of the NM results in a rapid reduction in synaptic current amplitude from the second EPSC onward in a train of EPSCs. This results from a reduction in the probability of transmitter release. Comparatively, when baclofen was applied, the first in a train of EPSCs was dramatically reduced in amplitude but subsequent EPSCs were bigger than in control conditions, by preventing synaptic depression and therefore enhancing synaptic strength. This action of baclofen was not observed at low frequency stimulation, suggesting that baclofen was

acting in a context dependent manner at this synapse. The enhancement of synaptic strength at high frequency stimulation is likely to result from the reduction in release probability, lowering the extent of vesicle depletion and postsynaptic receptor desensitisation following each presynaptic action potential. This reduction in receptor desensitisation may contribute to the ability of the NM to follow high frequency inputs accurately. If during high frequency stimulation extensive vesicle depletion were permitted to occur, there would be a concomitant reduction in synaptic strength, reducing the fidelity of this synapse. It is possible that baclofen is working in a similar manner to this in the MSO by enhancing the action of the inhibitory synaptic input at high frequencies. A brief examination of high frequency stimulation was attempted in this study but difficulties arose in that the synapse was subject to extensive temporal summation as a result of the multiple synaptic inputs it receives. This made it difficult to determine whether the synapse was undergoing facilitation or depression, so further examination was not conducted.

It must be noted that the role of inhibitory synaptic inputs to the MSO is a subject of great speculation, so the role of modulation at this synapse is difficult to discern. Further examination using more specific $GABA_B$ receptor antagonists needs to be conducted to determine whether $GABA_B$ receptors are active physiologically at this synapse.

6.42 Modulation via Metabotropic Glutamate Receptors (mGluRs)

Metabotropic glutamate receptors (mGluR) are G-protein-linked receptors that regulate intracellular second messenger systems and whose activation has also been shown here to modulate the evoked inhibitory synaptic current in the MSO. The sites of action of the metabotropic glutamate receptor agonists, 1*S*3*S*-ACPD and L-AP4 were not investigated using miniature current analysis although circumstantial evidence suggests that its site of action may be presynaptic. Firstly, Barnes-Davies & Forsythe (1995) have shown ACPD and L-AP4 to act presynaptically in the MNTB, a phenomenon which has also been observed elsewhere in the brain, including the hippocampus and cerebellum (reviewed by Schoepp & Conn, 1993). Secondly, L-AP4 is known to activate mGluRs 4, 6 and 7, which in turn are known to be presynaptic mGluRs and are negatively linked to adenylate cyclase (reviewed by Nakanishi, 1994; Saugstad, Segerson & Westbrook, 1995).

Assuming therefore that modulation of the inhibitory evoked synaptic current by mGluR activation is presynaptic, the question of what mGluR activation is actually doing remains to be

answered. There are a number of lines of evidence suggesting different mechanisms by which mGluR activation can suppress transmitter release, resulting in modulation of synaptic transmission. Firstly, there is evidence to suggest that presynaptic mGluRs modulate N- and L-type calcium channels in postsynaptic neurones (Sayer, Schwindt & Crill, 1992; Sahara & Westbrook, 1993) and more recently, Takahashi *et al.*, (1996) reported mGluR activation to suppress a high voltage activated P/Q type calcium conductance at a presynaptic terminal, thereby reducing calcium influx and neurotransmitter release. Secondly, there is evidence that presynaptic mGluRs act via potentiation of presynaptic K^+ channel currents (Sladeczek, Momiyama & Takahashi, 1993) so also acting indirectly on calcium channels. This was deduced since application of 4-AP reduced the modulatory action of ACPD on visual cortical neurones. Thirdly, mGluR activation could work by directly modulating the exocytotic machinery, a mechanism which was originally implicated in the MNTB (Barnes-Davies & Forsythe, 1995).

Barnes-Davies & Forsythe (1995) came to the conclusion that mGluR activation was acting directly on the exocytotic machinery by examining the action ACPD on paired pulse facilitation at the calyx of Held. Using the extracellular divalent concentrations of 2mM Ca^{2+} and 1mM Mg^{2+} the calyx of Held / MNTB synapse showed paired or triple pulse depression. They found that by lowering the extracellular calcium concentration, reducing the probability of transmitter release that the first EPSC of a train was reduced in amplitude. The second and third EPSCs in a train were then potentiated with respect to the first. This phenomenon can be explained by the residual calcium hypothesis (Katz & Miledi, 1968) where the first EPSC causes a transient increase in intracellular calcium concentration and therefore an increased probability of transmitter release in response to a second stimulus. Barnes-Davies and Forsythe (1995) used this paired pulse facilitation to examine the effect of ACPD at the calyx of Held. They found that ACPD had no effect on the magnitude of the paired pulse facilitation, suggesting that it did not alter the influx of calcium into the terminal. From this they deduced that mGlu receptor activation at this synapse is acting directly on the exocytotic machinery in the presynaptic terminal. However more recently, simultaneous recordings were made from the calyx of Held and postsynaptic MNTB neurones (Takahashi *et al.*, 1996) where it was reported that presynaptic P/Q type calcium channels were modulated by mGluR activation. An examination of paired pulse stimulation was attempted in my study but once again the multiple synaptic input to the MSO caused paired pulse stimulation to produce mixed results which were not readily interpreted since any action would also incorporate artifactual changes

resulting from threshold changes of the numerous axons. No further examination of paired pulse stimulation was therefore conducted.

Confirmation of both the site and mechanism of action of modulation by mGluR agonists, requires further study. Examination of the effect of mGluR agonists on miniature current amplitude and frequency, similar to that done for the action of baclofen above would be particularly useful. However, in light of the findings of Takahashi *et al.*, (1996) where direct recording techniques revealed a different mechanism of modulation by mGluR activation than indirect techniques (Barnes-Davies & Forsythe, 1995) at the same synapse, direct presynaptic recordings would be advantageous. However, unlike the MNTB, the MSO has the disadvantage that direct presynaptic recording is not possible so results of examination of presynaptic modulation using indirect techniques must be interpreted cautiously.

Once more, the role of modulation of the inhibitory synaptic current by mGluR activation remains undetermined. It is possible however, that mGluR activation could be working in a similar manner to that proposed of $GABA_B$ receptor activation in the NM by Brenowitz, David & Trussell (1998). Reduced release probability of neurotransmitter during a stimulus train could in turn enhance synaptic strength by limiting vesicle depletion and receptor desensitisation. The study by Brenowitz, David & Trussell (1998) was however at an excitatory synapse so the role of mGluR activation here may not be the same.

6.43 Modulation via 5HT Receptors

The evoked inhibitory synaptic current was also observed to be modulated by application of 5HT. 5HT can be excitatory or inhibitory and act at pre- or postsynaptic receptors. It appears to be acting as an inhibitor of synaptic transmission here but its precise location of action is unknown. There are 14 different 5HT receptor subtypes but $5HT_1$ and $5HT_2$ receptors are both located in the CNS and have been linked to postsynaptic inhibition. $5HT_{1B}$ receptors have been linked to presynaptic inhibition at both 5HT terminals and terminals releasing other transmitters (reviewed by Rang & Dale, 1991). Application of 5HT receptor specific antagonists will assist in identifying the 5HT receptors involved in this pathway therefore providing circumstantial evidence of their location. Once again though, to make a more accurate determination of the site of action of 5HT at this synapse, examination of it's effects on miniature currents is necessary.

6.44 Overview

Despite the clear modulation of the inhibitory synaptic current by GABA, glutamate and 5HT the role of this modulation is unresolved but may be involved in fine tuning of the inhibitory response to ensure the transmission of high fidelity timing information at his synapse. However, before physiological roles can be assigned to the modulation observed here, it will be first necessary to further investigate the receptor subtypes involved, and their respective locations. It is possible that modulation at this synapse may not be playing any physiological role in the auditory pathway, since no evidence has been provided here to suggest $GABA_B$, mGluR or 5HT receptors are active in physiological conditions. It would however seem likely that they are physiologically active since the receptors are clearly present in the MSO neuronal membrane, and all three transmitters, GABA, glutamate and 5HT are present in the brainstem.

Chapter 7 - Discussion

7 Final Discussion

Investigations into the methods by which vertebrates localise a sound source can be dated back as far as 1907 when Lord Rayleigh proposed the duplex theory for sound localisation. The duplex theory suggested that two methods of localisation occur in parallel, one where interaural phase or timing differences (ITDs) permits the localisation of low frequency sounds and the other where interaural intensity differences (IIDs) permits the localisation of high frequency sounds. This basic theory of sound source localisation is now widely accepted but the cellular methods by which it occurs is still a question which remains to be completely answered.

In 1948, Jeffress proposed a neuronal model of sound source localisation known as the delay line hypothesis. This model combined delay lines and coincidence detectors to generate a place map from which a sound source can be localised. The anatomical organisation of the medial superior olivary (MSO) nucleus lends itself to the delay line hypothesis proposed by Jeffress, although the model only incorporated excitatory inputs. However, it is now well established that the MSO, which forms a part of the binaural auditory pathway also receives inhibitory synaptic inputs. Despite this observation, many recent models of sound source localisation (e.g. Colburn, Han & Culotta, 1990; Han & Colburn, 1993) still only incorporate excitatory inputs. Brughera *et al.* (1996) more recently incorporated inhibitory inputs to their model of MSO function and although they failed to prescribe a role to the inhibition, they did propose that it may be involved in localisation of transient stimuli rather than steady state tones.

The role of inhibitory synaptic inputs to the MSO was also investigated by Grothe & Sanes (1993, 1994). They proposed that in addition to coincidence of excitatory synaptic inputs, synaptic inhibition is also important in the functioning of the MSO as a coincidence detector. They found that synaptic inhibition was only recruited at high stimulus intensities where it prolonged the refractory period following the first of two pulses, limiting the rate of action potential generation to high frequency stimulation. Funabiki, Koyano & Ohmori (1998) more recently suggested an involvement of $GABA_A$ receptor mediated inhibition in coincidence detection in the avian nucleus laminaris where the decay time course of excitatory synaptic inputs were found to accelerate on GABA application, sharpening the window of coincidence detection.

In this thesis, the MSO and some of the synaptic projections it receives has been studied. In particular the nature of the inhibitory synaptic input projecting from the ipsilateral medial

nucleus of the trapezoid body (MNTB) has been under scrutiny. Whilst this thesis does not address the issue of the role the MSO plays in sound source localisation directly, a good understanding of its physiology and pharmacology will hopefully go some way to contributing to a better understanding of this mechanism.

7.1 How Does the Anatomy and Physiology of the MSO Lend Itself to Sound Source Localisation?

The long established bipolar nature of MSO principal neurones is clearly displayed in figure 5.12 where the MSO neurones have been filled with the fluorescent dye, lucifer yellow. Difficulties in identification of MSO neurones was overcome in early experiments by filling them with lucifer yellow and post-experimentally identifying the neurones based on their known morphology.

Basic Membrane Properties

In chapter 3, some of the basic membrane properties of MSO neurones were reported. A rapidly inactivating inward sodium conductance and a slowly inactivating TEA sensitive outward potassium conductance were revealed. The existence of these two conductance types has been previously reported elsewhere in the brain stem auditory pathway (Forsythe & Barnes-Davies, 1993a; Brew & Forsythe, 1995; Wang *et al.*, 1998; Smith, 1995). Together with a dendrotoxin sensitive, low voltage activated potassium conductance these two conductances may underlie the mechanism by which MSO and MNTB neurones fire only a single action potential in response to a depolarising step. This ability to fire only a single action potential is important for MNTB and MSO neurones which are both involved in following high frequency auditory timing information. Wang *et al.* (1998) recently confirmed the presence of the *Shaw*-related potassium channel, $K_v3.1$ in mouse MNTB neurones and found that it contributed to high frequency firing in those neurones.

Excitatory Inputs

The bipolar morphology of MSO neurones forms the basis of the original theories regarding its involvement in sound source localisation. MSO neurones are orientated such that one dendrite projects toward the ipsilateral anterior ventral cochlear nucleus (AVCN) and the other toward

the midline, in the transverse plane. The MSO then receives a bilateral excitatory synaptic input from both the AVCN. The lateral dendrite receives an excitatory input from spherical bushy cells of the ipsilateral AVCN and the medial dendrite from the same cells in the contralateral AVCN. The nature of the excitatory input the MSO receives from the contralateral AVCN was investigated here and is thought to be mediated by NMDA and non-NMDA receptors, as has been found elsewhere in the auditory pathway (Forsythe & Barnes-Davies, 1993b; Otis Raman & Trussell, 1995). Consistent with other reports in the auditory pathway and elsewhere in the nervous system (Barnes-Davies & Forsythe, 1995; Wang *et al.*, 1998; Geiger *et al.*, 1995; Otis, Raman & Trussell, 1995) there is a suggestion that calcium permeable AMPA receptors may mediate fast excitatory synaptic transmission in the MSO. In the MNTB, AMPA receptors underlie large rapidly decaying EPSPs (Forsythe & Barnes-Davies, 1993b) which in turn cause the secure generation of a single action potential in response to a depolarising step (Forsythe & Barnes-Davies, 1993b, Brew & Forsythe, 1995; Wang *et al.*, 1998). As mentioned above, this single action potential generation contributes to the high reliability and temporal fidelity in the brain stem auditory pathway. AMPA receptors are likely to be performing a similar function here because like MNTB neurones, MSO neurones have been shown to respond to a depolarising step with the generation of a single action potential (Smith, 1995; Brew & Forsythe, 1996). The calcium permeability of AMPA receptors present in the auditory pathway may be contributing to temporal fidelity in this system at least in part by facilitating the termination of the excitatory postsynaptic potential through activation of calcium dependent potassium channels (Geiger *et al.*, 1995).

In addition to the fast excitatory synaptic inputs to the MSO, an NMDA receptor mediated input was also observed. The reversal potential of this synaptic current was relatively positive, a finding similar to that reported in the MNTB by Forsythe & Barnes-Davies (1993b) and which is likely to result from the non-specific cation permeability of the associated ion channel. Consistent with the well established characteristics of NMDA receptors, the current was subject to a voltage dependent magnesium block, so at negative holding potentials current flow was markedly rectified. Under normal physiological conditions, this voltage dependent block is likely to be relieved by depolarisation of the membrane, resulting from activation of the non-NMDA receptor mediated current. NMDA receptor activation is likely to be involved in long term pathological or physiological changes since its involvement in synaptic plasticity and excitotoxicity is well established (reviewed by Collingridge & Watkins, 1994).

Inhibitory Inputs

In this thesis there has been an extensive investigation of the characteristics of the inhibitory synaptic input the MSO receives from the ipsilateral MNTB. In order to accomplish this, pharmacological isolation of the inhibitory input was necessary, using excitatory amino acid antagonists. Examination of the inhibitory input revealed a strychnine sensitive current which reversed around the chloride equilibrium potential. These findings confirmed previous reports in which the amino acid, glycine was implicated as the neurotransmitter at this synapse (Smith, 1995; Grothe & Sanes, 1993, 1994).

The time course of the glycine receptor mediated inhibitory synaptic input was investigated and it's decay rate was fitted by a double exponential function which was both temperature- and voltage dependent. Glycine receptor mediated inhibitory synaptic transmission has been reported to be voltage dependent elsewhere in the central nervous system (e.g. Akaike & Kaneda 1989; Legendre, 1998; Stuart & Redman, 1990; Krupp, Larmet & Feltz, 1994) but no clear role has been ascribed to it. No attempt was made in this study to discern the underlying mechanism of the voltage dependence of the inhibitory synaptic input but it could be important to the functioning of the MSO because as the neurones depolarise, so the inhibitory synaptic current decay time course lengthens. Consequently, when the MSO receives bilateral excitation from the AVCN, the action of the inhibitory input will be enhanced. Such a finding was recently demonstrated in the avian nucleus laminaris when Funabiki, Koyano & Ohmori (1998) found that GABA application accelerated the time course of excitatory synaptic currents, thereby sharpening the window of coincidence detection.

One important finding of this study was the length and variability of the decay time course of the inhibitory synaptic current between neurones. A number of factors could account for this, one of which is the differential location of the synaptic inputs to the neurones. With this in mind an examination of the half width and 10-90% rise time of the evoked synaptic current was conducted both in individual neurones and across a population. In addition, the rise and decay time constants of miniature currents were also examined within individual neurones and across a population. Neither of these investigations revealed much correlation within individual neurones, suggesting that the synaptic inputs were not widely distributed in the neuronal membrane. Combined with the examination of the rate of switch off of the evoked synaptic current (figure 5.15) and previous immunohistochemical and electron microscopy studies (Clark, 1969; Oliver, Beckius & Schneiderman, 1995; Brunso-Bechtold, Henkel &

Linville, 1990; Kuwabara & Zook, 1992), these data confirm that the majority of the inhibitory synaptic inputs to the MSO are somatically located. However, examination of the half width and 10-90% rise time of the evoked synaptic current and of the rise and decay time constants of miniature currents across a population of MSO neurones revealed some correlation between these parameters. Barnes-Davies & Forsythe (1995) previously observed such a correlation at the calyx of Held / MNTB synapse and attributed this to some differences in receptor modulation or isoform expression. There is a well documented developmental heterogeneity of glycine receptor isoform expression over the first three postnatal weeks (Akagi & Miledi, 1988; Becker, Hoch & Betz, 1988; Langosch *et al.*, 1988; Hoch, Betz & Becker, 1989; Friauf, Hammerschmidt & Kirsch, 1997; Takahashi *et al.*, 1992). It is therefore quite possible that the correlation observed between the rising and falling phases of both the evoked synaptic and miniature currents results from expression of different proportions of adult and neonatal glycine receptor isoforms.

The developmental heterogeneity of glycine receptor isoform expression may also account for the variability in decay time constant observed between neurones. The first three weeks of postnatal development have been reported to be accompanied by a shortening of the single channel open time of glycine receptor ion channels (Takahashi *et al.*, 1992). In addition, an acceleration of the decay time course of evoked glycine mediated synaptic currents has also been reported with age (Takahashi *et al.*, 1992; Krupp, Larmet & Feltz, 1994). The neonatal isoform of the glycine receptor has also been reported to have a lower strychnine affinity than the adult isoform of the same receptor (Becker, Hoch & Betz, 1988).

Examination of a change in strychnine sensitivity with the aim of revealing differential glycine receptor isoform expression between neurones was not possible since it was very difficult in this preparation to construct a strychnine dose response curve. Examination of the decay time course of the inhibitory synaptic current was then conducted but no clear correlation was apparent between decay time course and age of the animal. However, it is likely that this study was of MSO neurones expressing a combination of adult and neonatal glycine receptor isoforms since the age of animals used spans the developmental change over period. In addition, the α_1 specific glycine receptor antagonist, CTB (Rundström *et al.*, 1994) also did not reveal differential expression of glycine receptor isoforms. This finding was however unsurprising since its action would also have been confounded by combined expression of both adult and neonatal glycine receptor isoforms. Despite difficulties in confirmation that the

variability in decay time course between neurones is an age dependent phenomenon, this is the most likely explanation and warrants further investigation.

Finally, an investigation of modulation of the inhibitory synaptic current was investigated. This revealed that the current was subject to extensive modulation by $GABA_B$, mGlu and 5HT receptors since the evoked synaptic current was depressed by agonists of all of these receptor types. Identification of the site of action of these modulators using miniature current analysis was only attempted for the $GABA_B$ receptor. Results of this suggested a presynaptic site of action, a finding which is consistent with that of others in the auditory pathway (Barnes-Davies & Forsythe, 1995; Otis & Trussell, 1996). $GABA_B$ receptor activation was recently reported by Brenowitz, David & Trussell (1998) to act in a context dependent manner in the avian nucleus magnocellularis where it enhanced excitatory synaptic strength during high frequency stimulation.

7.2 **Further Experiments**

Whilst extensive investigation of the physiology of the synaptic inputs was conducted in this thesis, a number of questions remain unanswered. A plethora of potential investigations still remain to be conducted before a complete understanding of the role the MSO plays in the auditory pathway can be achieved. Following, are a few important experiments which could be conducted, the results from which may assist in achieving a better understanding of the physiological role of the MSO.

1) In chapter 5, the rate of switch off of the inhibitory synaptic current was investigated but the findings were not conclusive. The rate of switch off appeared to occur over a double exponential time course, a finding which, based on the interpretation of Isaacson & Walmsley (1995a), suggested the presence of two locations of synaptic receptors. One caveat of this investigation was the possibility that the second, slow component of the time course over which the current switched off actually resulted from the dendrites acting as a current sink. In this case it is possible that the currents were all generated somatically and that the current was distributed along the dendrites and then re-invaded the soma when the holding potential was stepped to the reversal potential. A possible way to determine whether the morphology of the MSO neurones caused the double exponential time course of switch off of the synaptic current, or if it did indeed result from differential synaptic locations would be to conduct a similar

experiment on the excitatory inputs which are known to be distributed along the dendrites. If one assumes that synaptic location was responsible for the rate of switch off of the synaptic current, one would expect the switch off of the excitatory response to occur over a single exponential time course, but at a substantially slower rate.

2) Further experiments could be conducted to elaborate on the investigation of the presence of Ca^{2+} permeable AMPA receptors in the MSO by examining the spermine sensitivity of the inhibitory synaptic current. Calcium permeability is a relatively uncommon elsewhere in the central nervous system but seems to be reasonably common in the mammalian and avian auditory pathways. To conduct these investigations the intra- and extracellular calcium concentrations could be changed and the effect this has on the reversal potential of the AMPA receptor mediated current observed. In addition, spermine could be included in the intracellular patch solution to examine its effect on the current-voltage relationship of the AMPA receptor mediated current.

3) When examining the origin of the variability of the decay time course of the inhibitory synaptic current between neurones, it would be interesting to investigate whether the variability reflected the characteristic frequency of the MSO neurones. Since a frequency map of the MSO has been reported (Guinan, Norris & Guinan, 1972; Kuwabara & Zook, 1992) it would be possible to examine whether there was any correlation between decay time course and neuronal location within the nucleus. A record of the location of each neurone within the nucleus was not kept so no information to this end can be gleaned. However, it would be interesting to see if such a correlation occurred since this may be important to the functioning of the inhibitory input to sound source localisation.

4) An advantageous tool in this study would have been the ability to stimulate single MNTB neurones whilst recording from a single postsynaptic MSO neurone. This would have eliminated variability of the synaptic response resulting from different activation thresholds of MNTB neurones and allowed a more complete characterisation of a single MNTB to MSO synaptic projection. However, the large number of MNTB neurones meant that locating a particular one which was synapsing on the MSO being recorded from was very difficult to achieve. It may be possible in future experiments to achieve this by exploiting the tonotopic arrangement of characteristic frequency that exists between the MNTB and MSO nuclei.

Single MNTB stimulation would be a particularly useful tool when applying paired pulses to presynaptic MNTB neurones in order to examine if the synapse was subject to paired pulse facilitation or depression. With this technique, it would be useful to examine modulation at this synapse in a similar manner to that reported by Barnes-Davies & Forsythe (1995) in their examination of the effect ACPD had on paired pulse facilitation. In addition, modulation could be further examined using miniature current analysis, as was conducted for the action of baclofen at this synapse in my study.

5) Further experiments, both immunohistochemical and electrophysiological could be conducted to examine the developmental profile of glycine receptor expression in the MSO.

Immunohistochemical study would hopefully reveal the synaptic location of inhibitory glycine receptors on the MSO neuronal membrane and would eventually result in the construction of a developmental profile of the different isoforms of glycine receptor expression.

Electrophysiological experiments examining the single channel currents underlying the inhibitory synaptic currents recorded here could also be conducted to see how this changes with age.

Combined, these further electrophysiological and immunohistochemical studies may provide a clearer indication of why so much variability in decay time course of the inhibitory synaptic current was observed in this study.

References

References

Adams, J. C. & Mugnaini, E. (1990). Immunocytochemical evidence for inhibitory and disinhibitory circuits in the superior olive. *Hearing Research.* **49**, 281-298.

Akagi, H. & Miledi, R. (1988). Heterogeneity of Glycine Receptors and Their Messenger RNAs in Rat Brain and Spinal Cord. *Science.* **242**, 270-273.

Akaike, N. & Kaneda, M. (1989). Glycine-Gated Chloride Current in Acutely Isolated Rat Hypothalamic Neurons. *Journal of Neurophysiology.* **62(6)**, 1400-1409.

Altschuler, R. A., Betz, H., Parakkal, M. H., Reeks, K. A. & Wenthold, R. J. (1986). Identification of Glycinergic Synapses in the Cochlear Nucleus Through Immunocytochemical Localisation of the Postsynaptic Receptor. *Brain Research.* **369**, 316-320.

Aoshima, H., Inoue, Y., Ueda, E., Kitagawa, M. & Nishino, T. (1992). Minimal Model Analysing Response of Glycine Receptors Expressed in *Xenopus* Oocyte: Inhibition by a Lipid Hydroperoxide. *Journal of Biochemistry.* **111**, 523-528.

Aprison, M. H. & Daly, E. C. (1978). Biochemical Aspects of Transmission at Inhibitory Synapses: The Role of Glycine. *Advances in Neurochemistry.* **3**, 203-294.

Aprison, M. H. & Werman, R. (1965). The Distribution of Glycine in Cat Spinal Cord and Roots. *Life Sciences.* **4**, 2075-2083.

Ascher, P. & Johnson, J. W. (1994). The NMDA receptor, its channel, and its modulation by glycine. In: *The NMDA Receptor.* 2nd Edition. (Collingridge, G. L. & Watkins, J. C. Eds.) *Oxford University Press, Oxford.* pp177-205.

Banks, M. I. & Smith, P. H. (1992). Intracellular Recordings from Neurobiotin-labeled Cells in Brain Slices of the Rat Medial Nucleus of the Trapezoid Body. *Journal of Neuroscience.* **12(7)**, 2819-2837.

Barnes-Davies, M. & Forsythe, I. D. (1995). Pre- and postsynaptic glutamate receptors at a giant excitatory synapse in rat auditory brainstem slices. *Journal of Physiology.* **488.2**, 387-406.

Barnes-Davies, M. & Forsythe, I. D. (1996). AMPA receptor-mediated synaptic currents rectify with internal spermine in rat MNTB neurones *in vitro*. *Journal of Physiology.* **495.P**.

Baron, B. M., Harrison, B. L., Miller, F. P., McDonald, I. A., Salituro, F. G., Schmidt, C. J., Sorensen, S. M., White, H. S. & Palfreyman, M. G. (1990). Activity of 5,7-Dichlorokynurenic acid, a Potent Antagonist at the *N*-Methyl-D-aspartate Receptor-Associated Glycine Binding Site. *Molecular Pharmacology*. **38**, 554-561.

Barron, S. E. & Guth, P. S. (1987). Uses and limitations of strychnine as a probe in neurotransmission. *Trends in Pharmacological Science*. **8**, 204-206.

Becker, C.-M. (1992). Convulsants Acting at the Inhibitory Glycine Receptor. In: *Handbook of Experimental Pharmacology*, Vol 102. *Selective Neurotoxicity* (Herken, H. & Hucho, F., Eds.). *Berlin, Heidelberg: Springer-Verlag.*

Becker, C.-M., Betz, H. & Schröder, H. (1993). Expression of inhibitory glycine receptors in postnatal rat cerebral cortex. *Brain Research*. **606**, 220-226.

Becker, C.-M., Hermans-Borgmeyer, I., Schmitt, B. & Betz, H. (1986). The Glycine Receptor Deficiency of the Mutant Mouse Spastic: Evidence for Normal Glycine Receptor Structure and Localization. *Journal of Neuroscience*. **6(5)**, 1358-1364.

Becker, C.-M., Hoch, W. & Betz, H. (1988). Glycine receptor heterogeneity in rat spinal cord during postnatal development. *EMBO Journal*. **7(12)**, 3717-3726.

Benavides, J., López-Lahoya, J., Valdivieso, F & Ugarte, M. (1981). Postnatal Development of Synaptic Glycine Receptors in Normal and Hyperglycinemic Rats. *Journal of Neurochemistry*. **37(2)**, 315-320.

Betz, H. (1990). Homology and Analogy in Transmembrane Channel Design: Lessons from Synaptic Membrane Proteins. *Biochemistry*. **29(15)**, 3591-3599.

Betz, H. & Becker, C.-M. (1988). Mammalian Glycine Receptor: Biology and Structure of a Neuronal Chloride Channels Protein. *Neurochemistry International*. **13(2)**, 137-146.

Betz, H., Graham, D., Pfeiffer, F. & Rehm, H. (1983). α-bungarotoxin and strychnine as tools to characterize neurotransmitter receptors of the central nervous system. In: *Toxins as Tools in Neurochemistry* (Hucho, F. & Ovchinnikov, Y. A., Eds.) *de Gruyter, Berlin and New York*, pp245-255.

Birch, P. J., Grossman, C. J. & Hayes, A. G. (1988). 6,7-Dinitro-quinoxaline-2,3-dion and 6-nitro,7-cyano-quinoxaline-2,3-dion antagonise responses to NMDA in the rat spinal cord via

an action at the strychnine-insensitive glycine receptor. *European Journal of Pharmacology.* **156**, 177-180.

Blanton, M. G., Lo Turco, J. J. & Kriegstein, A. R. (1989). Whole cell recording from neurons in slices of reptilian and mammalian cerebral cortex. *Journal of Neuroscience Methods.* **30**, 203-210.

Bledsoe JR., S. C., Snead, C. R., Helfert, R. H., Prasad, V., Wenthold, R. J. & Altschuler, R. A. (1990). Immunocytochemical and lesion studies support the hypothesis that the projection from the medial nucleus of the trapezoid body to the lateral superior olive is glycinergic. *Brain Research.* **517**, 189-194.

Bodian, D. (1966). Electron Microscopy: Two Major Synaptic Types on Spinal Motoneurons. *Science.* **151**, 1093-1094.

Bormann, J., Hamill, O. P. & Sakmann, B. (1987). Mechanism of anion permeation through channels gated by glycine and γ-aminobutyric acid in mouse cultured spinal neurones. *Journal of Physiology.* **385**, 243-286.

Bormann, J., Rundström, N., Betz, H. & Langosch, D. (1993). Residues within transmembrane segment M2 determine chloride conductance of glycine receptor homo- and hetero-oligomers. *EMBO Journal.* **12(10)**, 3729-3737.

Borst, J. G. G. & Sakmann, B. (1996). Calcium influx and transmitter release in a fast CNS synapse. *Nature.* **383**, 431-434.

Bourk, T. R., Mielcarz, J. P. & Norris, B. E. (1981). Tonotopic Organization of the Anteroventral Cochlear Nucleus of the Cat. *Hearing Research.* **4**, 215-241.

Brawer, J. R., Morest, D. K. & Kane, E. C. (1974). The Neuronal Architecture of the Cochlear Nucleus of the Cat. *Journal of Comparative Neurology.* **155**, 251-300.

Brenowitz, S., David, J. & Trussell, L. (1998). Enhancement of Synaptic Efficacy by Presynaptic $GABA_B$ Receptors. *Neuron.* **20**, 135-141.

Brew, H. M. & Forsythe, I. D. (1995). Two Voltage-Dependent K^+ Conductances with Complementary Functions in Postsynaptic Integration at a Central Auditory Synapse. *Journal of Neuroscience.* **15(12)**, 8011-8022.

Brew, H. M. & Forsythe, I. D. (1996). Neurones in two auditory nuclei in slices of at brainstem exhibit distinct electrophysiological properties. *Journal of Physiology.* **495.P**.

Brughera, A. R., Stutman, E. R., Carney, L. H. & Colburn, H. S. (1996). A Model with Excitation and Inhibition for Cells in the Medial Superior Olive. *Auditory Neuroscience.* **2**, 219-233.

Brunso-Bechtold, J. K., Henkel, C. K. & Linville, C. (1990). Synaptic Organisation of the Adult Ferret Medial Superior Olive. *Journal of Comparative Neurology.* **294**, 389-398.

Caird, D. & Klinke, R. (1983). Processing of Binaural Stimuli by Cat Superior Olivary Complex Neurons. *Experimental Brain Research.* **52**, 385-399.

Cant, N. B. (1991). Projections to the Lateral and Medial Superior Olivary Nuclei from the Spherical and Globular Bushy Cells of the Anteroventral Cochlear Nucleus. In: *Neurobiology of Hearing: The Central Auditory System* (Altschuler, R. A., Bobbin, R. P., Clopton B. M. & Hoffman D. W., Eds.). *Raven Press, New York.* pp99-120.

Cant, N. B. & Casseday, J. H. (1986). Projections from the Anteroventral Cochlear Nucleus to the Lateral and Medial Superior Olivary Nuclei. *Journal of Comparative Neurology.* **247**, 457-476.

Cant, N. B. & Hyson, R. L. (1992). Projections from the lateral nucleus of the trapezoid body to the medial superior olivary nucleus in the gerbil. *Hearing Research.* **58**, 26-34.

Carr, C. E. (1993). Delay Line Models of Sound Localization in the Barn Owl. *American Zoology.* **33**, 79-85.

Carr, C. E. & Konishi, M (1988). Axonal delay lines for time measurement in the owl's brainstem. *Proceedings of the National Academy of Science, USA.* **85**, 8311-8315.

Carr, C. E. & Konishi, M. (1990). A Circuit for Detection of Interaural Time Differences in the Brain Stem of the Barn Owl. *Journal of Neuroscience.* **10(10)**, 3227-3246.

Caspary, D. M. & Faingold, C. L. (1989). Non-*N*-methyl-D-aspartate receptors may mediate ipsilateral excitation at lateral superior olivary synapses. *Brain Research.* **503**, 83-90.

Casseday, J. H. & Covey, E. (1987). Central Auditory Pathways in Directional Hearing. In: *Directional Hearing. Spinger-Verlag.* pp109-145.

del Castillo, J. & Katz, B. (1954). Quantal components of the end-plate potential. *Journal of Physiology.* **124**, 560-573.

Changeux, J.-P., Giraudat, J. & Dennis, M. (1987). The nicotinic actylcholine receptor: molecular architecture of a ligand-regulated ion channel. *Trends in Pharmacological Science.* **8**, 459-465.

Clark, G. M. (1969). The ultrastructure of nerve endings in the medial superior olive of the cat. *Brain Research.* **14**, 293-305.

Clements, J. D. (1996). Transmitter timecourse in the synaptic cleft: its role in central synaptic function. *Trends in Neuroscience.* **19(5)**, 163-171.

Colburn, H. S., Han, Y. & Culotta, C. P. (1990). Coincidence model of MSO responses. *Hearing Research.* **49**, 335-346.

Cole, K. S. (1949). Dynamic Electrical Characteristics of the Squid Axon Membrane. *Archives Sci. Physiol.* **3**, 253-258.

Collingridge, G. L. & Watkins, J. C. (1994). The NMDA Receptor (2nd Edition). *Oxford University Press, Oxford.*

Coombs, J. S., Eccles, J. C. & Fatt, P. (1955). The Specific Ionic Conductances and the Ionic Movements Across the Motoneuronal Membrane that Produce the Inhibitory Post-Synaptic Potential. *Journal of Physiology.* **130**, 326-373.

Crow, G., Rupert, A. L. & Moushegian, G. (1978). Phase locking in monaural and binaural medullary neurons: Implications for binaural phenomena. *Journal of the Acoustical Society of America.* **64(2)**, 493-501.

Curtis, D. R., Duggan, A. W. & Johnston, G. A. R. (1971). The Specificity of Strychnine as a Glycine Antagonist in the Mammalian Spinal Cord. *Experimantal Brain Research.* **12**, 547-565.

Curtis, D. R., Hölsi, L., Johnston, G. A. R. & Johnston, I. H. (1968). The Hyperpolarisation of Spinal Motoneurones by Glycine and Related Amino Acids. *Experimental Brain Research.* **5**, 235-258.

Davidoff, R. A., Aprison, M. H. & Werman, R. (1969). The Effects of Strychnine on the Inhibition of Interneurons by Glycine and γ-aminobutyric Acid. *International Journal of Neuropharmacology.* **8**, 191-194.

Diamond, J. S. & Jahr, C. E. (1995). Asynchronous Release of Synaptic Vesicles Determines the Time Course of the AMPA Receptor-Mediated EPSC. *Neuron.* 15, 1097-1107.

Edwards, F. A., Konnerth, A. & Sakmann, B. (1990). Quantal analysis of inhibitory synaptic transmission in the dentate gyrus of rat hippocampal slices: a patch clamp study. *Journal of Physiology.* **430**, 213-249.

Edwards, F. A., Konnerth, A., Sakmann, B. & Takahashi, T. (1989). A thin slice preparation for patch clamp recordings from synaptically connected neurones of the mammalian central nervous system. *Pflugers Archives European Journal of Physiology.* **414**, 600-612.

Evans, R. H., Francis, A. A., Jones, A. W., Smith, D. A. S. & Watkins, J. C. (1982). The effects of a series of ω-phosphonic α-carboxylic amino acids on electrically evoked and excitant amino acid-induced responses in isolated spinal cord preparations. *British Journal of Pharmacology.* **75**, 65-75.

Falck, F. A. (1884). *Archiv f. d. ges. Physiol.* **34**, 530-575.

Falck, F. A. (1885). *Archiv f. d. ges. Physiol.* **36**, 285-308.

Forsythe, I. D. (1991). Microincubator for regulating temperature and superfusion of tissue-cultured neurons during electrophysiological or optical studies. *In Methods in neurosciences: ion channels and electrophysiology.* (Conn, P. M., Ed.) *Academic Press, Florida.* pp301-320.

Forsythe, I. D. (1994). Direct patch recording from identified presynaptic terminals mediating glutamatergic EPSCs in the rat CNS, *in vitro*. *Journal of Physiology.* **479.3**, 381-387.

Forsythe, I. D. (1995). A physiological function for polyamines? *Current Biology.* **5(11)**, 1248-1251.

Forsythe, I. D. & Barnes-Davies, M. (1993a). The binaural auditory pathway: membrane currents limiting multiple action potential generation in the rat medial nucleus of the trapezoid body. *Proceedings of the Royal Society B.* **251**, 143-150.

Forsythe, I. D. & Barnes-Davies, M. (1993b). The binaural auditory pathway: excitatory amino acid receptors mediate dual timecourse excitatory postsynaptic currents in the rat medial nucleus of the trapezoid body. *Proceedings of the Royal Society B.* **251**, 151-157.

Forsythe, I. D., Barnes-Davies, M. & Brew, H. M. (1995). The Calyx of Held: a Model for Tranmission at Mammalian Glutamatergic Synapses. In: *Excitatory Amino Acids and Synaptic Transmission*. 2nd Edition. (Wheal, H. & Thompson, A., Eds.) *Academic Press*. pp133-143.

Forsythe, I. D. & Redman, S. J. (1988). The dependence of motoneurone membrane potential on extracellular ion concentrations studied in isolated rat spinal cord. *Journal of Physiology*. **404**, 83-99.

Frerking, M., Borges, S. & Wilson, M. (1995). Variation in GABA Mini Amplitude Is the Consequence of Variation in Transmitter Concentration. *Neuron*. **15**, 885-895.

Frerking, M., Borges, S. & Wilson, M. (1997). Are Some Minis Multiquantal? *Journal of Neurophysiology*. **78**, 1293-1304.

Friauf, E., Hammerschmidt, B. & Kirsch, J. (1997). Development of Adult-Type Inhibitory Glycine Receptors in the Central Auditory System of Rats. *Journal of Comparative Neurology*. **385**, 117-134.

Funabiki, K., Koyano, K. & Ohmori, H. (1998). The role of GABAergic inputs for coincidence detection in the neurones of the nucleus laminaris of the chick. *Journal of Physiology*. **508.3**, 851-869.

Geiger, J. R. P., Melcher, T., Koh, D.-S., Sakmann, B., Seeburg, P. H., Jonas, P. & Moyner, H. (1995). Relative Abundance of Subunit mRNAs Determines Gating and Ca^{2+} permeability of AMPA Receptors in Principal Neurons and Interneurons in Rat CNS. *Neuron*. **15**, 193-204.

Giraudat, J., Dennis, M., Heidmann, T., Chang, J.-Y. & Changeux, J.-P. (1986). Structure of the high affinity binding site for noncompetitive blockers of the acetylcholine receptor: Serine-262 of the δ subunit is labeled by [^{3}H]chlorpromazine. *Proceedings of the National Academy of Science, USA*. **83**, 2719-2723.

Glendenning, K. K. & Baker, B. N. (1988). Neuroanatomical Distribution of Receptors for Three Potential Inhibitory Neurotransmitters in the Brainstem Auditory Nuclei of the Cat. *Journal of Comparative Neurology*. **275**, 288-308.

Godfrey, D. A., Parli, J. A., Dunn, J. D. & Ross, C. D. (1988). Neurotransmitter Microchemistry of the Cochlear Nucleus and Superior Olivary Complex. In: *World Congress of Neurosciences*. (Syka, J. & Masterton, R. B. Eds.) *New York, Plenum*. pp107-121.

Goldberg, J. M. & Brown, P. B. (1968). Functional Organisation of the Dog Superior Olivary Complex: An Anatomical and Electrophysiological Study. *Journal of Neurophysiology*. **31**, 639-656.

Goldberg, J. M. & Brown, P. B. (1969). Response of Binaural Neurons of Dog Superior Olivary Complex to Dichotic Tonal Stimuli: Some Physiological Mechanisms of Sound Localization. *Journal of Neurophysiology*. **32**, 613-636.

Graham, D., Pfeiffer, F. & Betz, H. (1983). Photoaffinity-Labelling of the Glycine Receptor of Rat Spinal Cord. *European Journal of Biochemistry*. **131**, 519-525.

Graham, D., Pfeiffer, F., Simler, R. & Betz, H. (1985). Purification and Characterization of the Glycine Receptor of Pig Spinal Cord. *Biochemistry*. **24**, 990-994.

Graham, L. T. JR., Shank, R. P., Werman, R. & Aprison, M. H. (1967). Distribution of some Synaptic Transmitter Suspects in Cat Spinal Cord: Glutamic Acid, Aspartic Acid, γ-aminobutyric Acid, Glycine, and Glutamine. *Journal of Neurochemistry*. **14**, 465-472.

Grenningloh, G., Rienitz, A., Schmitt, B., Methfessel, C., Zensen, M., Beyreuther, K., Gundelfinger, E. D. & Betz, H. (1987). The strychnine-binding subunit of the glycine receptor shows homology with nicotinic acetylcholine receptors. *Nature*. **328**, 215-220.

Grenningloh, G., Schmieden, V., Schofield, P. R., Seeburg, P. H., Siddique, T., Mohandas, T. K., Becker, C.-M. & Betz, H. (1990). Alpha subunit variants of the human glycine receptor: primary structures, functional expression and chromosomal localization of the corresponding genes. *EMBO Journal*. **9(3)**, 771-776.

Grissmer, S., Nguyen, A. N., Aiyar, J., Hanson, D. C., Mather, R. J., Gutman, G. A., Karmilowicz, M. J., Auperin, D. D. & Chandy, K. G. (1994). Pharmacological Characterization of Five Cloned Voltage-Gated K^+ Channels, Types Kv1.1, 1.2, 1.3, 1.5, and 3.1, Stably Expressed in Mammalian Cell Lines. *Molecular Pharmacology*. **45**, 1127-1234.

Grothe, B. & Sanes, D. H. (1993). Bilateral Inhibition by Glycinergic Afferents in the Medial Superior Olive. *Journal of Neurophysiology*. **69(4)**, 1192-1196.

Grothe, B. & Sanes, D. H. (1994). Synaptic Inhibition Influences the Temporal Coding Properties of Medial Superior Olivary Neurons: An *in vitro* Study. *Journal of Neuroscience*. **14(3)**, 1701-1709.

Grothe, B., Vater, M., Casseday, J. H. & Covey, E. (1992). Monaural interaction of excitation and inhibition in the medial superior olive of the mustached bat: An adaptation for biosonar. *Proceedings of the National Academy of Science USA*. **89**, 5108-5112.

Guinan, JR., J. J., Norris, B. E. & Guinan, S. S. (1972). Single Auditory Units in the Superior Olivary Complex II: Locations of Unit Categories and Tonotopic Organization. *International Journal of Neuroscience*. **4**, 147-166.

Gundersen, C. B., Miledi, R. & Parker, I. (1986). Voltage dependence of human brain glycine receptor-channels in Xenopus oocytes. *Journal of Physiology*. **40P**.

Hamill, O. P., Bormann, J. & Sakmann, B. (1983). Activation of multiple-conductance state chloride channels in spinal neurones by glycine and GABA. *Nature*. **305**, 805-808.

Han, Y. & Colburn, H. S. (1993). Point-neuron model for binaural interaction in MSO. *Hearing Research*. **68**, 115-130.

Held, H. (1893). Die centraleGehörleitung. *Arch. Anat. Physiol., Anat. Abt.* 201-248.

Helfert, R. H., Bonneau, J. M., Wenthold, R. J. & Altschuler, R. A. (1989). GABA and glycine immunoreactivity in the guinea pig superior olivary complex. *Brain Research*. **501**, 269-286.

Helfert, R. H. & Schwartz, I. R. (1986). Morphological Evidence for the Existence of Multiple Neuronal Classes in the Cat Lateral Superior Olivary Nucleus. *Journal of Comparative Neurology*. **244**, 533-549.

Helfert, R. H. & Schwartz, I. R. (1987). Morphological Features of Five Neuronal Classes in the Gerbil Lateral Superior Olive. *American Journal of Anatomy*. **179**, 55-69.

Helfert, R. H., Snead, C. R. & Altschuler, R. A. (1991). The Ascending Auditory Pathways. In: *Neurobiology of Hearing: The Central Auditory System* (Altschuler, R. A., Bobbin, R. P., Clopton B. M. & Hoffman D. W., Eds.) *Raven Press, New York*. pp1-26.

Hershkowitz, R. M. & Durlach, N. I. (1969). Interaural Time and Amplitude jnds for a 500-Hz Tone. *Journal of the Acoustical Society of America*. **46(6-2)**, 1464-1467.

Hille, B. (1992). Ionic Channels of Excitable Membranes. 2nd Edition. Sunderland, Massachusetts. Sinauer Associates.

Hoch, W., Betz, H. & Becker, C.-M. (1989). Primary Cultures of Mouse Spinal Cord Express the Neonatal Isoform of the Inhibitory Glycine Receptor. *Neuron*. **3**, 339-348.

Hodgkin, A. L. & Huxley, A. F. (1952). The dual effect of membrane potential on sodium conductance in the giant axon of *Loligo*. *Journal of Physiology*. **116**, 497-506.

Hodgkin, A. L., Huxley, A. F. & Katz, B. (1949). Ionic Currents Underlying Activity in the Giant Axon of the Squid. *Archives Sci. Physiol.* **3**, 129-130.

Hodgkin, A. L., Huxley, A. F. & Katz, B. (1952). Measurement of Current-Voltage Relations in the Membrane of the Giant Axon of *Loligo*. *Journal of Physiology*. **116**, 424-448.

Honoré, T., Davies, S. N., Drejer, J., Fletcher, E. J., Jacobsen, P., Lodge, D. & Nielsen, F. E. (1988). Qunioxalinediones: Potent Competitive Non-NMDA Glutamate Receptor Antagonists. *Science*. **241**, 701-703.

Hucho, F. (1986). The nicotinic acetylcholine receptor and its ion channel. *European Journal of Biochemistry*. **158**, 211-226.

Imoto, K., Methfessel, C., Sakmann, B., Mishina, M., Mori, Y., Konno, T., Fukuda, K., Kurasaki, M., Bujo, H., Fujita, Y. & Numa, S. (1986). Location of a δ-subunit region determining ion transport through the acetylcholine receptor channel. *Nature*. **324**, 670-674.

Irvine, D. R. F. (1986). Progress in Sensory Physiology 7: The Auditory Brainstem. (Ottoson, D., Ed.). *Springer-Verlag, Berlin, Heidelberg, New York, Tokyo.*

Isaacson, J. S. & Walmsley, B. (1995a). Receptors Underlying Excitatory Synaptic Transmission in Slices of the Rat Anteroventral Cochlear Nucleus. *Journal of Neurophysiology*. **73(3)**, 964-973.

Isaacson, J. S. & Walmsley, B. (1995b). Counting Quanta: Direct Measurements of Transmitter Release at a Central Synapse. *Neuron*. **15**, 875-884.

Jeffress, L. A. (1948). A Place Theory of Sound Localization. *Journal of Comparative Physiology and Psychology*. **41**, 35-39.

Johnson, J. W. & Ascher, P. (1987). Glycine potentiates the NMDA response in cultured mouse brain neurons. *Nature*. **325**, 529-531.

Kabashima, N., Shibuya, I., Ibrahim, N, Ueta, Y. & Yamashita, H. (1997). Inhibition of spontaneous EPSCs and IPSCs by presynaptic $GABA_B$ receptors on rat supraoptic magnocellular neurons. *Journal of Physiology*. **504.1**, 113-126.

Kandler, K. & Friauf, E. (1995). Development of Glycinergic and Glutamatergic Synaptic Transmission in the Auditory Brainstem of Perinatal Rats. *Journal of Neuroscience*. **15(10)**, 6890-6904.

Kanemasa, T., Gan, L., Perney, T. M., Wang, L.-Y. & Kaczmarek, L. K. (1995). Electrophysiological and Pharmacological Characterization of a mammalian *Shaw* Channel Expressed in NIH 3T3 Fibroblasts. *Journal of Neurophysiology*. **74(1)**, 207-217.

Katz, B. (1969). The Release of Neural Transmitter Substances. *Liverpool University Press*.

Katz, B. & Miledi, R. (1968). The Role of Calcium in Neurotransmitter Facilitation. *Journal of Physiology*. **195**, 481-492.

Kirsch, J., Langosch, D., Prior, P., Littauer, U. Z., Schmitt, B. & Betz, H. (1991). The 93-kDa Glycine Receptor-associated Protein Binds to Tubulin. *Journal of Biological Chemistry*. **266(33)**, 22242-22245.

Kirsch, J., Malosio, M.-L., Wolters, I. & Betz, H. (1993). Distribution of Gephyrin Transcripts in the Adult and Developing Rat Brain. *European Journal of Neuroscience*. **5**, 1109-1117.

Kiss, A. & Majorossy, K. (1983). Neuron Morphology and Synaptic Architecture in the Medial Superior Olivary Nucleus. *Experimental Brain Research*. **52**, 315-327.

Kleckner, N. W. & Dingledine, R. (1988). Requirement for Glycine in Activation of NMDA-Receptors Expressed in *Xenopus* Oocytes. *Science*. **241**, 835-837.

Kombian, S. B. Zidichouski, J. A. & Pittman, Q. J. (1996). $GABA_B$ Receptors Presynaptically Modulate Excitatory Synaptic Transmission in the Rat Supraoptic Nucleus In Vitro. *Journal of Neurophysiology*. **76(2)**, 1166-1179.

Korn, H. & Faber, D. S. (1991). Quantal analysis and synaptic efficacy in the CNS. *Trends in Neurosciences*. **14(10)**, 439-445.

Krupp, J., Larmet, Y. & Feltz, P. (1994). Postnatal change of glycinergic IPSC decay in sympathetic preganglionic neurons. *NeuroReport*. **5**, 2437-2440.

Kuhse, J., Betz, H. & Kirsch, J. (1995). The inhibitory glycine receptor: architecture, synaptic localization and molecular pathology of a postsynaptic ion-channel complex. *Current Opinion in Neurobiology*. **5**, 318-323.

Kuhse, J., Schmeiden, V. & Betz, H. (1990a). A Single Amino Acid Exchange Alters the Pharmacology of Neonatal Rat Glycine Receptor Subunit. *Neuron.* **5**, 867-873.

Kuhse, J., Schmieden, V. & Betz, H. (1990b). Identification and Functional Expression of a Novel Ligand Binding Subunit of the Inhibitory Glycine Receptor. *Journal of Biological Chemistry.* **265(36)**, 22317-222320.

Kungel, M. & Friauf, E. (1997). Physiology and pharmacology of native glycine receptors in developing rat auditory brainstem neurons. *Developmental Brain Research.* **102**,157-165.

Kuwabara, N. & Zook, J. M. (1992). Projections to the Medial Superior Olive From the Medial and Lateral Nuclei of the Trapezoid Body in Rodents and Bats. *Journal of Comparative Neurology.* **324**, 522-538.

Langford, T. L. (1984). Responses elicited from medial superior olivary neurons by stimuli associated with binaural masking and unmasking. *Hearing Research.* **15**, 39-50.

Langosch, D., Thomas, L. & Betz, H. (1988). Conserved quaternary structure of ligand-gated ion channels: The postsynaptic glycine receptor is a pentamer. *Proceedings of the National Academy of Science, USA.* **85**, 7394-7398.

LaVilla, I. (1898). Algunos detalles concernietes a la oliva superior y focos acusticos. *Rev. Trimest Micrograf.* **3**, 75-83.

Leake, P. A. & Snyder, R. L. (1989). Topographic Organization of the Central Projections of the Spiral Ganglion in Cats. *Journal of Comparative Neurology.* **281**, 612-629.

Legendre, P. (1997). Pharmacological Evidence for Two Types of Postsynaptic Glycinergic Receptors on the Mauthner Cell of 52-h-Old Zebrafish Larvae. *Journal of Neurophysiology.* 77, 2400-2415.

Legendre, P. (1998). A Reluctant Gating Mode of Glycine Receptor Channels Determines the Time Course of Inhibitory Miniature Synaptic Events in Zebrafish Hindbrain Neurons. *Journal of Neuroscience*, **18(8)**, 2856-2870.

Levitan, E. S., Schofield, P. R., Burt, D. R., Rhee, L. M., Wisden, W., Köhler, M., Fujita, N., Rodriguez, H. F., Stephenson, A., Darlison, M. G., Barnard, E. A. & Seeburg, P. H. (1988). Stuctural and functional basis for $GABA_A$ receptor heterogeneity. *Nature.* **335**, 76-79.

Lindsey, B. G. (1975). Fine Structure and Distribution of Axon Terminals from the Cochlear Nucleus on Neurons in the Medial Superior Olivary Nucleus of the Cat. *Journal of Comparative Neurology.* **160**, 81-103.

Magleby, K. L. & Stevens, C. F. (1972). The effect of voltage on the time course of end-plate currents. *Journal of Physiology.* **223**, 151-171.

Malenka, R. C. (1994). Synaptic Plasticity in the Hippocampus: LTP and LTD. *Cell.* **78**, 535-538.

Malosio, M.-L., Marquèze-Pouey, B., Kuhse, J. & Betz, H. (1991). Widespread expression of glycine receptor subunit mRNAs in the adult and developing rat brain. *EMBO Journal.* **10(9)**, 2401-2409.

Marmont, G. (1949). Studies on the Axon Membrane I. A New Method. *Journal of Cellular and Comparative Physiology.* **34**, 351-382.

Marvizón, J. C. G., Vázquez, J., Calvo, M. G., Mayor JR., F., Gómez, A. R., Valdivieso, F. & Benavides, J. (1986). The Glycine Receptor: Pharmacological Studies and Mathematical Modeling of the Allosteric Interaction Between the Glycine- and Strychnine-Binding Sites. *Molecular Pharmacology.* **30**, 590-597.

Masterton, B. & Diamond, I. T. (1967). Medial Superior Olive and Sound Localization. *Science.* **155**, 1696-1697.

Masterton, R. B. & Imig, T. J. (1984). Neural Mechanisms for Sound Localization. *Annual Review of Physiology.* **46**, 275-287.

Mayer, M. L., Partin, K. M., Patneau, D. K., Wong, L. A., Vyklicky Jr, L., Benveniste, M. & Bowie, D. (1995). Desensitization at AMPA, Kainate and NMDA Receptors. In: *Excitatory Amino Acids and Synaptic Transmission.* 2nd Edition. (Wheal, H. & Thompson, A. Eds.) *Academic Press.* pp89-98.

Mayer, M. L., Westbrook, G. L. & Guthrie, P. B. (1984). Voltage-dependent block by Mg^{2+} of NMDA responses in spinal cord neurones. *Nature.* **309**, 261-263.

Moore, J. K. (1986). Cochlear Nuclei: Relationship to the Auditory Nerve. In: *Neurobiology of Hearing: The Cochlea.* (R. A. Altschuler, D. W. Hoffman & R. P. Bobbin. Eds.) *Raven Press, New York.* pp283-301.

Moore, M. J. & Caspary, D. M. (1983). Strychnine blocks binaural inhibition in lateral superior olivary neurons. *Journal of Neuroscience.* **3(1)**, 237-242.

Morest, D. K. (1968). The Collateral System of the Medial Nucleus of the Trapezoid Body of the Cat, its Neuronal Architecture and Relation to the Olivo-Cochlear Bundle. *Brain Research.* **9**, 288-311.

Nakanishi, S. (1994). Metabotropic Glutamate Receptors: Synaptic Transmission, Modulation and Plasticity. *Neuron.* **13**, 1031-1037.

Narahashi, T., Moore, J. W. & Scott, W. R. (1964). Tetrodotoxin Blockage of Sodium Conductance Increase in Lobster Giant Axons. *Journal of General Physiology.* **47**, 965-974.

Neher, E. & Sakmann, B. (1976). Single-channel currents recorded from membrane of denervated frog muscle fibres. *Nature.* **260**, 799-802.

Nernst, W. (1888). Zur Kinetik der in Lösung befindlichen Körper: Theorie der Diffusion. *Z. Phys. Chem.* 613-637.

Noda, M., Takahashi, H., Tanabe, T., Toyosato, M., Kikyotani, S., Furutani, Y., Hirose, T., Takashima, H., Inayama, S., Miyata, T. & Numa, S. (1983). Structural Homology of *Torpedo californica* acetylcholine receptor subunits. *Nature.* **302**, 528-532.

Nowak, L., Bregestovski, P., Ascher, P, Herbert, A. & Prochiantz, A. (1984). Magnesium gates glutamate-activated channels in mouse central neurones. *Nature.* **307**, 462-465.

Oliver, D. L., Beckius, G. E. & Shneiderman, A. (1995). Axonal Projections From the Lateral and Medial Superior Olive to the Inferior Colliculus of the Cat: A Study Using Electron Microscopic Autoradiography. *Journal of Comparative Neurology.* **360**, 17-32.

Olney, J. W., Price, M. T., Samson, L. & Labruyere, J. (1986). The role of specific ions in glutamate neurotoxicity. *Neuroscience Letters.* **65**, 65-71.

Osen, K. K. (1969). Cytoarchitecture of the Cochlear Nuclei in the Cat. *Journal of Comparative Neurology.* **136**, 453-484.

Otis, T. S., Raman, I. M. & Trussell, L. O. (1995). AMPA receptors with high Ca^{2+} permeability mediate synaptic transmission in the avian auditory pathway. *Journal of Physiology.* **482.2**, 309-315.

Otis, T. S. & Trussell, L. O. (1996). Inhibition of Transmitter Release Shortens the Duration of the Excitatory Synaptic Current at a Calyceal Synapse. *Journal of Neurophysiology.* **76(5)**, 3584-3588.

Pearce, R. A. (1993). Physiological Evidence for Two Distinct $GABA_A$ Responses in Rat Hippocampus. *Neuron.* **10**, 189-200.

Perney, T. M. & Kaczmarek, L. K. (1997). Localization of a High Threshold Potassium Channel in the Rat Cochlear Nucleus. *Journal of Comparative Neurology.* **386**, 178-202.

Perney, T. M., Marshall, J., Martin, K. A., Hockfield, S. & Kaczmarek, L. K. (1992). Expression of the mRNAs for the Kv3.1 Potassium Channel Gene in the Adult and Developing Rat Brain. *Journal of Neurophysiology.* **68(3)**, 756-766.

Peyret, D., Campistron, G., Geffard, M. & Aran, J.-M. (1987). Glycine Immunoreactivity in the Brainstem Auditory and Vestibular Nuclei of the Guinea Pig. *Acta Otolaryngol (Stockh).* **104**, 71-76.

Pfeiffer, F., Graham, D. & Betz, H. (1982). Purification by Affinity Chromatography of the Glycine Receptor of Rat Spinal Cord. *Journal of Biological Chemistry.* **257(16)**, 9389-9393.

Pfeiffer, F., Simler, R., Grenningloh, G. & Betz, H. (1984). Monoclonal antibodies and peptide mapping reveal structural similarities between the subunits of the glycine receptor of rat spinal cord. *Proceedings of the National Academy of Science, USA.* **81**, 7224-7227.

Pfeiffer, R. R. (1966). Classification of Response Patterns of Spike Discharges for Units in the Cochlear Nucleus: Tone-Burst Stimulation. *Experimental Brain Research.* **1**, 220-235.

Poljak, S. (1926). The Connections of the Acoustic Nerve. Journal of Anatomy. 60, 465-469.

Ramón y Cajal, S. (1909). Histologie du systeme nerveux de l'homme et des vertebrates. Paris: Maloine.

Rang, H. P. & Dale, M. M. (1991). Chemical Transmitters and Drug Action in the Central Nervous System. In: *Pharmacology. Churchill Livingstone.* pp573-605.

Rayleigh, Lord, O. M. (1907). On our Perception of Sound Direction. *Philosophical Magazine.* **13**, 214-232.

Rhode, W. S., Oertel, D. & Smith, P. H. (1983). Physiological Response Properties of Cells Labeled Intracellularly with Horseradish Peroxidase in Cat Ventral Cochlear Nucleus. *Journal of Comparative Neurology.* **213**, 448-463.

Robertson, B. (1997). The real life of voltage-gated K^+ channels: more than model behaviour. *Trends in Pharmacological Sciences.* **18**, 474-483.

Rothman, S. M. (1985). The Neurotoxicity of Excitatory Amino Acids is Produced by Passive Chloride Influx. *Journal of Neuroscience.* **5(6)**, 1483-1489.

Rundström, N., Schmieden, V., Betz, H., Bormann, J. & Langosch, D. (1994). Cyanotriphenylborate: Subtype-specific blocker of glycine receptor chloride channels. *Proceedings of the National Academy of Science USA.* **91**, 8950-8954.

Ryall, R. W., Piercey, M. F. & Polosa, C. (1972). Strychnine-Resistant Mutual Inhibition of Renshaw Cells. *Brain Research.* **41**, 119-129.

Sahara, Y. & Westbrook, G. L. (1993). Modulation of Calcium Currents by a Metabotropic Glutamate Receptor Involves Fast and Slow Kinetic Components in Cultured Hippocampal Neurons. *Journal of Neuroscience.* **13(7)**, 3041-3050.

Sanes, D. H. (1990). An *in vitro* Analysis of Sound Localization Mechanisms in the Gerbil Lateral Superior Olive. *Journal of Neuroscience.* **10(11)**, 3494-3506.

Sassoè-Pognetto, M., Kirsch, J., Grünert, U., Greferath, U., Fritschy, J. M., Möhler, H., Betz, H. & Wässle, H. (1995). Colocalization of Gephyrin and $GABA_A$-Receptor subunits in the Rat Retina. *Journal of Comparative Neurology.* **357**, 1-14.

Saugstad, J. A., Segerson, T. P. & Westbrook, G. L. (1995). Modulation of Ion Channels and Synaptic Transmission by Metabotropic Glutamate Receptors. In: *Excitatory Amino Acids and Synaptic Transmission.* 2nd Edition. (Wheal, H. & Thompson, A. Eds.) *Academic Press.* pp77-88.

Sayer, R. J., Schwindt, P. C. & Crill, W. E. (1992). Metabotropic Glutamate Receptor-Mediated Suppression of L-Type Calcium Current in Acutely Isolated Neocortical Neurons. *Journal of Neurophyiology.* **68(3)**, 833-842.

Scheibel, M. E. & Scheibel, A. B. (1974). Neuropil Organization in the Superior Olive of the Cat. *Experimental Neurology.* **43**, 339-348.

Schmanns, H. & Friauf, E. (1994). K^+- and transmitter-induced rises in$[Ca^{2+}]_i$ in auditory neurones of developing rats. *NeuroReport.* **5**, 2321-2324.

Schmieden, V., Grenningloh, G., Schofield, P. R. & Betz, H. (1989). Functional expression in *Xenopus* oocytes of the strychnine binding 48kd subunit of the glycine receptor. *EMBO Journal.* **8(3)**, 695-700.

Schmeiden, V., Kuhse, J. & Betz, H. (1992). Agonist pharmacology of neonatal and adult glycine receptor α subunits: identification of amino acid residues involved in taurine activation. *EMBO Journal.* **11(6)**, 2025-2032.

Schmitt, B., Knaus, P., Becker, C.-M. & Betz, H. (1987). The M_r 93000 Polypeptide of the Postsynaptic Glycine Receptor Complex Is a Peripheral Membrane Protein. *Biochemistry.* **26**, 805-811.

Schoepp, D. D. & Conn, P. J. (1993). Metabotropic glutamate receptors in brain function and pathology. *Trends in Pharmacological Science.* **14**, 13-20.

Schofield, P. R., Darlison, M. G., Fujita, N., Burt, D. R., Stephenson, F. A., Rodriguez, H., Rhee, L. M., Ramachandran, J., Reale, V., Glencorse, T. A., Seeburg, P. H. & Barnard, E. A. (1987). Sequence and functional expression of the $GABA_A$ receptor shows a ligand-gated receptor super-family. *Nature.* **328**, 221-227.

Schröder, S., Hoch, W., Becker, C.-M., Grenningloh, G. & Betz, H. (1991). Mapping of Antigenic Epitopes on the α_1 Subunit of the Inhibitory Glycine Receptor. *Biochemistry.* **30**, 42-47.

Seeburg, P. H. (1993). *The TINS/TiPS Lecture.* The molecular biology of mammalian glutamate receptor channels. *Trends in Neuroscience.* **16(9)**, 359-365.

Shelton P. A., Davies, N. W., Antoniou, M., Grosveld, F., Needham, M., Hollis, M., Brammer, W. J. & Conley, E. C. (1993). Regulated Expression of K^+ Channel Genes in Electrically Silent Mammalian Cells by Linkage to β-Globin Gene-Activation Elements. *Receptors and Channels.* **1**, 25-37.

Sladeczek, F., Momiyama, A. & Takahashi, T. (1993). Presynaptic inhibitory action of a metabotropic glutamate receptor agonist on excitatory transmission in visual cortical neurons. *Proceedings of the Royal Society, B.* **253**, 297-303.

Smith, A. J. & Forsythe, I. D. (1996). Glycinergic synaptic responses between identified neurones in the rat auditory pathway *in vitro*. *Journal of Physiology.* **495.P**.

Smith, A. J. & Forsythe, I. D. (1997). Time-course and modulation of inhibitory glycinergic synaptic currents in the medial superior olive (MSO). *Society for Neuroscience Abstracts.*

Smith, P. H. (1995). Structural and Functional Differences Distinguish Principal From Nonprincipal Cells in the Guinea Pig MSO Slice. *Journal of Neurophysiology.* **73(4)**, 1653-1666.

Sprosen, T. S. & Woodruff, G. N. (1990). Polyamines potentiate NMDA induced whole-cell currents in cultured striatal neurons. *European Journal of Pharmacology.* **179**, 477-478.

Stotler, W. A. (1953). An experimental study of the cells and connections of the superior olivary complex of the cat. *Journal of Comparative Neurology.* **98**, 401-431.

Stuart, G. J. & Redman, S. J. (1990). Voltage dependence of Ia reciprocal inhibitory currents in cat spinal motoneurones. *Journal of Physiology.* **420**, 111-125.

Sullivan, W. E. & Konishi, M. (1986). Neural map of interaural phase difference in the owl's brainstem. *Proceedings of the National Academy of Science, USA.* **83**, 8400-8404.

Takahashi, T., Forsythe, I. D., Tsujimoto, T., Barnes-Davies, M. & Onodera, K. (1996). Presynaptic Calcium Current Modulation by a Metabotropic Glutamate Receptor. *Science.* **274**, 594-597.

Takahashi, T. & Momiyama, A. (1991). Single-Channel Currents Underlying Glycinergic Inhibitory Postsynaptic Responses in Spinal Neurons. *Neuron.* **7**, 965-969.

Takahashi, T., Momiyama, A., Hirai, K., Hishinuma, F. & Akagi, H. (1992). Functional correlation of fetal and adult forms of glycine receptors with developmental changes in inhibitory synaptic receptor channels. *Neuron.* **9**, 1155-1161.

Todd, A. J., Spike, R. C., Chong, D. & Neilson, M. (1995). The Relationship Between Glycine and Gephyrin in Synapses of the Rat Spinal Cord. *European Journal of Neuroscience.* **7**, 1-11.

Triller, A., Cluzeaud, F., Pfeiffer, F., Betz, H. & Korn, H. (1985). Distribution of Glycine Receptors at Central Synapses: An Immunoelectron Microscopy Study. *Journal of Cell Biology.* **101**, 683-688.

Tsuchitani, C. & Boudreau, J. C. (1966). Single Unit Analysis of Cat Superior Olive S Segment with Tonal Stimuli. *Journal of Neurophysiology.* **29**, 684-697.

Twyman, R. E. & MacDonald, R. L. (1991). Kinetic Properties of the Glycine Receptor Main- and Sub-Conductance States of Mouse Spinal Cord Neurones in Culture. *Journal of Physiology*. **435**, 303-331.

Uchizono, K. (1967). Synaptic Organization of the Purkinje Cells in the Cerebellum of the Cat. *Experimental Brain Research.* **4**, 97-113.

Unwin, N. (1989). The Structure of Ion Channels in Membranes of Excitable Cells. *Neuron.* **3**, 665-676.

Vandenberg, R. J., French, C. R., Barry, P. H., Shine, J. & Schofield, P. R. (1992). Antagonism of ligand-gated ion channel receptors: Two domains of the glycine receptor α subunit form the stychnine-binding site. *Proceedings of the National Academy of Science, USA.* **89**, 1765-1769.

Vandenberg, R. J., Handford, C. A. & Schofield, P. R. (1992). Distinct Agonist- and Antagonist-Binding Sites on the Glycine Receptor. *Neuron.* **9**, 491-496.

Vater, M. (1995). Ultrastructural and Immunocytochemical Observations on the Superior Olivary Complex of the Mustached Bat. *Journal of Comparative Neurology.* **358**, 155-180.

Walmsley, B. (1991). Central Synaptic Transmission: Studies at the Connection Between Primary Afferent Fibres and Dorsal Spinocerebellar Tract (DSCT) Neurones in Clarke's Column of the Spinal Cord. *Progress in Neurobiology.* **36**, 391-423.

Wang, H., Kunkel, D. D., Schwartzkroin, P. A. & Tempel, B. L. (1994). Localization of Kv1.1 and Kv1.2, Two K Channel Proteins, to Synaptic Terminals, Somata, and Dendrites in the Mouse Brain. *Journal of Neuroscience.* **14(8)**, 4588-4599.

Wang, L.-Y., Gan L., Forsythe, I. D. & Kaczmarek, L. K. (1998). Contribution of the Kv3.1 potassium channel to high-frequency firing in mouse auditory neurones. *Journal of Physiology.* **509.1**, 183-194.

Wang, Y.-X., Wenthold, R. J., Ottersen, O. P. & Petralia, R. S. (1998). Endbulb Synapses in the Anteroventral Cochlear Nucleus Express a Specific Subset of AMPA-Type Glutamate Receptor Subunits. *Journal of Neuroscience.* **18(3)**, 1148-1160.

Warr, W. B. (1966). Fiber Degeneration Following Lesions in the Anterior Ventral Cochlear Nucleus of the Cat. *Experimental Neurology.* **14**, 453-474.

Weiser,M., Vega-Saenz de Miera, E., Kentros, C., Moreno, H., Franzen L., Hillman, D., Baker, H. & Rudy, B. (1994). Differential Expression of *Shaw*-related K^+ Channels in the Rat Central Nervous System. *Journal of Neuroscience*. **14(3)**, 949-972.

Wenthold, R. J., Huie, D., Altschuler, R. A. & Reeks, K. A. (1987). Glycine Immunoreactivity Localized in the Cochlear Nucleus and Superior Olivary Complex. *Neuroscience*. **22(3)**, 897-912.

Whittingham, T. S., Lust, W. D. & Passonneau, J. V. (1984). An *in vitro* model of ischemia: Metabolic and electrical alterations in the hippocampal slice. *Journal of Neuroscience*. **4**, 793-802.

Wong, E. H. F., Kemp, J. A., Priestley, T., Knight, A. R., Woodruff, G. N. & Iversen, L. L. (1986). The anticonvulsant MK-801 is a potent *N*-methyl-D-aspartate antagonist. *Proceedings of the National Academy of Science, USA*. **83**, 7104-7108.

Wu, S. H. & Kelly, J. B. (1992). Binaural Interaction in the Lateral Superior Olive: Time Difference Sensitivity Studied in Mouse Brain Slice. *Journal of Neurophysiology*. **68**, 1151-1159.

Wu, S. H. & Kelly, J. B. (1994). Physiological evidence for ipsilateral inhibition in the lateral superior olive: synaptic responses in mouse brain slice. *Hearing Research*. **73**, 57-64.

Wu, S. H. & Kelly, J. B. (1995). Inhibition in the Superior Olivary Complex: Pharmacological Evidence From Mouse Brain Slice. *Journal of Neurophysiology*. **73(1)**, 256-269.

Wu, S. H. & Oertel, D. (1984). Intracellular Injection with Horeseradish Peroxidase of Physiologically Characterized Stellate and Bushy Cells in Slices of Mouse Anteroventral Cochlear Nucleus. *Journal of Neuroscience*. **4(6)**, 1577-1588.

Yin, T. C. T. & Chan, J. C. K. (1988). Neural Mechanisms Underlying Interaural Time Sensitivity to Tones and Noise. In: *Auditory Function* (Edelman, G. M., Gall, W. E. & Cowan, W. M. Eds.) *John Wiley & Sons*. pp385-430.

Yin, T. C. T. & Chan, J. C. K. (1990). Interaural Time Sensistivity in the Medial Superior Olive of the Cat. *Journal of Neurophysiology*. **64(2)**, 465-488.

Yost, W. A. & Dye, R. H. (1991). Properties of Sound Localization by Humans. In: *Neurobiology of Hearing: The Central Auditory System* (Altschuler, R. A., Bobbin, R. P., Clopton B. M. & Hoffman D. W. Eds.). *Raven Press, New York.* pp389-410.

Young, A. B. & Snyder, S. H. (1973). Strychnine Binding Associated with Glycine Receptors of the Central Nervous System. *Proceedings of the National Academy of Science, USA.* **70(10)**, 2832-2836.

Young, A. B. & Snyder, S. H. (1974). Strychnine Binding in Rat Spinal Cord Membranes Associated with the Synaptic Glycine Receptor: Cooperativity of Glycine Interactions. *Molecular Pharmacology.* **10**, 790-809.

Zarbin, M. A., Wamsley, J. K. & Kuhar, M. J. (1981). Glycine Receptor: Light Microscopic Autoradiographic Localization with [^{3}H]Strychnine. *Journal of Neuroscience.* **1(5)**, 532-547.

Zhang, S. & Trussell, L. O. (1994). Voltage clamp analysis of excitatory synaptic transmission in the avian nucleus magnocellularis. *Journal of Physiology.* **480.1**, 123-136.

Zwislocki, J. & Feldman, R. S. (1956). Just Noticeable Differences in Dichotic Phase. *Journal of the Acoustical Society of America.* **28(5)**, 860-864.

Appendices

Appendix 1 - Solutions

A Extracellular Solutions

i) HEPES buffered extracellular solution

Compound	Concentration (mM)	MWt
NaCl	135	58.44
KCl	3	74.56
HEPES	10	238.30
Glucose	10	180.16
Sucrose	45	342.30

The above compounds were added to ~900ml of milli-Q water. The pH was adjusted to 7.2 using 1M NaOH. The osmolarity was checked to be ~320mOsM and was made up to 1 litre with milli-Q water. Sucrose was added if necessary to adjust the osmolarity. The solution was stored at 2-5°C and 2mM $CaCl_2$ and 1mM $MgCl_2$ were added prior to use.

ii) Bicarbonate buffered artificial CSF

Compound	Concentration (mM)	MWt
NaCl	125	58.44
KCl	2.5	74.56
Glucose	10	180.16
NaH_2PO_4	1.25	156.01
Na-Pyruvate	2	110.00
Myo-inositol	3	180.2
Ascorbic acid	0.5	176.13
$NaHCO_3$	26	84.01

The above compounds were added to 2 litres of milli-Q water. The solution was then gassed for at least 30 minutes with 95%O_2 / 5%CO_2 such that the pH was 7.4. 2mM $CaCl_2$ and 1 mM $MgCl_2$ were added and the solution was stored at 2-5°C until use.

iii) Bicarbonate buffered low Na^+ artificial CSF

Compound	Concentration (mM)	MWt
KCl	2.5	74.56
Glucose	10	180.16
NaH_2PO_4	1.25	156.01
Ascorbic acid	0.5	176.13
Sucrose	250	342.30
$NaHCO_3$	26	84.01

The above compounds were added to 2 litres of milli-Q water. The solution was then gassed for at least 30 minutes with 95%O_2 / 5%CO_2 such that the pH was 7.4. 1mM $CaCl_2$ and 2mM $MgCl_2$ were added and the solution was stored at 2-5°C until use.

B. **Intracellular Patch Solutions**

i) Solution used for MEL cells.

Compound	Concentration (mM)	MWt
K^+ Gluconate	100	234.2
KCl	30	74.56
HEPES	10	238.3
EGTA	2	380.4
$MgCl_2$	2	203.31

The above compounds were added to ~80ml of milli-Q water and the pH adjusted to ~7.3 using 1M NaOH. The osmolarity was checked to be ~310mOsM and was made up to 100ml with milli-Q water. Sucrose was added if necessary to adjust the osmolarity. The solution was then frozen in 2ml aliquots to be defrosted for use on the day of an experiment

ii) KCl solution used for MSO neurones

Compound	Concentration (mM)	MWt
KCl	130	74.56
HEPES	10	238.3
EGTA	5	380.4
$MgCl_2$	1	203.31

The above compounds were added to ~80ml of milli-Q water and the pH adjusted to ~7.3 using 1M KOH. The osmolarity was checked to be ~310mOsM and was made up to 100ml with milli-Q water. Sucrose was added if necessary to adjust the osmolarity. The solution was then frozen in 2ml aliquots to be defrosted for use on the day of an experiment

iii) CsCl solution used for MSO neurones

Compound	Concentration (mM)	MWt
CsCl	130	168.4
EGTA	5	380.4
$MgCl_2$	1	203.31
HEPES	10	238.3
Sucrose	30	342.3

The above compounds were added to ~80ml of milli-Q water and the pH adjusted to ~7.3 using 1M CsOH. The osmolarity was checked to be ~310mOsM and was made up to 100ml with milli-Q water. Sucrose was added if necessary to adjust the osmolarity. The solution was then frozen in 2ml aliquots to be defrosted for use on the day of an experiment.

iv) $CsMeSO_4$ solution used for MSO neurones

Compound	Concentration (mM)	MWt
$CsMeSO_4$	130	228.0
EGTA	5	380.4
$MgCl_2$	1	203.31
HEPES	10	238.3
Sucrose	25	342.3

The above compounds were added to ~80ml of milli-Q water and the pH adjusted to ~7.3 using 1M CsOH. The osmolarity was checked to be ~310mOsM and was made up to 100ml with milli-Q water. Sucrose was added 133.5mM if necessary to adjust the osmolarity. The solution was added to intracellular patch solution (iii) in appropriate quantities as to produce intracellular chloride concentrations of: 5.9mM and 34.5mM.

C. **Junction Potentials**

Junction potentials are formed at the interface between two differently charged solutions When determining the reversal potential of the synaptic current, different proportions of intracellular patch solutions iii and iv were used, generating intracellular chloride concentrations ($[Cl^-]_i$)of 132.0mM, 34.5mM and 5.9mM. The extracellular artificial CSF (extracellular solution ii) was used throughout, producing an extracellular chloride concentration ($[Cl^-]_o$) of 133.5mM. The following documents the junction potentials generated using these different concentrations of chloride in the intracellular solution. When determining the reversal potential of the synaptic current, the discrepancy of the holding potential was adjusted by adding the junction potential.

$[Cl^-]_o$ (mM)	$[Cl^-]_i$ (mM)	Junction potential (mV)
133.5	132.0	2.7
133.5	34.5	5.26
133.5	5.9	8.22

Appendix 2 - Abbreviations

Abbreviation	*Full Name*
(1*S*,3*S*)-ACPD	(1*S*,3*S*)-1-Aminocyclopentane-1,3-dicarboxylic acid
ACSF	Artificial cerobrospinal fluid
AMPA	(α)-2-amino-3-[3-hydroxy-5-methylisoxazol-4-yl] propanic acid.
4-AP	4-amino pyridine
L-AP4	L(+)-2-amino-4-phosphonobutyric acid
DL-AP5	(±)-2-amino-5-phosphono-pentanoic acid
AVCN	Anterior ventral cochlear nucleus
BF	Best frequency
$CaCl_2$	Calcium chloride
CHO Cells	Chinese hamster ovary cells
CN	Cochlear nucleus
CNQX	6-cyano-7-nitroquinoxaline-2,3-dione
CNS	Central nervous system
CsCl	Caesium chloride
CSF	Cerebrospinal fluid
$CsMeSO_4$	Caesium methyl sulphonate
CsOH	Caesium hydroxide
CTB	Cyanotriphenyl borate
DAT	Digital audio tape
DCN	Dorsal cochlear nucleus
DNLL	Dorsal nucleus of the lateral lemniscus
DNQX	6,7-dinitro-7-quinoxaline-2,3-dione
DTX-I	Dendrotoxin I
EAA	Excitatory amino acid
EGTA	Ethylene glycol-bis(β-aminoethyl ether)-N,N,N',N'-tetra-acetic Acid
EPSC	Excitatory postsynaptic current
EPSP	Excitatory post synaptic potential
GABA $_{(A\ /\ B)}$	γ-aminobutyric acid (A or B type receptor)

GHK equation	Goldman Hodgkin Katz equation
GluR	Glutamate receptor
$GlyR_{(N/A)}$	Glycine receptor (neonatal or adult)
HEPES	N-(2-hydroxyethyl)piperazine-N'-(2-ethanesulphonic acid)
IC	Inferior colliculus
IID	Interaural intensity difference
IPSC	Inhibitory postsynaptic current
ITD	Interaural time difference
KCl	Potassium chloride
KOH	Potassium hydroxide
LL	Lateral lemniscus
LNTB	Lateral nucleus of the trapezoid body
LSO	Lateral superior olive
LTP	Long term potentiation
mAb	Monoclonal antibody
MEL cells	Murine erythroleukaemia cells
$MgCl_2$	Magnesium chloride
mGluR	Metabotropic glutamate receptor
MGN	Medial geniculate nucleus
mIPSC	Miniature inhibitory postsynaptic current
MK801 (Dizocilpine)	(+)-5-methyl-10,11-dihydro-5*H*-dibenzo[*a*,*d*]cyclohepten-5,10-imine maleate
MNTB	Medial nucleus of the trapezoid body
MSO	Medial superior olive
MWt	Molecular weight
nAChR	Nicotinic acetylcholine receptor
NaCl	Sodium chloride
$NaHCO_3$	Sodium hydrogen carbonate
NaH_2PO_4	Sodium hydrogen phosphate
NaOH	Sodium hydroxide
NM	Nucleus magnocellularis
NMDA	*N*-methyl-D-aspartate
PBS	Phosphate buffered saline

PON	Periolivary nucleus
PVCN	Posterior ventral cochlear nucleus
SEM	Standard error of the mean
SOC	Superior olivary complex
TEA	Tetraethyl ammonium
TTX	Tetrodotoxin
VCN	Ventral cochlear nucleus
VNLL	Ventral nucleus of the lateral lemniscus
$[X]_i$	Intracellular concentration of X
$[X]_o$	Extracellular concentration of X